QUANTIFICATION OF DIETARY TITANIUM DIOXIDE (E171) IN NEW ZEALAND FOOD PRODUCTS TO ESTIMATE POPULATION INTAKE AND ITS ROLE IN THE PATHOGENESIS OF METABOLIC DYSFUNCTION–ASSOCIATED STEATOTIC LIVER DISEASE (MASLD)

A thesis presented in partial fulfilment of the requirements for the degree of

Doctor of Philosophy (PhD)

in

Health Sciences

at Massey University, Wellington

New Zealand.

Jangrez Khan

2026

Abstract

Titanium dioxide (TiO_2) is commonly used as a food additive (E171) and has long served as a whitening and opacifying agent in confectionery and processed foods. However, its safety has become the subject of debate, with regulatory bans in several regions following concerns over potential toxicity and health risks associated with nanoparticles. New Zealand (NZ) has not yet imposed bans on E171, and the level of E171 and titanium (Ti) in NZ foods is unknown.

TiO_2 has been implicated in liver toxicity, oxidative stress, and metabolic dysfunction; however, its role in metabolic disorders such as metabolic dysfunction–associated steatotic liver disease (MASLD) remains elusive. This thesis presents a representative food survey of Ti intakes/exposure alongside an *in vitro* study to investigate the potential link between TiO_2 and the pathogenesis of MASLD.

A quantitative, comprehensive food survey was conducted to analyse Ti levels in the diet and subsequent population exposure. This survey distinguished between natural Ti intakes and habitual consumption of products containing added TiO_2. A representative range of foods across ten categories was analysed for Ti concentrations using graphite furnace atomic absorption spectroscopy (GFAAS). Using 14-day food intake data from the New Zealand Total Diet Study (NZTDS), the Ti intakes (mg/14 days) were estimated and converted to daily intake doses (mg/kg-bw/day) across age, gender, and ethnicity groups.

A human hepatoma HepG2 cell line was used in conjunction with oleic acid (OA) treatment to establish a steatotic model and evaluate the effects of TiO_2 (Titanium (IV) oxide nano powder with 21 nm primary particles - P21) and E171 (heterogeneous particle size). Cellular uptake of TiO_2 (E171 and P21) was assessed using a turbidity meter, while cytotoxicity was determined by trypan blue exclusion and neutral red uptake assays. The effects of E171 and P21 on steatosis were investigated using Oil Red O (ORO) staining, complemented by biochemical assays for triglycerides and cholesterol using commercially available kits. Oxidative stress responses were further examined by measuring reactive oxygen species (ROS), total antioxidant capacity (TAC), nitric oxide (NO), and lipid peroxidation (malonaldehyde; MDA).

The food survey (43 composites and 180 targeted items) revealed wide variation in Ti concentrations across NZ dietary intakes. Background levels were consistently low in plant- and dairy-based foods (<0.1–0.7 mg/kg), with natural contributions evident in eggs (1.17 mg/kg), meats (0.765–0.854 mg/kg), dried fruits, berries, and tea leaves (4.77 mg/kg). Among the 180 targeted items, confectionery products displayed a heavy-tailed distribution, with several globally recognised brands containing E171 at concentrations exceeding 1000–2200 mg/kg, while chocolate-based items ranged from <0.05 to 2076 mg/kg. Toothpaste analysis confirmed that personal care products are the most

concentrated point source of TiO_2, with levels up to 6349 mg/kg (0.63% w/w), 2–3 times higher than confectionery and 50–100 times higher than coated chocolates. Overall, the composite survey established a consistent background dietary Ti intake of 500–750 µg/day (0.5–0.75 mg/day), mainly attributable to natural sources, while targeted analysis highlighted residual high-dose products and habitual consumption of these products elevates baseline intake and can push exposure beyond upper levels.

In vitro, HepG2 steatotic models revealed that E171 and P21 selectively exacerbate cytotoxicity, triglyceride accumulation, and oxidative stress under lipid overload, without significantly altering cholesterol storage or lipid droplet formation. ROS levels increased dose-dependently in steatotic cells but remained unchanged in non-steatotic cells. In contrast, NO activity and MDA levels were stable, indicating no progression to inflammatory signalling or lipid peroxidation.

Overall, this study demonstrates that TiO_2 exposure in NZ is modest and largely background-driven, with only a small number of residual high-dose products contributing to elevated intake. TiO_2 does not universally drive steatosis but selectively perturbs triglyceride metabolism and ROS regulation under metabolic stress. These findings provide a timely baseline for a permitted but declining E171 landscape in NZ and highlight the importance of metabolic context in shaping TiO_2 toxicity.

Acknowledgements

In the name of Allah, the Most Gracious and the Most Merciful.

First and foremost, I would like to express my deepest gratitude to my supervisor, **Dr. Beth Mallard**, whose extreme support, kindness, and invaluable guidance have been a constant source of strength throughout my PhD journey. Her encouragement and wisdom have shaped not only my research but also my personal growth.

I extend my special gratitude to **Dr. Nick Kim** and **Dr. Collette Bromhead** for their generous guidance and for sitting with me at the lab bench, patiently teaching me everything I needed to know. Their dedication and hands-on mentorship have been genuinely inspiring. My sincere thanks also go to **Dr. Marlena Kruger** and **Dr. Penelope Truman**, whose immense guidance and support throughout my PhD were instrumental in helping me navigate challenges and achieve milestones. A special thanks to the Head of School, **Dr. Rachel Page**, for her generous support and guidance. My supervisory team has been the backbone of my academic journey. They were not only there for my academic progress but also stood by me during personal struggles and life phases throughout my PhD. Their doors were always open to me, without restriction of time, and their compassion made all the difference.

I am grateful to the technical staff, especially **Karishma Deo**, for her expertise and for ensuring my experiments ran smoothly. I also sincerely thank the administrative staff, **Alicia Jacob** and **Jill Brakensiek** for their constant support and assistance throughout my PhD journey. I would like to sincerely thank the science technicians at Massey University and Victoria University for their support and assistance in demonstrating/conducting the titanium dioxide characterisation work.

Beyond academia, I owe heartfelt thanks to my family, friends, and companions. Special appreciation goes to **Ahmad Hassan** and **Dr. Tasmia**, who stood by me through thick and thin, offering unwavering support. I am equally indebted to **Dr. Atif Islam** and **Dr. Mehwish Abbasi** for their immense support throughout this journey. I want to express my heartfelt gratitude to my dear friends, **Dr. Imran Khan**, **Riaz Ali**, and **Dr**. **Haroon Ahmad**, for their unwavering support and companionship. Their encouragement, emotional strength, and the many cherished memories we shared have been a source of comfort throughout my hardships and life's challenges.

To my beloved brothers and sisters, I am deeply grateful for your prayers and support. Above all, I owe everything to my father, **Wakeel Khan**, whose endless blessings have been the foundation of my success. I lovingly remember my late mother, **Zareen Taja**, whose memory continues to inspire me and to whom I dedicate this study. I also thank my younger brother, **Haider Khan**, **Fatima**, and my nephew **Zayyan Khan** for their cheerful encouragement throughout this journey.

Finally, I reserve my deepest gratitude for my wife, **Dr. Rabia**. Her immense support and encouragement carried me through the most difficult times. This achievement was not possible without her, and indeed, nothing in my life is achievable without her presence. Everything I have accomplished, and all the fortune in my life, is because of her. My beloved daughters, **Merwah Khan** and **Zunairah Khan**, have been my little butterflies throughout this journey. Their laughter, energy, and endless curiosity cheered me up in the most challenging times. They reminded me that life is not only about research and deadlines, but also about love, play, and the simple happiness of being together.

And to you all, my heartfelt thanks for your prayers, support, and encouragement throughout this journey.

Jangrez Khan

Table of contents

List of Figures

List of Tables

Abbreviations

2c37	Cytochrome P450 2C37
8-oHdG	8-hydroxy-2'-deoxyguanosine (marker of oxidative DNA damage)
A/G	Albumin to globulin ratio
A20	TNFAIP3 (tumour necrosis factor alpha-induced protein 3)
Acyl-CoA	Acyl coenzyme A
AFP	Alpha-fetoprotein
ALB	Albumin
ALP	Alkaline phosphatase
ALT	Alanine aminotransferase
Apaf-1	Apoptotic protease-activating factor 1
AST	Aspartate aminotransferase
ATF6	Activating transcription factor 6
Bax	Bcl-2-associated X protein
Bcl-2	B-cell lymphoma 2
BNIP3	BCL2/adenovirus E1B 19 kDa protein-interacting protein 3
BRIP1	BRCA1 interacting protein C-terminal helicase 1
BUN	Blood urea nitrogen
Calpain 2	Calcium-activated neutral protease 2
Caspase-1/Caspase-3	Cysteine-aspartic acid protease 1/3
Caspase-9	Cysteine-aspartic acid protease 9
CAT	Catalase
CCL20	Chemokine (C-C motif) ligand 20
CD36	Cluster of differentiation 36
CD68	Cluster of differentiation 68 (macrophage marker)
CDKN1A	Cyclin-dependent kinase inhibitor 1A (p21)

CEA	Carcinoembryonic antigen
ChE / PChE	Cholinesterase / Pseudocholinesterase
Cho / Chol	Cholesterol
CHOP	C/EBP homologous protein
ChREBP	Carbohydrate response element-binding protein
CK	Creatine kinase
c-Myc	Cellular myelocytomatosis oncogene
Co	Cobalt
Col1α1	Collagen type I alpha 1 chain
collagen I	Type I collagen
Cox2	Cyclooxygenase 2
CPT1	Carnitine palmitoyltransferase 1
Creatinine	Waste product from muscle metabolism
CRP	C-reactive protein
Ctgf	Connective tissue growth factor
CXCL2	Chemokine (C-X-C motif) ligand 2
cyclin D	Cyclin D (cell cycle regulator)
CYP1A	Cytochrome P450 1A
CYP1A1	Cytochrome P450 family 1 subfamily A member 1
Cyp2b10	Cytochrome P450 2B10
Cyp2b9	Cytochrome P450 family 2 subfamily B member 9
Cyp2c70	Cytochrome P450 family 2 subfamily C member 70
Cyp4a14	Cytochrome P450 family 4 subfamily A member 14
Cyto-c	Cytochrome c
D.BIL	Direct bilirubin
DNA	Deoxyribonucleic acid

DNAJC15	DnaJ heat shock protein family (Hsp40) member C15
DNMT3a	DNA (cytosine-5)-methyltransferase 3 alpha
DNMT3b	DNA (cytosine-5)-methyltransferase 3 beta
ECM	Extracellular matrix
ER	Endoplasmic reticulum
ES1	ES1 homolog, mitochondrial
FABP1	Fatty acid binding protein 1
FAM114A2	Family with sequence similarity 114 member A2
FATP	Fatty acid transporter proteins
FFA	Free fatty acids
Fibronectin	Extracellular matrix glycoprotein involved in cell adhesion and wound healing
GADD45A	Growth arrest and DNA damage-inducible alpha
GATA3 / GATA4	GATA-binding protein 3 / 4
GATD3A	Glutamine amidotransferase domain-containing protein 3A
GCLC	Glutamate–cysteine ligase catalytic subunit
GDF15	Growth differentiation factor 15
GI tract	Gastrointestinal tract
GLB	Globulin
Glu	Glucose
GPx	Glutathione peroxidase
GRP78	Glucose-regulated protein 78
GSH	Reduced glutathione
GSK-3β	Glycogen synthase kinase 3 beta
GSSG	Oxidized glutathione
GST	Glutathione S-transferase
GZMA	Granzyme A

H1-2	Histone H1.2
H_2O_2	Hydrogen peroxide
HADHB	Hydroxyacyl-CoA dehydrogenase trifunctional multienzyme complex subunit beta
HBDH	α-Hydroxybutyrate dehydrogenase
HCC	Hepatocellular carcinoma
HDL / HDL-Cho	High-density lipoprotein cholesterol
HepaRG	Human hepatic progenitor cell line
HepG2	Human liver carcinoma cell line
HepG2/C3A	Subclone of HepG2 with enhanced liver-specific functions
HIF-1α	Hypoxia-inducible factor 1 alpha
HO-1	Heme oxygenase 1
Hsp	Heat shock protein
HSP60 / HSP70	Heat shock protein 60 / 70
HSP70	Heat shock protein 70
Huh7	Human hepatoma cell line
IFN-γ	Interferon gamma
IgG	Immunoglobulin G
IgM	Immunoglobulin M
IKK1 / IKK2	IκB kinase 1 / 2
IL-10	Interleukin 10
IL-12	Interleukin 12
IL-1α	Interleukin 1 alpha
IL-1β	Interleukin 1 beta
IL-2	Interleukin 2
IL-4	Interleukin 4
IL-5	Interleukin 5

IL-6	Interleukin 6
IL-6	Interleukin 6
IL1β	Interleukin-1 beta
ILK	Integrin-linked kinase
iNOS	Inducible nitric oxide synthase
INSIG1	Insulin-induced gene 1
IR	Insulin receptor
IRE1α/β	Inositol-requiring enzyme 1 alpha/beta
ISCA2	Iron-sulfur cluster assembly 2 homolog
IV	Intravenous
IκB	Inhibitor of kappa B
JNK1	c-Jun N-terminal kinase 1
LAP	Leucine aminopeptidase
LDH	Lactate dehydrogenase
LDL-C	Low-density lipoprotein cholesterol
LDL-Cho	Low-density lipoprotein cholesterol
LPO	Lipid peroxidation
LX-2	Human hepatic stellate cell line
MAPK	Mitogen-activated protein kinase
MASH	Metabolic dysfunction-associated steatohepatitis
MASLD	Metabolically-dysfunction-associated steatotic liver disease
MBD2	Methyl-CpG-binding domain protein 2
MCP-1	Monocyte chemoattractant protein-1
MDA	Malondialdehyde
MDK	Midkine
MIP-2	Macrophage inflammatory protein-2

min	minutes
Mn	Manganese
Mo	Molybdenum
Mrp3	Multidrug resistance-associated protein 3
MT	Metallothionein
nbn	Nibrin (gene involved in DNA damage response)
NF-κB	Nuclear factor kappa-light-chain-enhancer of activated B cells
NIK	NF-κB-inducing kinase
NLRP10	NOD-like receptor family pyrin domain containing 10
NLRP3	NOD-like receptor family pyrin domain containing 3
NO	Nitric oxide
Nos2	Nitric oxide synthase 2
NQO1	NAD(P)H quinone dehydrogenase 1
Nrf2	Nuclear factor erythroid 2–related factor 2
O_2-	Superoxide anion
Oapt1	Organic anion transporting polypeptide 1
Ogg1	8-oxoguanine DNA glycosylase 1
P	Phosphorus
p38 MAPK	p38 Mitogen-Activated Protein Kinase
p53	Tumor protein p53
PC	Phosphatidylcholine
PChe	Pseudocholinesterase
p-eIF2α	Phosphorylated eukaryotic initiation factor 2 alpha
PERK	Protein kinase RNA-like endoplasmic reticulum kinase
PI3K/AKT	Phosphoinositide 3-kinase / Protein kinase B signaling pathway
p-p38	Phosphorylated p38 mitogen-activated protein kinase

PPARα	Peroxisome proliferator-activated receptor alpha
Rb	Retinoblastoma protein
RNS	Reactive nitrogen species
ROS	Reactive oxygen species
SCARA3	Scavenger receptor class A member 3
Smad-2	Mothers against decapentaplegic homolog 2
SOD	Superoxide dismutase
SPP1	Secreted phosphoprotein 1 (also known as osteopontin)
SREBP1c	Sterol regulatory element-binding protein 1c
STAT1 / STAT3 / STAT6	Signal transducer and activator of transcription 1 / 3 / 6
T.BIL	Total bilirubin
T2DM	Type 2 diabetes mellitus
TAC	Total antioxidant capacity
TBA	Total bile acids
TBARS	Thio barbituric acid reactive substances
T-bet	T-box transcription factor TBX21
TBIL	Total bilirubin
TC	Total cholesterol
TCHO / TC	Total cholesterol
TEM	Transmission electron microscopy
TF	Transcription factor
TF Genes	Transcription factor genes
TG	Triglycerides
TGF-β	Transforming growth factor beta
TGF-β1R	Transforming growth factor beta 1 receptor
THLE-2	Human liver epithelial cell line

Ti	Titanium
Ti_2O_3	Dititanium trioxide (Titanium (III) oxide)
Timp1	Tissue inhibitor of metalloproteinases 1
TiO_2	Titanium dioxide
TiO_2 NPs	Titanium dioxide nanoparticles
TiO_3	Titanium trioxide
TLR2 / TLR4	Toll-like receptor 2 / 4
TLR-4	Toll-like receptor 4
TNF-α	Tumour necrosis factor alpha
TOS	Total oxidant status
TP	Total protein
TP53	Tumour protein p53
UHRF-1	Ubiquitin-like with PHD and RING finger domains 1
UPR	Unfolded protein response
VEGF	Vascular endothelial growth factor
VEGFA	Vascular endothelial growth factor A
VLDL	Very low-density lipoproteins
Wnt3 / Wnt4	Wingless-type MMTV integration site family member 3 / 4
XBP1-s	Spliced X-box binding protein 1
XBP1-t	Total X-box binding protein 1
yrs	years
ZNF562	Zinc finger protein 562
α-Sma	Alpha-smooth muscle actin
β-catenin	Beta-catenin
γH2A	Phosphorylated histone H2A variant (γ-H2AX, DNA damage marker)

CHAPTER 1: Introduction

1.1 Titanium dioxide as a food additive

Titanium (Ti) is the seventh most abundant metal and the ninth most prevalent element in Earth's crust. Titanium dioxide (TiO_2) is widely used as a whitening and opacifying agent in selected medicines, foods, and cosmetics. Ti as a metal and its uses, unique properties, and crystalline forms are discussed in detail in **Section 2.2**.

TiO_2 is widely utilised across industries in macro- and micro-scale forms, serving as a pigment and food additive. While macro-sized (1–1000 µm) particles are largely inert, micro-sized TiO_2 (0.1–10 µm) used in foods often exhibits a broad particle size distribution, including a significant number of particles (17-36%) in the nano range, i.e., <100 nm, which are known as titanium dioxide nanoparticles (TiO_2 NPs). Engineered nano-TiO_2 (~21 nm) exhibits distinct physicochemical properties, including enhanced surface reactivity and photocatalytic potential (Luo et al., 2020; Shang et al., 2024; Weir et al., 2012; Younes et al., 2021). As a food additive, TiO_2 is known as E171 in the European Union (EU), and INS171 in the United States (US) (Korotcenkov, 2020b). It is commonly used in food and consumer products such as toothpaste, coatings, preserved fruits, chewing gum, coated candies, carbonated drinks, dairy products, tattoo ink, sauces, icings, beauty creams, cake decorations, food colours, and dressings (Chen et al., 2013; Keller et al., 2013; Lim et al., 2018; Lomer et al., 2000; Ortiz & Alster, 2012; Peters et al., 2014; Weir et al., 2012). TiO_2 NPs, although not the dominant component in E171, are biologically relevant due to their potential for increased reactivity and bioavailability (Fiordaliso et al., 2022). E171 contains enough TiO_2 NPs to raise safety concerns in the context of ingestion and long-term exposure (Barreau et al., 2021; Younes et al., 2021).

1.2 Consumption of E171

In the food industry, various nanomaterials at low concentrations are used as additives to maintain nutrient bioavailability, extend shelf life, and enhance sensory characteristics, including texture, flavour, colour, and consistency. Although for many years, food additives including E171, were regarded as harmless, more recently the potential adverse effects have been more closely considered (Warheit, 2024; Younes et al., 2021).

Reported consumption rates of E171 vary significantly, with estimates for children ranging from 0.6 mg/kg/day to more than 6.9 mg/kg/day, while adult intake is as low as 0.3 mg/kg/day (Bachler et al., 2015; Lomer et al., 2000; Rompelberg et al., 2016; Weir et al., 2012; Younes et al., 2021). The daily dietary intake of E171 is across different age groups and cultures; however, due to lower body mass and disproportionately higher consumption of E171-containing products, children were found to be

the most highly exposed group. Children are more likely to consume food that may contain TiO_2 (Bischoff et al., 2021; Li et al., 2018; Weir et al., 2012). The National Diet and Nutrition Survey (NDNS) and the Diet and Nutrition Survey of Infants and Young Children (DNSIYC) were used to estimate E171 exposure across age groups in the UK. This report revealed that the average daily intake of E171 ranged from 3.3–11 mg/kg-bw/day. Moreover, the 95th percentile total exposures for E171 ranged from 9.1 to 26 mg/kg-bw/day (COT, 2024).

1.3 Emerging potential health risks and regulatory actions

In the late 1960s, due to TiO_2's low solubility and chemical inertness, the EU and the US Food and Drug Administration designated food-grade titanium dioxide (E171) as safe for consumption (Commission Regulation EU, 2012; Korotcenkov, 2020a). Currently, in the US, the maximum concentration of E171 as a food additive is 1% (FDA, 2024; Heringa et al., 2016). In contrast, the EU allowed the addition of E171 to food at *quantum satis* levels (meaning only as much as necessary) until its use was officially banned in 2022 (Baranowska-Wójcik et al., 2022; Heringa et al., 2016; Rompelberg et al., 2016; Younes et al., 2021). In New Zealand (NZ), the regulation of E171 as a food additive is governed by Food Standards Australia New Zealand (FSANZ). E171 is currently permitted as a food additive in NZ, classified as a colouring agent, and no maximum limit is specified, meaning it can be used according to the manufacturer's specifications (FSANZ, 2022; Warheit, 2024). Research over the last decade has challenged perspectives on the safety and low toxicity of TiO_2 (TiO_2 NPs and E171) containing products.

In 2010, TiO_2 NPs were classified as a group 2B carcinogen (a substance possibly carcinogenic to humans, based on limited evidence) by the International Agency for Research on Cancer (IARC, 2010) for humans (by inhalation). Since those initial reports, several studies have documented the adverse effects of TiO_2 NPs across various routes of administration, including inhalation, intravenous, dermal, and oral (Hong et al., 2014; Hu et al., 2015; Ogunsuyi et al., 2022; Talamini et al., 2019). The European Food Safety Authority (EFSA) Panel on Food Additive and Nutrient Sources added to Food (ANS Panel) re-evaluated the usage of TiO_2 in 2016 and 2018 over the concerns raised about its genotoxic and carcinogenic potential, but both EFSA reports concluded that these concerns were unfounded (EFSA, 2016; Younes et al., 2018). However, in 2020, E171 use was suspended in France for one year, and in 2021, EFSA declared it unsafe for use as a food additive (Boutillier et al., 2021). In 2022, the EU also banned the use of E171 as a food additive, as it potentially has genotoxic effects and is no longer considered safe (Younes et al., 2021). Subsequently, many countries, including Switzerland, Jordan, Saudi Arabia, Qatar, Yemen, Oman, Turkey, and Israel, replicated the ban. However, others, including NZ, Australia, Canada, and the US, have chosen not to regulate the use of E171 (TDMA, 2022).

These safety concerns and regulations have prompted several countries to assess population exposure to E171. The EU, through EFSA, conducted a detailed safety assessment using national intake data from member states, while France carried out a 5-year market screening (2018–2022) (Bucher et al., 2024). In contrast, Australia and NZ published the FSANZ report, which is based primarily on previously published data, rather than direct market sampling of food products, meaning their assessments do not reflect real-time market composition (FSANZ, 2022).

1.4 TiO_2 and the liver

TiO_2 NPs have been shown to induce toxicity in various organs, including lungs, brain, kidneys, spleen, and liver. As the body's main detoxification organ, the liver not only eliminates exogenous compounds (Kalra et al., 2025) but also regulates key metabolic processes, including glucose, insulin signalling, inflammation, and lipid metabolism (Watt et al., 2019).

Several studies have investigated the hepatic effects of TiO_2 (see **Appendices 2.1** and **2.2** for details). TiO_2 NPs have been found to accumulate in the liver with slow excretion (Chen et al., 2009; Liang et al., 2009; Shakeel et al., 2016). After intravenous administration, they rapidly accumulate in the liver, with ~69% detected within 5 min and ~80% after 15 min, marking the liver as a key site of deposition and toxicity (Huggins & Froehlich, 1966). Similarly, studies in rodents using oral administration confirm predominant hepatic accumulation (Abd-Elhakim et al., 2023; Valentini et al., 2019). Increasing evidence indicates TiO_2 can induce hepatotoxicity by disrupting physiological pathways in the liver (Ma et al., 2023; Zhao et al., 2021). Accumulation of TiO_2 NPs in the liver is associated with steatosis, oxidative stress, endoplasmic reticulum (ER), and mitochondrial stress, leading to reactive oxygen species (ROS), reactive nitrogen species (RNS), inflammation, necrosis, and apoptosis *in vitro* and *in vivo* (Cui et al., 2010; Cui et al., 2011; Gilbert et al., 2021; Hassanein & El-Amir, 2018; Jia et al., 2017; Nie et al., 2021; Shirdare et al., 2022; Wang et al., 2013) (for details, see **Section 2.7**).

Increased ROS in the liver plays an important role in the pathogenesis of various metabolic disorders, such as obesity, insulin resistance (IR), type 2 diabetes (T2M), and metabolic dysfunction-associated steatotic liver disease (MASLD), previously known as non-alcoholic fatty liver disease (NAFLD). MASLD progresses from simple steatosis to metabolic dysfunction-associated steatohepatitis (MASH), characterised by liver inflammation and fibrosis, leading to cirrhosis, liver failure, and hepatocellular carcinoma (HCC) (see **Figure 2.4**) (Targher et al., 2024).

ROS play a key role in the pathogenesis of diabetes by disrupting the functioning of pancreatic β-cells (insulin-producing cells in pancreatic islets), further reducing insulin sensitivity, which is also a crucial risk factor for MASLD (Eguchi et al., 2021; Fridlyand & Philipson, 2006; Yeo et al., 2013). Oral administration of TiO_2 NPs increases ROS, leading to insulin resistance and elevated plasma glucose

levels in mice (Hu et al., 2015). The oxidative hepatic environment in obesity promotes the signal transduction and activation of transcription programs (STAT-1 and STAT-3). This activation leads to the recruitment of T cells and promotes liver damage as disease progresses, culminating in malignant transformation (Grohmann et al., 2018). The involvement of ROS in initiating oxidative stress, inflammation, and cellular damage is well-established in the pathogenesis of MASLD and its associated risk factors, including IR, T2DM, and obesity. Given the documented ability of TiO_2 NPs to induce ROS, a plausible link between TiO_2 NPs exposure and the onset and progression of MASLD warrants further investigation.

1.5 Rationale and focus

Despite growing global concern over its safety, E171 remains permitted in NZ food products. FSANZ acknowledged these concerns and issued a call for data to reassess its safety in Australia and NZ. Based on existing international data, FSANZ concluded that there is insufficient evidence to warrant a ban on E171 (FSANZ, 2021). Despite this position, there is currently no comprehensive dietary exposure survey that quantifies E171 consumption in NZ. This lack of localised data presents a significant gap in understanding population-level exposure, particularly given the widespread availability of E171-containing food products in NZ supermarkets.

Both the changing regulatory environment and the growing emphasis on assessing real-world E171 consumption have been driven by accumulating evidence of TiO_2 NPs toxicity in various experimental models (Bischoff et al., 2025; Younes et al., 2021). Previous studies have demonstrated that TiO_2 NPs can induce adverse biological effects, including oxidative stress, inflammation, and genotoxicity (Younes et al., 2021). The liver is a primary target organ of E171, with research indicating potential impacts on liver function and health following oral exposure. TiO_2 NPs increase the serum levels of liver injury markers *in vivo* (Abbasi-Oshaghi et al., 2019; Azim et al., 2015; Niu et al., 2017; Sallam et al., 2022b; Salman et al., 2021) and induce cytotoxic effects, including restricted cell growth, increased apoptosis, and cell cycle arrest *in vitro* (Sha et al., 2011). These adverse outcomes, particularly oxidative stress, inflammation, and apoptosis, are key contributors to the pathogenesis of MASLD.

MASLD is a multifactorial condition linked with cardiometabolic risk factors such as obesity, insulin resistance, and type 2 diabetes, all of which are highly prevalent in NZ. One third of NZ adults are obese, and over 300000 New Zealanders have diabetes (mainly T2DM), suggesting that there is potentially a large proportion of the population with MASLD, mostly undiagnosed (Diabetes NZ, 2024). Although studies have shown the hepatotoxic effects of TiO_2, a possible role in MASLD remains unexplored.

The current study reports the outcome of an assessment of dietary Ti levels in food items and consumer products available in the NZ market. Additionally, this project investigated whether TiO_2 exacerbated steatosis and/or oxidative stress in an *in vitro* model of MASLD in human cells.

1.6 Research objectives

The overall aims of this research were two-fold. Firstly, to investigate the concentration of Ti in a sample of food available in NZ, in order to estimate the dietary Ti intakes of the NZ population. Secondly, to determine whether TiO_2 NPs (P21) or E171 exacerbate lipid accumulation or other pathways associated with MASLD in a human liver (HepG2) cell model of steatosis.

Objective 1: To identify the food groups most likely to contribute to Ti intake, including the prevalence and levels of E171 in commonly used products, distinguishing between natural baseline intakes and those attributable to the food additive E171.

Objective 2: To estimate dietary intakes of Ti in NZ across age, gender, and ethnicity categories and to assess potential upper intakes among frequent consumers.

Objective 3: To investigate the role of E171 and P21 in inducing steatosis in HepG2 cells and its impact on oleic acid-induced steatotic HepG2 cells.

Objective 4: To investigate the role of E171 and P21 in the induction of oxidative stress in steatotic HepG2 cells.

1.7 Thesis structure

This thesis follows the traditional monograph format and is organised into eight chapters, along with references and appendices. The structure is as follows:

Chapter 1 provides an introductory section to the research topic, outlining its background and significance, and outlines the overall aims and objectives for this PhD study.

Chapter 2 provides a comprehensive review of relevant literature, critically examining prior research to identify gaps and inform the research direction.

Chapter 3 outlines the general methods employed across the various experiments conducted in this study. It provides a detailed account of the experimental procedures, materials, protocols, and data analysis techniques applied to interpret the results.

Chapters 4 and **5** address the first and second research objectives, respectively, related to Ti levels in NZ food and estimated intake among New Zealanders.

Chapters 6 and **7** address the third and fourth research objectives, related to the effects of TiO_2 on a HepG2 cell model of steatosis.

Chapter 8 summarises the main findings of the study and highlights the limitations encountered during the research. It critically evaluates the implications of these findings within the context of existing literature, proposes directions for future investigation that could build upon the insights gained from this thesis, and further advance understanding in the field.

References list all the sources cited in this thesis.

Appendices include supplementary information and some data not included in the main text.

CHAPTER 2: Literature review

A review article entitled "Hepatotoxicity of titanium dioxide nanoparticles" based on parts of the literature reviewed in this chapter has been published by the author of this thesis (Khan et al., 2025).https://doi.org/10.1002/jat.4626

2.1 Titanium metal

Titanium (Ti) is a silver-coloured metal valued for its low density, high strength, and corrosion resistance (See **Table 2.1** for chemical and physical properties of Ti). Ti is an abundant element in the Earth's crust, occurring at a concentration of ~4400 ppm, which corresponds to about 0.6% by weight, thus making it the ninth most abundant element in the crust (Buettner & Valentine, 2012; Klein & Russell, 1973), and is the second most abundant transition metal, after iron (Emsley, 2011; Kaim et al., 2013). It occurs within mineral deposits, mainly rutile (a crystal form of TiO_2), ilmenite ($FeTiO_3$), and titanite ($CaTiSiO_5$), which are widely distributed in the Earth's crust and lithosphere and are found in all living things, water bodies, rocks, and soils (Emsley, 2011). The most common oxidation state of Ti is +4, but +3 and +2 states also exist. Metallic Ti, TiO_2, and $TiCl_4$ (used in making smoke screens) are the compounds most widely used in industry (Warheit et al., 2007). The chemical and physical properties are summarised in **Table 2.1**.

Table 2.1 Chemical and physical properties of Ti.

Symbol	Ti
Discovery	1791 by William Gregor
Named by	Martin Heinrich Klaproth in 1795
Appearance	Silvery grey-white metallic
Atomic weight/Atomic number	47.867 / 22
Block/Group/Period	d/4/4
Electron configuration/ electrons/ shell	$3d^2\ 4s^2$/ 2, 8, 10, 2
Phase at STP	Solid
Melting point	1941 K (1668 °C, 3034 °F)
Boiling point	3560 K (3287 °C, 5949 °F)
Density (near RT)	4.506 g/cm^3
Oxidation states	+2, +3 (numerous), +4 (most common, covalent bonding)
Isotopes/abundance	^{46}Ti, ^{47}Ti, ^{48}Ti, ^{49}Ti, ^{50}Ti/ 8.25%, 7.44%, 73.72%, 5.41%, 5.18%.

Allotropic forms	A hexagonal α, body-centred cubic (lattice) β
Titanium-containing minerals	Anatase, brookite, ilmenite, perovskite, rutile, and titanite (sphene), Akaogiite (very rare)

Ti metal is widely used in the aircraft and spacecraft industries due to its high tensile strength, extraordinary corrosion resistance, lightweight nature, and ability to withstand extreme temperatures. Additionally, it has several applications in the chemical and paper pulp industries due to its corrosion resistance and chemical inertness. For example, it is used as tubing and for lining vessels, which are used in nitric acid and acetaldehyde production (Boyer, 2010). Ti and its alloys are commonly used in the medical and dental fields due to their exceptional corrosion resistance and mechanical properties. They are mainly used in implant devices to replace defective hard tissues, such as artificial hip or knee joints, bone plates, dental implants, and dental products, including crowns, bridges, and dentures (Jin et al., 2022). Additionally, it is widely used in dairy products, as a colour additive in confectionery, and bread flours as an alternative flour bleaching agent (Hu et al., 2010; Samat et al., 2016)

2.2 Titanium dioxide (TiO_2) chemical properties

Four prominent oxides of Ti are titanium monoxide (TiO), titanium dioxide (TiO_2), titanium trioxide (TiO_3), and dititanium trioxide (Ti_2O_3) (Jin et al., 2022). Structurally, the Ti atom is octahedrally coordinated to oxygen, but the positions of the octahedral structure differ across the different crystalline forms (Diebold, 2003). TiO_2 occurs naturally in three crystallographic forms: rutile, anatase, and brookite. Both rutile and anatase are used as food additives. Anatase is a more chemically reactive form (De Matteis et al., 2021). Rutile and anatase exist in a tetragonal structure, whereas brookite is orthorhombic. The metastable anatase and brookite can be thermally restructured into the more thermodynamically stable rutile (Ropers et al., 2017), depending on the mineral's industrial purpose. Anatase quickly converts into rutile at a temperature >700°C, and rutile melts at temperatures between 1830–1850°C. However, anatase is predominantly used in commercial products due to its higher photocatalytic activity than brookite and rutile (Chen & Mao, 2007; Cihlar et al., 2021; Fagan et al., 2016; Higashimoto, 2019; Jing et al., 2013).

TiO_2 is a cheap, abundant, extremely bright, and white pigment having a high refractive index with a molecular weight of 79.9 g/mol, boiling point of 2972°C, melting point of 1843°C, and relative density of 4.26 g/cm³ at 25°C (Sayes et al., 2006). Due to its properties like ease of availability, biocompatibility, high specific surface area, long-term photostability, strong oxidising properties, antibacterial properties, anti-corrosive, and low toxicity, it is widely used in paints (artist's paint and house paint), enamels, lacquers, plastics, and paper coatings (Chen et al., 2020; Kaewklin et al., 2018; Yin et al., 2013). TiO_2 is used in a variety of drugs and cosmetics because it acts as an effective sunscreen,

protecting against short-wave ultraviolet radiation. TiO_2 serves as a clouding agent and is assimilated into dry beverages and tobacco wrappings. It is also used in the pharmaceutical industry as a component of tablets (Weir et al., 2012).

The most common Ti compound is TiO_2, which constitutes almost 95% of all Ti consumed (US Geological Survey, 2025). In 2024, 9.93 million tonnes were produced. The global market for TiO_2 is expected to increase by 6.5% between 2024 and 2030, from USD 21.64 billion (in 2024) with a revenue forecast of USD 31.79 billion in 2030. The projected increase in the TiO_2 market value is driven by rising production and consumption, as well as moderate price growth, with demand as the primary factor. The most significant contributor to market growth is increasing demand from end-use sectors such as paints and coatings, plastics, cosmetics, and paper (Grand View Research, 2024).

TiO_2 NPs are inorganic materials with a diameter of 1–100 nm and are among the top five nanoparticles used in consumer products. TiO_2 NPs are currently widely used in various industries, including paints (48%), plastics (19%), resin (10%), papermaking (8%), fibre (3%), rubber (2%), and others (medicine, food, and cosmetics; 10%) (Baranowska-Wójcik et al., 2022).

TiO_2 does not occur in a pure, food-safe white form in nature, so it is extracted and refined from titanium-bearing ores. Primary source is ilmenite ($FeTiO_3$), the most common and widespread ore. Rutile, which is nearly pure TiO_2, is abundant in beach sands. Other sources include titanium slag, leucoxene (altered ilmenite), and minor natural anatase (Sampath et al., 2023; Christie & Brathwaite., 1998).

Food-grade TiO_2 is produced through two primary industrial routes: the sulfate process and the chloride process. The sulfate process begins with lower-grade ores such as ilmenite, which is digested in concentrated sulfuric acid to form a titanyl sulfate solution. This solution is purified, then hydrolysed with water or steam to precipitate hydrated titanium dioxide (metatitanic acid). The precipitate is filtered, washed thoroughly, and calcined at high temperatures (900–1000°C) to form the final TiO_2 crystals, most often in the anatase form that is preferred for many food applications. In comparison, in the chloride process, the ore is reacted with chlorine gas and carbon at very high temperatures to produce titanium tetrachloride ($TiCl_4$) vapor. This vapor is carefully distilled for purification and then oxidised with oxygen to yield TiO_2, typically in the rutile crystal form (Maldybayev et al., 2024; Gázquez, 2014). After the base TiO_2 is synthesised by either process, it undergoes additional steps to convert it into food-grade material. The calcined powder is finely ground to achieve the desired particle size distribution, usually averaging 200–300 nm with some nanoparticles present. It is then extensively washed and filtered to remove residual acids, sulfates, iron, and heavy metals such as lead and arsenic until the purity reaches at least 99% TiO_2. The material is rigorously tested in batches for compliance

with food additive specifications, including limits on contaminants, acid-soluble substances, and microbial safety. Only material that meets these strict purity and safety criteria is certified and packaged as food-grade TiO_2 (E171) (McNulty, 2007; Briñas et al., 2024; Warheit, 2024).

2.3 Route of entry and absorption of TiO_2 NPs

Ti is present in the human body at trace levels, ranging from 10–20 mg, making it the 14th most abundant element (Buettner & Valentine, 2012). Despite its abundance and bioactivity (its ability to interact favourably with biological tissues), Ti has not been demonstrated to be essential for human health. There are no known biomolecules or physiological processes that depend on Ti for their function, metabolism, or completion of biological pathways. Interestingly, some organisms have been observed to sequester Ti preferentially, suggesting a potential biological role; however, its essentiality remains unconfirmed (Buettner & Valentine, 2012; Merian et al., 2004).

TiO_2 NPs can enter the body via oral ingestion, intravenous administration, dermal exposure, medical implantation, and intranasal or intratracheal inhalation (Coelho et al., 2016; EFSA, 2019; Gilbert et al., 2021; Hamilton, 2013; Jacobs et al., 1991; Keller et al., 1995; Lima et al., 2004; Patri et al., 2009; Praphawatvet et al., 2020; Sul, 2010; Yang et al., 2008; Zierden & Valentine, 2015). However, human exposure to TiO_2 primarily occurs through dietary intake, mainly from products that contain E171 as a food additive. Animal studies have shown that orally administered TiO_2 NPs are preferentially absorbed in the small intestine, enter circulation, and accumulate in the liver, pancreas, spleen, kidneys, and even the brain (Younes et al., 2021). The routes of entry, absorption, accumulation, and elimination of TiO_2 NPs are shown in **Figure 2.1**.

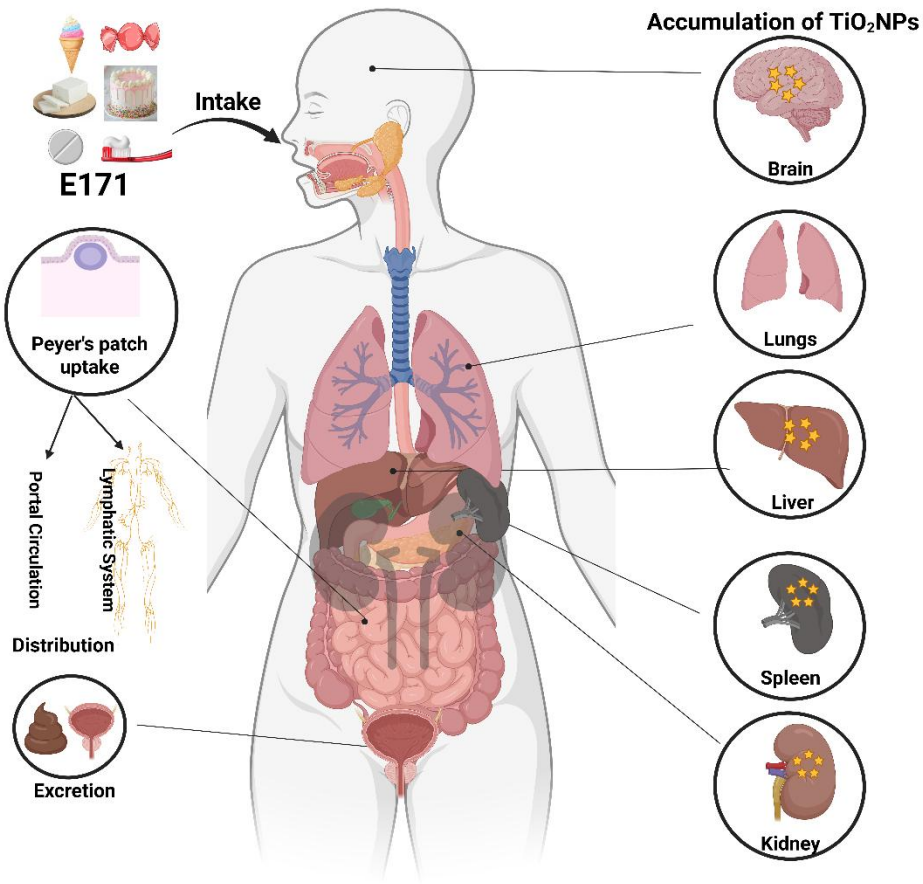

Figure 2.1 Routes of entry, absorption, distribution, accumulation, and excretion of TiO_2 NPs.
TiO_2 NPs can enter the human body through several exposure routes, with oral ingestion being the most common due to their widespread use in food additives, pharmaceuticals, and personal care products. Upon ingestion, food components and TiO_2 NPs are separated in the stomach, and a small percentage of particles are taken up by the small intestine, from which they enter the bloodstream. These particles then accumulate in different organs, including the brain, lungs, liver, spleen, and kidneys. Despite their limited absorption, the body attempts to eliminate TiO_2 NPs through faecal excretion, which remains the primary route for unabsorbed particles. Figure created with BioRender.

2.3.1 Oral route

The mechanism by which orally ingested TiO_2 NPs enter systemic circulation remains to be fully elucidated. However, human studies suggest small particles of TiO_2 NPs are more readily absorbed through the gastrointestinal (GI) tract, with peak blood Ti levels occurring 8–12 hours post-ingestion (Bockmann et al., 2000). Similarly, Pele et al. (2015) assessed blood Ti concentrations in seven volunteers and peak absorption reached approximately 10 µg/L at 6–8 hours post-ingestion, consistent with earlier findings. Studies on E171 indicate low oral systemic bioavailability (proportion of TiO_2 particles from E171 that enter the bloodstream and become available to organs and tissues after oral ingestion), i.e., less than 0.5% in mice and likely under 1% in rats, despite detectable levels in blood and tissues (Younes et al., 2021).

Ingested TiO_2 NPs can accumulate in the major organs like the liver, kidneys, spleen, and lung tissues, causing toxicity, while the unabsorbed fraction is defaecated (Kreyling et al., 2017). The absorption, potential toxicity, and properties of NPs are influenced by their presence in the GI tract. Studies on rodents and human volunteers indicate that once TiO_2 passes the intestinal barrier, it reaches the bloodstream and is then transported to different organs, including the liver, brain, spleen, and kidneys (Medina-Reyes et al., 2020; Pele et al., 2015; Ropers et al., 2017). In rodents, a range of effects have been reported following TiO_2 NPs administration, including stomach and intestinal inflammation (Talamini et al., 2019), liver cell necrosis, progression of colon tumours, lesions to cardiovascular tissue, nephrotoxicity (Wang et al., 2007), as well as the enhancement of anxiety disorders (Medina-Reyes et al., 2020; Urrutia-Ortega et al., 2016).

Although the exact pathways of TiO_2 particle absorption in humans remain poorly understood, a limited number of *ex vivo* and *in vivo* studies have offered some insight. A Porcine buccal model was used to investigate the absorption of 28, 36, and 148 nm TiO_2 particles. Interestingly, all the particles crossed the mucosal layer and penetrated the oral epithelium, but smaller NPs displayed deeper penetration, indicating a size-dependent effect (Teubl et al., 2015a). TiO_2 NPs can be effectively absorbed, internalised, and stored by Caco-2 cell monolayers (a human epithelial cell line) and tend to aggregate or agglomerate in the cytosol, with or without being enveloped in cytoplasmic vesicles. Additionally, differentiated Caco-2 cell monolayers have been shown to internalise TiO_2 NPs within 4 hours of exposure by the process of transcellular absorption (Pedata et al., 2019). Translocation into lymphatic and blood circulation can lead to the deposition of TiO_2 NPs within tissues and organs after ingestion, as demonstrated in a rat model (Geraets et al., 2014).

2.3.2 Intravenous route

Intravenous (IV) administration of TiO_2 NPs has been commonly used in research to study biodistribution, toxicity, and therapeutic potential. After IV administration, a high burden of TiO_2 particles was observed in the liver and spleen of rats (Fabian et al., 2008; Geraets et al., 2014; Xie et al., 2011). Moreover, at six hours post-IV administration, TiO_2 was predominantly localised in the liver (94%), with smaller amounts in the spleen (2.0%), lung (0.17%), kidney (0.023%), heart (0.014%), and blood (0.026%). After 30 days, levels in the liver and spleen remained stable, while those in the lung, kidney, and blood declined slightly but significantly (Shinohara et al., 2014). Single and repeated IV exposure of TiO_2 in rat models resulted in rapid distribution of Ti to all major organs, with the liver being the primary site of accumulation, followed by spleen and lungs. At 24 hours post-exposure, total recovery of Ti ranged from 64–95% in males and 59–108% in females, indicating substantial systemic distribution and excretion. Over 90 days, Ti levels declined slightly up to 26%, suggesting gradual clearance or redistribution from tissues (Geraets et al., 2014).

2.3.3 Dermal route

The skin serves as a physical barrier that actively prevents the entry of foreign particles into the body. A variety of products, such as sunscreens and cosmetics, contain TiO_2 NPs, and our skin is regularly exposed to them. However, our skin has a tough outer layer of stratum corneum, which prevents inorganic particles from entering the body (Pflücker et al., 2001). However, physical disruption to the skin can disturb the barrier function of the stratum corneum; hence, *in vitro* or *in vivo* studies usually investigate TiO_2 NPs penetration in both stripped skin (mimics an injured skin) and intact skin (H. Shi et al., 2013). Several studies have reported that TiO_2 does not penetrate the skin beyond the epidermis, regardless of the particle size of TiO_2 (Crosera et al., 2015; Schulz et al., 2002; Shi et al., 2013). In a murine model, 60 days of exposure resulted in complete dermal penetration and tissue accumulation of TiO_2 NPs. Histopathological analysis revealed marked alterations in both hepatic and dermal tissues, predominantly attributed to dysregulated oxidative stress (Wu et al., 2009).

2.3.4 Respiratory route

TiO_2 NPs can enter the human body through respiratory exposure, especially in industrial environments where TiO_2 is used in pigments, coatings, or nanomaterials (Shi et al., 2013). Most inhaled TiO_2 NPs are deposited in the upper airways, where coughing and mucociliary mechanisms effectively clear them. A fraction of smaller particles can reach the alveolar regions (Dreno et al., 2019). There, alveolar macrophages play a key role in engulfing and removing these particles. However, some nanoparticles may evade clearance, cross the alveolar epithelium, and enter the pulmonary capillaries, allowing for limited systemic distribution (Dar et al., 2020; Dreno et al., 2019; Kreyling et al., 2002). Importantly, lung pathologies associated with TiO_2 exposure, such as inflammation, oxidative stress, and tissue damage, are primarily driven by local interactions within the respiratory tract. These effects do not require the particles to enter the bloodstream. Instead, they result from direct cellular responses to particle deposition, including the activation of immune cells, the release of ROS, and the disruption of epithelial integrity (Shi et al., 2013). Rodent studies demonstrate that inhalation of TiO_2 can lead to the development of lung pathologies including lung tumours (Baan et al., 2006), lung inflammation (Bermudez et al., 2002), breakdown of alveolar membranes as a result of the body's immune response (Chen et al., 2006), as well as lung tissue scarring (Ma et al., 2019). Inhalation of anatase TiO_2 NPs is more toxic than the rutile forms (Schaudien et al., 2025; Warheit et al., 2003; Warheit & Brown, 2019; Warheit et al., 2007). However, an inhalation concentration of up to 35 mg/m^3 was found to be safe for the lungs and does not cause chronic pulmonary overload (Christensen et al., 2011; Rashid et al., 2021).

Following exposure through inhalation, ingestion, or other routes (mentioned above), TiO_2 nanoparticles are absorbed into systemic circulation and subsequently internalised by cells.

2.3.5 Reported cellular uptake mechanisms

In vitro studies have shown that cellular uptake of TiO_2 nanoparticles primarily occurs through endocytic pathways, with variations depending on NP properties, cell type, and exposure conditions (Bhattacharya et al., 2009; Di et al., 2017; Lankoff et al., 2012). In most cell types, the main mechanisms involve clathrin-mediated endocytosis, caveolae-mediated endocytosis, macropinocytosis, and phagocytosis. However, these processes are influenced by nanoparticle characteristics such as primary size (often 10–100 nm for efficient uptake), shape, surface charge, coating, and agglomeration state in biological media, as well as the formation of a protein corona that alters how cells recognise and internalise the particles (Lammel et al., 2019; Behzadi et al., 2017).). Brandão et al. (2020) reported concentration and time-dependent uptake of 25 nm TiO_2 nanoparticles in HepG2 cells, confirmed by flow cytometry, and attributed internalisation to endocytosis. Another study on the fish liver cells (RTL-W1) reported that TiO_2 nanoparticles are mainly internalised via caveolae-mediated endocytosis (Lammel et al., 2019). Overall, these studies demonstrate that TiO_2 nanoparticles are efficiently internalised by human liver cell lines, primarily through active endocytic mechanisms.

2.4 Accumulation and biodistribution of TiO_2 NPs

Oral ingestion or inhalation of TiO_2 NPs leads to accumulation in the GI tract, lungs, heart and cardiac muscle, kidneys, spleen, and the liver. Moreover, it has been reported that prolonged exposure of TiO_2 NPs disturbs the homeostasis of lipids and glucose in rats and mice (Faddah et al., 2013; Liu et al., 2010; Song et al., 2016). Oral administration (single dose) of different-sized TiO_2 NPs in mice demonstrated that smaller NPs (25 nm) accumulate mainly in the spleen and smaller amounts in the lungs and kidneys; alternatively, larger NPs (80 nm) accumulate in the liver (Wang et al., 2007). Ma et al. (2009) reported that intraperitoneal injection of TiO_2 anatase nanoparticles in mice, administered daily over 14 days, led to tissue-specific accumulation of the nanoparticles. The distribution indicated that the liver was the primary site of TiO_2 NPs deposition.

TiO_2 particles are subsequently distributed to various organs in order of decreasing concentration: mesenteric lymph nodes, liver, spleen, kidney, lungs, heart, and reproductive organs. Post-mortem analysis of 15 human samples revealed that the spleen and liver are primary sites of food-grade TiO_2 bioaccumulation (Heringa et al., 2018). Sequential blood levels of Ti in six volunteers after the ingestion of 23–45 mg of TiO_2 in the form of gelatine capsules were investigated, and they observed that smaller particles had greater absorption with a 5–10-fold increase above baseline in blood Ti levels, peaking

at 8–12 h post ingestion (Bockmann et al., 2000). Similarly, in seven volunteers who ingested 100 mg of food-grade TiO_2, blood concentrations were measurable and showed correlated patterns, with a peak of only 10 µg/L occurring 6–8 hours after ingestion, consistent with previous findings (Pele et al., 2015).

Previously, it was indicated in a study that the primary elimination route of TiO_2 was through faeces, indicating minimal GI absorption (Cho et al., 2013). However, in a separate study involving orally dosed rats, elimination of the absorbed TiO_2 was found to be very slow, with only small amounts excreted over 90 days, suggesting potential for tissue accumulation over time (Cho et al., 2013; Geraets et al., 2014).

2.5 Biological half-life of TiO_2 NPs

In rats, when TiO_2 NPs (25 or 75 nm) enter the circulation, they deposit in the liver and spleen, where they exhibit a biological half-life of more than 30 days, resulting in a high risk of bioaccumulation given the chronic daily exposure (Kreyling et al., 2017; Martins et al., 2017; Shinohara et al., 2014). Moreover, the half-lives of absorbed TiO_2 particles were estimated to be 200–450 days (Younes et al., 2021). According to the EFSA panel on food Additives and Nutrient Sources (ANS Panel), after IV administration, TiO_2 NPs exhibit slow clearance from body tissues. This slow elimination raised concerns about the potential for accumulation in organs, as the calculated half-lives varied significantly, ranging from 28 to 650 days depending on the specific organ involved; however, minimal data is available on TiO_2 in human studies (Additives & Food, 2016).

Available human data suggest that the biological half-life of Ti following TiO_2 exposure may exceed 320 days, while in mice, estimates reach up to 640 days (Ramoju et al., 2020). In orally dosed rat models, elimination was notably slow, with only minimal excretion observed over 90 days (Cho et al., 2013; Geraets et al., 2014). Despite limited systemic absorption, it is well established that the majority of ingested TiO_2 is excreted via faeces, indicating low GI uptake (Cho et al., 2013).

2.6 Toxicity of TiO_2 NPs

Toxicity studies (*in vivo*) have shown that inhalation of TiO_2 NPs caused lung inflammation and a dose-dependent increase in bronchoalveolar lavage fluid (BALF) total cell and neutrophil counts, total protein content, enzyme activities, and alveolar macrophages in rats and mice (Grassian et al., 2007; Ma et al., 2009). Furthermore, *in vitro* studies reviewed by Wang et al. (2015) have shown that TiO_2 NPs induce oxidative stress and apoptosis in the human alveolar basal epithelial adenocarcinoma (A549) cell line.

Both *in vitro* and *in vivo* studies have identified toxic effects of TiO_2 NPs, including alterations in the cell cycle, nuclear membrane constriction, and apoptosis (Acar et al., 2015; Coccini et al., 2015; Hu et

al., 2011; Valdiglesias et al., 2013). Additionally, TiO_2 NPs have been reported to generate ROS, induce single-strand breaks and oxidative lesions in DNA, and damage cellular components, including DNA, proteins, and lipids. Furthermore, they interact with the epithelial layer of the small intestine, compromising tight junction integrity and increasing intestinal permeability, suggesting interference with the nutrient absorption process (Jugan et al., 2012; Petković et al., 2011).

2.7 Mechanisms of TiO_2 NPs toxicity in the liver

The liver is the most important organ for the detoxification of toxins and xenobiotics. Regardless of the route of administration, TiO_2 NPs accumulate in the liver and pose a risk of toxicity depending on dose, exposure duration, and particle characteristics (Cui et al., 2010; Cui et al., 2011; Gilbert et al., 2021; Hassanein & El-Amir, 2018; Jia et al., 2017; Nie et al., 2021; Shirdare et al., 2022; Suker & Jasim, 2018; Wang et al., 2013). The reported mechanisms by which TiO_2 NPs cause toxicity in the liver include the generation of ROS (Jia et al., 2017; Shrivastava et al., 2014), oxidative stress (Chen et al., 2019; Chen et al., 2020; Wang et al., 2014), inflammation (Abbasi-Oshaghi et al., 2019; Hong et al., 2020), steatosis, histopathological changes (fibrosis, and damaged lobular structure) (Azim et al., 2015; Cui et al., 2011; Talamini et al., 2019; Wang et al., 2007; Wang et al., 2013; Zhao et al., 2021), DNA damage, necrosis, apoptosis, and cell death (Cui et al., 2010; Jia et al., 2017; Orazizadeh et al., 2020; Sallam et al., 2022a). *In vitro* studies on cultured human and rat liver cells have also shown cytotoxic effects of TiO_2 NPs (Sha et al., 2011). Similarly, TiO_2 NPs induced alterations in cell viability, increased ROS levels, decreased glutathione (GSH) levels, and distorted cellular morphology in a human hepatocarcinoma cell line (HepG2 cells) (Abbasi-Oshaghi et al., 2019). In addition, cell growth inhibition, increased apoptosis, cell cycle arrest at the G1 stage, and induction of ROS-mediated ER stress via activation of the Protein kinase R-like endoplasmic reticulum kinase/activating transcription factor 6/ Bcl-2–associated X protein (PERK/ATF6/Bax) axis were observed in HepG2 cells (Li et al., 2020).

Appendices 2.1 and **2.2** provide details of all *in vivo* and *in vitro* studies reporting the pathological effects of TiO_2 NPs in the liver to date. **Figure 2.2** shows an overview of key hepatotoxic processes induced by TiO_2 NPs.

2.7.1 Biochemical parameters and histopathological changes in the liver

Biochemical parameters such as alanine aminotransferase (ALT), aspartate aminotransferase (AST), lactate dehydrogenase (LDH), and alkaline phosphatase (ALP) serve as indicators of liver function and cellular integrity (Lala et al., 2023). Oral administration of TiO_2 NPs has been shown to increase the serum levels of liver injury markers (ALT, AST, LDH, ALP) in rodents in a dose-dependent and statistically significant manner (for details see **Appendix 2.1**). Elevated serum levels of these enzymes indicate hepatocellular injury, which corresponds to various histopathological liver changes, including focal

degeneration of hepatocytes, spotty necrosis, hydropic degeneration, liver oedema, congestion, Kupffer cell hypertrophy, swelling, vacuolisation, nuclear membrane collapse, and overall cell death (Ali et al., 2019; Azim et al., 2015; Hassanein & El-Amir, 2017; Moradi et al., 2019; Shirdare et al., 2022; Wang et al., 2013). The mechanism of TiO_2 NPs induced liver injury is discussed in the sections below.

2.7.2 Oxidative, mitochondrial, and ER stress

Oxidative stress damages lipids, carbohydrates, proteins, and DNA in mammalian cells (Kohen & Nyska, 2002). Oxidative stress and apoptosis induced by ROS are reported as the key factors in intracellular TiO_2 NPs-induced organ injury and toxicity (Long et al., 2007). TiO_2 NPs promote the generation and accumulation of ROS and induce indirect oxidative DNA damage in cells. Excessive ROS production disrupts the balance of the liver's oxidant/antioxidant system, leading to lipid peroxidation and liver cell apoptosis (Su et al., 2019). Additionally, TiO_2 NPs have been shown to induce the formation of apoptotic bodies in mammalian cells (Dhupal et al., 2018; Shukla et al., 2013) and to modify cellular macromolecules, including proteins. These modified proteins, known as protein adducts, trigger immune surveillance mechanisms, leading to immune cell infiltration and hepatic inflammation by activating stress and inflammatory signalling pathways (Conde de la Rosa et al., 2022). Transmission electron microscopy (TEM) studies have confirmed that TiO_2 NPs enter cells via the cell membrane and induce oxidative stress by disrupting the balance between oxidants and antioxidants. Moreover, TiO_2 NPs interact with organelles like mitochondria, the ER, and the Golgi apparatus. Mitochondrial disruption impairs electron transport and adenosine triphosphate (ATP) synthesis, leading to increased ROS production and ER stress, which interferes with protein folding and calcium signalling, amplifying oxidative damage (Chen et al., 2019; Li et al., 2020).

Mitochondria are one of the main organelles affected by TiO_2 NPs, where they can either physically accumulate in mitochondria, disrupting membrane integrity and ATP synthesis (Barkhade et al., 2021; Chen et al., 2018) or induce mitochondrial dysfunction indirectly via ROS generation and oxidative signalling pathways (Chen et al., 2019; Li et al., 2020). TiO_2 NPs cause morphological alterations by damaging mitochondrial membranes, swelling and ballooning of mitochondria, and overall decreasing the activity of mitochondria in hepatic cells (Chen et al., 2019; Jia et al., 2017; Teubl et al., 2015; Yang et al., 2017). TiO_2 NPs interfere with the activity of electron transport chain components, including mitochondrial complex I (nicotinamide adenine dinucleotide dehydrogenase) and complex II (succinate dehydrogenase). Alterations in these enzymes result in defective oxidative metabolism that can lead to mitochondrial cytopathy (Waseem et al., 2022). Also, TiO_2 NPs induced changes in these complexes may result in an aberrant mitochondrial permeability transition pore, further causing uncoupling of oxidative phosphorylation and depletion of ATP (Chen et al., 2018; Mehndiratta et al., 2002; Waseem et al., 2022).

The ER controls the accurate folding of proteins. Accumulation of misfolded proteins in the ER causes ER stress, which activates an unfolded protein response (UPR). The UPR either maintains homeostasis or triggers cell death to inhibit the accumulation of damaged cells (Cao et al., 2017). The UPR has three signal transducers: protein kinase RNA-like ER kinase; inositol-requiring enzyme 1 alpha/beta (IRE1α/β); and activating transcription factor 6 (ATF6). During ER stress, PERK (ER-resident protein) mediates signal transduction and, together with ATF6 and IRE1, triggers either ROS-ER stress-mediated apoptosis or autophagy (Li et al., 2022; Liu et al., 2015).

Nanoparticle-induced ER stress is an early biomarker for evaluating nanotoxicity. TiO_2 NPs increase the expression of PERK, Bax, and ATF6 in HepG2 cell lines. TiO_2 NPs induce ER stress, activating PERK/ATF6 signalling pathways, and contributing to the TiO_2-mediated apoptosis in HepG2 cells (Bischoff et al., 2021; Hu et al., 2020; Li et al., 2020). The PERK–eIF2α–ATF4 pathway up-regulates the UPR target genes and induces the folding and excretion of proapoptotic protein C/EBP homologous protein (CHOP), which regulates both lipogenesis and hepatic steatosis (Hernández-Gea et al., 2013; Hu et al., 2020; Li et al., 2020). Thus, TiO_2 NPs can induce ER stress in liver cells; however, further studies are needed to elucidate their role in mediating ER stress, apoptosis, and autophagy in these cells.

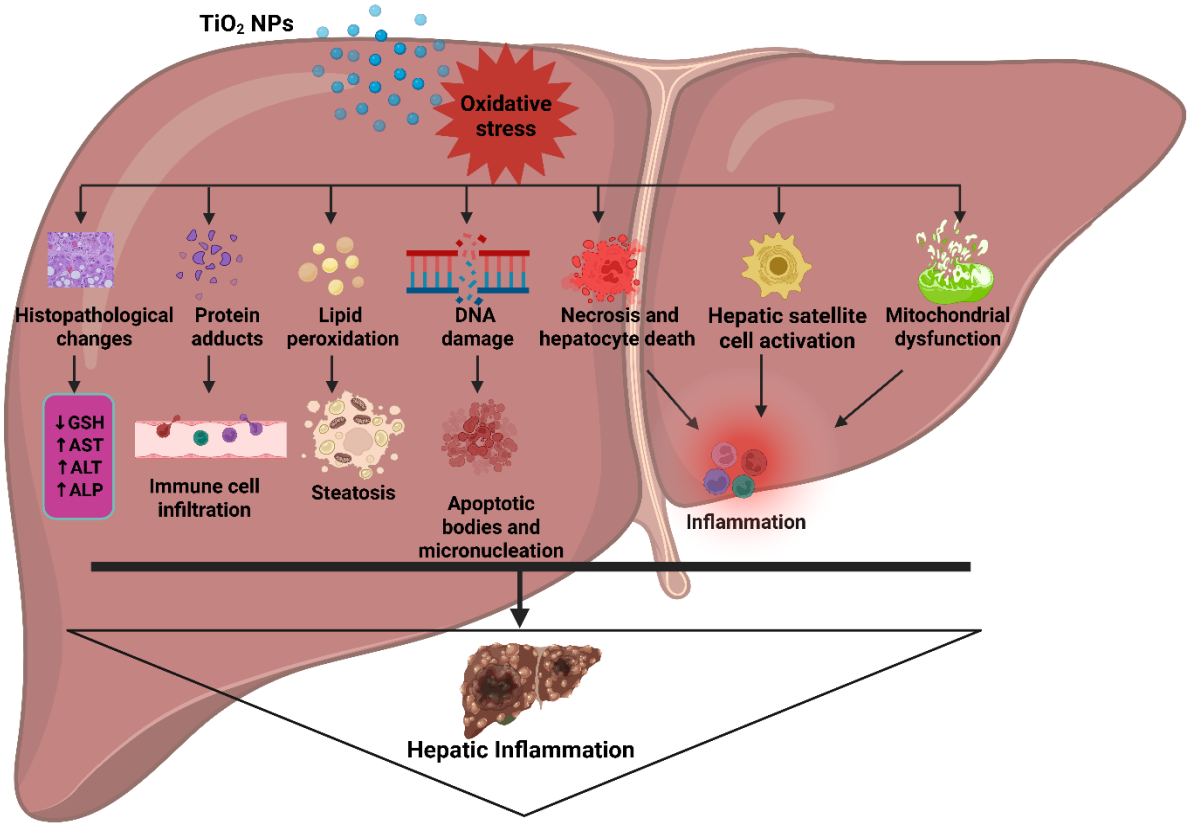

Figure 2.2 TiO_2 NP-induced oxidative stress triggers inflammation.
TiO_2 NPs induce oxidative stress and cause hepatic inflammation by changing the histopathology of the liver, generating protein adducts, lipid peroxidation, necrosis, hepatocyte death, mitochondrial dysfunction, and DNA

damage. **Abbreviations:** AST aspartate transaminase; ALT alanine transaminase; ALP alkaline phosphatase; GSH Glutathione.

2.7.3 Apoptosis, necrosis, and inflammation

Oral administration of TiO_2 NPs has been shown to induce chromatin condensation, nuclear fragmentation, and apoptosis i*n vitro* (Cui et al., 2010; Zhu et al., 2012). TiO_2 NPs increase the expression of pro-apoptotic genes, including p53, Bax, Cyto-c, Apaf-1, caspase-9, and caspase-3, and reduce the expression of anti-apoptotic gene B-cell lymphoma 2 (Bcl-2), indicating that TiO_2 NPs can mediate apoptosis via the caspase-dependent signalling pathway. This pathway has been demonstrated *in vitro* in HepG2 cells (Shukla et al., 2013) and *in vivo,* in rat liver (Abbasi-Oshaghi et al., 2019). Studies using immunoblot analysis in both tissue samples and *in vitro* cell models demonstrated that TiO_2 NPs activate the intrinsic pathway of apoptosis by increasing the expression of pro-apoptotic proteins and decreasing the levels of anti-apoptotic protein (Sallam et al., 2022b; Sallam et al., 2022a; Shukla et al., 2014). TEM studies of liver cells of mice have shown that TiO_2 NPs cause the breakdown of nucleolus, dispersed chromatin, apoptosis, and apoptotic cell bodies (Jia et al., 2017). This shows that TiO_2 NPs can induce liver apoptosis and structural damage.

Another study reported that TiO_2 NPs increase pro-apoptotic factors (Bax, caspase-3, and p53) and decrease Bcl-2 in the rat liver (Abbasi-Oshaghi et al., 2019). The caspases and Bcl-2 proteins are the main regulators of the apoptotic pathway. Translocation of Bax into mitochondria alters the permeability of cytochrome C and further stimulates post-mitochondrial caspases that lead to apoptotic cell death (Wang et al., 2014). Necrosis is one of the primary features of liver injury and upregulates the expression of apoptotic genes (p53, p38, TNF-α, caspase-3, caspase-8, caspase-9). This suggests the role of TiO_2 NPs in causing cell necrosis through ROS (Abbasi-Oshaghi et al., 2019; Moradi et al., 2019; Morgan et al., 2018; Sallam et al., 2022b).

TiO_2 NPs activate mitogen-activated protein kinase (MAPK) and nuclear factor kappa B (NF-κB) inflammatory signalling cascades, leading to transient liver inflammation due to increased levels of pro-inflammatory cytokine tumour necrosis factor α (TNF-α), decreased expression of NF-κB inhibitor A20 (anti-inflammatory gene), and reduced cell viability *in vitro* (Chen et al., 2016). In addition, oral administration of TiO_2 NPs in rats causes infiltration of white blood cells, inflammation, Kupffer cell enlargement, sinusoidal dilation with the accumulation of inflammatory cells, and hepatocyte necrosis (Shirdare et al., 2022). Abbasi-Oshaghi et al. (2019) have reported that TiO_2 NPs induce inflammatory responses by increasing the expression of TNF-α (a pro-inflammatory cytokine) and inducible nitric oxide synthase (iNOS) (primary source of ROS) levels dose-dependently in the rat liver. Zhao et al. (2021) have shown that high-dose oral administration of TiO_2 NPs causes severe oxidative stress, hepatic inflammation, fibrosis, and apoptosis in the liver of mice, and these effects were exacerbated

with fructose-induced metabolic syndrome. These results suggest that some populations, such as those with metabolic syndrome, may be more at risk of adverse health outcomes associated with TiO_2 NPs.

Overall, these studies suggest that TiO_2 NPs may induce necrosis, apoptosis, inflammation, and other liver impairments via ROS generation, DNA damage, ER stress, and mitochondrial stress (Mohammadinejad et al., 2019). The proposed molecular mechanisms by which TiO_2 NPs induce apoptosis, necrosis, and inflammation are summarised in **Figures 2.2** and **2.3**. However, the role of TiO_2 NPs in molecular signalling pathways that regulate autophagy in liver cells remains elusive.

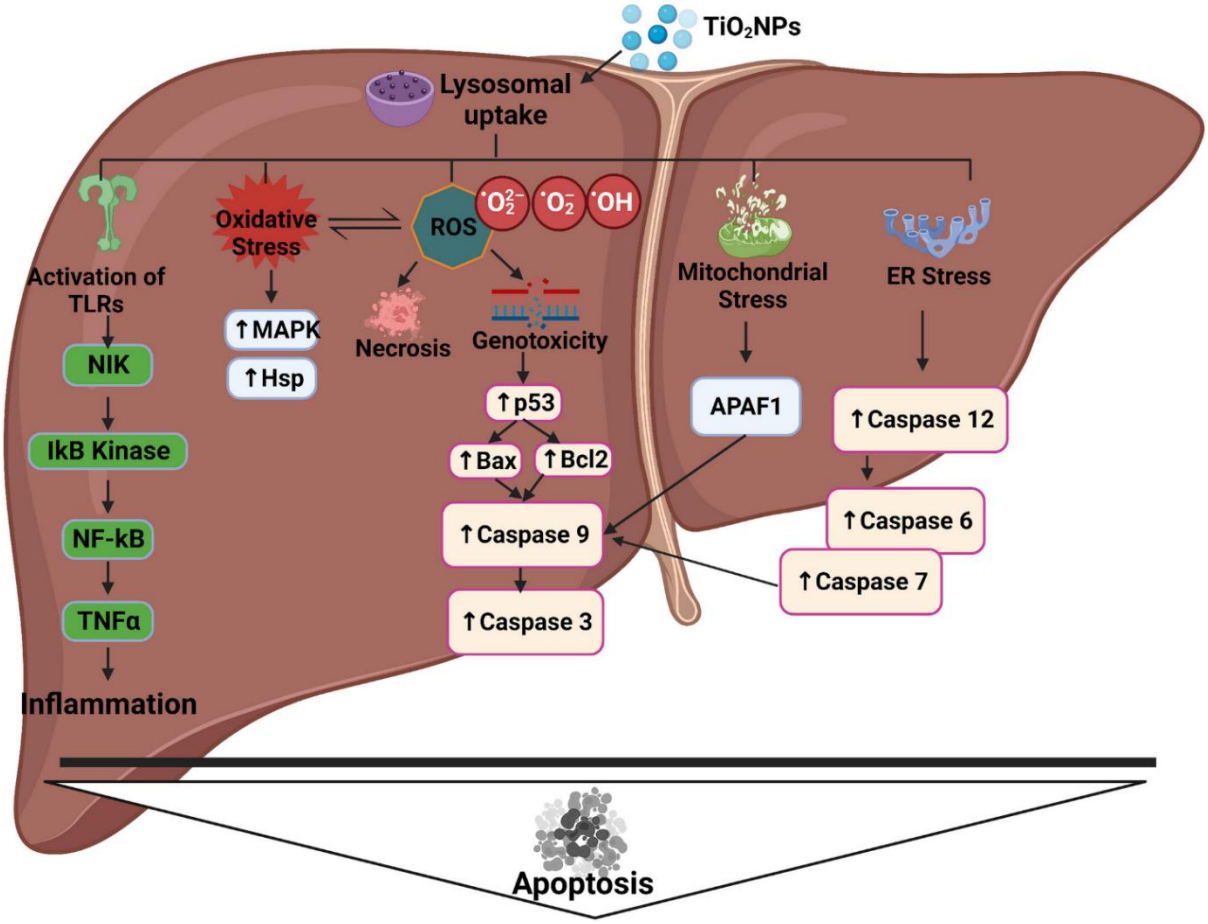

Figure 2.3 Proposed mechanisms of hepatotoxicity induced by TiO_2 NPs.
In the liver, TiO_2 NPs activate Toll-like receptors (TLRs) and enhance NF-κB-inducible kinase (NIK), leading to a nuclear factor-kappa B (NF-κB) response and cellular inflammation. TiO_2 NPs induce oxidative stress, generate ROS species, and increase the expression of stress protein Hsp (heat shock protein) and activate the MAPK (mitogen-activated protein kinases) signalling pathway. TiO_2 NPs increase p53 expression, which in turn increases Bax and Bcl2 expression, thereby increasing caspases 3 and 9 expression and leading to apoptosis. TiO_2 NPs can also induce mitochondrial and ER stress, mediated by apoptotic protease-activating factor 1 (APAF1) and caspases (12, 6, and 7). Figure created with BioRender. **Abbreviations:** APAF1 Apoptotic protease activating factor-1; Bax Bcl-2-associated X; Bcl2 B-cell lymphoma 2; IKB inhibitory subunit κB; Hsp Heat shock protein; MAPK mitogen-activated protein kinase; NIK nuclear factor κB-inducing kinase; NF-κB nuclear factor-kappa B; NPs: Nanoparticles; TLRs toll-like receptors; TNFα Tumor necrosis factor-alpha.

2.7.4 Genotoxicity

Genotoxicity is defined as the ability of biological or chemical agents to damage the genetic information in the cells, triggering genomic instability and mutations, and probably causing various diseases, including cancer (Phillips & Arlt, 2009). Oral exposure of TiO_2 NPs in mice and rats causes DNA damage, increases the expression of pro-apoptotic proteins (Bax), p53, and decreases the expression of anti-apoptotic proteins (Bcl-2), leading to apoptosis and distorted liver function (Abdel-Wahhab et al., 2021a; Orazizadeh et al., 2020; Sallam et al., 2022a; Shukla et al., 2014). Fatma et al. (2021) have shown that TiO_2 NPs induce structural and numerical chromosomal aberrations in lymphocytes. *In vivo* studies have confirmed that TiO_2 NPs cause chromosomal aberrations, DNA breaks, and can induce genotoxicity in liver, spleen, and thymus cells (Ali et al., 2019; Chakrabarti et al., 2019; Manivannan et al., 2020).

2.8 Metabolic dysfunction-associated steatotic liver disease (MASLD)

MASLD, formerly known as Non-alcoholic Fatty Liver Disease (NAFLD) is a liver pathology that corresponds to the accumulation of fat (triglycerides) (≥5%) in the liver (steatosis) in the absence of secondary causes of steatosis, such as significant alcohol consumption, viral hepatitis, other chronic liver and hereditary disorders (Chalasani et al., 2012; Marjot et al., 2020). MASLD encompasses a wide range of histological abnormalities and develops in four main stages. Firstly, fatty liver (steatosis), which is fat accumulation in liver cells and is usually diagnosed during tests carried out for other reasons. Second, metabolic-associated steatohepatitis (MASH, formerly non-alcoholic steatohepatitis, NASH) is a more serious form of MASLD in which the steatosis is accompanied by inflammation. Third, fibrosis: insistent inflammation that results in the formation of scar tissue around the liver; however, the liver is still working normally. Finally, MASH cirrhosis, which is the most severe stage, is characterised by the liver becoming shrunken, scarred, and lumpy with permanent damage that can lead to liver failure and MASH-related hepatocellular carcinoma (HCC) (**Figure 2.4**) (Loomba & Chalasani, 2015; Loomba et al., 2015).

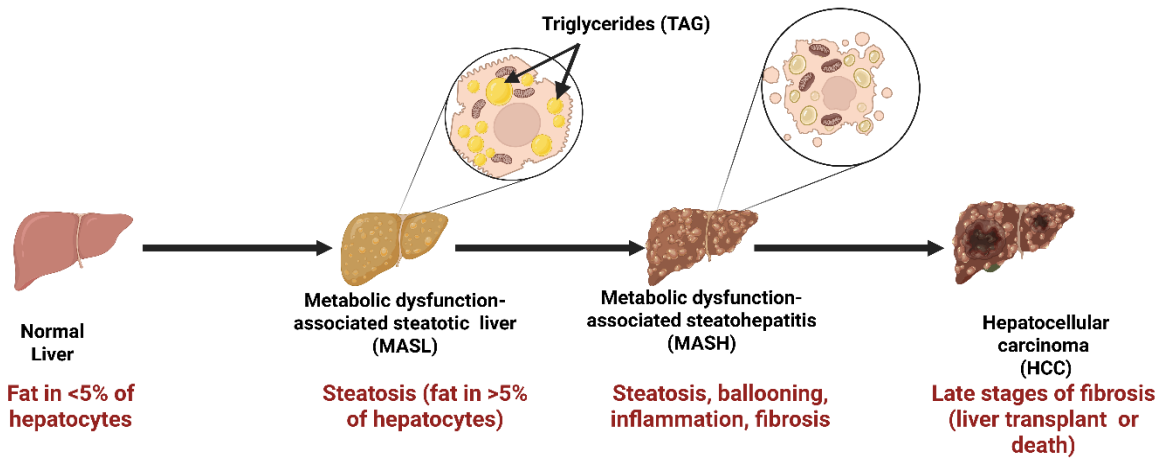

Figure 2.4 Progression of MASLD.
The development of MASLD is divided into four stages: simple steatosis (MAFL), metabolic-associated steatohepatitis (MASH), liver cirrhosis, and, eventually, hepatocellular carcinoma (HCC). Figure created with BioRender.

2.8.1 Global epidemiology of MASLD

Both the incidence and prevalence of MASLD are rising rapidly worldwide. MASLD is the most common cause of chronic liver disease, with an estimated global prevalence of 38% in 2022 (Koliaki et al., 2025; Riazi et al., 2022; Younossi et al., 2023). MASLD was one of the major causes of cirrhosis and malignancy-related mortality in NZ (Hsiang et al., 2015), with national data indicating a notable rise in liver cancer deaths peaking around 2019. According to Hsiang et al. (2015), the incidence of liver transplantation for MASLD has increased substantially, making it the third most common indication for chronic liver disease requiring transplantation. This trend is mirrored in the rising cases of HCC associated with MASLD, reflecting broader public health challenges linked to obesity, insulin resistance, and metabolic syndrome across Australasia (Howell et al., 2022; Zhou et al., 2025).

2.8.2 Risk factors for MASLD

MASLD has multiple risk factors, among which obesity and type 2 diabetes mellitus (T2DM) are the most dominant risk factors (Wang et al., 2025). Obesity is a major global health problem, and it is anticipated that by 2030, more than 1 billion adults will be obese worldwide (Lobstein et al., 2022). According to the NZ Health Survey (2023/24), approximately one in three adults was obese (34.2% or nearly 1.5 million). In NZ, the prevalence of obesity varies by ethnicity: Pacific (69.5%), Māori (46.9%), European/Other (33.5%), and Asian adults (17.8%). In addition, 11.7% children (age group: 2–14 years) were graded as obese (NZ Health survey, 2025). With rising obesity, NZ has an increased risk of MASLD-linked complications leading to cirrhosis (Adams et al., 2020).

Type 2 diabetes (T2DM, non-insulin dependent or adult-onset) is a serious public health concern affecting 6.28% (462 million individuals) of the world's population (Khan et al., 2020). MASLD and T2DM are two pathological disorders that act synergistically, increasing the overall risk of adverse

hepatic and extra-hepatic effects. T2DM is an established risk factor for the faster progression of MASLD to MASH, and cirrhosis/HCC (Lonardo et al., 2019; Mantovani et al., 2020; Targher et al., 2018). Previous research has shown that a bidirectional association between MASLD and diabetes exists and that MASLD may lead to the development of diabetes (Targher et al., 2016). Recently, a meta-analysis reported that ~65% of people with T2DM have MASLD globally (Younossi et al., 2024). In NZ, 5% of the population has T2DM, and this is predicted to increase to 7% by 2040. The prevalence of diabetes is approximately 2–3 times higher in adults (age group: 25–39 years) of Māori and Pacific ethnicity compared to those of European ethnicity (Edgar & Mateparae, 2020; Ministry of Health, 2018).

2.8.3 Pathogenesis of MASLD in humans

MASLD is a multifactorial disease with multiple modifiers, including diet, lifestyle, gut microbiota, environmental factors, hormonal imbalance, and genetic/epigenetic factors that modulate the accumulation of free fatty acids (FFA) in the liver (Jiménez-González et al., 2025; Li et al., 2024; Moretti et al., 2024). One of the major factors is insulin resistance, which leads to the deposition of FFAs and increased fat accumulation in the liver. This results in lipotoxicity caused by increased oxidative stress, ER stress, misfolding of proteins, inhibition of autophagy, and mitochondrial damage within the liver cells (Mota et al., 2016; Vesković et al., 2023). ROS and RNS mediate oxidative stress and play a key role in the pathogenesis of MASLD, leading to MASH. This high production of ROS not only causes mitochondrial damage, lipid peroxidation, and low-density lipoprotein oxidation but also leads to inflammation, hepatic stellate cells activation, fibrosis, necrosis, cirrhosis, and ultimately, HCC (Clare et al., 2022; Raza et al., 2019; Spahis et al., 2017; Zhang et al., 2025).

Metabolic pathways, energy metabolism, and cell cycle control are key mechanisms that drive progression from MASLD to MASH and HCC. In hepatocytes, mitochondrial activities, including β-oxidation, electron transfer, production of ATP, and generation of ROS, regulate fat metabolism and energy homeostasis (Mao et al., 2006; Radosavljevic et al., 2024). During the initial steatosis phase of MASLD, mitochondria facilitate and split lipotoxic FFAs into stable triglycerides by storing them in fat droplets, thus preventing oxidative stress (Radosavljevic et al., 2024; Savage et al., 2006; Steinberg et al., 2025). However, a chronic high-fat/high-fructose diet causes accumulation of lipids in hepatocytes due to the accumulation of toxic metabolites and cellular metabolic reprogramming (Chakravarthy et al., 2005; Li et al., 2025; Muriel et al., 2021; Smajis et al., 2020). These variations cause lipotoxicity due to discrepancies in hepatic metabolism and excessive production of FFAs (Li et al., 2025; Li et al., 2009). ER stress is also a major contributor to liver cell injury and carcinogenesis in MASH (Magkos et al., 2010; Xu et al., 2025; Yamada et al., 2025). Overall, the crosstalk among oxidative stress, ER stress, and mitochondrial stress due to the accumulation of FFAs plays a role in the development of MASLD, MASH,

and its progression to HCC (Li et al., 2025; Radosavljevic et al., 2024; Smajis et al., 2020; Stefan et al., 2011; Yamada et al., 2025) (**Figure 2.5**).

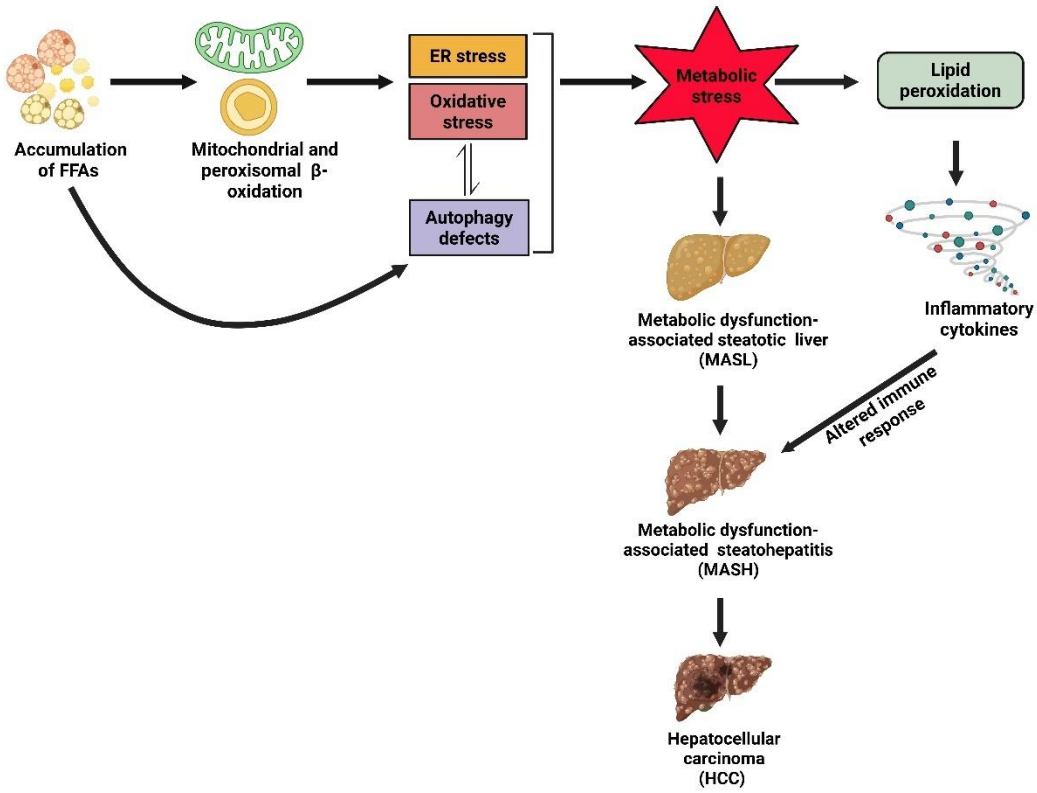

Figure 2.5 Pathogenesis of MASLD.
Factors that contribute to the pathogenesis of MASLD include dysregulated lipid metabolism, oxidative stress, ER stress, mitochondrial and peroxisomal β-oxidation, altered immune response, environmental pollutants, endocrine defects, and gut-microbiota imbalance, acting together in a genetic/epigenetic environment. Figure created with BioRender.

Lipid metabolism primarily occurs in the liver. Besides synthesising fatty acids, the liver also exports them, redistributes them to other tissues, and uses them as energy substrates (Ipsen et al., 2018; Nguyen et al., 2008). The interactions between nuclear receptors, hormones, and transcription factors maintain hepatic lipid homeostasis. Any disruption in these pathways may lead to FFA retention in the liver and the subsequent development of MASLD. Accumulation of FFA in the liver occurs due to an imbalance between the acquisition of lipids and lipid disposal, which are tightly controlled by four major pathways, including 1) uptake of circulating lipids, 2) *de novo* lipogenesis, 3) fatty acid oxidation, and 4) export of lipids in very low-density lipoproteins (VLDL) (Ipsen et al., 2018; Ma et al., 2025).

Hepatic lipid uptake is facilitated by special fatty acid transporter proteins, cluster of differentiation 36 (CD36), and caveolins (surface organelles in various animal cells) that are localised in the plasma membrane of hepatocytes (Koo, 2013; Mashek, 2013). The transport of these hydrophobic fatty acids

is then facilitated by fatty acid binding protein 1 (FABP1) to various cellular compartments within the cytoplasm. In addition to transportation, FABP1 facilitates the storage and utilisation of fatty acids and their derivatives (acyl-CoA). FABP1 protects against lipotoxicity by binding cytotoxic FFAs and promoting their oxidation or by incorporating fatty acids into triglycerides (Ipsen et al., 2018).

In the liver, *de novo* lipogenesis occurs when acetyl-CoA (originating from excess carbohydrates) is converted into new fatty acids. These newly generated fatty acids then undergo a series of steps, including desaturation, elongation, and esterification, and are finally either stored as triglycerides or exported as VLDL particles. Thus, an increase in *de novo* lipogenesis can result in hepatic steatosis and/or hypertriglyceridemia, and may also cause steatohepatitis, as saturated fatty acids, like palmitate, can cause inflammation and apoptosis (Ipsen et al., 2018; Listenberger et al., 2003).

Elevated *de novo* lipogenesis is one of the major characteristics of MASLD patients (Carli et al., 2024; Diraison et al., 2003; Donnelly et al., 2005; Lucaciu et al., 2025). Although regulation of *de novo* lipogenesis is complex, it is mainly controlled by two key transcription factors, namely, sterol regulatory element-binding protein 1c (SREBP1c) and carbohydrate regulatory element-binding protein (ChREBP). SREBP1c is activated by insulin and liver X receptor α, while ChREBP is activated by carbohydrates (Carli et al., 2024; Eberlé et al., 2004; Sanders & Griffin, 2016; Yamashita et al., 2001).

Oxidation of fatty acids primarily occurs in the mitochondria and is regulated by peroxisome proliferator-activated receptor alpha (PPARα) (Carli et al., 2024; Dikalov et al., 2024; Kersten & Stienstra, 2017; Koo, 2013; Rao & Reddy, 2001; Reddy & Hashimoto, 2001). Mitochondria, peroxisomes, and cytochromes are the main organelles that mediate the oxidation of fatty acids in mammalian cells. Entrance of fatty acids into the mitochondria is dependent on carnitine palmitoyl transferase 1 (CPT1); however, mitochondria are unable to oxidise very long-chain fatty acids. Long-chain fatty acids are then metabolized through β-oxidation in peroxisomes. In cytochromes, ω-oxidation occurs in case of lipid overload, such as in MASLD. Overall, these processes generate significant amounts of ROS, oxidative stress, and toxic dicarboxylic acids, which promote inflammation and disease progression (Begriche et al., 2013; Carli et al., 2024; Kersten & Stienstra, 2017; Nassir & Ibdah, 2014; Rao & Reddy, 2001).

Apart from fatty acid oxidation, another mechanism to reduce hepatic lipid content is to export triglycerides. Being hydrophobic, fatty acids can only be exported from the liver after being packaged into water-soluble VLDL particles together with phospholipids, cholesterol, and apolipoproteins (Fabbrini et al., 2008; Perry et al., 2014). MASLD patients have diminished export of fatty acids, resulting in more hepatic lipid content, following intracellular lipid accumulation, which leads to steatosis, lipotoxicity, liver damage, and fibrosis (Charlton et al., 2002; Fabbrini et al., 2008; Horton et

al., 1999; Nagaya et al., 2010; Nakamuta et al., 2009). These four major pathways, which, when disrupted, cause the accumulation of fats in hepatocytes, have been summarised in **Figure 2.6**.

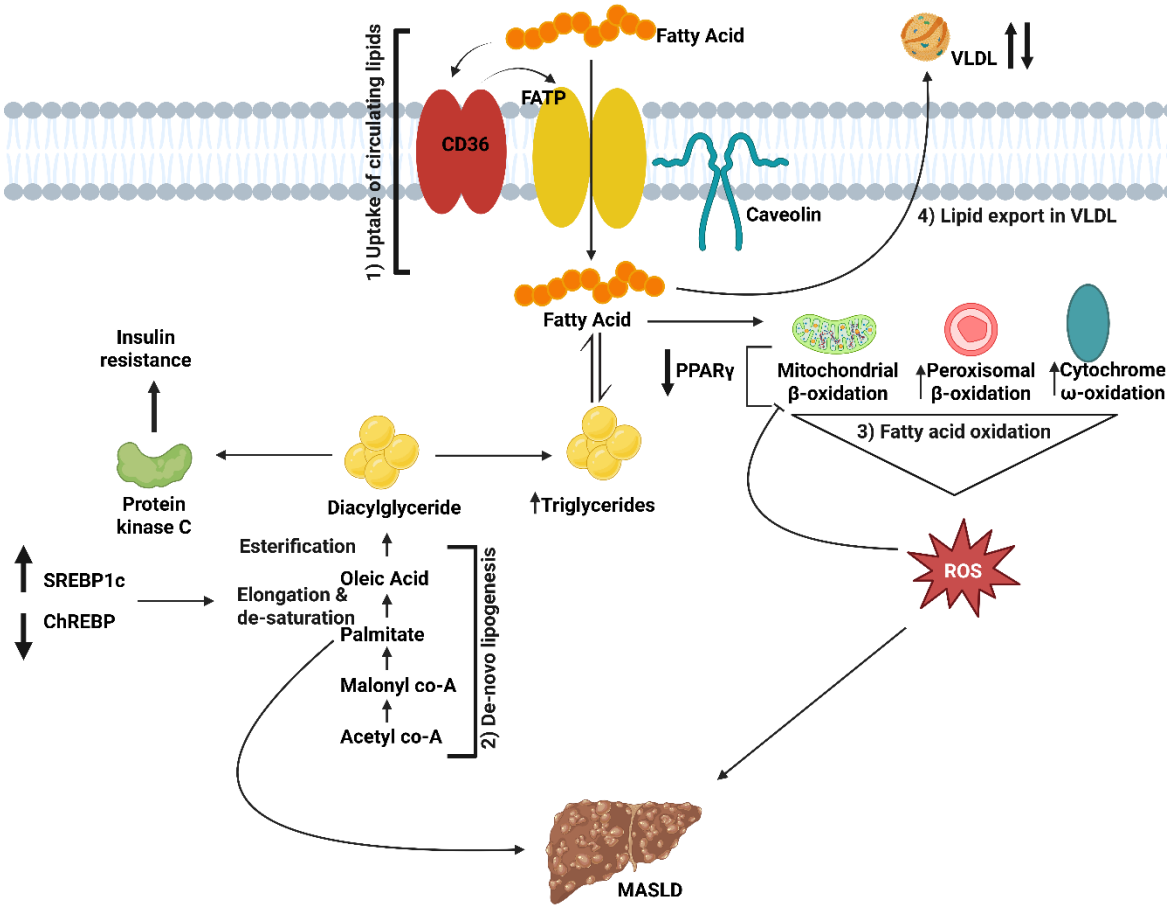

Figure 2.6 Molecular mechanism of lipid accumulation in MASLD.
Accumulation of fatty acids in the liver occurs due to an imbalance between the acquisition of lipids and lipid disposal, which are tightly controlled by four major pathways, including uptake of circulating lipids; *de novo* lipogenesis; oxidation of fatty acids, and export of lipids in very low-density lipoproteins (VLDL). Figure created with BioRender. **Abbreviations:** CD 36 cluster of differentiation 36; ChREBP Carbohydrate response element (ChRE)-binding protein; FATP fatty acid transport proteins; PPARγ peroxisome proliferator-activated receptor γ; SREBP-1 Sterol Regulatory Element-binding Protein-1; VLDL Very-low-density lipoprotein.

The literature reviewed in this chapter indicates that the toxicity of TiO_2 NPs shares several pathological mechanisms with MASLD. The overlapping features, such as oxidative stress, inflammation, lipid accumulation, mitochondrial dysfunction, altered lipid metabolism, and fibrosis, highlight the liver's vulnerability to both metabolic and nanoparticle-induced toxicity. The major pathological features shared by TiO_2 NPs-induced hepatotoxicity and MASLD are summarised in **Table 2.2**.

Table 2.2 Major pathological features shared by MASLD and TiO_2 NPs-induced toxicity.

Feature	MASLD Features	TiO_2 NPs toxicity features	References
Oxidative stress	Elevated ROS leads to lipid peroxidation and cell damage.	TiO_2 NPs generate ROS, causing oxidative injury to hepatocytes.	(Jia et al., 2017; Li & Tang, 2024; Orazizadeh et al., 2014; Sang et al., 2012; Vacca et al., 2020; Wang et al., 2024)
Inflammatory response	ER stress-mediated inflammation, cirrhosis, activation of the transcription factors NF-κB, JNK, and TGF-β.	ER stress mediated inflammation, autophagy, mitochondrial damage, oxidative stress, increased levels of NF-κB, TNF-α, interleukins (2, 4, 6, 8, 10, 18, 1-β), and TGF-β.	(Jia et al., 2017; Sang et al., 2012; Shirdare et al., 2022; Vacca et al., 2020)
Lipid accumulation (Steatosis)	Fat accumulation (hepatic steatosis).	Obesity in high-fat diet-fed mice was observed. Onset of steatosis with Neuropeptide Y expression in male rats.	(Marjot et al., 2020; Tassinari et al., 2023; Zhu et al., 2021)
Mitochondrial dysfunction	Impaired energy metabolism and apoptosis.	TiO_2 NPs damage mitochondrial membranes, cause mitochondrial dysfunction and reduce ATP production.	(Arumugam et al., 2023; Natarajan et al., 2015; Waseem et al., 2022)
Lipid metabolism	Altered lipid metabolism.	Altered lipid metabolism.	(Chen et al., 2019; Chen et al., 2020)
Fibrosis potential	Progression to liver fibrosis in advanced stages.	Long-term TiO_2 exposure may activate hepatic stellate cells, promoting fibrosis.	(Hagström et al., 2024; Hong et al., 2020)
Insulin resistance	Increased plasma glucose levels by inducing IR.	Increased plasma glucose levels by inducing IR.	(Hu et al., 2016; Marjot et al., 2020)

Cellular apoptosis	Hepatocyte death due to lipotoxicity and inflammation.	TiO_2 NPs induce apoptosis via oxidative and inflammatory pathways.	(Abbasi-Oshaghi et al., 2019)

2.8.4 Models for studying MASLD

MASLD is a multifactorial condition influenced by the interplay of genetic, metabolic, dietary, and environmental factors. It is closely associated with insulin resistance, obesity, dyslipidaemia, and T2D, and often coexists with other components of metabolic syndrome. The progression from simple steatosis to inflammation and fibrosis involves oxidative stress, ROS generation, lipotoxicity, and immune-mediated mechanisms, making MASLD a dynamic disease (Dua et al., 2025). Previous research into MASLD has relied on both *in vivo* and *in vitro* models to study its complex pathophysiology. *In vivo* models, primarily rodent models, are fed high-fat, high-sugar, or methionine-choline-deficient diets that closely mimic the metabolic and histological features of MASLD observed in humans. These models allow understanding of systemic interactions among the liver, adipose tissue, gut microbiota, and immune system, making them invaluable for understanding disease progression (Alshawsh et al., 2022; Cui et al., 2025; Vacca et al., 2024). In contrast, *in vitro* models offer a controlled environment to dissect the cellular and molecular mechanisms underlying MASLD. As elevated FFAs play a key role in the disease development, *in vitro* models typically replicate MASLD by adding high levels of FFAs to the culture medium, commonly oleic acid and/or palmitic acid, which facilitate lipid accumulation in the hepatocytes (Cominguez et al., 2022; Wang et al., 2022). Other models incorporate metabolic stressors, such as fructose, which promote *de novo* lipogenesis and oxidative stress, further contributing to hepatic fat accumulation (Howes et al., 2025; Huang et al., 2025). A wide range of cell lines has been used to replicate MASLD features, including steatosis, expression of inflammatory markers, oxidative stress, and apoptosis *in vitro* (**Table 2.3**).

Table 2.3 Commonly used cell lines used for *in vitro* MASLD modelling.

Cell Line	Origin	MASLD Features	References
HepG2	Human hepatocellular carcinoma	Apoptosis, steatosis	(Cao et al., 2022; Green et al., 2015; Green et al., 2018; Gunn et al., 2017; Khalifa et al., 2022; Li et al., 2022; Malekpour-Dehkordi et al., 2022; Müller & Sturla, 2019; Poornima et al., 2022; Ramos et al., 2022; Shahmoradi et al., 2023; Wang et al., 2022; Zhang et al., 2021)

HepG2/C3A	Clonal derivative of HepG2	Oxidative stress, expression of inflammatory markers	(Filippi et al., 2015; Kermanizadeh et al., 2012; Müller & Sturla, 2019; Ramos et al., 2022)
HepaRG	Human hepatocellular carcinoma	Steatosis, MMP, oxidative stress, cell viability	(Müller & Sturla, 2019; Ramos et al., 2022; Tolosa et al., 2016)
Huh7	Human hepatocellular carcinoma	Steatosis, ER stress, apoptosis	(Gunn et al., 2017; Khamphaya et al., 2018; Müller & Sturla, 2019; Takahara et al., 2017; Wang et al., 2022)
LX-2	Human hepatic stellate cells	Activation of stellate cells	(Barbero-Becerra et al., 2015; Müller & Sturla, 2019; Ramos et al., 2022)
THLE-2	Immortalised normal human liver epithelial cells	Oxidative stress, expression of inflammatory markers, insulin resistant phenotype	(Şahin et al., 2024; Sefried et al., 2018)

HepG2 cells are human-derived hepatocellular carcinoma cells, like tumour cells in hepatoblastoma, but retain the features of normal hepatocytes. They exhibit lipid uptake and storage, lipoprotein metabolism, and glucose handling, all of which are crucial for studying hepatic steatosis and metabolic dysfunction. Their ability to take up exogenous fatty acids and lipoprotein residues makes them helpful in modelling fat accumulation in liver cells (Arzumanian et al., 2021; Donato et al., 2015). Moreover, HepG2 cells are cost-effective and highly reproducible, making them suitable for testing drug toxicity, nanoparticle interactions, and metabolic responses. Despite limitations such as low fatty acid oxidation, cancer-like phenotype, and reduced expression of some drug-metabolising enzymes, their accessibility and functional relevance make them a widely used model for early-stage liver disease research (Arzumanian et al., 2021; Donato et al., 2015).

In summary, the literature highlights the role of Ti and its compounds, particularly TiO_2, in biological systems. The chemical and physical properties of Ti influence its behaviour upon exposure, and various routes of entry and absorption have been documented in both human and animal models. Once internalised, TiO_2 NPs exhibit tissue-specific accumulation and biodistribution, with the liver as a primary target organ. Toxicological studies reveal that TiO_2 can induce oxidative and nitrosative stress, inflammation, and cellular damage, contributing to hepatic dysfunction. These mechanisms are particularly relevant in the context of MASLD, where risk factors such as obesity, insulin resistance, and lipid dysregulation intersect with environmental exposures. The pathogenesis of MASLD involves interactions between lipid accumulation, oxidative stress, and inflammatory signalling. *In vitro* models, especially those using HepG2 cells, provide valuable platforms for dissecting these pathways and

evaluating the hepatotoxic potential of TiO_2. Collectively, this body of evidence underscores the importance of understanding TiO_2's role in liver health and metabolic disease.

CHAPTER 3: Methods

3.1 Overview

This chapter outlines the methodology employed to address the research objectives of this study. The methods are divided into three parts:

1. Part A: This section describes the methodology used in the quantification of E171 levels in food (based on the NZ Total Dietary Study) and selected food and consumer items available in NZ. The primary results relating to these topics are presented in **Chapters 4** and **5** of this thesis.
2. Part B: This section details the experimental protocols used to characterise E171 and P21 and the assessment of its cytotoxic effect in a dose-dependent manner on normal and steatotic HepG2 cells. Primary results for these parts of the research are provided in **Chapters 6** and **7**.
3. Part C: Data processing.

Part A. Methodologies relating to dietary intake assessment and food and product testing

Approach, selection of categories, and development of composite groups

3.2 Overall methodology

For the dietary survey, the overall methodology started with selecting a representative range of foods across 10 food categories. Foods within each category (e.g., dairy products) were purchased and analysed to determine the concentrations of the target constituent, Ti (mg/kg). For each food category (and constituent), the average concentration (mg/kg) was multiplied by the intake of that food (g/14 days) for each age and gender group to estimate the total amount of the constituent (mg) consumed over two weeks. These amounts contributed by each food group were then summed to estimate overall 14-day and daily (mg/day) intakes across all foods consumed. Daily intakes were, in turn, divided by body weight (bw) to express the results as daily intake doses (mg/kg-bw/day). NZ food intake estimates for the 10 age, gender, and ethnicity categories were based on Smith et al. (2017), kindly provided by the Ministry for Primary Industries (MPI). These intake estimates were used in the most recently published New Zealand Total Diet Study (NZTDS), published in May 2018, and based on a food surveying round undertaken in 2016. According to Pearson et al. (2018), 14-day intakes for 128 foods were drawn from the following categories (numbers in brackets): Fruits and vegetables (37); Dried fruits (3); Meat/chicken/fish (21); Dairy products (12); Drinks (14); Instant foods (9); Breads and breakfast foods (18); Chocolate and snacks (7); Sauces (3); and Other foods (4). Food intakes allocated in this study were therefore the same as those used in the most recently published NZTDS. Fourteen-day intake data provided in Smith et al. (2017) (their Appendix B, Tables D and E) were transferred to a Microsoft Excel spreadsheet format and then checked for transcription accuracy. Care was taken to

ensure that intake figures remained faithful to the original data during the survey design phase, for example, when allocating a specific food to its correct composite as outlined below.

3.3 Development of the composite groups

For the development of the composite groups, foods were allocated to 40 groups, spread over 9 major (operational) categories, as follows:

3.3.1 Fruits

1. Pip fruit/Kiwi fruit
2. Stone fruit
3. Citrus
4. Berries
5. Tomato
6. Others

3.3.2 Vegetables and fungi

1. Root vegetables
2. Tubers
3. Leafy vegetables
4. Squash/Creeping vegetables
5. Seed/Other
6. Dried fruits

3.3.3 Grain and cereal-based foods (carbohydrate-rich)

1. Bread
2. Rice or rice-based
3. Breakfast cereals
4. Pasta, spaghetti, noodles
5. Biscuits
6. Cakes

3.3.4 High protein foods (meat/chicken/fish/other)

1. Chicken
2. Beef
3. Pork
4. Fish
5. Other seafood
6. Eggs
7. Nuts
8. Others (composite foods, tofu, and beans)

3.3.5 Dairy foods

1. Milk
2. Milk products 1
3. Milk products 2

3.3.6 Drinks (beverages) and soup

1. Water
2. Juices and carbonated beverages
3. Warm or caffeinated beverages (further divided into 32A Tea, 32B Coffee Instant, and 32C Other)
4. Alcoholic drinks
5. Soup

3.3.7 Spreads, condiments and flavourings

1. Spreads
2. Condiments and flavourings
3. Snack foods and chocolate

3.3.8 Infant foods

1. Infant foods (further divided into 38A Pre-school and 38B Toddler categories)

3.3.9 Others

1. Sugar

2. Oil

Two of the composites (32; Warm or caffeinated beverages and 38; Infant foods) were further subdivided during the laboratory operations to allow for better discrimination between types of foods. All composites were designed in a way that they could be allocated overall 14-day intake figures based on Smith et al. (2017) which were also used in the most recently published NZTDS. This step involved tracking the intakes for specific foods, and some substitutions in cases where two foods were sufficiently similar.

Each of the 40 main composite groups comprised between 1 and 4 key foods, and a total of 136 key foods were analysed in this part of the study. **Appendix 4.1** provides further details on the key foods analysed and their 14-day intakes across the 10 age and gender groups.

For many of the 'key foods' shown in **Appendix 4.1**, more than one brand, variety, or example was included in the composite to represent that food more comprehensively. For example, Composite Group 1 Pipfruit/kiwifruit comprised examples of apples, pears, and kiwifruit. The key food 'apple' included three different types of apples. The highest number of individual foods in any composite was nine.

The major categories themselves can be related to dietary food groups (e.g., fruits) but were also designed to accommodate similarities and differences in sample handling and preparation requirements. For example, before the ashing step, vegetables were chopped and weighed, whereas the approach with a preformulated liquid beverage was to evaporate a specific volume to dryness (see **Section 3.5**).

3.4 Sample collection

All samples except beef, chicken, and liver were purchased from local supermarkets: Woolworths (previously branded as Countdown), Pak ‘n Save, and New World, in the Wellington region of NZ. Beef, chicken, and liver samples were bought at a Wellington butchers’ shop.

As part of the standard methodology of an NZTDS, samples are collected from four NZ centres (two in the North Island and two in the South Island) on four occasions spread over a year (four quarters). The most recent sampling occurred during 2024, and the corresponding 2024 NZTDS report is still in preparation. The reason for geographical spread is that some products are seasonal, and/or levels of some constituents (e.g., pesticide residues) in some products may vary with season or geographical location.

In this study, samples were collected at supermarkets in one city (Wellington) from September 2024 to January 2025. For Ti in foods, it is expected that results for samples collected in Wellington will also represent those from other locations in NZ, and that any seasonal changes will be undetectable or negligible. This is because levels of natural Ti in foods are relatively low, and those in seasonal foods such as fruits or vegetables are often near or below the detection limit (DL) for Ti, regardless of when or where they are sampled. Significantly, most supermarket supply chains operate countrywide, and many non-seasonal foods are probably the same product sold across the country. This is mainly because the NZ supermarket industry is characterised as a duopoly, with 90% of the market share and 80% of the grocery trade dominated by two companies: Foodstuffs (the owners of Pak ‘n Save, New World, and Four Square) and Woolworths (previously branded as Countdown). The sample collection in this survey (from Foodstuffs and Woolworths) covered both companies that comprise the NZ supermarket duopoly (Styles, 2024).

All foods listed in the NZTDS were purchased in the order of the composite design (1–40). Samples were chosen that were thought to represent a reasonable proportion of the regular diet. Fruits and vegetables were bought fresh and processed on the same day, in the order specified in the composites table (see **Section 3.3** above and **Appendix 4.1**).

Sample purchase, preparation, and analysis were undertaken in batches (rather than collecting all foods first and storing them until analysis) so that the time between purchase and analysis was always kept to a reasonable minimum (same day or overnight). When short-term storage was necessary, perishable items were stored under suitable conditions (usually refrigeration) to prevent changes in their overall composition before sample processing and analysis.

3.5 Sample preparation

3.5.1 Glassware and reagents

All glassware used in this study was acid-washed, triple-rinsed with distilled water, and dried to remove any contaminants or traces of the tested elements. All equipment, including work surfaces used for food preparation, was thoroughly cleaned, and stainless-steel knives were used for chopping.

3.5.2 Treatment of samples

Samples were prepared as they would typically be for cooking or for eating uncooked; bananas, oranges, onions, potatoes, and carrots were peeled; apples and pears were not peeled, and shells were discarded from eggs. Fruits and vegetables in the same composites were chopped (with a stainless-steel knife), mixed, and shaken in a bowl with a tight lid to achieve thorough mixing.

Composite food samples were prepared based on the consumption of individual foods (with reference to the ratio of intakes of every key food in the composite, **Appendix 4.1**), to around a mixture of 100 g. The amount of all food in each composite was thoroughly mixed to achieve uniformity.

Subsamples of the composites were analysed in triplicate. The typical sample weight of each subsample was mostly around 10 g (example composite design is shown in **Figure 3.1**). However, for some samples, the weight was adjusted, or a different approach was taken, based on the nature of the food. The most significant difference in approach was for the pre-prepared liquid foods (cold drinks, milk, water, and sauces). In the case of these, up to 80 mL/85 g of each sample was first added to an acid-washed pre-weighed Pyrex beaker, weighed, and then evaporated in a laboratory oven at 95 °C. The evaporation step took 1–3 days, depending on the sample. The residue was then re-weighed and ashed (**Section 3.5**) as usual. Other weight or sample preparation exceptions included foods as whole chunks (some chocolates), foods in the form of pastes (pouches and ice creams), or foods where it would be ideal to lower the detection level. All such variations led to either an increase or a decrease in sample weight, ranging from 4 g to 85 g.

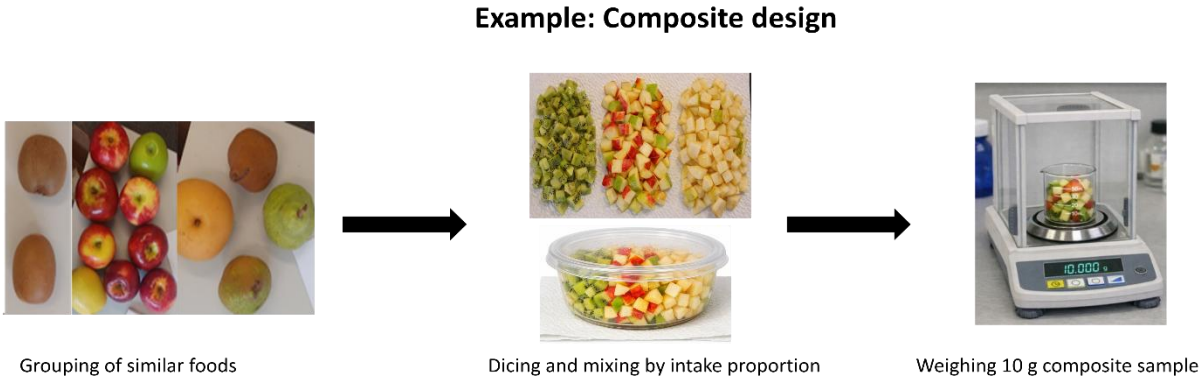

Figure 3.1 Overview of example composite design

3.5.3 Ashing

Ashing is performed to remove organic components from food samples, simplify acid digestion, and prepare the final sample solution matrix (El Hosry et al., 2023). This was performed by placing the Pyrex beakers with their samples in a muffle furnace in a predetermined order. The ashing step was maintained at 650 °C for 12–16 hours in batches of 4 triplicate (12 beakers per run).

There are two approaches to ashing. 'Wet ashing' involves the use of oxidising acids (often with other oxidising agents) and can be a long and complex process but is required for inorganic substances that are volatile. 'Dry ashing' involves the use of heat alone (El Hosry et al., 2023). One advantage of testing for Ti and TiO_2, which was used in this step, is that both substances have high melting points (1660 °C for Ti metal and 1843 °C for TiO_2). This means there is no need for wet ashing; the samples can be dry-ashed. Furthermore, the ashing step can also be carried out at quite a high temperature (650 °C) without loss of Ti by volatilisation, removing all the organic matter while retaining all the Ti. Higher temperatures than 650 °C were possible and were also trialled, but ran into a limitation that the Pyrex beaker can start to deform over time at temperatures above approximately 760 °C, because the softening point of Pyrex is 820 °C. In this study, 650 °C was found to be an optimal temperature for sample preparation for analysis of Ti, and also allowed later testing for chromium (Cr, melting points 1907 °C for Cr metal, and 2435 °C for Cr_2O_3) and zinc (Zn, melting points 419.5 °C for Zn metal, and 1975 °C for ZnO) in the same acid digest solutions. Consistent with the lower melting point of Zn and some of its compounds, a modest but tolerable loss of about 15% Zn may have occurred during the 650 °C ashing step (see **Section 3.5**)

After ashing, the beakers were allowed to cool and carefully transferred (to avoid loss of inorganic ash) for re-weighing to determine the ash weight. In this step, the weight of the beaker plus ash was recorded, and then the initial weight of the empty beaker was subtracted to obtain the ash weight.

3.5.4 Acid digestion and sample workup

The sample digestion method adapted from Leone (1973) was used for the analysis of TiO_2. This was further validated through test digestions of E171 and its ashed E171 residue in agar (see **Table 3.2**), as well as samples of Ti metal powder. This method involves the use of concentrated sulfuric acid (H_2SO_4) and was trialled both with and without additional sodium sulfate (Na_2SO_4), to boost the concentration of sulfate anions (SO_4^{2-}), which act as a complexing agent for $Ti4^+$ in acid solution. Matrix-matched dilutions were compared with those from a 1000 mgTi/L ICP/AAS calibration standard solution (Merck, as $(NH_4)_2TiF_6$ in H_2O, traceable to SRM from NIST). Results with and without Na_2SO_4 were equivalent, indicating that this reagent was unnecessary. A general rule for trace element analyses is that it is best

to use the simplest approach with the possible steps, to avoid potential for contamination from added reagents or sample manipulations (Hoenig, 2001).

In the final adapted method, 20 mL concentrated AR grade H_2SO_4 (Sigma-Aldrich, USA) was carefully added to each 100 mL Pyrex beaker (containing the food ash). Beakers were covered with a watch glass, swirled, and transferred to a hot plate in a fume cupboard. Solutions were heated to simmering, covered with watch glasses in a fume cupboard. Samples were simmered on a hotplate for 60 min, and swirled occasionally, until the solution turned clear. After this, the hotplate was turned off, and the beakers were allowed to cool.

In their concentrated form, the digest solutions were capable of dissolving acid-hardened filter papers. For this reason, the cooled digest samples were diluted 3–4 times before filtering by adding 60 mL of distilled water to each beaker and swirling. Sample solutions were then filtered into 100 mL volumetric flasks through Whatman #541 paper to remove any undigested particles. For most samples, there were very few of these in evidence. An exception was for some toothpastes (tested as individual products, see **Chapter 5**) where significant amounts of insoluble inorganic material were present after digestion; this material was thought to be insoluble aluminium sulfate formed by reaction of alumina (Al_2O_3) with sulfuric acid. Alumina and aluminium lactate (which would form alumina during ashing) are both widely used in toothpastes. The presence of this insoluble material in the toothpaste digests did not interfere with the detection of Ti.

Each sample beaker and filter paper were rinsed three times, and the volume was raised to 80 mL with distilled water. Subsequently, 4 mL of AR 30% hydrogen peroxide (H_2O_2) (Sigma-Aldrich, Merck Life Science Ltd, Auckland) was added to each flask to develop any colour. The volume was made up by adding distilled water to reach the 100 mL mark, then capped and mixed by inversion to achieve a final sulfuric acid concentration of 20%.

The addition of H_2O_2 in the presence of SO_4^{2-} ions has the effect of converting dissolved titanium to a yellow-orange coloured 'titanium peroxide' complex. This reaction is rapid and linked to peroxo (O_2^{2-}) ligands becoming coordinated to the Ti(IV) centre, with sulfate ions (SO_4^{2-}) influencing the coordination environment. The resulting species has been identified as $[Ti(O_2)SO_4]\cdot nH_2O$; however, its exact structure may vary depending on pH, concentration, and other conditions. For samples containing sufficient Ti(IV), the complex forms at sufficiently high concentrations to produce an immediate colour change from clear to yellow-orange.

3.6 Analysis

3.6.1 Concentration ranges and instrumental options

During this study, it was established that colour development is usually evident in samples containing E171 (under our experimental conditions of approximately 10 g of food and a 100 mL volume), with the exception of a few food samples that contained E171 at unusually low concentrations (see **Chapter 5**). Colour development is useful because any samples in this category are suitable for analysis by UV-visible (UV-vis) spectroscopy. This is more straightforward than Graphite Furnace Atomic Absorption Spectroscopy (GFAAS). The GFAAS determination, in turn, is not influenced by the presence of H_2O_2, so that digest samples which showed no colour-change remained suitable for GFAAS testing. In this study, all but one of the composite samples tested as part of the food survey (this chapter) showed no colour-change and required analysis by GFAAS. By contrast, a reasonable proportion of samples tested in the targeted survey involving foods more likely to contain E171 (see **Chapter 5**) showed a colour change when H_2O_2 was added to the digest solutions. In most cases, this corresponded with the E171 product labelling, confirming that the UV-visible method remains suitable for detecting foods containing E171. A notable distinction was that the two concentration ranges usually differed by at least two orders of magnitude. It was found that when E171 is present in a food at a level that makes the coloured complex visible, the Ti concentration is typically several hundred times higher than the natural Ti concentration in foods. Testing any of the coloured samples by GFAAS required substantial dilution to match the GFAAS calibration range, even when the colour was faint.

3.6.2 UV-vis spectrophotometry

All samples that developed visible colours (as a representation of the presence of high levels of added titanium in the food samples) were measured via their UV-vis absorbances.

Where colour was evident, titanium concentrations were quantified using a colourimetric method on a direct reading spectrophotometer (Hach DR/2000, Hach Lange NZ, Auckland, NZ) at a wavelength of 410 nm. Acid-matched standard solutions of concentrations 0 (blank), 5, 12.5, 25, and 50 mg/L were prepared from a 1000 mgTi/L stock standard solution that had been prepared by acid digestion of Ti powder. Before use, the stock standard was validated (after suitable dilution) by comparison with a commercial 1000 mg Ti/L ICP/AAS calibration standard (Merck, as $(NH_4)_2TiF_6$ in H_2O) on both the GFAAS and UV-vis instruments.

Samples with a colour more intense than that of the highest calibration standard (50 mg/L) were diluted to ensure they remained within the calibration range. A typical UV-vis calibration graph obtained in this study is shown in **Figure 4.1B**.

3.6.3 Graphite furnace atomic absorption spectroscopy (GFAAS)

All samples that did not produce any colour were subjected to GFAAS. Analysis was carried out at 364.2675 nm using an Analytik Jena ContraAA 700 tandem continuum source GFAAS/FAAS (Analytik Jena GmbH, Jena, Germany), which employs a xenon lamp and provides exact wavelength resolution. The GFAAS furnace heating programme is shown in **Table 3.1**, and the standard curve for Ti obtained by GFAAS is shown in **Figure 4.1A**.

For GFAAS measurements, samples were diluted by a factor of five to a final sulfuric acid strength of 4% and run against matrix-matched standards. During method development, it was determined that diluting the acid digests by a factor of 5 (from 20% to 4% sulfuric acid) reduced the noise to give an optimal signal-to-noise ratio and good peak reproducibility, to yield an equivalent DL as for undiluted 20% sulfuric acid samples, but with no matrix-modifier required. Dilution also slightly extended furnace lifetimes, as 20% sulfuric acid is very corrosive.

Table 3.1 GFAAS furnace heating program for the measurement of Ti in food extracts.

Step number	Step	Temperature (°C)	Ramp time (s)	Holding time (s)
1	Drying # 1	80	6	20
2	Drying # 2	90	3	20
3	Drying # 3	110	5	10
4	Pyrolysis	350	50	20
5	Pyrolysis	1400	300	10
6	Gas adaption	1400	0	5
7	Atomise	2600	1500	10
8	Clean	2700	500	4

The GFAAS is capable of dispensing 20 µL of sample volumes by autosampler, and hence the standards were prepared by autosampler dilution (4, 8, 12, 16, and 20 µL), which covered the range (100, 200, 300, 400, and 500 µg/L) of Ti. Each standard and sample was run in triplicate.

The upper limit of the heating programme for Ti analysis was 2700 °C (**Table 3.1**), which is at the extreme end of the tolerance for high-purity graphite (and pyrolytic-carbon-coated) GFAAS tubes. For this reason, samples were analysed in relatively small batches. To control for tube degradation during a run, calibration was undertaken both before and after each sample batch. This allowed a dynamic correction factor to be applied to offset the progressive signal reduction caused by graphite tube degradation. Across both composite and single-sample testing (**Chapters 4** and **5**), including method

development, the GFAAS component consumed about 20 graphite tubes. The methodology used in the quantification of E171 levels in food and consumer items is summarised in **Figure 3.2.**

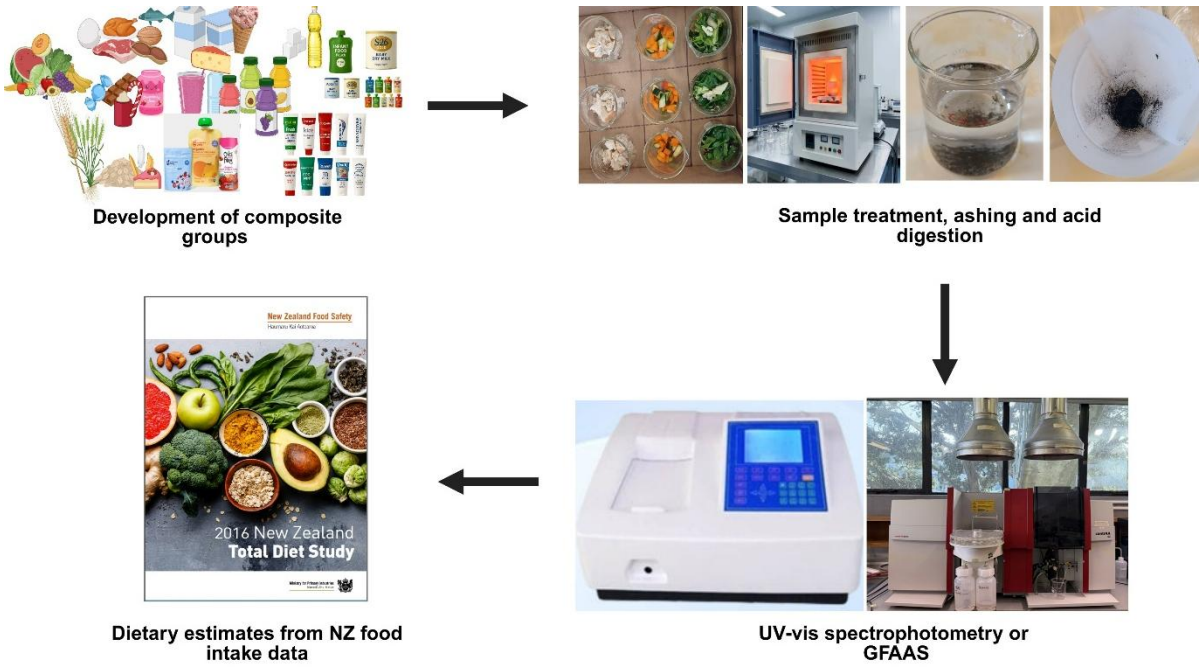

Figure 3.2 Overview of analytical steps in E171 quantification

As a general observation, Ti concentrations in foods and other samples are either relatively low or, where E171 was added, relatively high, with no samples in between. Whereas colourimetric analysis was confirmed to be appropriate for samples to which E171 had been added, GFAAS was required for the analysis of all natural food samples. The two main concentration zones for Ti in foods (either low or high) are separated by two to three orders of magnitude.

3.7 Quality assurance

3.7.1 Recovery of E171 from agar

To mimic the experimental method for analysing Ti in food, five samples of E171 in agar were prepared by adding 0.134 g of E171 to 1 g of agar and processed and analysed in the same way as standard food samples. This was to test the overall recovery of E171 from a food-like sample, which could be affected by losses during the ashing step, the proportion recovered during the acid extraction step, and the accuracy of the analytical measurement step. Recoveries were calculated based on the analytical measurements of [Ti] converted to [TiO_2] equivalents. Recovery values for all five samples and one sample of E171 powder are given in **Table 3.2**.

Table 3.2 Percent recovery of Ti from powder and agar samples.

Sample type	Percent recovery
E171 powder	101.9
E171 in agar	95.7
E171 in agar	91.5
E171 in agar	107.1
E171 in agar	85.2
E171 in agar	87.8
N	6
Mean	94.9
Standard deviation	8.4
%RSD	8.9

Notes: E171: titanium dioxide, N = number of samples.

The mean recovery was 95%, demonstrating acceptable accuracy. On average, the (apparent) loss of Ti was only around 5%. The relative standard deviation was <10%, indicating tolerable precision for the repeat analysis of equivalent samples. There was no evidence to suggest that the presence of the agar matrix (representing organic matter in a food sample) caused a lower recovery (range 85–107%) compared with recovery from a sample of E171 powder (102%) (**Table 3.2**). This indicates that the 12–16-hour 650 °C ashing step does not alter the structural composition of E171 in a way that reduces its subsequent dissolution in concentrated sulfuric acid. Instead, the ashing step seems to act as a simple reversal process, converting matrix-bound E171 back to E171 powder.

It is possible that ashing at 650 °C may alter some of the natural forms of Ti in foods. However, in the oxidising environment of the muffle furnace, any organically bound or other Ti species are likely to be converted to TiO_2 so that they will become equivalent to E171.

Overall, these results demonstrated the suitability of the sample preparation and analysis methodologies used to measure Ti in food samples in this study.

3.7.2 Zinc and chromium testing

Testing for Zinc (Zn) and Chromium (Cr) in the same composite samples was undertaken to assess the reliability of the composite sampling and dietary intake estimation methodologies used in this study.

Intake estimates for Zn in NZ can be directly compared because Zn has already been included in previous NZTDS. Cr intakes have not been previously reported in NZTDS or other NZ surveys, but adult intake estimates are available from overseas studies.

In theory, natural dietary intakes of Ti should also fall somewhere between those of Cr (which are lower) and Zn (which are higher), so intake estimates for these two elements should bracket the intake estimates for Ti. Zn and Cr testing was therefore mainly used as a quality assurance measure: a means of validating the overall dietary intake estimate methodology used in this study for Ti. However, an assessment of Cr and Zn intakes in New Zealanders in 2024 is an additional outcome of this study.

Some aspects of the analytical methodology used for Ti, particularly the digestion with concentrated sulfuric acid, are not commonly used for determinations of Zn or Cr, but this was not seen to be a limitation, for the following reasons:

- Although the majority of trace element testing makes use of digestion with nitric acid (with or without other reagents such as peroxide), this is partly for ease of use and subsequent analysis: chloride (from HCl) and sulfate (from H_2SO_4) can cause more significant interferences on ICP and AAS than nitrate (from HNO_3). Hydrofluoric acid (HF) is not generally used because it is too hazardous to human health. The default modified nitric acid digestion approach used in commercial laboratories is a compromise and often referred to as a ‘pseudo-total’ extraction, because it results in incomplete recoveries for some elements and matrices, such as Cr in soils. By contrast, it was expected that the concentrated sulfuric acid digestion conditions used in this study (for dissolution of Ti and TiO_2) would have quantitatively recovered all available Cr and Zn in the food ash samples, because concentrated acid is a powerful oxidising agent.
- With respect to the 650 °C ashing step used for Ti, losses of Cr would not be expected because of the high melting points of Cr and its compounds (see **Section 4.3.1**). Some ashing losses may have occurred for Zn, but the magnitude of those (if any) could also be assessed by reference to intake estimates obtained in the last published NZTDS. For this study, the aim was to determine whether the overall methodology provides estimates of Zn intake in the same order of magnitude as those in the NZTDS and how close they are.

Cr and Zn analyses were carried out on the most diluted (4% sulfuric acid) digest solutions, against matrix-matched standards. For Cr, GFAAS analysis was performed at 357.868 nm using the heating programme shown in **Figure 4.2B** and **Table 3.3**. For Zn, analyses were carried out on the same instrument, operated in Flame AAS (FAAS) mode at 213.857 nm using an air-acetylene flame. The sensitivity of Cr determinations by GFAAS is relatively low, whereas the sensitivity of Zn determination by FAAS is very high. For this reason, the standards for both Cr and Zn were the same range of 0, 0.25, 0.5, 1, and 2 mg/L, with most sample measurements occurring at the lower end of this calibration range for both elements.

Table 3.3 GFAAS furnace heating program for the measurement of Cr in food extracts.

Step number	Step	Temperature (°C)	Ramp time (s)	Holding time (s)
1	Drying # 1	80	6	20
2	Drying # 2	90	3	20
3	Drying # 3	110	5	10
4	Pyrolysis	350	50	20
5	Pyrolysis	1300	300	10
6	Gas adaption	1300	0	5
7	Atomise	2300	1500	4
8	Clean	2450	500	4

Part B. Methodologies relating to cell culture testing

3.8 Acquisition and characterisation of food-grade TiO_2 (E171) and P21

Food-grade TiO_2 (E171) was kindly provided by NZ distributors of Jiangsu Hushen Titanium White Technology (China), Sensient Technologies (USA), and purchased from a local baking supply store in NZ. Titanium (IV) oxide nano powder with 21 nm primary particle (P21) was purchased from Sigma-Aldrich, USA (Cat. No. 718467). Material acquired from the three sources was labelled E171A, E171B, E171C, and P21, and characterised using the methods outlined below.

3.8.1 Scanning electron microscopy (SEM) and transmission electron microscopy (TEM)

SEM imaging was performed using a JEOL JSM-6500F field emission scanning electron microscope (JEOL, Tokyo, Japan), while TEM characterisation was carried out using a JEOL JEM-2100F transmission electron microscope.

SEM and TEM characterisation was performed to assess the morphology of TiO_2 (E171 and P21) samples. The E171 samples were analysed by SEM using 150,000x to 300,000x magnification and 10 kV of electron acceleration. For sample preparation, a water suspension of E171 particles was freshly prepared and sonicated for 2 min. The mixture was dropped onto the SEM sample stub, and samples were air-dried at room temperature (RT) and imaged without coating. At least six images per sample were taken for further size analysis.

The morphology of P21 was analysed by TEM. The samples were analysed by TEM operating at 200kV using a digital camera at x100K magnification (Gatan 832.J45UO; Gatan Inc., Pleasanton, California, USA). The sample was placed in a 1.5 mL Eppendorf sample vial and dispersed in ethanol using a sonication bath. A Pasteur pipette was used to dispense a small drop of the sample onto a formvar-coated, carbon-coated 3 mm copper grid. The sample was air-dried and plasma-coated at RT overnight before insertion in the TEM machine for analysis. At least 10 images of the sample were captured to investigate size distributions using Fiji (version 2.16.0). The characterisation of the size of the E171 particles was performed from several pictures of each sample using Fiji software (Schindelin et al., 2012). High-resolution SEM and TEM images were analysed using the line segment tool, with multiple regions of interest selected to ensure representative sampling. Each particle's longest axis was measured in nm, calibrated using the image scale bar. A total of 100 individual particles were measured per image to minimise sampling bias.

3.8.2 Powder X-ray diffraction spectroscopy (XRD)

XRD was used to characterise the crystalline structure of TiO_2 NPs in E171 and P21. XRD identifies phase composition (anatase, rutile, brookite) based on diffraction peak patterns. Crystalline phases of

E171 and P21 were analysed by X-ray powder diffractometry (Rigaku Spider diffractometer, Japan). A Rigaku spider diffractometer equipped with a MicroMax MM007 rotating anode generator (Cu α radiation, 1.54180 Å), high-flux osmic multilayer mirror optics, and a curved image plate detector was used to perform XRD analysis. All particles (in powdered form) were placed on the XRD specimen holder and pressed with a glass slide to ensure uniform sample thickness. The sample values were then analysed in Microsoft Excel.

3.8.3 Energy dispersive spectroscopy (EDS) and energy-dispersive X-ray spectroscopy (EDX)

The elemental composition of E171 and P21 was determined using SEM in EDX mode and TEM equipped with an EDS detector. For E171, analysis was conducted using a FEI Quanta 200 SEM (FEI Electron Optics, Eindhoven, Netherlands) operating in EDX mode to identify and quantify major elements. The sample was mounted on conductive carbon tape, and representative regions were imaged under an accelerating voltage suitable for X-ray generation. EDAX point analysis and elemental mapping were performed to determine the distribution and concentration of key elements.

For P21, high-resolution elemental mapping was performed using a JEOL TEM equipped with an EX-37001 Solid Silicon Drift Detector. The EDS analysis was conducted at a magnification of x600K with a 50 nm scale bar for precise localisation and identification of Ti and associated elements. Data from both instruments were processed to generate spectra and elemental maps, which were used to interpret the elemental composition and spatial distribution within the samples.

3.8.4 Dynamic light scattering (DLS)

The hydrodynamic diameter, zeta potential (ZP), and polydispersity index (PDI) were measured using a Malvern Zetasizer (model ZEN 3600, UK). The samples E171 and P21 in a concentration of 0.05% were freshly prepared from the stock (1000 µg/mL) and dispersed by sonicating for 30 min in deionised water (DI) and Dulbecco's Modified Eagle Medium (DMEM) (supplemented with 10% FBS and 1% penicillin/streptomycin). 1 mL of each sample was put in a cuvette, and the software instructions were followed to run the analyses. Before each analysis, the cuvette was thoroughly cleaned with DI water. Three independent experiments were performed for each sample. Before the experiment, the pH and refractive index (RI) of the dispersion media (DI and DMEM) were recorded.

3.9 *In vitro* studies

3.9.1 Cell culture and treatment

HepG2 cells were obtained from the American Type Culture Collection (ATCC, USA). Cells were passaged five times before cryopreservation in liquid nitrogen and served as stock for the experimental work.

Cells from the original stock were cultured and passaged to establish a working stock. For storage, cell concentration was adjusted to approximately 2×10^6 cells/mL with cell culture medium (Dulbecco's Modified Eagle Medium (DMEM; Sigma-Aldrich) supplemented with 4.5 mM glucose, 2 mM glutamine, 10% foetal bovine serum (FBS; Thermo Fisher Scientific), and 1% penicillin-streptomycin (Sigma-Aldrich, USA) and 10% v/v DMSO was added. The cells were then aliquoted into 1 mL cryotubes and frozen for 24 hours using a Mr Frosty freezing container (Thermo Fisher Scientific) containing isopropyl alcohol, placed in a -80°C freezer. After 24 hours, the cryotubes were then transferred to liquid nitrogen for storage.

Frozen cells were thawed before being added to a 15 mL Falcon tube containing prewarmed cell culture medium. The tube was centrifuged for 3 min at 200 × g, and the supernatant was discarded to remove the dimethyl sulfoxide (DMSO)-containing culture media in which the cells were frozen. The cells were then transferred to $25cm^2$ (T25) Nunc cell culture flasks (Thermo Fisher Scientific) containing prewarmed DMEM. Cells were incubated at 37 °C in a humidified atmosphere with 5% CO_2 incubator (ESCO, Singapore) until reaching 75–80% confluence.

Once the cells had reached ~80% confluence, they were transferred to a 75 cm^2 (T75) Nunc cell culture flask. To transfer the cells, the cell culture medium was removed, and the cells were washed twice with warm phosphate-buffered saline (PBS), then detached by adding Trypsin-EDTA (0.25%) (Thermo Fisher Scientific) and incubating for 10 min. Prewarmed cell culture medium was then added to inactivate the Trypsin-EDTA. Cells were then added to a 50 mL Falcon tube and centrifuged for 3 min at 200 × g. The supernatant was discarded, and the cell pellet was resuspended in 1 mL of cell culture medium. The cells were then transferred to the T75 flask containing around 15 mL of warm cell culture medium. Cells were then incubated until they reached ~80% confluency, at which time, they were either passaged or plated for different experiments in respective plate types.

For the cell passage or plating, cells were detached from the flask, centrifuged, and the cell pellet resuspended as described above. Cells were then counted using a haemocytometer. For cells being passaged, 2×10^6 cells were added to a new T75 flask containing approximately 15 mL of warm cell culture medium. Cells to be plated for the subsequent experiments were adjusted to the appropriate concentrations as described in the sections that follow. HepG2 cells were cultured for no more than 15 passages throughout the experiments.

Cell passaging and plating were performed in an aseptic environment using a biological safety cabinet. The cabinet was sterilised by UV irradiation for 15 min every time it was used, and the surfaces were cleaned with 70% ethanol before and after each use.

3.9.2 Optimisation of steatotic HepG2 cell model

To establish a steatotic model, an initial dose-response experiment was performed to identify a concentration of OA that induces moderate lipid accumulation without causing significant cytotoxicity. HepG2 cells were treated following the protocol described by Zhang et al. (2021). HepG2 cells were cultured at a density of 2×10^5/well in 24-well plates for 24 hours in DMEM supplemented with 10% FBS. Cells were subjected to serum starvation for 6 hours in DMEM containing 1% BSA without FBS to enhance OA uptake. Cells were then treated with OA at varying concentrations (0.1, 0.25, 0.5, 0.75, 1 mM) for 48 hours to induce lipid accumulation. After treatment, cells were washed three times with PBS to remove residual OA. OA quantification was performed using Oil Red O (ORO) staining.

3.10 Reagents and assays

3.10.1 Preparation and dispersion of E171 and P21 particles

E171 and P21 stock solutions were prepared for cellular exposure following standardised dispersion protocols to ensure reproducibility and minimise agglomeration. E171 and P21 were weighed separately into sterile centrifuge tubes (Thermo Fisher Scientific) and dispersed in PBS at 10 mg/mL each. The solutions were vortexed for 5 min and further diluted to a stock concentration of 1 mg/mL. For cell exposure, the stock solutions were sonicated in a bath sonicator (Soniclean, Australia) for 30 min to promote uniform dispersion. TiO_2 NPs were then serially diluted in complete culture medium to the desired treatment concentrations (5, 50, 100, 200 µg/mL). Each treatment was thoroughly vortexed immediately before use. Each concentration of TiO_2 NPs was made fresh immediately before the experiment to minimise aggregation and ensure consistent exposure conditions.

3.10.2 Oleic acid preparation

An oleic acid (OA; Sigma-Aldrich) stock solution was prepared following the protocol described by (Khalifa et al., 2022). OA was dissolved at a final concentration of 12 mM in PBS (137 mM NaCl, 10 mM phosphate, 2.7 mM KCl, pH 7.4) containing 11% fatty acid-free BSA (Sigma-Aldrich, USA) to enhance solubility and mimic physiological conditions. The mixture was sonicated using a bath sonicator (SONICLEAN, Australia) for two cycles of 5 min each to ensure proper dispersion. The solution was then incubated overnight at 37 °C with continuous shaking using a shaking incubator (Innova 4230, USA). Following incubation, the OA solution was sterilised by filtration through a 0.22 µm membrane filter (Sigma-Aldrich), aliquoted into sterile tubes, and stored at 4 °C until use.

3.10.3 Cell viability assays

3.10.3.1 MTT (3-(4,5-dimethylthiazol-2-yl)-2,5-diphenyltetrazolium bromide) assay

The MTT assay measures cell viability by detecting metabolic activity. MTT is a yellow tetrazolium salt and living cells with active mitochondria reduce MTT to purple formazan crystals. The amount of formazan formed is proportional to the number of viable cells (Ghasemi et al., 2021).

The MTT reagent was obtained from Thermo Fisher Scientific. An MTT stock solution (12 mM) was prepared by adding 1 mL of sterile PBS to 5 mg of MTT (5x). The solution was vortexed until dissolved and kept at 4 °C overnight. The following day, the solution was vortexed and filtered with a 0.2 µm membrane filter. Cells were grown at a density of 1×10^4/well overnight in a 96-well plate (Thermo Fisher Scientific). Twenty-four hours after cells were seeded, DMEM with different OA concentrations (0, 0.1, 0.25, 0.5, 0.75, 1 mM) was added to the cells for 48 hours. Cells were then washed with PBS before 100 µL of a mixture of MTT stock solution and DMEM (1:6) was added to each well. The plate was incubated at 37 °C in the 5% CO_2 incubator for 4 hours. The media was then carefully discarded by slowly inverting the plate, after which 100 µL dimethyl sulfoxide (DMSO) was added to each well. To dissolve the formazan crystals, the plate was placed on a shaker for 15 min at RT. Finally, absorbance was measured at 590 nm. Results were calculated using a microplate reader (FLUOstar Omega, BMG Labtech Pty, Melbourne, Australia). Cell viability was calculated using the standard formula [Viability (%) = (Absorbance of treated cells/ Absorbance of control cells) x 100] based on corrected absorbance values. Blank wells containing only culture medium and MTT reagent, without cells, were included to account for background absorbance, and their average values were subtracted from all sample and control readings to eliminate non-specific interference. Untreated HepG2 cells served as the negative control and were designated as representing 100% viability, providing a baseline against which the effects of various treatment concentrations were normalised.

3.10.3.2 Trypan blue exclusion assay

The trypan blue exclusion assay was employed to measure both cell number and viability of HepG2 cells following treatment with TiO_2 (E171 and P21) with/without OA. Live cells with intact membranes exclude the dye and remain unstained, while dead cells with compromised membranes absorb trypan blue and appear blue under the microscope. HepG2 cells were seeded in a 6-well plate (Cat. No. 140675, Thermo Fisher Scientific) at a density of 1×10^5 cells/well for 24 hours. Cells were treated with varying concentrations of (0, 5, 50, 100, 200 µg/mL) of E171 and P21 with and without OA for 48 hours. After treatment, adherent cells were washed with PBS, then trypsinised and centrifuged at 200 × g for 5 min. The cell pellet was resuspended in PBS, and an aliquot of the cell suspension was mixed 1:1 with 0.4% trypan blue solution (Sigma-Aldrich). The mixture was incubated at RT for 2–3 min. Stained and unstained cells were counted using a haemocytometer under a light microscope (Olympus

CKX41SF, Auckland, NZ). Viable cells excluded the dye and appeared clear, whereas non-viable cells took up the dye and appeared blue. All experiments were performed in triplicate. Cell viability was calculated using the formula, Viability (%) = (Number of viable cells/ Total number of cells) x 100.

3.10.3.3 Neutral red uptake assay

The neutral red uptake (NRU) assay was performed to evaluate the cytotoxic effects of E171 and P21 on HepG2 cells, with results based on lysosomal integrity and cell viability. Viable cells actively take up and bind the dye, while damaged or non-viable cells show reduced uptake due to lysosomal membrane disruption. The amount of dye retained is quantified spectrophotometrically, reflecting cell viability (Rodrigues et al., 2023). To optimise the number of cells per well for seeding, HepG2 cells were seeded into 96-well plates at a varying density of 0–4 x 10^4 cells/well and incubated for 48 hours at 37 °C in a humidified atmosphere containing 5% CO_2. The medium was removed, and the cells were gently washed with PBS. A neutral red (NR) working solution (40 µg/mL in serum-free medium) was prepared from neutral red stock solution (4 mg/mL; 40 mg neutral red dye in 10 mL PBS). The NR working solution was centrifuged for 10 min at 4000 g to sediment dye crystals. A 100 µL aliquot of NR working solution was added to each well, and the mixture was incubated for 2 hours at 37 °C to allow dye uptake by viable cells. Post-incubation, cells were washed with 150 µL of PBS/well and the NR dye was then extracted using NR destain solution (50% ethanol, 49% distilled water, and 1% glacial acetic acid). Plates were gently shaken for 10 min to ensure complete dye solubilisation. Absorbance was measured at 540 nm using a microplate reader.

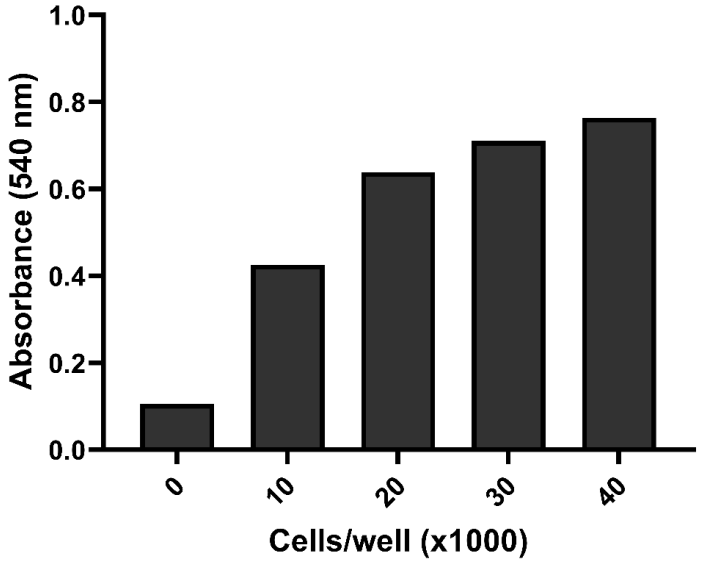

Figure 3.3 Relationship between the number of cells per well and the absorbance at 540 nm after neutral red uptake assay.

The optimal cell density, as shown in **Figure 3.3**, was determined to be 2×10^4 cells per well. For subsequent experiments with E171 and P21, wells were seeded with 2×10^4 cells and treated with varying concentrations of E171 and P21 (0, 5, 50, 100, and 200 µg/mL), both in the presence and absence of OA (0.25 mM) dispersed in culture medium. Cells were incubated for 48 hours following treatment. For neutral red uptake, the aforementioned steps for cell optimisation were followed. All experiments were performed in triplicate, and the resulting data were analysed to assess the dose-dependent cytotoxic effects of E171 and P21.

3.11 Oil red O (ORO) staining

ORO staining detects intracellular neutral lipids by binding to neutral lipids such as triglycerides and lipid droplets (cholesteryl esters) in HepG2 cells, allowing visual assessment of steatosis under a microscope. For quantification, the bound dye is eluted with isopropanol and measured spectrophotometrically, reflecting lipid accumulation (Du et al., 2023).

Based on the initial screening, 0.25 mM OA was selected as the optimal concentration for inducing steatosis. In subsequent experiments, cells were treated with or without 0.25 mM OA, with or without E171 or P21 at 5, 10, or 50 µg/mL for 48 hours. Following treatment, cells were washed with PBS and fixed with 10% formalin (Sigma-Aldrich, USA) in PBS at 37 °C for 2 hours. Formalin was removed with a pipette, and cells were washed twice with ddH_2O. Cells were treated with 60% isopropanol for 5 min at RT and then allowed to dry completely. ORO stock solution (ORO; Sigma-Aldrich) was prepared by diluting 0.35 g of ORO in 100 mL of isopropanol (Sigma-Aldrich) using a stirrer, filtering through a 0.22 µm membrane filter, and storing at RT. The ORO working solution was prepared by mixing 6 mL of ORO stock solution with 4 mL of ddH_2O, allowing it to sit at RT for 20 min, then filtering. ORO working solution (2 mL) was added to each well, and the mixture was incubated at RT for 10 min. ORO working solution was removed, and cells were washed 5 times with ddH_2O. Stained cells were visualised using a light microscope equipped with a digital camera (EP50, Olympus, Auckland NZ), and images were captured at 20× magnification. For ORO quantification, the cells were dried with a low-heat hairdryer to ensure complete evaporation of residual moisture. ORO dye was eluted from the dried cells by adding 1 mL of 100% isopropanol and incubating for 10 min with gentle shaking. This solution was then transferred to a 1.5 mL microcentrifuge tube. Optical density (OD) was measured at 500 nm in the plate reader using 100% isopropanol as a blank.

3.12 Haematoxylin staining

Haematoxylin counterstaining was performed following ORO staining to enhance cellular contrast and facilitate morphological assessment. While ORO selectively stains neutral lipids in red, haematoxylin selectively binds to nucleic acids, staining cell nuclei blue-purple. For haematoxylin staining, 2 mL of Mayer haematoxylin (potassium alum 50 g, distilled water 1000 mL, haematoxylin 1 g, sodium iodate 0.2 g, acetic acid 20 mL) was added to each well for 1 min, then washed 5 times with ddH_2O, followed by imaging.

3.13 Triglyceride quantification assay

The triglyceride quantification assay operates by enzymatically hydrolysing triglycerides into glycerol and FFAs. The liberated glycerol is then oxidised, generating hydrogen peroxide, which reacts with a probe to produce a colourimetric or fluorometric signal. The intensity of this signal is directly proportional to the triglyceride concentration.

Triglyceride was quantified in TiO_2 NPs treated HepG2 cells using a commercially available Triglyceride Quantification Kit (Abcam, Cambridge, UK), following the manufacturer's instructions. Cells were seeded at a density of 8×10^5/well in a 6-well plate. After 24 hours, cells were treated with E171 or P21 (at 0, 5, or 50 µg/mL) with or without OA for 48 hours. Cells were then trypsinised and washed with cold PBS twice. Cells were resuspended and homogenised in 1 mL of 5% Nonidet P-40 substitute (Sigma-Aldrich, USA) by gently pipetting, followed by slowly heating the samples to 95–100°C in a thermomixer for 2–5 min. Samples were then centrifuged for 2 min at 13000 x g to remove any insoluble material. Supernatants were transferred to a new Eppendorf tube (1.5 mL) and diluted 10-fold with ddH_2O. Samples and standards (50 µL each) were loaded into a flat-bottom black 96-well plate (BMG LabTech, Ortenberg, Germany), and 2 µL of cholesterol esterase/lipase was added to each well. The samples were then gently mixed and incubated for 20 min at RT in the shaker. Master mix (containing assay Buffer, oxiRed™ Probe, and Enzyme Mix VI) was prepared according to the manufacturer's protocol, and 50 µL was added to each well, and the plate was incubated for 60 min at RT in the dark. Fluorescence intensity was measured at an excitation wavelength of 544 nm and an emission wavelength of 590–10 nm, using a microplate reader.

Triglyceride concentrations were calculated using a standard curve generated from known triglyceride standards (0–1 nmol/well) included in the kit. The concentration of triglycerides (mM) was calculated using the formula, triglyceride = (B/V) × D, where B is the amount of triglyceride from the standard curve, V is the sample volume, and D is the dilution factor applied before assay setup.

3.14 Total cholesterol (TCHO) quantification assay

Total intracellular cholesterol levels were measured in TiO_2 NPs treated HepG2 cells using a commercially available Total Cholesterol Assay Kit (Abcam, Cambridge, UK), following the manufacturer's protocol. Cells were seeded at a density of 8×10^5/well in a 6-well plate. After 24 hours, cells were treated with E171 or P21 at 0, 5, or 50 µg/mL, with or without OA for 48 hours. Cells were then trypsinised and washed with cold PBS twice.

After treatment, HepG2 cells were harvested and lysed by adding 200 µL of Chloroform: Isopropanol: NP-40 substitute (7:11:0.1) to all samples. Cell lysis was achieved by homogenising the samples at high speed for 2 min using a homogeniser (ULTRA-TURRAX T-10, IKA-Werke GmbH & Co. KG, Staufen, Germany). The lysates were centrifuged at 10000 × g for 10 min at 4 °C to remove cellular debris. To remove chloroform, the organic phase was transferred to a new Eppendorf tube (1.5 mL) and air dried at 50 °C for 40 min. To further remove chloroform traces, samples were centrifuged using a vacuum concentrator attached to an aspirator pump for 30 min, until any residual organic solvent was removed, yielding a dry pellet. Dried lipids were dissolved in 200 µL of the assay buffer provided in the kit and vortexed until the mixture was homogeneous. Samples were diluted 1:10 according to the manufacturer's instructions, and the fluorometric reaction mix was prepared as specified in the protocol. For each reaction, 50 µL of the fluorometric reaction mix was added to 50 µL of standards, controls, and sample wells in a black, clear-bottom 96-well plate (Thermo Fisher Scientific). The contents were mixed using a horizontal shaker and incubated for 60 min at 37 °C, protected from light. Fluorescence intensity was then measured at an excitation wavelength of 544 nm and an emission wavelength of 590–10 nm.

A standard curve (0–0.5 µg/well) was generated and used to calculate the total cholesterol concentration of the unknown samples in (µM) by using the formula, Total cholesterol concentration = (A/V) x D, where A is amount of cholesterol determined from standard curve, V is volume of sample added into the reaction well and D is the dilution factor.

3.15 Reactive oxygen species (ROS) detection

ROS generation was assessed using the commercially available peroxide-sensitive fluorescent probe 2',7'-dichlorofluorescein diacetate (H_2DCFDA) (Thermo Fisher Scientific). HepG2 cells were seeded at a density of 2×10^4 cells per 100 µL in a black, clear-bottom 96-well plate for 24 hours. After 24 hours, cells were incubated with 5 µM H_2DCFDA for 1 hour at 37 °C in the dark to allow probe uptake and oxidation, followed by treatment with E171 or P21 at 5 or 50 µg/mL, with or without OA, for 5 hours. After incubation, cells were washed with PBS to remove excess dye. The resulting intracellular fluorescence of dichlorofluorescein (DCF), indicative of ROS levels, was measured using a microplate

reader with excitation and emission wavelengths set at 544 nm and 590–10 nm, respectively. Hydrogen peroxide (1000 µM) was used as a positive control for ROS induction. Corrected absorbances were obtained by subtracting the absorbance values of treated cells from those of blanks containing the same amount of DMEM and E171/P21. Fluorescence intensity was measured at Ex/Em=485/535 nm, and values were expressed as relative fluorescence units (RFU).

3.16 Total antioxidant capacity (TAC) assay

The TAC of HepG2 cells was measured using a commercially available TAC Assay (Abcam, UK) following the manufacturer's protocol. Cells were seeded at a density of 8×10^5/well in a 6-well plate. After 24 hours, cells were treated with E171 or P21 at 5 or 50 µg/mL) with or without OA for 48 hours. Cells were trypsinised and washed with cold PBS twice. Cells were resuspended in 100 µL of ddH20 followed by homogenisation with a homogeniser (ULTRA-TURRAX, T-10, IKA-Werke GmbH & CO, Stauffen, Germany). Cell homogenate was kept on ice for 10 min, followed by centrifugation at 10000 × g for 10 min at 4 °C to remove debris; the supernatant was collected for analysis. Aliquots (50 µL) of cell lysates were diluted 1:1 with 50 µL of protein mask (to inhibit protein-based antioxidant activity, allowing selective quantification of small-molecule antioxidants) and added to a 96-well plate. Subsequently, 100 µL of Cu^{2+} working solution was added to each sample and standard well. The plate was incubated at RT for 90 min on a shaker, in the dark. Absorbance was measured at 570 nm. Antioxidant capacity was calculated using a standard curve (0–20 nmol/well) generated from Trolox standards (commonly used as a reference compound for quantifying antioxidant capacity (Silvestrini et al., 2023). The values are expressed as Trolox equivalents (mM) by formula, Antioxidant Capacity = (B/V) x D, where B is the amount of antioxidant activity in the sample well derived from the standard curve, V is the volume of sample added to the well, and D is the dilution factor, if the sample was diluted before assay setup.

3.17 Nitric oxide (NO) quantification assay

NO levels were measured in HepG2 cells using a commercially available Nitric Oxide Assay Kit (Sigma-Aldrich, USA) following the manufacturer's instructions. Cells were seeded at a density of 8×10^5/well in a 6-well plate. After 24 hours, cells were treated with E171 or P21 at 5 or 50 µg/mL with or without OA for 48 hours. Cells were trypsinised and washed with cold PBS twice. After experimental treatments, cell culture supernatants were collected and centrifuged at 14000 × g for 5 min to remove debris. The clarified supernatants were subjected to deproteinisation prior to NO analysis. For this, 8 µL of zinc sulfate solution (0.3 M) was added to each sample and vortexed briefly. Subsequently, 8 µL of sodium hydroxide (2N) solution was added, followed by another vortexing step. The mixture was then centrifuged at 14000 × g for 10 min at 4 °C to remove precipitated proteins. The resulting clear supernatant was collected and used for NO quantification.

A volume of 100 µL sample was mixed with 200 µL Griess reagents (containing sulfanilamide and N-(1-naphthyl) ethylenediamine dihydrochloride) in a 96-well plate and incubated at 37 °C for 60 min. Absorbance was measured at 540 nm. Nitrite concentrations were calculated using a standard curve (0–100 µmol/well) generated from sodium nitrite standards provided in the kit by formula, Nitric Oxide (µM) = (OD_{Sample}– OD_{Blank}/slope) x DF, where DF stands for dilution factor.

3.18 Lipid peroxidation assay

Lipid peroxidation was assessed to evaluate oxidative damage in HepG2 cells following treatment with TiO_2 NPs and/or OA. The assay was performed using a commercially available Lipid Peroxidation (MDA) Assay Kit (Abcam, UK), which quantifies malondialdehyde (MDA), a stable end-product of lipid peroxidation. Cells were seeded at a density of 8×10^5/well in a 6-well plate. After 24 hours, cells were treated with E171 or P21 at 5 or 50 µg/mL with or without OA for 48 hours. After treatment, cells were washed with cold PBS, harvested, and lysed using the kit's lysis buffer. Cell lysis was performed by homogenising the samples on ice, followed by sonication until the lysates appeared visually clear. Lysates were centrifuged at 13000 × g for 10 min to remove cellular debris. The supernatant was collected for analysis and kept on ice. Aliquots of the cell lysates (200 µL) were mixed with the kit developer mix (600 µL) and incubated at 95 °C for 60 min. After cooling to RT, samples were centrifuged to remove precipitates. The absorbance was measured at 532 nm. MDA concentrations were calculated using a standard curve (0–0.5 nmol/well) generated from known MDA standards and expressed as MDA amount (µM).

3.19 Measurement of E171 and P21 cellular uptake in HepG2 cells by turbidity meter

To evaluate the cellular uptake of E171 and P21, a methodology modified from (Zhang et al., 2021) was used. HepG2 cells were seeded into 12-well plates at a density of 3×10^5/well and incubated overnight for 24 hours at 37 °C. Following initial incubation, cells were treated with/without 0.25 mM OA and E171 or P21 (at 5, 10, or 50 µg/mL) for six hours. After treatment, cells were washed three times with PBS to remove unbound nanoparticles and media. Cells were then detached using 0.25% trypsin-EDTA solution and collected by centrifugation at 200 × g for 5 min. To remove any loosely adhered particles, the cell pellets were resuspended in PBS and centrifuged three additional times, with supernatant decanted after each wash. The final cell pellets were ashed in a muffle furnace for 12 hours to eliminate organic material. The resulting ash was digested in 20 mL of concentrated sulfuric acid on a hot plate until complete dissolution. The digested samples were then diluted to a final volume of 80 mL with DI water to ensure complete release of internalised or surface-adhered nanoparticles. The Ti content in the digested samples was quantified using a turbidity meter (Hach, USA) at 410 nm. Each sample was measured in triplicate, and the average value was recorded. The entire experiment was repeated three times, and a 20% sulfuric acid solution was used as a negative control to account

for background turbidity. To calibrate the instrument for Ti detection, a standard curve was generated by digesting various concentrations of E171/P21 powder (0, 2.5, 5, 10, 20, 25, 50 µg/mL) in 25% sulfuric acid solution. The resulting absorbance values were used to generate a calibration equation, and the amount (µg) of sorbed E171/P21 was calculated from the standard curve and reported as % recovered.

3.20 Microscopy and image acquisition

Microscopic analysis was performed to visualise cellular morphology, evaluate cytotoxicity, and staining outcomes following various treatments.

For all assays, cells were examined using a light microscope (CKX41, Olympus, Japan) at 20× magnification equipped with a digital camera (EP50, Olympus, Japan). All images were acquired under consistent exposure settings and analysed using EP50 imaging software.

Part C. Data processing

3.21 Statistical analyses

Summary statistics relating to the dietary survey (**Chapter 4**) and individual product testing (**Chapter 5**) parts of this study were derived using standard statistical functions in Microsoft Excel. Most of the mathematical calculations were also undertaken using (suitably formatted and populated) Microsoft Excel spreadsheets.

Statistical analysis of cell cultures was performed using one-way or two-way ANOVA, as appropriate, and Tukey's multiple-comparison test, with a significance level set at $p<0.05$. Statistical analysis was performed using GraphPad Prism (Prism 10 for Windows, version 10.6.1; GraphPad Software, La Jolla, California, USA).

CHAPTER 4: Estimation of dietary intakes of Ti in NZ residents

4.1 Introduction

The amount of titanium (Ti) in the human body is estimated to range from 10–20 mg, making Ti the fourteenth most abundant element (Buettner & Valentine, 2012). This body burden represents a balance of inputs and losses, where essentially all quantifiable inputs can be assumed to be dietary – through ingestion of Ti in food. Like many trace elements, dietary intakes of Ti may come from both natural and anthropogenic sources.

The most common Ti compound is titanium dioxide (TiO_2), which constitutes almost 95% of all Ti consumed (Gázquez et al., 2014). TiO_2 was approved as a food additive in 1966 in the US, by the Food and Drug Administration (FDA), while in the EU it was approved as a food additive in 1969. In the food industry, TiO_2 is known as E171 in the EU, and INS 171 in the US (Boutillier et al., 2022; Parrino & Palmisano, 2020). Since then, it has been used as a food additive throughout the world and is present in food products, including preserved fruits, chewing gum, coated candy, dairy products, sauces, icings, and other consumer products such as toothpaste, tattoo ink, beauty creams, sunscreen, and medicinal tablets (La Maestra et al., 2021).

Before E171 was approved as a food additive in 1969, natural sources would have predominated dietary intake. The chemical forms of Ti across natural food sources have not been characterised. Still, they may range from food-associated soil minerals (e.g., TiO_2 and $FeTiO_3$) to complexes with biological ligands to oligomeric clusters. Ti(III) and Ti(IV) are the most common oxidation states of Ti, and under most aerobic environmental conditions, Ti(IV) is favoured. It is not known whether Ti is an essential element in humans (Zierden & Valentine, 2015). However, if it is required, it is sufficiently abundant that dietary deficiency is unlikely to occur, and attempts to induce a Ti-deficient diet have been unsuccessful (Buettner & Valentine, 2012). At the outset of this study, the natural baseline intake of Ti in adults was not precisely known but could be estimated in order of magnitude terms. Assuming a mean [Ti] in food of 0.3 mg/kg, ingestion of 2.5 kg of food per day, and a 70 kg body weight gives an estimated intake of 10 µg/kg-bw/day.

In the decades since approval of E171 as a food additive, this source would have become a significant to major component of total Ti intakes in many countries. E171 is also likely to have become the sole anthropogenic dietary source of Ti of any significance. However, it should be recognised that for this source of Ti, biological activity will be determined by the fact that E171 comprises highly inert and insoluble particle (Skocaj et al., 2011). In E171, the presence of Ti could be seen as being 'almost incidental,' or at least a secondary factor, in relation to potential health effects. Health effects from E171 are likely to be related to the presence of insoluble particles, and possibly their surface

mineralogy, but not their internal makeup. Active Ti(IV) biochemistry is unlikely to be a significant factor, in the way that it may (potentially) be with a component of natural dietary Ti.

Overall, natural dietary Ti sets a baseline that has not been well characterised but may include various Ti(IV) complexes and compounds, and (with some foods) potential inorganic micromineral forms from soils. E171 technically adds to the dietary Ti baseline but is likely to primarily act as a vehicle for the delivery of inert insoluble particles. Active Ti(IV) biochemistry is unlikely to play a more than minor part in the biological effects of E171.

Studies of dietary Ti have been complicated by both the relative difficulty of testing for Ti and the presence of E171. The first factor has meant that relatively few studies have been undertaken, compared with (for example) toxic heavy elements such as arsenic, lead, cadmium, or mercury. The second factor has led to dietary intake estimates including E171. A term such as 'baseline' will usually reflect a typical modern intake estimate (with E171 present), rather than a natural intake (E171 absent). Results may be reported as either concentrations of Ti or of TiO_2 (E171). With these provisos, studies/reports representing the estimated intakes of Ti (as TiO_2 equivalents) in both children and adults are compiled in **Table 4.1**.

Table 4.1 Studies reporting the estimated consumption of TiO_2 in children and adults.

Country/area	Estimated intake (mg/kg/day) in		References
	Adults	Children	
UK	1	2–3	(Weir et al., 2012)
US	1–2	0.2–0.7	(Weir et al., 2012)
Denmark	0.7–1.4	1.7–2.6	(Bachler et al., 2015)
Netherlands	0.6-0.7	1.3–1.5	(Sprong et al., 2016)
Europe	0.3-4	0.5–3.7	(EFSA, 2016)
Europe	0.3-3.8	0.6–6.9	(Younes et al., 2021)

It might be noted here that these estimates are substantially higher than might be expected from natural dietary Ti (estimated above as being in the likely area of 10 µg/kg-bw/day for Ti in a 70 kg adult, approximately 17 µg/kg-bw/day as TiO_2 equivalents). For example, even the low-end estimates for European adults of 300 µg/kg-bw/day **(Table 4.1)** are about 18 times higher than this figure. This difference underscores the significance of E171 as a dominant dietary Ti source when it is present in a significant proportion of food items.

Food surveys to assess E171 consumption in a population provide essential data on exposure levels and potential health impacts. By evaluating real-world consumption and associated risks, these surveys can contribute to understanding the exposure risks. Globally, there have been few food surveys analysing population exposure to E171 **(Table 4.1)**.

TiO_2-containing food and consumer products are readily available on NZ supermarket shelves. However, prior to this research, no surveys of dietary Ti or E171 intake among the NZ population have been conducted.

The most systematic dietary intake survey carried out in NZ is the periodic (5–10 yearly) New Zealand Total Diet Study (NZTDS), undertaken by New Zealand Food Safety, a branch of MPI. Each NZTDS covers a range of contaminant elements, but Ti is omitted.

Furthermore, potential intakes in NZ cannot be reliably derived from historical estimates from other jurisdictions (as shown in **Table 4.1**). This is for two reasons:

- Changes between (formerly comparable) jurisdictions: the ban on use of E171 as a food additive in the EU countries, with ongoing use in others (the US, Australia, New Zealand), is likely to have altered the consumption picture between countries that ban this use of E171, and those that do not.
- Changes over time: manufacturers that export to EU countries will have been altering the formulations of applicable product lines to meet the updated requirements. With larger-scale manufacturers that have used E171, e.g., the confectionery company Mars Inc., more product lines will likely become E171-free to meet EU market requirements, and the same products will be sold into Australian and NZ markets. This factor implies that in some countries, E171 intakes will now be lower than they were at the date of a previous research publication. It should also be noted that all of the studies referenced here were conducted pre-ban. In addition, although NZ intakes have not previously been quantified, they may have been decreasing in response to the ban on E171 in significant offshore markets. It should be acknowledged that it has been recognised that the use of E171 in NZ may pose various (unspecified and unquantified) risks to the food industry.
- King et al. (2024) identified the use of E171 as a food additive as one of 166 so-called ‘emerging’ food risks for NZ, in the context of ‘horizon scanning’ for substances that may cause risks for the NZ food industry, in order to prioritise research needs. In this context, E171 was categorised with 53 other substances as “no action at this time (keep watch).” This categorisation can be interpreted as meaning that risks to the NZ food industry (as a whole, including food production, importing, exporting, or retailing) from the presence of E171 in

some products are currently thought to be low, but of possible future concern. Ranking possible risks to the food industry in this way is an important exercise for prioritising research funding but is no substitute for research on the actual presence of E171 in NZ products, and dietary intake estimates of Ti and E171 in NZ.

Thus, there are significant gaps in our understanding of Ti or E171 in NZ products, the likely exposures of New Zealanders, and the future ability to assess any potential public health implications of those exposures. This research was undertaken to begin to address these gaps.

The aims of the study set out in **Chapters 4** and **5** are therefore as follows:

1. To estimate dietary intakes of Ti in NZ across 10 age, gender, and ethnicity categories.
2. To identify which food groups are likely to contribute the most to these intakes.
3. To distinguish between natural baseline intakes and those attributable to E171.
4. To identify the foods most likely to contain E171, and its prevalence and levels in food types where it has been commonly used.
5. To estimate the possible (upper) intakes of E171 in individuals who may routinely use or consume one or more E171-containing food products.

Aims 1–3 relate to average dietary intakes and are explored in this chapter. Aims 4 and 5 relate to prevalence in individual foods and possible upper-end intakes and are the focus of **Chapter 5**.

For the broad intake estimates (this chapter), the methodologies adopted parallel those used in the NZTDS. The survey year is 2024, and the 10 age, gender, and ethnicity categories are as used in the most recently published NZ Total Diet Study Pearson et al. (2018): males 19–24 yrs, males >25 yrs; females >25 yrs; Pacific females >15 yrs; Pacific males >15 yrs; boys 11–14 yrs; girls 11–14 yrs, children 5–15 yrs; pre-school children 1–3 yrs; and infants 6–12 mo.

4.2 Methods

Details of the methodology, including laboratory operations applied in this part of the study, are provided in **Chapter 3** (**Section 3.2**).

As outlined above, the overall methodology adopted in this study was based on that used in the most recently published NZTDS Pearson et al. (2018), with a selection of a representative range of foods across 10 food categories. NZ food intake estimates for the 10 age, gender, and ethnicity categories were based on Smith et al. (2017), kindly provided by the MPI. For the development of the composite groups, foods were allocated to 40 groups across 10 major categories. Each of the 40 main composite groups comprised between 1 and 4 key foods, and a total of 136 key foods were analysed in this part of the study. **Appendix 4.1** provides complete information on the key foods analysed and their 14-day intakes across 10 age and gender groups, with many of these foods represented by composites that include multiple brands, varieties, or examples to ensure comprehensive representation.

All samples were purchased from Wellington supermarkets, Woolworths (formerly Countdown), Pak ‘n Save, and New World, except beef, chicken, and liver, which were sourced from a local butcher. Composite food samples were prepared by combining individual foods to a total of around 100 g. The amount of all food on each composite was properly mixed to achieve uniformity.

Analytical methods in brief (see **Section 3.2** for full details) involved digestion of weighed subsamples in concentrated sulfuric acid, followed by filtration, dilution, and the addition of hydrogen peroxide to form the peroxotitanium (IV) sulfate complex. Analysis was by UV-visible spectroscopy for samples containing enough Ti to show a visible colour, and Graphite Furnace Atomic Absorption Spectroscopy (GFAAS) for the lower-level (colourless) samples. Example calibration curves for each method are shown in **Figures 4.1** and **4.2**.

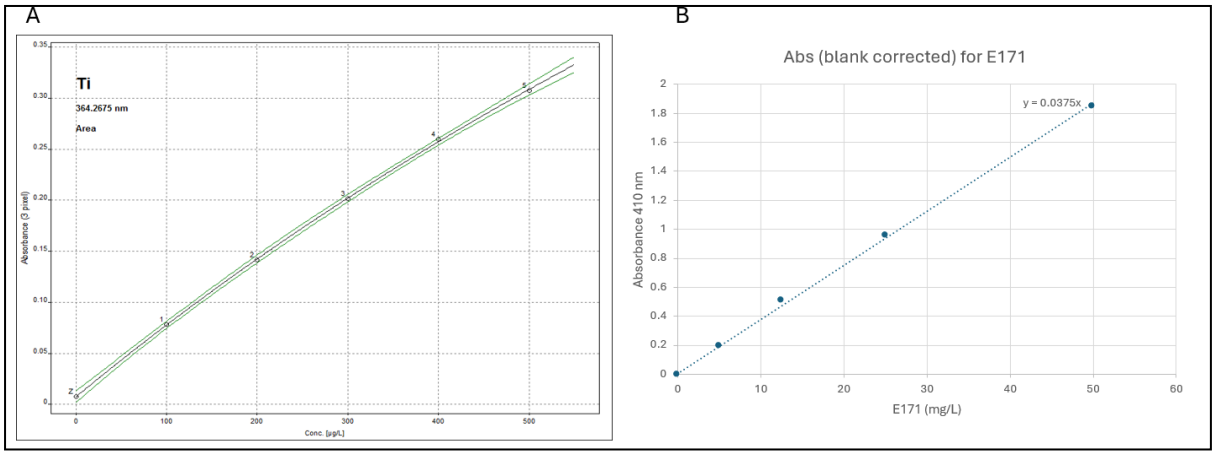

Figure 4.1 Example standard curves for Ti obtained by GFAAS (A) and UV-vis spectrophotometry (B).

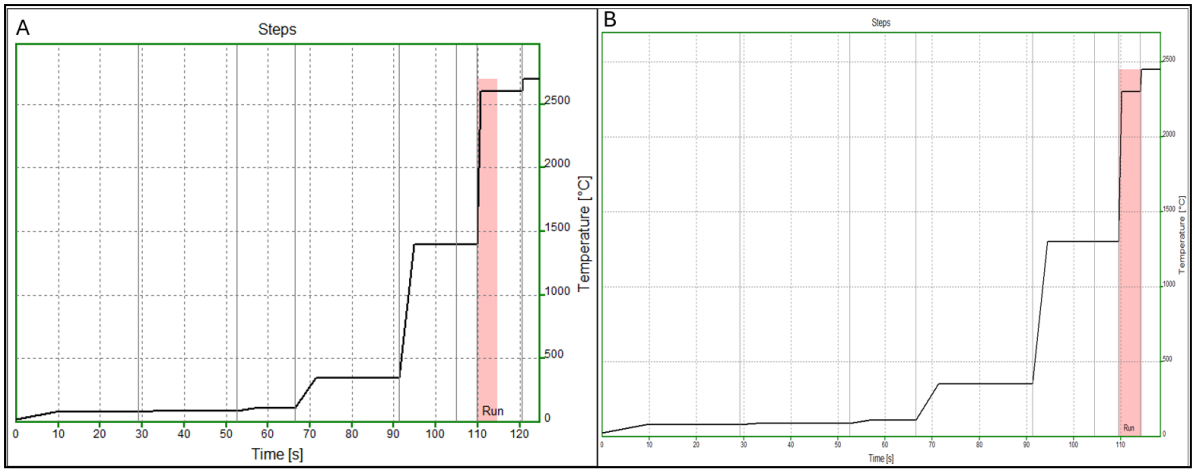

Figure 4.2 GFAAS furnace heating steps used for analysis of Ti (A, see also Table 3.1) and Cr (B, see also Table 3.3).

4.3 Results and discussion

4.3.1 Concentrations of Ti, Zn, and Cr in food composites

Mean wet weight concentrations of Ti, Zn, and Cr in the food composites (as consumed) are provided in **Table 4.2**. Classification of food composites is based on individual food consumption from NZTDS 2016, followed by grouping similar foods into composites. Ash weight concentrations of Ti in the food composites are provided in **Appendix 4.2**.

Table 4.2 Concentrations of Ti, Zn and Cr in the food composite samples (mg/kg wet weight, as consumed, each value is the mean of 3 measurements). Non-detects are shown to two decimal places.

Major (operational) category	Composite No.	Composite group	Metal concentration (mg/kg, as consumed)		
			Ti	Zn	Cr
Fruits	1	Pip fruit/Kiwi fruit	0.368	2.34	0.014
	2	Stone fruit	<0.31	3.76	0.023
	3	Citrus	<0.21	1.11	0.011
	4	Berries	0.427	1.20	0.024
	5	Tomato	<0.14	1.53	0.014
	6	Others	<0.35	2.56	0.006
Vegetables and fungi	7	Root vegetables	<0.32	7.57	0.002
	8	Tubers	0.352	2.37	0.008
	9	Leafy vegetables	0.387	4.97	0.002
	10	Squash/Creeping veg	<0.15	2.41	0.006
	11	Seed/Other	0.46	3.63	0.023
	12	Dried fruits	0.686	3.64	0.101
Grain and cereal-based foods (carbohydrate rich)	13	Bread	0.417	9.95	0.024
	14	Rice or rice-based	0.612	6.04	0.018
	15	Breakfast cereals	0.673	23.1	0.078
	16	Pasta, spaghetti, noodles	<0.38	8.36	0.016
	17	Biscuits	0.631	5.61	0.042
	18	Cakes	<0.36	3.44	0.034

(Table 4.2 continues over…)

Table 4.2 continued….

Major (operational) category	Composite No.	Composite group	Metal concentration (mg/kg, as consumed)		
			Ti	Zn	Cr
High protein foods (meat/chicken/fish / other)	19	Chicken	0.765	10.4	0.039
	20	Beef	0.815	59.4	0.034
	21	Pork	0.854	17.0	0.024
	22	Fish	<0.37	3.25	0.055
	23	Other seafood	0.579	38.5	0.072
	24	Eggs	1.17	17.6	0.012
	25	Nuts	0.709	25.3	0.109
	26	Others (composite foods, tofu, and beans)	<0.16	6.12	0.040
Dairy foods	27	Milk	<0.1	1.30	0.009
	28	Milk products 1	<0.33	11.9	0.038
	29	Milk products 2	14.8, 0.814[a]	0.345	0.029
Drinks (beverages) and soup	30	Water	<0.03	0.013	<0.001
	31	Juices and carbonated beverages	<0.01	0.057	0.002
	32A	Tea	0.006	14.9	0.001
	32B	Coffee instant & drinking chocolate	0.065	6.53	0.029
	32C	Caffeinated beverage	<0.01	0.027	0.003
	33	Alcoholic drinks	<0.01	0.176	0.005
	34	Soup	<0.1	0.405	0.022

(Table 4.2 continues over…)

Table 4.2 continued….

Major (operational) category	Composite No.	Composite group	Metal concentration (mg/kg, as consumed)		
			Ti	Zn	Cr
Spreads, condiments and flavourings	35	Spreads	0.39	0.425	0.012
	36	Condiments and flavourings	<0.13	0.298	0.038
Snack foods and chocolate	37	Snack foods and chocolate	<0.24	9.64	0.082
Preschool and infant foods	38A	Pre-school (1-3 years)	<0.24	11.1	0.048
	38B	Infant foods (6-12 mo)	0.647, 0.350[b]	23.3	0.033
Others	39	Sugar	<0.21	0.046	0.003
	40	Oil	<0.39	<0.01	0.001

*Notes:
[a]for Composite 29, the original measurement was 14.8 mg/kg, but this was traced to one product. Following analysis of 11 individual products, the original result was found to be *unrepresentative* (the E171-containing product accounted for only 9% of the sample set); therefore, the refined estimate for this composite group is 0.814 mg/kg. See text for more details.
[b]for Composite 38B, the original mean was 0.647 mg/kg, but one of the three subsamples was suspected to be an outlier. Further analysis was undertaken for 13 individual foods in this category to provide a more reliable estimate of the mean, which was 0.350 mg/kg. See text for more details.

4.3.2 Ti results by food type

FSANZ permits E171 in food under Good Manufacturing Practice (GMP), with no set legal limit in Australia or NZ (FSANZ, 2022). However, in the US, the legal limit for E171 in food is 1% by weight (USFDA, 2016), which corresponds to 0.6% (or 6000 mg/kg) Ti (Younes et al., 2021). Concentrations of Ti in all the food composites analysed were well below this value.

4.3.2.1 Eggs

In this study, the highest concentration of Ti (1.17 mg/kg) was found in the 'eggs' composite (Composite 24, **Table 4.2**). In comparison, a previous study by Altun et al. (2019) reported levels of naturally occurring Ti in free-range hen eggs across three seasons (spring, summer, and autumn), ranging from 2.13 to 3.94 mg/kg.

Altun et al. (2019) employed a digestion approach similar to that used in other validated studies, applying a mixed nitric acid/hydrogen peroxide solution (0.75 65% HNO_3 + 0.25 30% H_2O_2). Using this method, they reported a recovery of 101% for titanium in the Certified Reference Material NIST 1515 Apple Leaves, which contains 10 mg Ti/kg. These results suggest that the values reported for the tested

eggs are likely reliable. Results from this study (1.17 mg/kg) are 1.8–3.3 times lower than those of Altun et al. (2019), though they are in the same order of magnitude. Differences of this type may come down to the type of egg production system and how it determines feed type and feeding habits. For example, assuming that ingested soil makes a significant contribution to Ti intakes in chickens, free-range hens are likely to consume more soil than cage-free hens (which are housed in a barn but range within that area), which may, in turn, ingest more soil than fully caged hens.

In contrast, Dobrzański et al. (2020) reported that the levels of Ti in egg white and egg yolk were in the range 0.04–0.17 mg/kg. These results seem unusually low compared to those of Altun et al. (2019) or to those of this study by 1–2 orders of magnitude. Dobrzański et al. (2020) did not report recovery of Ti from a known sample, so their results for this element are not considered validated. A low recovery may have resulted from the authors' multi-element analysis with a nitric acid digestion step, with no additional oxidising agent (H_2O_2 or equivalent), or from an aspect of their microwave digestion methodology that was not as rigorous as that used by other authors. As part of the method development for this thesis, both Ti powder and E171 were found to be largely resistant to dissolution in concentrated nitric acid.

4.3.2.2 High protein foods

The high-protein food category in this study (**Table 4.2**) included composites of chicken, beef, pork, fish, seafood, and nuts, with Ti levels ranging from <0.16 to 0.854 mg/kg. Ti concentrations in beef, pork, and chicken were 0.815, 0.854, and 0.765 mg/kg, respectively. These findings are consistent with those reported by An et al. (2024), indicating Ti levels in chicken ranging from 0.4 to 0.91 mg/kg.

Once again, at least one source provides a substantially lower figure for Ti in meat products. Wu et al. (2016) reported values of 0.0006 mg/kg in beef and 0.0003 mg/kg in pork. These authors used a simple nitric acid digestion (1 g sample to 5 mL conc. HNO_3 heated to 160 °C for four hours and then a hot plate at 110 °C to remove the acid), with quantification for 14 trace elements (Cd, Hg, Pb, As, Cr, Cu, Fe, Zn, Mn, Mo, Ni, Co, Se and Ti) in 22 meat samples.

Ti concentrations reported by Wu et al. (2016) in beef and pork are therefore between 667–3000 times lower than the 0.4–0.91 mg/kg range determined by An et al. (2024) which encompasses approximately 0.8 mg/kg results for beef and pork from this study. Such unusually low results probably reflect incomplete dissolution of Ti during an acid-digestion step intended for standard trace-element analysis.

These comparisons suggest the following:

- A proportion of literature values for Ti in food samples may be orders of magnitude lower than their actual values.

- This may more commonly occur when authors have used a standard nitric acid extraction to quantify a range of trace elements, and Ti has been included with the elements subsequently assayed (typically by ICP-MS) in sample digest solutions. Apparently, low values may reflect resistance of Ti to nitric acid dissolution, though there may be exceptions depending on other aspects of the extraction conditions.
- If there is a choice between two order-of-magnitude ranges, the higher one may be more credible.
- The most reliable papers will be those for which Ti recovery has been quantified and reported against reference samples (e.g., as in **Table 3.2** of this study, or the Apple Leaves assessed by (Altun et al., 2019).

In what follows, results from other workers are reported as they are, but the above aspects should be borne in mind.

4.3.2.3 Fruit and vegetables

For the various fruit and vegetable composites, concentrations range from <0.15 to 0.686 mg/kg (**Table 4.2**). The lowest levels (below the DL of 0.15 mg/kg) were observed in squash composites, while the highest (0.686 mg/kg) were detected in dried fruits, followed by berries (0.427 mg/kg). Previous researchers have also reported varying Ti concentrations across different produce. For example, Bakshi et al. (2019) reported a Ti concentration of 2.31 mg/kg in tomatoes, whereas in this study the value was 0.41 mg/kg. Another study by Trebolazabala et al. (2017) reported a range of 0.3–1 mg/kg in tomatoes, and the results in this study fall in this range. Similarly, the Ti concentration of 0.46 mg/kg found in mushrooms (**Table 4.2**) is in the range of 0.03–1.81 mg/kg reported by Siwulski et al. (2021) Although our findings across various fruits and vegetables are consistent with the existing literature, slight variations may be attributed to factors such as soil composition and geographical differences.

4.3.2.4 Grain and cereal-based foods

Concentrations of Ti in the grain and cereal-based foods group (including rice, breakfast cereals, pasta, spaghetti, noodles, biscuits, and cake) were found to range from <0.36 to 0.673 mg/kg (**Table 4.2**).

The concentration in rice (0.612 mg/kg) falls within the range of results (0.01–3 mg/kg) reported by other workers. These include Chung et al. (2018): 0.01–0.31 mg/kg; Xia et al. (2022); 2.4–3 mg/kg; Kollander et al. (2023): 0.01–0.38 mg/kg; and De La Cruz et al. (2024): 0.04–0.42 mg/kg for Italian rice. Results for rice in this study are thus slightly higher than the top end of four studies, but well below the bottom end of the range reported by Xia et al. (2022). Variations between studies may be

attributable to several factors, including differences in rice varieties, environmental contamination, soil composition, agricultural practices, and processing methods.

4.3.2.5 Dairy foods

Within the dairy foods operational category (**Table 4.2**), the 'milk' composite (Composite 27) comprised three actual dairy milk products (dairy milk, 0.5% fat, dairy milk, 3.25% fat, and a flavoured milk), and one non-dairy milk (soy milk) (**Appendix 4.1**). The method involved evaporating 80 mL samples (**Section 4.2.4**) before ashing to achieve the lowest attainable quantification limits. Despite this, Ti was undetectable in the milk composite at a quantification limit of 0.1 mg/kg (**Table 4.2**). Ti was also below the limit of detection (<0.33 mg/kg) in Composite 28 (Milk products 1), which comprised butter, cheese, and yoghurt (**Appendix 4.1**).

In Composite 29 (Milk products 2), Ti was detected at a comparatively high level of 14.8 mg/kg. This composite contained a mix of dairy and 'dairy-like' foods, namely: ice cream, dairy dessert, and coconut cream (**Appendix 4.1**). Further investigation was undertaken by individually testing the following 11 ice-cream, cheesecake, and related products from seven brands (see also **Chapter 5**):

- Kapiti: Triple Chocolate 1 L, Marlborough Salted Caramel 1 L, and White Chocolate and Raspberry 1 piece;
- Lotte: Yukimi Frozen Dessert Vanilla 1 pack;
- Mochi Ice: Coconut ice cream bites 6 pieces (manufacturer redacted)
- Much Moore: Premium Awesome Boysenberry Stracciatella 2L;
- Oreo: Frozen Cookie Sandwich 1 pack;
- Sara Lee: Strawberry Coulis Cheesecake 410 g; and
- Tip Top: Boysenberry Ripple 2L, Slushy Lemonade and Raspberry 1 pack, French Vanilla 2L.

It was established that the high result for 'Dairy products 2' composite was due to one product within containing 96.1 mg/kg Ti, presumably as E171. This was the Mochi Ice product (Coconut ice cream bites 6 pieces; manufacturer redacted).

From results for the 11 products, it was evident that the presence of high Ti (obvious E171) in this food category is not particularly common (1 of 11 samples, or 9% of the sampled set). Excluding this product, concentrations ranged from less than detectable (the lowest DL was 0.31 mg/kg for Tip Top French Vanilla) to 2.46 mg/kg (Oreo Frozen Cookie Sandwich), and the mean value (N=10) was 0.814 mg/kg. Including the anomalous product (N=11) brought the mean up to 9.48 mg/kg, which is in a similar range to the 14.8 mg/kg determined for the original 'Dairy foods 2' composite.

Due to the low (9%) prevalence of E171 in this grouping of foods, the decision was made to exclude the Mochi Ice product from this grouping when calculating 'typical' dietary intake estimates and make use of the lower 0.814 mg/kg figure as being more representative for those purposes (**Table 4.2**). At the same time, it was recognised that a higher routine personal consumption of a specific product would result in a higher individual intake of Ti (and E171). This aspect of 'idiosyncratic' exposure is modelled in **Section 5.4** (**Chapter 5**) for example scenarios.

Results found for [Ti] in the current survey for milk composite (Composite 27: <0.1 mg/kg, **Table 4.2**) are consistent with those of Rompelberg et al. (2016), who reported a [Ti] range of <0.05 (their reported quantification limit) and 0.63 mg/kg (mean 0.31 mg/kg) for raw cow's milk from the Netherlands. Similarly, results for the other two dairy-related composites in this study (Composites 28 and 29: <0.33, and 0.81 mg/kg, **Table 4.2**) are in the ranges reported by the same authors for [Ti] in regular and processed dairy products. These were a mean of 0.47 mg/kg (range <0.05–1.46 mg/kg) for regular dairy products (i.e., milk, yoghurt), and a mean of 0.12 mg/kg (range <0.05–0.57 mg/kg) for processed dairy products (Rompelberg et al., 2016).

4.3.2.6 Drinks and beverages, including soup

Ti concentrations in the drinks (beverages) and soup operational group (**Table 4.2**) were consistently low, ranging from 0.006 to 0.065 mg/kg. Composites within this group included water, juices, and carbonated beverages, tea, instant coffee, drinking chocolate, caffeinated drinks, alcoholic drinks, and soup. For juices, Demir et al. (2020) recorded Ti concentrations between 0.01 and 0.07 mg/kg; the <0.01 mg/kg result for Composite 31 (juices and carbonated drinks) in **Table 4.2** is consistent with this range.

In the case of tea and powdered drinks, the test samples were reasonably-sized (10 g) solids, and the results reported were adjusted assuming specific weights, extraction proportions, and dilutions with 150 mL of water to provide a concentration 'as consumed.' The adjustments and assumptions made for tea, coffee, and drinking chocolate are shown in **Table 4.3**.

Table 4.3 Assumptions made for tea, coffee and drinking chocolate to convert [Ti] from the value measured in the food composite, to a concentration 'as consumed.'

Variable	Unit	Tea	Coffee and drinking chocolate
[Ti] as determined in dry power or leaves	µg/g=mg/kg	4.77	1.44
Weight per drink	g	2.62	6.78[a]
Proportion extracted into the drink	0–1	0.07[b]	1.0
Amount extracted into the drink	µg	0.87	9.75
Water dilution volume[c]	mL=g	150	150
Concentration as ingested	µg/g=mg/kg	0.006	0.065

Notes:
[a] 6.78 g is half the weight of one sachet of the drinking chocolate; based on volume, this was felt to be realistic for most powdered drinks (e.g., powdered coffee);
[b] It was assumed that 7% of the Ti in the leaves is extracted into hot water. This figure is probably realistic as an upper estimate, but may still be an overestimate. It is similar to normal metal bio accessibility through the GI tract, which contains an extraction acid (HCl) and enzymes;
[c] For this calculation, the water is assumed to have no Ti (this is consistent with the NZTDS approach, which assumes distilled water).

For dry tea leaves, the Ti concentration found in this study (4.77 mg/kg, **Table 4.3**) is consistent with the detected range of 2.0–6.9 mg/kg reported by Lim et al. (2021) in an X-ray fluorescence spectroscopy study of 75 commercial teas. The purpose of that study was to establish whether multi-element analysis could be used to trace the regional origin of tea samples, rather than being a dietary intake study. The distinction between [Ti] in the dry product and [Ti] as consumed (**Table 4.3**) is important to bear in mind when taking results of studies involving analysis of tea, powder coffees, powdered hot chocolate, or other products that undergo considerable dilution (and for tea, a partial extraction step) before ingestion. Failure to take these factors into account could result in an erroneous finding that tea, coffee, and other hot beverages dominate Ti intakes.

As another point of comparison, we could expect that [Ti] in tea leaves, derived from the *Camellia sinensis* plant, should be in keeping with [Ti] in plant leaves, in general. This is the case, though [Ti] in plant leaves is quite variable. Dumon and Ernst (1988) noted that, in terrestrial plants, titanium accumulates in a species-specific and organ-specific pattern, with increased concentrations in senescing leaves. Lyu et al. (2017) noted that [Ti] in a tabulation of over 51 plant species (two hyperaccumulators excluded) ranged from 1 to 578 mg/kg with a mean of 33.4 mg/kg. Nineteen of the 51 species (37%) were in the 2–7 mg/kg range, including the results for the tea leaves (4.77 mg/kg) tested as part of this study (**Table 4.3**).

4.3.2.7 Infant foods

The 'infant foods' category was initially planned as a single composite (Composite 38), but subsequently divided into two, to allow for differences in the types of foods eaten by infants (6-12 months age) compared with pre-school toddlers (1–3 years). Composite 38A represented foods eaten by pre-school children, and Composite 38B represented foods consumed by infants (**Appendix 4.1**).

Composite 38A contained [Ti] at <0.24 mg/kg, the DL for the sample tested (**Table 4.2**). In the case of Composite 38B, one of the three subsamples showed a result (0.900 mg/kg) that was more out of keeping with the other two subsamples (0.477 and 0.564 mg/kg) than it should have been, given that these were all the same homogenised composite sample. For this reason, 13 further foods in this category from across the brands Farex (1 item), Natureland (2 items), Only Organic (1 item), Smiling tums (2 items), Watties (4 items), and Aptamil GOLD$^+$, and Karicare GOLD$^+$ (2 items) were analysed individually to provide a more reliable estimate of the mean for infant foods that are sold as such. The mean Ti concentration in these samples plus the two accepted composite results (N=15) was 0.350 mg/kg, with a range from 0.155 to 0.788 mg/kg and a standard deviation of 0.233 mg/kg. The mean value of 0.350 mg/kg was therefore taken as the most reliable estimate of [Ti] for infant foods sold as such.

4.3.2.8 Subsection summary

Overall, Ti results for food types sampled in this survey were consistent with those found from overseas research, where comparisons could be made, with two provisos:

- There is evidence that in some published literature, reported concentrations of Ti in food are up to three orders of magnitude lower than the likely true range, as determined by other researchers and through this study. This vulnerability is not universal but probably relates to the incomplete recovery of Ti from the food sample during a standard nitric acid digestion. In this study, sample digestion was in (heated) concentrated sulfuric acid, in which both E171 and Ti powder will dissolve.
- Where intake estimates involve drinks made from powders or leaves, it would not be appropriate to make use of a concentration as determined. Instead, allowance should be made for both extraction and dilution (**Table 4.3**). For Ti, failure to take these factors into account could lead to the false conclusion that intakes are dominated by tea drinking.

In the composite food survey, only one sample tested positive for suspected E171. This low proportion of samples containing E171 clearly suggests that its presence may not be as prevalent (in NZ in 2024) as has usually been assumed. This topic is further investigated in **Chapter 5**, which focuses more closely on foods that are more likely to contain E171. As outlined above, due to its unrepresentative nature,

this item was excluded from the mean estimate for the composite in which it originally appeared (Composite 29, Milk Products 2). For this study, the Ti concentrations in food composites and the subsequent dietary intake estimates (**Section 4.3.5**) therefore best describe the natural baseline for Ti.

4.3.3 Ti in foods - summary statistics and weighted means

Table 4.4 provides summary information across all composites and weighted mean concentrations for each of the 10 age and gender groups. Overall, 153 samples were tested in this part of the study: the 43 original composites were analysed in triplicate (129 samples), and further testing was undertaken for 24 individual foods to obtain the most reliable estimates to represent food composites 29 (Milk products 2) and 38B (Infant foods).

Table 4.4 Summary of Ti concentrations across all 43 composites, and weighted means for all food consumed by each age and gender group based on dietary composition.

Category	Statistic	Value(s)
Numbers and detections	Total number of samples	129
	Total number of composites	43
	Number of composite non-detects	15
	Percent detects, percent non-detects	62.5, 37.5
Concentrations in foods (mg/kg, as eaten)	Mean (ND=0, **ND=0.5DL**, ND=DL)	0.269, **0.321**, 0.377
	Standard deviation (ND=0.5DL)	0.296
	Median (ND=0.5DL)	0.180
	Geometric mean (ND=0.5DL)	0.170
	Minimum (as detected)[b]	<0.01
	Maximum	1.17
Weighted mean [Ti] across all foods consumed, allowing for dietary composition (mg/kg)	Males 19 to 24 years	0.225
	Males 25 years +	0.200
	Females 25 years +	0.193
	Pacific Females 15 years +	0.240
	Pacific Males 15 years +	0.253
	Boys (11 to 14 years)	0.282
	Girls (11 to 14 years)	0.263
	Children (5 to 5 years)	0.259
	Pre-school (1 to 3 years)	0.236
	Infants (6 to 12 months)	0.302

Notes: [a.] Weighted means are calculated based on amounts of each composite ingested over 14 days (see **Section 4.3.5** for details), and are across all foods, including water and drinks. [b.] For tea, the calculated

'as consumed' value of 0.006 mg/kg is below the <0.01 minimum due to assumptions about extraction and dilution into 150 mL of water – see the text and **Table 4.3**.

Overall, Ti was detected in almost two-thirds (62.5%) of the samples and not detected in the other approximately one-third (37.5%). Assigning non-detects to 0.5DL (DL detection limit, or half the DL expressed as the concentration in food), the overall mean concentration of Ti in foods tested was 0.321 mg/kg or 321 µg/kg (**Table 4.5**). This value is relatively insensitive to how non-detects are treated, varying by only ±16 % (from 0.269 mg/kg when non-detects are set to zero to 0.377 mg/kg when non-detects are set to the DL).

Weighted mean figures for each group are also presented in **Table 4.4**, for convenience. These are calculated by dividing the amounts of each composite ingested over 14 days by the total weight of food consumed over the same period (see **Section 4.3.5** for granular detail) and are across all foods, including water and drinks. These figures allow you to estimate a person's total Ti intake for any of the 10 specified age and gender groups, based solely on the overall amount of food eaten. For example, if a 19–24 yrs old male ingests 2.5 kg of food per day with the composition as used in the last published NZTDS, the amount of Ti they will consume is estimated as 0.225 mgTi/kg x 2.5 kg food = 0.56 mgTi/day. (**Table 4.8** in **Section 4.3.5** shows the average food consumption figures that were used in the last NZTDS, for the ten age and gender groups.)

Interestingly, these weighted means are relatively invariant. They range from 0.193 mg/kg (for 25+ year females) to 0.302 mg/kg (for 6–12-month infants) (**Table 4.4**). The mean and standard deviation are 0.245 mg/kg and 0.04 mg/kg, respectively, giving a %RSD of only 14%.

From this analysis it is already apparent that as a weighted average, infant diets (0.302 mg/kg) may only contain about 26% more Ti than weighted average food ingested by the other nine age and gender groups (0.239 mg/kg), and only 7% more than the corresponding figure for 11–14 yrs old boys (0.282 mg/kg). This implies that body weight will be the main factor determining higher Ti intakes in infants, when expressed as doses (on a mg/kg body weight basis).

4.3.4 Relative abundances of Cr and Zn

4.3.4.1 Relative abundances in the foods

Mean concentrations of Zn and Cr in the food composites are also provided in **Table 4.2**. As outlined in **Section 3.5,** the primary purpose of this testing was to assess the reliability of the overall dietary intake estimation methodology applied for Ti when the same method is applied to Zn and Cr. This is possible because external intake estimates are available for both Zn (from the last published NZTDS) and Cr (from overseas research). During the study, another interesting aspect emerged: despite their different magnitudes, a close correlation exists between [Ti] and [Cr] concentrations across various food categories, and this translates into a similar correlation in natural intakes. Zn and Cr results for

the food composites are therefore presented in this section, and will be discussed further in **Section 4.3.6**, after the intake estimates for Ti.

The first aspect to examine is which foods have the highest and lowest concentrations of Ti, Zn, and Cr. Mean concentrations of the three trace elements in each operational food grouping, and ratios of Ti/Cr and Zn/Ti, are shown in **Table 4.5**. In assessing this data, a distinction was made between the major food groups by mass (**Table 4.5A**) and "other and minor" food groups (**Table 4.5B**). The latter category (including drinks, snack foods, and chocolate, spreads and flavourings, and infant foods) presents a complication for interpreting any 'natural signal' that may exist: one reason for this is that more highly processed foods are more distant from the point of primary production, and/or may be fortified. Results for the major groupings are also expressed as a percentage of the food grouping containing the most of each element in **Table 4.6**.

Table 4.5 Mean concentrations and ratios of Ti/Cr and Zn/Ti in the operational food groupings used in the composite food survey. Mean concentrations for Ti are calculated with non-detects set to 0.5DL.

Table 4.5A	Mean concentrations (mg/kg)			Element ratios	
Food category - major groups	**Ti**	**Cr**	**Zn**	**Ti/Cr**	**Zn/Ti**
Fruits	0.213	0.015	2.08	13.9	9.8
Vegetables and fungi	0.353	0.024	4.10	14.9	11.6
Grain and cereal-based foods	0.451	0.035	9.42	12.8	20.9
High protein foods (meat/chicken/fish/other)	0.644	0.048	22.2	13.4	34.5
Dairy and related	0.341	0.025	4.53	13.5	13.3
Overall major group mean	0.400	0.030	8.46	13.7	18.0
Std dev	0.160	0.013	8.13	0.8	10.1
%RSD	40.1	42.6	96.1	5.8	56.2

Table 4.5B	Mean concentrations (mg/kg)			Element ratios	
Food category - other or minor groups	**Ti**	**Cr**	**Zn**	**Ti/Cr**	**Zn/Ti**
Drinks (beverages) and soup	0.031	0.012	4.41	2.6	144
Spreads, condiments, and flavourings	0.225	0.025	0.36	9.0	1.6
Snack foods and chocolate	0.120	0.082	9.64	1.5	80.3
Infant foods	0.235	0.041	17.2	5.8	73.1
Others	0.150	0.002	0.05	75.0	0.3
Overall other/minor group mean	0.152	0.032	6.33	18.8	59.8
Std dev	0.084	0.031	7.20	31.6	60.4
%RSD	55.0	96.9	114	168	101

Table 4.6 Mean concentrations of each element expressed as percentages of the highest concentration group, which in all three cases is found in the high-protein foods (set to 100%).

Operational group	Percent of the highest concentration		
	Ti	Cr	Zn
Fruits	33.0	31.9	9.4
Vegetables and fungi	54.8	49.2	18.5
Grain and cereal-based foods	70.0	73.4	42.5
High protein foods (meat/chicken/fish/other)	100	100	100
Dairy and related	53.0	52.6	20.4

In magnitude terms, Ti concentrations in the major food groupings are 'approximately equidistant' between those of Cr and Zn. On average, there is 14 times more Ti than Cr, and 18 times more Zn than Ti (**Table 4.5A**). Results show that the highest concentrations of both Ti and Zn occur in the high protein foods group (red meat, chicken, fish, and others). The second-highest value for Zn was in infant foods, some of which will be fortified with Zn. The highest Cr was in snack foods and chocolate, but the high-protein foods group ranked second. Taking these out to focus only on the major food groupings (**Table 4.5B**, **Table 4.6),** a clear picture emerges, which suggests that in natural foods, Ti and Cr follow each other remarkably closely. At the same time, Ti and Zn, and Cr and Zn, are also reasonably closely related.

Specifically, Ti, Zn, and Cr are all at their highest concentrations in the meat/chicken/fish composite. For Ti and Cr, relative concentrations in foods (as percent of highest) match each other in all five of the major food categories (**Table 4.7**), in this order:

[1] high protein foods (meat, chicken, fish, etc) (highest, assigned 100%) >

[2] grain and cereal-based foods (70–73% of the highest concentration) >

[3] and [4] dairy and related (52–53% of highest)=vegetables and fungi (49–55% of highest) >

[5] fruits (32–33% of the highest)

Ti and Cr concentrations in these 'closer to natural' food groupings are highly correlated, with Pearson's correlations of R=0.993, p<0.0001, slope=1.0 over the first five categories (**Table 4.5A**)**.**

To the author's knowledge, a close correlation between Cr and Ti across food types has not been previously reported. Future research could explore this topic.

Zn follows the same order as Cr–Ti, through the relative concentrations differ from those of Ti and Cr, and this appears to partly reflect disproportionately higher concentrations of Zn in the high protein food category. For Zn, the order and relative proportions are:

[1] high protein foods (meat, chicken, fish, etc) (highest, assigned 100%) >

[2] grain and cereal-based foods (42.5% of the highest concentration) >

[3] and [4] dairy and related foods (20.4% of highest) ~ vegetables and fungi (18.5% of highest)

[5] fruits (9% of the highest)

All three elements, therefore, show the same rankings in major food groupings, but the relationship between Ti and Cr is remarkably close.

4.3.4.2 Relative abundances in the ash

As outlined in the methodology (**Section 3.2**), ash weights were also recorded in this study. Ash weight concentrations of Ti, Cr, and Zn in the five main food groupings are shown in **Table 4.7**. These figures represent the concentration of elements in the inorganic component of each food, after all organic matter and water have been removed.

Table 4.7 Mean concentrations and relative proportions of Ti, Zn, and Cr in the inorganic ash of the five main food groupings used in the composite food survey.

Operational group	Mean ash weight concentration (mg/kg)			Element ratios in the ash	
	Ti	Cr	Zn	Ti/Cr	Zn/Ti
Fruits	76.9	4.3	662	18.0	8.6
Vegetables and fungi	44.8	1.8	805	24.3	18.0
Grain and cereal-based foods	54.2	3.4	721	16.0	13.3
High protein foods	48.8	3.0	1527	16.4	31.3
Dairy foods	49.0	2.5	1022	19.7	20.9
Mean	54.7	3.0	948	18.9	18.4
Std dev	12.9	0.9	352	3.4	8.6
%RSD	23.5	30.7	37.1	17.8	46.6

Results show that the inorganic component of the five main food groupings is about 55 mg/kg Ti, and this does not change by a large amount from group to group (range 45–77 mg/kg and RSD 24% (**Table 4.7**). Similarly, Cr makes up an average of 3 mg/kg of the inorganic components with an RSD of 30%, and Zn averages 950 mg/kg with an RSD of 37%.

On average, Ti concentrations in the ash are equidistant between those of Cr and Zn. The average ratios of Ti/Cr and Zn/Ti in the inorganic components are 18.9 and 18.4, respectively. These compare with ratios of 13.7 and 18.0 determined for the whole foods (**Table 4.5A**). In magnitude terms, these results are as expected, because Ti, Cr, and Zn species in foods should be oxidised during ashing and conserved in the inorganic ash. The slightly higher Ti/Cr ratio in the ash is influenced by the vegetable and fungi group (ratio of 24.3) and may be an artefact of ash weight measurement uncertainties. This is because the ash weight measurements were calculated as the difference between the weight of an empty Pyrex beaker (about 150 g) and the weight of the same beaker, after heating and cooling, containing the ash (itself weighing only a fraction of a gram). For some samples containing a very low inorganic content, such as aqueous drinks, the calculated ash weight was a small negative number on the four-figure decimal balance, reflecting analytical balance measurement error, along with a possibility that a small but perhaps detectable amount of Pyrex may also be lost from beakers during ashing.

4.3.5 Dietary Ti intake estimates in 10 age and gender groups

Estimated dietary intakes of Ti can be calculated by multiplying the mean concentrations of Ti in each composite food by the weight of that food ingested and summing the products. Estimated intakes of each food composite were derived from 14-day data reported in Smith et al. (2017), which also served

as the basis for estimates made in the most recently published NZTDS (Pearson et al., 2018). Some data assignment and rearrangement for specific foods tested in this study was undertaken to ensure alignment with their correct composite groups, and a cross-check was run to ensure that no intake data was lost or overlooked. These overall average 14-day and daily food intakes for the ten age and gender groups are shown in **Table 4.9.**

Table 4.8 Average overall food intakes of various age and gender groups as used in the last published New Zealand Total Diet Study (Smith et al., 2017).

Demographic group	14-day consumption (g of food)	1-day consumption (kg of food)
Infants (6 to 12 months)	8837	0.631
Pre-school (1 to 3 years)	18706	1.336
Children (5 to 5 years)	23308	1.665
Girls (11 to 14 years)	25403	1.815
Boys (11 to 14 years)	28926	2.066
Males 19 to 24 years	43760	3.126
Males 25 years +	44858	3.204
Females 25 years +	36348	2.596
Pacific Females 15 years +	32567	2.326
Pacific Males 15 years +	41300	2.950

4.3.6 Detailed intake estimates (every food composite)

Fourteen-day Ti intake estimates of the 10 age and gender groups for every food composite are presented in **Table 4.9**. For these estimates, non-detects (NDs) were set to half the DL. Overall intake estimates are provided in **Table 4.10**.

As reported in **Section 4.3.3**, Ti was below the estimated DL in 37.5% (15 of 40) food composites (**Table 4.4**). Raw results for these samples were recorded, but for reporting (**Table 4.2**), these composites are shown as <DL as that would apply to the food composite; for example, the 'citrus' composite contained Ti at less than 0.21 mg/kg (<0.21 mg/kg). When a substantial proportion of foods show non-detections (NDs), how they are treated can create uncertainties in intake estimates. In the intake calculations, results below DL can be set equal to the detection limit (ND=DL), zero (ND=0), or half the detection limit (0.5DL), which is the most common approach. In this study, it was also possible to use the raw data to compare the results with those of the other three methods. A sensitivity analysis was undertaken to determine the influence of this factor, and the results are shown in **Table 4.11**.

Table 4.9 Ti intake estimates as 14-day values (µg/14 days) for every food composite, across the 10 age and gender groups (NDs set to half DL).

Major category	Comp-osite No	Composite group	Males 19–24 yrs	Males >25 yrs	Females >25 yrs	Pacific females >15 yrs	Pacific males >15 yrs	Boys 11–14 yrs	Girls 11–14 yrs	Children 5–15 yrs	Pre-school 1–3 yrs	Infants 6–12 mo
Fruits	1	Pip fruit/Kiwi fruit	310	321	272	272	321	405	442	461	210	123
	2	Stone fruit	64	76	84	71	76	44	46	58	40	36
	3	Citrus	68	82	87	57	57	129	199	174	74	37
	4	Berries	84	67	62	62	67	24	39	47	34	17
	5	Tomato	72	112	100	62	100	88	86	25	28	20
	6	Others	201	159	137	179	159	101	80	133	145	128
Vegetables and fungi	7	Root vegetables	79	99	78	60	99	85	66	60	33	20
	8	Tubers	785	654	406	537	731	682	598	415	197	116
	9	Leafy vegetables	174	192	151	111	207	213	147	81	52	27
	10	Squash/Creeping veg	56	79	83	56	79	45	33	22	29	23
	11	Seed/Other	166	161	156	80	161	149	114	101	57	39
	12	Dried fruits	21	21	14	14	21	21	21	21	68	45

(Table 4.9 continues over…)

Table 4.9 continued…

Major category	Comp-osite No	Composite group	Males 19–24 yrs	Males >25 yrs	Females >25 yrs	Pacific females >15 yrs	Pacific males >15 yrs	Boys 11–14 yrs	Girls 11–14 yrs	Children 5–15 yrs	Pre-school 1–3 yrs	Infants 6–12 mo
Grain and cereal-based foods (carbo-hydrate rich)	13	Bread	769	636	490	516	563	927	673	677	238	142
	14	Rice or rice-based	781	695	508	545	891	331	216	234	39	23
	15	Breakfast cereals	206	284	152	226	270	180	154	169	192	101
	16	Pasta, spaghetti, noodles	445	396	301	334	516	253	245	185	115	65
	17	Biscuits	203	182	143	143	182	398	301	301	328	145
	18	Cakes	135	124	75	79	139	68	103	50	33	14
High protein foods (meat / chicken / fish / other)	19	Chicken	1046	656	577	932	1432	834	566	445	203	106
	20	Beef	489	482	346	569	795	538	342	273	200	134
	21	Pork	405	278	172	201	301	286	171	115	102	51
	22	Fish	157	169	139	193	214	83	50	45	34	24
	23	Other seafood	96	108	73	73	108	9	9	0	0	0
	24	Eggs	362	314	321	189	314	257	222	187	128	70
	25	Nuts	50	50	46	46	50	25	25	25	0	0
	26	Others (composite foods, tofu, and beans)	315	251	143	218	208	230	216	130	85	48

(Table 4.9 continues over…)

Table 4.9 continued…

Major category	Comp-osite No	Composite group	Males 19–24 yrs	Males >25 yrs	Females >25 yrs	Pacific females >15 yrs	Pacific males >15 yrs	Boys 11–14 yrs	Girls 11–14 yrs	Children 5–15 yrs	Pre-school 1–3 yrs	Infants 6–12 mo
Dairy foods	27	Milk	840	876	667	657	876	736	560	630	1189	243
	28	Milk products 1	155	167	170	96	92	150	142	116	273	233
	29	Milk products 2	366	285	228	519	610	444	407	537	497	171
Drinks (beverages) and soup	30	Water	90	93	126	126	93	148	148	157	106	57
	31	Juices and carbonated beverages	121	48	34	43	58	46	38	36	34	13
	32A	Tea	5	28	33	17	17	1	1	1	0	0
	32B	Coffee instant & drinking chocolate	287	521	385	261	261	65	69	52	20	7
	32C	Caffeinated beverage	7	3	3	3	3	2	2	0	0	0
	33	Alcoholic drinks	68	57	17	10	57	0	0	0	0	0
	34	Soup	63	63	85	38	63	38	38	25	13	8

(Table 4.9 continues over…)

Table 4.9 concluded…

Major category	Comp-osite No	Composite group	Males 19–24 yrs	Males >25 yrs	Females >25 yrs	Pacific females >15 yrs	Pacific males >15 yrs	Boys 11–14 yrs	Girls 11–14 yrs	Children 5–15 yrs	Pre-school 1–3 yrs	Infants 6–12 mo
Spreads, condiments and flavourings	35	Spreads	169	144	119	131	140	113	81	89	47	35
	36	Condiments and flavourings	62	45	32	38	45	49	39	29	13	8
Snack foods and chocolate	37	Snack foods and chocolate	88	66	64	48	61	190	166	128	45	25
Infant foods	38A	Infant foods - preschool	0	0	0	0	0	0	0	0	109	0
	38B	Infant foods - toddler	0	0	0	0	0	0	0	0	0	2234
Others	39	Sugar	34	48	38	37	49	24	24	14	6	4
	40	Oil	54	46	28	28	46	21	15	10	9	3

Table 4.10 Estimated 14-day and daily intakes of Ti in the 10 demographic groups, both as ingested and as a dose per kilogram of body weight.

Titanium intakes and doses	Males 19–24 yrs	Males >25 yrs	Females >25 yrs	Pacific Females >15 yrs	Pacific Males >15 yrs	Boys (11–14 yrs)	Girls (11–14 yrs)	Children (5–6 yrs)	Pre-school (1–3 yrs)	Infants (6–12 mo)
14-day Ti intake (µg/14 days)	9946	9133	7142	7872	10528	8427	6891	6256	5020	4591
Single day Ti intake (µg/day)	710	652	510	562	752	602	492	447	359	328
Average body weight (NZTDS 2016/18)	79.5	86.7	73.3	88.1	98.1	54.0	54.0	23.0	13.0	9.0
Estimated daily dose of Ti (µg/kg-bw/day)	8.9	7.5	7	6.4	7.7	11.1	9.1	19.4	27.6	36.4
Estimated daily dose in TiO_2 equivalents (µg/kg-bw/day)	14.9	12.6	11.6	10.6	12.8	18.6	15.2	32.4	46	60.8

Table 4.11 Dietary intake estimates calculations using original values, or by setting non-detections to half the detection limit (0.5DL), and setting non-detects to zero (ND=0).

'Original analytical data' refers to the raw GFAAS readings, which in some cases were below the apparent detection limit. These values could be set to 0, set to 0.5 detection limit (0.5DL, the standard approach), or set to the detection limit (ND=DL).

Estimated intakes as µg/day	Males 19–24 yrs	Males >25 yrs	Females >25 yrs	Pacific Females >15 yrs	Pacific Males >15 yrs	Boys (11–14 yrs)	Girls (11–14 yrs)	Children (5–6 yrs)	Pre-school (1–3 yrs)	Infants (6–12 mo)
Based on original analytical data	701	639	500	556	745	582	478	432	322	329
With non-detects set to 0.5DL	710	652	510	562	752	602	492	447	359	328
With non-detects set to zero	484	434	332	389	532	421	328	302	187	256
With non-detects set to DL	939	873	690	737	974	782	656	592	531	400
Ratios of the intake estimates (µg/day)										
ND = 0 / original data	0.69	0.68	0.67	0.70	0.71	0.72	0.69	0.70	0.58	0.78
ND = 0 / 0.5DL approach	0.68	0.67	0.65	0.69	0.71	0.70	0.67	0.68	0.52	0.78
0.5DL approach / ND=DL approach	0.76	0.75	0.74	0.76	0.77	0.77	0.75	0.76	0.68	0.82
0.5DL approach / original data	1.01	1.02	1.02	1.01	1.01	1.03	1.03	1.04	1.11	1.00

4.3.7 Overall intake estimates

Estimated daily Ti intakes as ingested across the 10 age and gender groups (**Table 4.10**) range from 328 µg/day for infants, to 752 µg/day for Pacific males (>15 yrs), a factor of only two times.

All three adult (>15 yrs old) male groups show very similar intakes: mean 705 µg/day and a range of 652–752 µg/day. For the two comparable adult female groups, the figures are about 24% lower than those of males, with a mean intake of 536 µg/day. For 11–14 yrs old children, the picture is very similar, with a mean of 547 µg/day, and the estimated intake for girls is 18% lower than that of boys.

Expressed on a dose basis, intakes across both males and females (>15 yrs) are all very similar and average 7.5 µg/kg-bw/day, with quite a narrow range from a low of 6.4 µg/kg-bw/day for Pacific females to a high of 8.9 µg/kg-bw/day (for 19–24 yrs old males). Children (11–14 yrs of age) show slightly higher intakes, with a mean of 10.1 µg/kg-bw/day for boys and girls. Pre-school children and infants show the highest intakes, of 27.6 and 36.3 µg/kg-bw/day, respectively (**Table 4.10**).

Thus, pre-school children and infants ingest about half (54%) the Ti as adults (means of 343 compared with 637 µg/day), but experience about 4.3 times the dose expressed on a body-weight basis (mean of 32 compared with 7.5 µg/kg-bw/day). Results of this study show that higher relative doses of Ti in pre-school children and infants are entirely due to their lower body weights. On average, the pre-school children and infants weigh 11 kg (as a mean), which is a factor of 7.7 times lower than the mean weight of the five <15 y 'adult' groups (mean body weight 85 kg).

This finding relates to natural dietary Ti, reflecting the nature of the food composites and the way that detections of E171 in the two food composites that were likely to contain it were handled (**see Sections 4.3.1** and **4.3.2**). Some children may also ingest more Ti than adults on an idiosyncratic basis, as is assumed in much of the E171 literature (Bischoff et al., 2025). For example, a particular child may routinely consume a preferred confectionery which contains E171, increasing their overall daily Ti intake (as ingested) to more than that of an adult. Results of this study demonstrate that such an outcome would require the presence of E171, because natural intakes of Ti in pre-school children and infants (as ingested) are about half those of adults (**Table 4.10**).

Idiosyncratic exposures and the presence and prevalence of E171 in food products most likely to contain it are the subject of **Chapter 5**.

Intakes and doses can also be expressed as TiO_2 equivalents, the unit more commonly used for studies focused on E171 in food. Estimated daily intakes of TiO_2 in this study are 0.0116–0.0149 mg/kg-bw/day for adults (**Table 4.10**), significantly lower than previously reported values from studies overseas. For example, adult intakes in the UK, US, Denmark, and the Netherlands ranged from 0.6 to 2 mg/kg/day

(Bischoff et al., 2025), while the EFSA documented a broader range of 0.3 to 4 mg/kg/day (Younes et al., 2021).

Differences between the results of this study and previous overseas studies are significant, and may be caused by up to three interrelated factors:

1. Results of this survey primarily reflect natural Ti intakes from food, estimated at the beginning of this chapter to be in the order of 10 µg/kg/day for a 70 kg adult. Evidence for E171 was found in only one composite (Composite 29), and a single outlier in another (Composite 38B) (see footnote to **Table 4.2**). Further testing of foods in those groups was undertaken to develop the best estimate in each case. It is thought that the results from this study show no to minimal influence from the presence of E171. It is possible that NZ foods may contain less E171 on average than US or European foods.
2. Previous estimates commonly include assumptions about E171 exposures, which go on to dominate total intake estimates. In some cases, the focus is only on E171, and in others, natural Ti intakes are commonly assumed to be a low (or negligible) baseline.
3. E171 usage in foods may have been declining over time in response to regulatory controls in some jurisdictions influencing product formulations across multiple markets, so that a new survey may show a lower result than an older survey, regardless of country. This factor reflects the prevalence of E171 (presence or absence). This aspect is examined further in **Chapter 5**.

4.3.8 Uncertainties introduced by non-detections

Overall, uncertainties in the overall intake estimates introduced by the food composites showing non-detections are relatively modest (**Table 4.11**). Interestingly, using raw data provides estimates comparable to those from the 0.5DL approach. Compared with those two approaches, setting ND=0 or ND=DL yields estimates that are typically about one-third lower or higher, respectively. The largest variance is for preschool children (1–3 yrs), where setting ND=0 reduces the estimated intake to about half that obtained with ND=0.5DL (**Table 4.11**). For the purposes of this study, the best estimates are regarded as those obtained using the 0.5DL approach, because (a) in reality, very few to no foods should have zero Ti (ND=0), because Ti occurs naturally, and (b) probabilistically, it is *unlikely* that every composite showing a non-detection would happen to have Ti at the detection limit (Ti=ND).

4.3.9 Contributions from individual composites

Fourteen-day Ti intakes for each of the 43 food composites are shown in **Table 4.9**. Among males aged 19–24 yrs, the highest intake of Ti was observed in the composite group of chicken, amounting to 1046

µg over a 14-day period. This value was even higher in Pacific males aged 15 years or older, where Ti consumption reached 1432 µg over 14 days (**Table 4.9**).

For younger age groups, distinct dietary sources contributed to the highest Ti intake. Pre-school children (aged 1–3 yrs) exhibited the highest consumption in the composite group of milk, with an intake level of 1189 µg per 14 days. In infants aged 6–12 months, the highest Ti intake was observed in the composite infant food group, reaching 2234 µg per 14 days.

Conversely, the lowest Ti intake was observed in tea (Composite 32A), the only composite comprising a single food. This partly reflects assumptions made when converting from the concentration in tea leaves (4.77 mg/kg) to an estimated Ti concentration in tea as consumed (0.006 mg/kg), that 7% of the Ti was extracted from 2.62 g of leaves per drink, into a 150 mL dilution volume (**Table 4.3**). Among males aged 19–24 years, Ti consumption was recorded at 5 µg over 14 days. This intake increased to 28 µg/14 days in males older than 25 years and 33 µg/14 days in females older than 25 yrs.

These findings indicate that specific foods influence Ti exposure, but it may be more informative to examine the results at a less granular level than for individual food composites. For this reason, intakes were also estimated for each of the ten operational food categories.

4.3.10 Contributions from food categories

Percentage contributions of each operational food category to daily intakes of Ti are shown in **Table 4.12**. Proportional Ti intakes for the first seven age and gender groups are illustrated in **Figure 4.3**.

Table 4.12 Percentage (%) contributions of each operational food group to daily intakes of Ti.

Major (operational) category	Males 19–24 yrs	Males >25 yrs	Females >25 yrs	Pacific Females >15 yrs	Pacific Males >15 yrs	Boys (11–14 yrs)	Girls (11–14 yrs)	Children (5–6 yrs)	Pre-school (1–3 yrs)	Infants (6–12 mo)
Fruits	8.7	9.4	10.9	9.7	7.8	9.6	12.9	15.3	12.8	8.9
Vegetables and fungi	13.1	13.4	12.6	11	12.4	14.8	14.7	11.7	9.6	5.8
Grain and cereal-based foods (carbohydrate rich)	29.0	28.9	26.7	26.4	27.9	28.5	28	28.8	22.6	11.5
High protein foods (meat/chicken/fish/other)	29.5	25.8	26.3	31.4	33.1	27.3	23.2	19.8	16.4	9.3
Dairy and related (milk, yoghurt, cheese, butter, ice-cream, desserts)	9.4	9.7	10.5	11.8	10.5	11.7	12.4	15.8	30.0	12.6
Drinks and soup	6.3	8.8	9.3	6.2	5	3.5	4.2	4.3	3.7	1.8
Spreads, condiments and flavourings	2.1	1.9	1.9	1.9	1.6	1.7	1.5	1.7	1.2	0.9
Snack foods and chocolate	0.9	0.7	0.9	0.6	0.6	2.2	2.4	2.0	1.0	0.5
Infant foods	0	0	0	0	0	0	0	0	2.3	48.5
Others	1.2	1.3	1.1	1	1.1	0.7	0.7	0.5	0.4	0.2
Sum	100	100	100	100	100	100	100	100	100	100

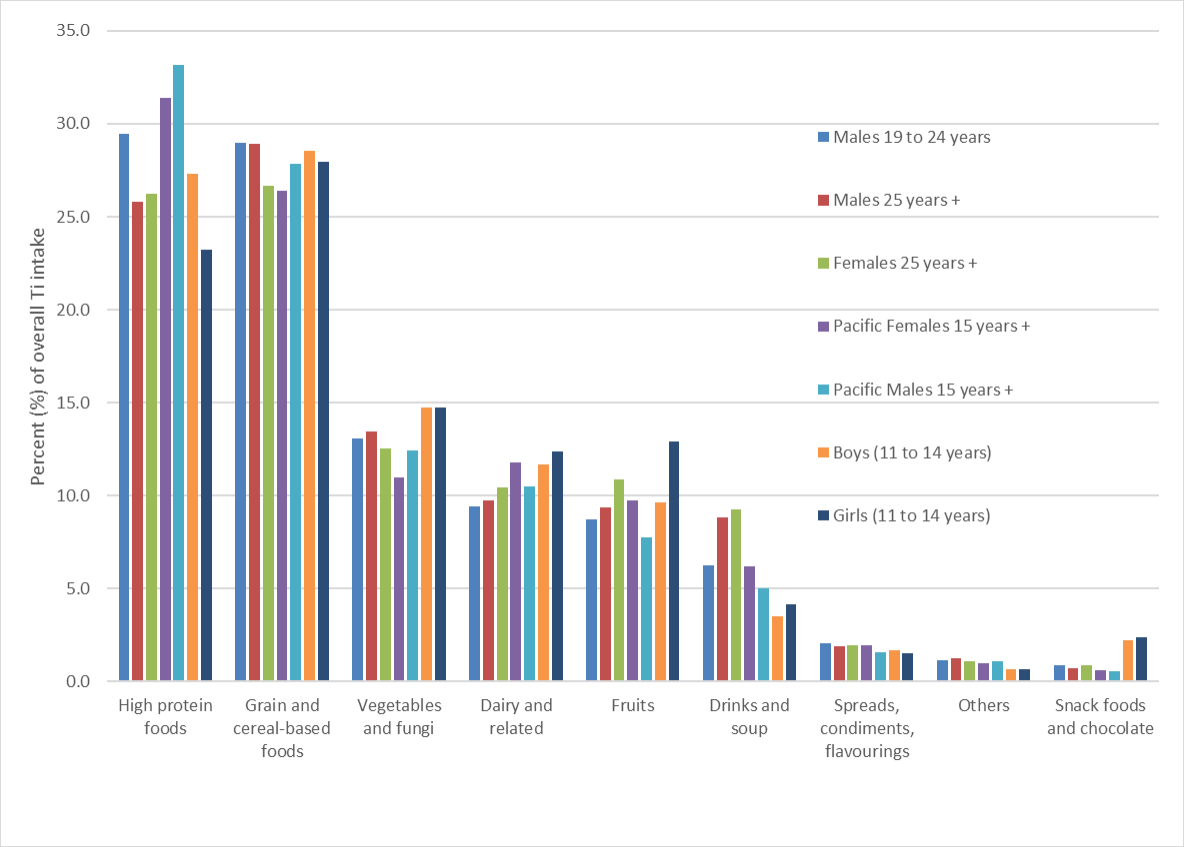

Figure 4.3 Percentage contribution of each food category to dietary Ti intakes in the seven age and gender categories comprising all adults and all children older than 11 years of age.

Across the first seven age and gender groups (including all adults >15 years, and both boys and girls of 11–14 years), the pattern is the same. Over half (56.0%) of dietary Ti comes from two food categories, each contributing an equal amount: high-protein foods (mean 28.1%) and grain- and cereal-based foods (mean 27.9%). Another one-third (mean 33.9%) comes from the three other main food categories, also in almost equal amounts: vegetables and fungi (13.1%), dairy and related (10.9%), and fruits (9.9%). The final ~10% is from the other four minor food categories, namely: drinks and soups (6.2%), spreads and condiments (1.8%), snack foods and chocolate (1.2%), and others (1.0%).

Moving to younger children: for 5-6 yrs olds (**Table 4.12**), the general pattern remains the same, but more (~16%) Ti is contributed from the dairy and related group, and slightly less (~20%) comes from high-protein foods. This trend continues into the 1–3 yrs old children, in which for the first time dairy and related foods represent the highest single contribution (30% of Ti intakes), which causes the relative contributions from cereals (23%) and high-protein foods (16%) to be proportionately lower. These differences between younger (1–6 yrs) children and older children (all groups >14 yrs) reflect the higher relative intake of dairy products in the diets of younger children. In other respects, the patterns are the same.

Infants show a distinct apparent difference compared with the other nine age and gender groups, with about half (48.5%) of the Ti coming directly from infant foods (**Table 4.12**). However, infant foods are predominantly formulated from the other five major food categories, including grains and cereals, fruits, vegetables, high-protein foods, and dairy products. On closer inspection, the proportional contributions of each food type to Ti intakes in infants are therefore likely to follow the same patterns as for the other age and gender groups, if contributions from the infant food category could be allocated back to each of those parent food categories.

4.3.11 Comparison to intakes of Cr and Zn

Results for concentrations of Cr and Zn in food composites and ash were presented in **Section 4.3.4**. On average, Ti concentrations in food were found to sit between those of Cr and Zn: there is 14 times more Ti than Cr, and 18 times more Zn than Ti (**Section 4.3.4**). As with Ti, the Cr and Zn data can be converted to estimated intakes. Results are shown in **Appendices 4.3** and **4.4** and summarised in **Tables 4.13 and 4.14**.

Table 4.13 Estimated intakes of Zn and Cr for each of the 10 age and gender groups, and comparison of results for Zn with those reported in the 2016/18 NZTDS.

Figures are as ingested. Note that for Zn, intakes are expressed in mg/day, whereas for Cr, intakes are expressed in µg/d.

Group	Estimated Zinc intakes			Estimated Cr intakes, µg/day
	This study, mg/day	As reported in the last NZDTS (mid-bound mean), mg/day	Percent (%) of NZTDS 2016/18 estimate	
Males 19 to 24 years	12.1	13.9	86.9	49.8
Males 25 years +	11.2	12.7	88.2	53.1
Females 25 years +	8.5	9.3	91.3	40.1
Mean[a] male and female 25 years +	9.8	11	89.7	46.6
Pacific Females 15 years +	10.0	11.5	86.8	39.5
Pacific Males 15 years +	13.6	15.3	88.7	49.3
Boys (11 to 14 years)	10.6	12.5	85.2	36.6
Girls (11 to 14 years)	8.2	10	81.9	31.1
Children (5 to 6 years)	6.9	8	86.7	26.7
Pre-school (1 to 3 years)	5.6	6.4	87.1	22.2
Infants (6 to 12 months)	13.8, 7.72[b]	5.8	238, 132[b]	26.1

Notes: [a] Male and female 25 yrs+ means were calculated from the two rows above; [b] Zn intakes in infants were sensitive to the proportion of infant formula, and whether it is Zn-fortified. The first value includes a Zn-fortified formula, and the second excludes it.

Table 4.14 Intake estimates (as ingested) for Zn, Ti, and Cr in the 10 age and gender groups in the same units (μg/day), and the relative position of Ti.

Group		Intakes (as ingested, μg/day)			Intake ratios	
		Zn	Ti	Cr	Zn/Ti	Ti/Cr
Males 19 to 24 yrs		12079	710	49.8	17.0	14.3
Males 25 yrs +		11204	652	53.1	17.2	12.3
Females 25 yrs +		8488	510	40.1	16.6	12.7
Mean male and female 25 yrs +		9846	581	46.6	16.9	12.5
Pacific Females 15 yrs +		9984	562	39.5	17.8	14.2
Pacific Males 15 yrs +		13565	752	49.3	18.0	15.2
Boys (11–14 yrs)		10648	602	36.6	17.7	16.5
Girls (11–14 yrs)		8189	492	31.1	16.6	15.8
Children (5–6 yrs)		6936	447	26.7	15.5	16.8
Pre-school (1–3 yrs)		5575	359	22.2	15.5	16.2
Infants (6–12 months)		7720	328	26.1	23.5	12.6
All groups ages 11 yrs +	Mean	10594	611	42.8	17.3	14.4
	Std dev	1915	98.5	8.1	0.6	1.5
	%RSD	18.1	16.1	18.9	3.2	10.7
Infants, pre-schoolers and young children	Mean	6743	378	25.0	18.2	15.2
	Std dev	1086	61.7	2.5	4.6	2.3
	%RSD	16.1	16.3	9.8	25.4	15.1

As for concentrations in food, intakes of Ti are approximately halfway between those of Zn and Cr (**Table 4.14**). For all groups aged 11 yrs and above, the mean Ti intake (as ingested) is 611 μg/day, which is 17 times lower than the intake of Zn (10594 μg/day), and 14 times higher than the intake of Cr (42.8 μg/day). This demonstrates that although Ti is not ingested at levels similar to those of the essential element Zn, it is not an 'ultra-trace' type of dietary element either. Rather, it is relatively abundant compared with elements such as Cr, which may or may not be essential (EFSA, 2006; EFSA,

2017; Jeejeebhoy, 1999; Vincent, 2010, 2013), or Co which is essential (Genchi et al., 2023). As outlined in the introduction to this chapter, it remains possible that at some level, Ti may be essential.

Results for Zn in this study show good agreement with the mid-bound mean reported in the most recently published NZTDS (**Table 4.13**). Results in this study are 10-15% lower than the NZDTS figures, but this is likely to reflect a small amount of Zn being lost during the 650 °C ashing step used for Ti in this study due to the relatively low melting point of Zn (**Section 3.2**). In other respects, the close alignment in Zn intake estimates between the two studies provides support for the reliability of the intake methodology used in this study.

Chromium (Cr) intakes in NZ have not been previously reported. According to Pearson (Pers. Comm. 2025), Cr was measured in samples processed for the last published NZTDS. Still, those results were not published due to the additional complication of factoring in discussion relating to toxicological differences between chromium's two main oxidation states (Cr(III) and Cr(VI)). However, some older overseas estimates of total Cr intakes are available for comparison.

Cr intake data in the US are limited, as the National Health and Nutrition Examination Survey (NHANES) does not report it. Small studies suggest average intakes of 29 μg/day for women and 54 μg/day for men (Anderson et al., 1992, 1993), with well-balanced diets providing around 27 μg per 2,000 kcal. A 2018 Italian study found a median intake of 57 μg/day (Filippini et al., 2018). Intake data estimates attributable to consumption of dietary supplements containing Cr (including some multivitamin products) are scarce, but NHANES III estimated a median of 23 μg/day among users.

Cr is often considered a nutrient, though its essentiality remains unsettled. Nutrient reference values for chromium, jointly set by the Australian Government Department of Health and the NZ Ministry of Health, recommend Adequate Intakes (AIs) of 35 μg/day for men and 25 μg/day for women aged 19–70 yrs, with increased needs during pregnancy (30 μg/day) and lactation (45 μg/day). For children aged 1–13 yrs, AIs range from 0.2–25 μg/day. These values align with US recommendations and are based on limited evidence, primarily from urinary excretion studies (NHMRC, 2006). The US Institute of Medicine (2001) set AIs for Cr due to insufficient data for estimated average requirements and Recommended Dietary Allowances. AIs are 25 μg/day for women (14–50), 20 μg/day for older women, 30 μg/day in pregnancy, and 45 μg/day in lactation. For men, AIs are 35 μg/day (14–50) and 30 μg/day for older men. For children (1–13 yrs), AIs range from 0.2 to 25 μg/day depending on age (National Research Council, 2002). In contrast, EFSA does not consider Cr an essential nutrient and has not established any Population Reference Intakes, AIs, or Tolerable Upper Intake Levels (ULs) for chromium. Chromium is the only mineral for which the U.S. and EU differ in their assessment of essentiality (EFSA, 2006; EFSA, 2017).

Intakes of Cr determined in this study (**Table 4.13**) are within these measured ranges and recommended intake values.

Overall, the intake estimates for Zn and Cr obtained in this study, using the same foods, composites, and methodology as applied to Ti, are in good agreement with available external estimates, the most recently published NZDTS for Zn, and overseas estimates for Cr. The fact that intakes of these two elements also bracket those of Ti is also helpful. Together, these results confirm that the Ti intake estimates in this study are likely reliable.

4.4 Discussion and summary – key findings

4.4.1 Ti in foods

The concentration of Ti varied widely across food categories analysed in this study (**Sections 4.3.2** and **4.3.3**), with the highest level detected in the eggs composite (1.17 mg/kg) and among high-protein foods, beef, pork, and chicken exhibited relatively elevated Ti levels (0.815, 0.854, and 0.765 mg/kg, respectively). In contrast, other items in this category ranged from below detection to 0.854 mg/kg. Fruit and vegetable composites showed a broader range (<0.15–0.686 mg/kg), with dried fruits and berries containing the highest values. Grain- and cereal-based foods, including rice, pasta, and baked goods, contained Ti concentrations ranging from <0.36 to 0.673 mg/kg. Dairy products demonstrated notable variability, while the milk composite showed moderate levels, the 'Milk products 2' composite reached 14.8 mg/kg due to a single item, 'Mochi Ice', containing 96.1 mg/kg Ti, likely from the additive E171. Beverages and soups consistently exhibited low Ti levels (0.006–0.065 mg/kg), except for dry tea leaves, which contained 4.77 mg/kg. Infant foods were stratified into two composites to reflect age-specific dietary patterns, enabling more accurate exposure assessment. Composite 38A showed Ti levels below detection (<0.24 mg/kg), while Composite 38B had inconsistent subsample results. A broader analysis (N=15) yielded a reliable mean Ti concentration of 0.350 mg/kg for infant foods.

4.4.2 Ti intakes

Estimated intakes of Ti were in the range of 500–750 µg/day for all age and gender groups 11 yrs and older, and relate to the amount of food ingested (**Table 4.10**). At the low end of this relatively narrow range are girls (11–14 yrs, 492 µg/day) and adult females (>25 yrs, 510 µg/day); and at the high end are slightly younger males (19–24 yrs, 710 µg/day) and Pacific males (752 µg/day). Younger children had lower daily intakes that mainly reflect lower food consumption: from 328 µg/day for infants (6–12 months old) to 447 µg/day for children (5–6 yrs). During the study, it was determined that Ti intake for any individual, regardless of age or gender, could also be estimated by multiplying the amount of food consumed by that person in a day by the weighted mean Ti across the foods eaten by that group. The weighted means are provided in **Table 4.4**.

In terms of which foods contribute the most natural Ti intakes (**Table 4.12**; **Figure 4.3**), over half (56.0%) of dietary Ti is from two food categories: high protein foods (28%) and grain and cereal-based foods (also 28%). Another third (mean 34%) comes from the three other main food categories, also in almost equal amounts: vegetables and fungi, dairy and related, and fruits. Among the youngest children, there is a clear dominance of infant foods. Still, it should be recognised that these are derived from the other five main food categories so that they can be seen as pre-formulated dietary composite samples.

On an ingested dose basis (µg/kg–bw/day), some more distinct differences emerge between the doses received by all groups, 15 and older and those of the five younger groups. These are primarily driven by body weight differences, which also bring some of the other groups closer together. Thus, adult (>25 yrs) males and females experience approximately the same daily dose (7.5 µg/kg/day for the males, and 7.0 µg/kg/day for females; **Table 4.10**). The average dose for all five groups >15 yrs is also 7.5 µg/kg/day, at an average body weight of 85.1 kg. Moving to boys and girls (11–14 yrs, 54 kg body weight), the average dose increases to 10.1 µg/kg/day. In this group, the ingested amount of Ti is slightly lower than that of adults, but the dose received is 1.34 times higher, due to a body weight that is 1.57 times lower. This trend continues in younger (5–6 yrs) children (assumed body weight 19.4 kg), preschoolers (13 kg), and infants (9 kg), in which the estimated Ti doses increase to 19.4, 27.6, and 36.4 µg/kg/day, respectively.

In **Section 4.1** of this chapter, it was noted that natural intakes of Ti are not well characterised but might be expected to be in the order of 10 µg/kg/day, assuming a mean [Ti] in food of 0.3 mg/kg, ingestion of 2.5 kg of food per day, and a 70 kg body weight. Adjusting that estimate for the average 85 kg adult body weight used for the first five age and gender groups in the NZTDS, the figure would bring it down slightly to 8–9 µg/kg/day. Remarkably, this turns out to be a good match for the average Ti intake of 7.5 µg/kg/day for these groups found in this study. Expressed in TiO_2 equivalents, this works out as 12.5 µg/kg/day (see **Table 4.10**).

Equally notable, these figures are well below previous estimates of TiO_2 consumption in adults (**Table 4.1**). For example, the lower end of the previously estimated TiO_2 intake range for Europeans is 0.3 mg/kg/day, or 300 µg/kg/day (**Table 4.1**). This is 25 times higher than the dose estimated for New Zealanders in this study, from food sampled in 2024.

These observations, and the fact that E171 was only detected in one product within one composite sample in this survey (which was excluded through further sampling), lead to three conclusions:

1. E171 was not readily detected in NZ foods sampled in 2024, suggesting it may now be absent or rare in most food categories;

2. The intake and dose estimates in this chapter relate to natural Ti, rather than added E171;
3. Higher intakes reported in previous decades by workers in other countries (**Table 4.1**) are almost certainly dominated by the presence of E171 in a higher proportion of the foods sampled in those countries, and in the years that the sampling occurred.

This survey may therefore be the first to characterise natural Ti intakes, and in doing so, uncover a close correlation between Ti and Cr in foods and the diet (see below).

These ideas are further explored in **Chapter 5**, where the focus is on foods most likely to contain E171, which then leads on to modelling possible exposures among habitual consumers. As will be shown (**Section 5.3**), reaching the intakes reported in **Table 4.1** of this chapter would readily be possible for a person who happens to consume one or more products containing E171 habitually. Under those circumstances, the E171 quickly becomes the dominant source of Ti. However, the likelihood of encountering such products and the prevalence of E171 in foods that historically contained it appear to have decreased.

4.4.3 Relationships between Ti, Cr, and Zn

The concentration of Ti across major food groups ranged from Cr to Zn, with ~14 times more Ti than Cr and 18 times more Zn than Ti. All three elements showed their highest concentrations in high-protein foods, followed by grain- and cereal-based foods, dairy products, and fruits. Ti and Cr exhibited a highly correlated distribution across the five major food categories, with consistent Ti/Cr ratios, indicating a strong natural co-occurrence. This natural correlation between Ti and Cr has not been reported previously and would be worth further investigation. In previous surveys, relationships between Ti and other elements would have been masked by the swamping effect of E171 on the natural Ti signal.

Zn followed the same pattern as Ti and Cr, but with some more noticeable concentration differences, mainly in high-protein foods. Estimated daily intakes further reflected this order, for individuals aged 11 and above, the mean Ti intake was 611 µg/day, positioned between Cr (42.8 µg/day) and Zn (10594 µg/day). These findings confirm that Ti, while not essential like Zn, is not an ultra-trace element and is relatively abundant in the diet compared to Cr.

CHAPTER 5: Evaluating the levels of E171 in selected food items from NZ supermarkets

5.1 Introduction

As noted in previous chapters, titanium dioxide (TiO_2; E171) is a common food additive used as a whitening agent to enhance the visual appeal of processed foods (Bucher et al., 2024), as a filler, for texture, or (in toothpaste) as an abrasive.

In **Chapter 4**, which focused on dietary intakes, one finding was that the prevalence of E171 in food composites appeared lower than might have been expected, at least based on overseas literature, suggesting that dietary E171 consumption would be difficult to avoid. Only two of the composite food samples contained E171. In each case, the E171 was traceable to a single food product within the composite, which was considered unrepresentative of that food category. One outcome was that the dietary exposure estimates provided in **Chapter 4** most closely reflect natural Ti intakes.

This left open questions about (a) the prevalence of E171 in products available on the NZ market that are most likely to contain it, and (b) possible idiosyncratic intakes of E171 in people who habitually consume one or more products containing it at elevated levels.

Several overseas studies have quantified E171 concentrations across different foods and related products. Some of these studies have taken a broad approach, whereas others have targeted foods more likely to contain E171. To the author's knowledge, no such study has previously been carried out in NZ.

The two main objectives of this part of the study were:

(1) To carry out the first NZ survey of this type, selectively targeting food (and other product) categories that are most likely to contain E171, and

(2) To estimate reasonable upper-end dietary exposures of E171 that could exist in people who habitually consume one or more products containing it at elevated levels.

Products targeted included items that explicitly list E171 on their labelling, are processed in ways that may introduce TiO_2 as an additive, may contain it based on their appearance, and/or have previously been found to contain E171 in previous (overseas) research. Given the widespread presence of TiO_2, there is a reasonable possibility that E171 may be present even when not declared on packaging. A subsidiary aim of objective (a) was to establish the accuracy of product labelling, or the extent of mislabelling, if any.

Table 5.1 provides an overview of detected E171 concentrations across various categories of processed foods in seven previous studies: (Bucher et al., 2024; Cao et al., 2024; Kim et al., 2018; Lim et al., 2018; Lomer et al., 2000; Peters et al., 2014; Sungur et al., 2020; Weir et al., 2012).

As the focus is on identifying food types most likely to contain E171, the summary statistics in **Table 5.1** apply only to cases where Ti was detected (i.e., values below the DL were excluded from the means and other statistics shown in **Table 5.1**). Sampling in each of the seven studies was not usually representative, in the sense that most (though not all) of the seven surveys specifically targeted food categories which were likely to, or known to, contain E171. It is also worth noting that some authors have reported Ti concentrations (as measured), whereas others converted their results to equivalent TiO_2 (E171) units. Concentrations shown in **Table 5.1** are standardised as [Ti] for purposes of comparison, where [Ti] = 0.5993 [TiO_2].

Table 5.1 Summary of results in cases where E171 was detected across seven previous studies undertaken at different times and in different countries. Highlighted cells show cases where [Ti] exceeds 100 mg/kg.

General group	Corresponding composite number in baseline dietary survey (Table 4.2)	Number of samples where Ti detected	Concentration as titanium [Ti], mg/kg				
			Mean	Median	Geometric mean	Minimum	Maximum
Fruits and vegetables	8, 11 and 12	5	102	64.2	22.7	1.8	366
Grains and related products incl. cereals, biscuits and cakes	14, 15, 16, 17 and 18	34	561	27.9	35.2	0.6	6120
Milk, dairy products and soy milk	27, 28, 29	26	237	1.1	6.8	0.2	1800
Drinks, juices, carbonated beverages, warm beverages, alcoholic beverages	31, 32, 33	10	92	43	35	1.4	369
Spreads and condiments	35,36	21	687	185	79.5	0.2	3590
Confectionery incl. chocolate	37	177	674	272	151	0.6	5300
Others (sugar, oils)	39	2	3.0	3.0	3.0	3.0	3.0
Icings and cake decorations	not applicable	45	1514	492	311	0.4	11478
Powdered drinks, drink syrups, coffee creamers, & unidentified drinks	not applicable	25	585	90	101	4.2	4692
Dietary supplements	not applicable	6	1014	672	447	18	3222
Toothpaste	not applicable	3	3573	3020	3460	2800	4900
Other	not applicable	7	157	24.0	37.8	6.7	840

Previous surveys summarised in **Table 5.1** indicate that the highest number of detections across the seven studies has been in the confectionery category (177 detections in total). However, this is a frequently targeted category, so sampling is not representative. However, it has not been uncommon to find E171 in confectionery, icings and cake decorations, some grain-based products such as biscuits and cakes, some dairy products, including (on occasion) cheese, and powdered drinks. Toothpastes are not often included in such surveys, but are a category for which individual products are most likely to contain E171.

Across all products sampled in the seven previous studies, Ti concentrations were the highest on average in the limited number of toothpaste samples tested (**Table 5.1**). Among food items, icings and decorations also exhibited high Ti levels, averaging 1514 mg/kg, but with a broad range from 0.4 mg/kg to 11478 mg/kg.

Within each category (e.g., confectionery), the mean values in **Table 5.1** might be seen as an upper estimate of the possible average for the food as consumed if a person ate across the range of products in that category. This would be an upper estimate because the data excludes the non-detections. The maximum values are the highest amounts detected in a single product. Across a population, the proportion of individuals consuming food from a given category with the highest E171 level detected would be low, because these cases represent people who habitually consume a specific food that happens to contain high E171.

Focusing on foods (excluding toothpastes and dietary supplements), and cases where detected means and maxima exceed 200 mgTi/kg, the seven previous studies reviewed suggest that E171 exposures would have been most likely to occur from consumption of: some confectionery including iced cakes, some baked goods (cakes and biscuits), some spreads and condiments, some powdered or other drinks, and some dairy products (**Table 5.1**).

Although sample selection was informed by previous research identifying categories of foods likely to contain E171 (**Table 5.1**), there are two differences between this and prior work.

The first is that this is the first NZ survey. There may be differences in the prevalence and levels of E171 in some categories of foods purchased in NZ, compared with comparable foods from other countries.

The second is that this is the newest survey, and it falls after enough time has passed for the effects of the regulatory change restricting the use of E171 as a food additive in the European Union (Chapter 1) to be felt. This change will have altered the practices of the larger food and confectionery manufacturers to ensure continued access to their products in the EU markets. In keeping with this idea, Blaznik et al. (2021) reported a significant decrease in the use of E171 in the food supply of Slovenia after the EFSA report concluding that E171 can no longer be considered a safe food additive.

For efficiency reasons, once a manufacturing chain is amended to ensure continued market access, there would be little incentive to provide a different product (still containing E171) to other markets (for example: Australia, NZ, the US), especially when they may also move to restrict E171 in the future, and if there is little downside to removing it. It is therefore possible that the prevalence and/or levels of E171 in NZ foods may have decreased in recent years, without this being noticed or known. Although there is no previous NZ survey to compare this study's results with, this is a potentially important factor to bear in mind when interpreting this study's results alongside those of previous workers.

5.2 Methods

The targeted survey involved collecting and analysing 180 individual food items (see **Appendix 5.1**) from supermarkets in Wellington, NZ. Samples were collected during November 2024. The selection of categories and foods was based on:

1. Food categories found to contain E171 in previous studies (**Section 5.1**, **Table 5.1)**;
2. Products listing E171 or TiO_2 on the package; and
3. Further investigation of the two composites found to contain higher Ti (one with suspected E171) in the dietary survey study (**Chapter 4**).

The analytical methods used were the same as those applied in the composite food survey (**Chapter 4**) and are detailed in **Section 3.2**. Briefly, these involved digesting weighed subsamples in concentrated sulfuric acid, filtering, diluting, and adding hydrogen peroxide to form the peroxotitanium (IV) sulfate complex. Analysis was by UV-visible spectroscopy for samples containing enough Ti to show a visible colour, and GFAAS for the lower-level (colourless) samples. Example calibration curves for each method are shown in **Figures 4.1** and **4.2**.

5.3 Results and discussion

5.3.1 Analytical results and summary statistics

Concentrations of Ti and TiO_2 (E171) determined in each of the 180 products are provided in **Appendix 5.2**. Summary statistics organised by product type are shown in **Table 5.2** (confectionery) and **Table 5.3** (non-confectionery foods and toothpastes). Consumed or chewed food items comprised 163 of the 180 samples. **Table 5.4** shows the proportions of this set that fall above and below specific concentration thresholds (**Table 5.4A**) and percentiles of the results distribution (**Table 5.4B**), for both Ti and TiO_2 equivalents.

For this assessment, results were designated as a positive E171 detection when the concentration of Ti is (a) >5.0 mg Ti/kg food, and (b) >100 mg Ti/kg ash. Applying these thresholds, the presence of E171 was confirmed in 38 (21%) of the 180 samples (**Table 5.5**). This hit-rate seems lower than might have

been expected based on previous work undertaken outside NZ and given that this survey was specifically designed to target foods most likely to contain E171. The prevalence of E171 in NZ foods in 2024, along with the accuracy of labelling, is discussed further in **Section 5.4**.

Results for products in which E171 was detected, as [TiO_2] equivalents in mg/kg and percentages (%) in both the product and the inorganic ash, are provided in **Table 5.6**. Within each product type listed in **Table 5.6**, E171 concentrations are ranked from highest to lowest.

Table 5.2 Summary statistics relating to confectionery (For the complete dataset, see Appendix 5.2).

Confectionery category	Type	N	Non-detects	Ti concentration (mg/kg, wet-weight basis)[a]						Presence of E171			E171 concentration in samples where detected ($mgTiO_2$/kg, wet weight)[b]			
				Mean	Std dev	Median	Geo-metric mean	Min	Max	E171 labels	E171 detect-ions	Percent containing E171 (%)	Mean	Std dev	Min	Max
Chocolate	Chocolate-containing bars	23	7	0.72	0.90	0.49	0.47	<0.35	4.43	1	0	-	-	-	-	-
	Chocolate-containing items (other)	7	4	1.58	2.28	0.45	0.52	<0.05	6.01	0	0	-	-	-	-	-
	Chocolate-containing sweets	12	0	309	446	3.34	19.6	0.29	1240	5	4	41.7	1230	650	474	2080
	Chocolates	**7**	**3**	**0.66**	**0.34**	**0.57**	**0.59**	**<0.62**	**1.15**	**0**	**0**	**-**	**-**	**-**	**-**	**-**
	All chocolate confectioneries	**53**	**14**	**74.7**	**249**	**0.57**	**1.16**	**<0.05**	**1240**	**6**	**5**	**9.4**	**1230**	**650**	**474**	**2080**
Flour or cereal-based	Biscuits	8	3	0.47	0.37	0.41	0.37	<0.28	1.28	1	0	-	-	-	-	-
	Biscuits (chewable bars)	3	0	172	149	234	50.4	1.96	280	2	2	66.7	429	53.5	391	467
	Cakes	5	0	1.15	0.55	1.07	1.03	0.43	1.89	0	0	-	-	-	-	-
	All flour/cereal confectioneries	**16**	**3**	**32.8**	**87.9**	**0.79**	**1.28**	**<0.28**	**280**	**3**	**2**	**12.5**	**429**	**53.5**	**391**	**467**
Sugar-based	Cake decorations	8	2	21.0	31.5	5.61	3.40	<0.38	84.1	5	4	50.0	69.4	57.4	17.3	140
	Cake icings	2	0	858	555	858	763	465	1250	2	2	100	1430	927	776	2090
	Chewable candies	29	15	35.6	142	0.42	0.94	<0.14	753	9	8	27.6	214	433	9.75	1260
	Chewing gums	6	0	224	543	2.37	6.17	1.21	1330	2	1	16.7	2220	-	2220	2220
	Hard candies	7	0	285	464	2.00	7.72	<0.30	1077	4	3	42.9	1110	864	139	1800
	Pharmaceutical (chewable and hard)	4	2	0.53	0.43	0.37	0.420	<0.42	1.16	0	0	-	-	-	-	-
	All sugar confectioneries	**56**	**19**	**112**	**311**	**0.74**	**2.15**	**<0.14**	**1330**	**22**	**18**	**32.1**	**577**	**796**	**9.75**	**2220**
Confectioneries - all categories combined		**125**	**36**	**86.2**	**266**	**0.680**	**1.56**	**<0.05**	**1330**	**31**	**25**	**20.0**	**696**	**772**	**9.75**	**2220**

Notes: [a]Non-detects were set to 0.5DL for the purposes of calculating means, standard deviation, medians, and geometric means; [b] Thresholds used: for this assessment, results were designated as a positive E171 detection when (a) mgTi/kg food >5.0 mg/kg, and (b) mgTi/kg ash >100 mg/kg.

Table 5.3 Summary statistics relating to non-confectionery foods and other products.

Food category	Type	N	Non-detects	Ti concentration (mg/kg, wet-weight basis)[a]						Presence of E171			E171 concentration in samples where detected ($mgTiO_2$/kg, wet weight)[b]			
				Mean	Std dev	Median	Geo-metric mean	Min	Max	E171 labels	E171 detect-ions	Percent containing E171 (%)	Mean	Std dev	Min	Max
Dairy products	Ice creams / dairy desserts	10	1	10.3	30.2	0.55	0.89	<0.15	96.1	0	1	10.0	160	-	160	160
	Cheese	1	1	<0.86	-	-	-	<0.86	<0.86	0	0	-	-	-	-	-
	All dairy products	11	2	9.4	28.8	0.43	0.83	<0.15	96.1	0	1	9.1	160	-	160	160
Drink additives	Powder and syrup	2	1	0.29	0.34	0.29	0.15	<0.09	0.53	0	0	-	-	-	-	-
Drinks (non-dairy)	Energy, sports or fruit drinks	5	3	0.21	0.23	0.12	0.13	<0.07	0.61	0	0	-	-	-	-	-
	Plant-based milks	5	2	0.07	0.04	0.07	0.06	<0.06	0.11	0	0	-	-	-	-	-
	All (non-dairy) drinks	10	5	0.14	0.17	0.08	0.09	<0.06	0.61	0	0	-	-	-	-	-
Food additives or ingredients	Liquid food colorants	4	0	56400	57700	27900	41500	26800	143000	4	4	100	94100	96300	44700	239000
Grain-based foods	Bread	1	1	<0.23	-	-	-	<0.23	<0.23	0	0	-	-	-	-	-
Infant foods	Baby foods	13	11	0.25	0.18	0.18	0.21	<0.29	0.79	0	0	-	-	-	-	-
Pharmaceuticals / Nutraceuticals	Tablets	2	0	2.79	3.10	2.79	1.73	<1.2	4.99	0	0	-	-	-	-	-
Toothpastes and related products	Toothpastes (10) and denture cream (1)	10	1	1260	1340	865	222	<0.83	3800	7	8	80.0	2630	2210	20	6350

Notes: [a]Non-detects were set to 0.5DL for the purposes of calculating means, standard deviation, medians, and geometric means; [b] Thresholds used: for this assessment, results were designated as a positive E171 detection when (a) mgTi/kg food >5.0 mg/kg, and (b) mgTi/kg ash >100 mg/kg.

Table 5.4A. Proportions of consumed or chewed food items above and below specific thresholds. (N=163; excludes food additives, pharmaceutical tablets, and toothpastes) – 5.4B. Concentration distribution percentiles.[a]

A

Category	Expressed as [Ti]		Expressed as [TiO_2]	
	Number	Percentage	Number	Percentage
Total food items	163	100	163	100
Below 0.5 mg/kg	88	54.0	53	32.5
Above 0.5 mg/kg	75	46.0	110	67.5
Above 5 mg/kg	27	16.6	31	19.0
Above 50 mg/kg	18	11.0	19	11.7
Above 500 mg/kg	8	4.9	10	6.1
Above 1000 mg/kg	4	2.5	8	4.9
Above 2000 mg/kg	0	0	1	0.6

B

Percentile	[Ti], mg/kg	[TiO_2], mg/kg	[TiO_2], %
10	0.12	0.20	0.00002
20	0.21	0.36	0.00004
30	0.26	0.44	0.00004
40	0.39	0.65	0.00006
50	0.46	0.76	0.00008
60	0.70	1.17	0.00012
70	1.20	2.00	0.00020
80	2.48	4.13	0.00041
90	83.7	140	0.014
95	684	1141	0.114
99	1279	2135	0.213

[a] Percentiles were calculated based on log-normalised data to correct for skew.

Table 5.5 Summary statistics relating to E171 detections.

Variable	Number	Percentage (%)
Total sample size	180	100
E171 detected	38	21.1
E171 labelling present	42	23.3
E171 labelling with presence confirmed	35	19.4
E171 labelling but no E171 detected	7	3.9
E171 detected but with no labelling	3	1.7

Table 5.6 Results for products in which E171 was detected, as [TiO_2] equivalents in mg/kg and percentages (%) in both the product and the inorganic ash.

Identity	Type	E171 Label	E171 in the product		E171 in the ash	
			mg/kg	%	mg/kg	%
Foods (ranked highest to lowest)						
Peak	Chewing gums	Yes	2223	0.22	24928	2.5
Ready-made white icing	Cake icings	Yes	2086	0.21	702231	70.2
M&Ms chocolate crispy	Chocolate-containing sweets	Yes	2076	0.21	145335	14.5
Swirly heart pops raspberry flavoured	Hard candies	Yes	1797	0.18	949016	94.9
M&Ms sweets cookie dough	Chocolate-containing sweets	Yes	1572	0.16	164603	16.5
Unicorn spinner lollipop	Hard candies	Yes	1387	0.14	2026920*	100*
M&Ms chocolate brownie	Chocolate-containing sweets	Yes	1327	0.13	95331	9.5
Woolworths Lollies Milk Bottles	Chewable candies	Yes	1256	0.13	220025	22.0
Pettinice white icing	Cake icings	Yes	776	0.08	442764	44.3
M&Ms milk chocolate	Chocolate-containing sweets	Yes	704	0.07	50292	5.0
Darrell Lea chocolates minty crunchy balls	Chocolate-containing sweets	Yes	474	0.05	44990	4.5
Strawberry flavoured thick shake bar (manufacturer redacted)	Biscuits (chewable bars)	No	467	0.05	48821	4.9
Tasti milkies choc vanilla snack size bars	Biscuits (chewable bars)	Yes	391	0.04	28762	2.9
Sour lollies	Chewable candies	Yes	311	0.03	799398	79.9
Coconut ice cream bites 6 pieces (manufacturer redacted)**	Ice cream biscuits	No	160	0.02	34085	3.4
Sugar natural crystal pink 90g	Cake decorations	Yes	140	0.01	78179	7.8
Oki Doki Christmas candy cane with jellybean	Hard candies	Yes	139	0.01	1254466*	100*
Sprinkle medley dancing unicorn 80g	Cake decorations	Yes	91.3	0.01	131119	13.1

[Continued over…]

Table 5.6 continued…

Identity	Type	E171 Label	E171 in the product		E171 in the ash	
			mg/kg	%	mg/kg	%
Party Times eggs	Chewable candies	Yes	54.9	0.01	208721	20.9
Sprinkle medley vintage pearl 80g	Cake decorations	Yes	28.8	0.00	76527	7.7
Sour peaches	Chewable candies	Yes	28.0	0.00	35305	3.5
Maycey's sour fruit mix	Chewable candies	Yes	19.8	0.00	25248	2.5
Skittles	Chewable candies	Yes	17.9	0.00	50143	5.0
Medley natural blue 85g	Cake decorations	Yes	17.3	0.00	58627	5.9
Skittles sweets fruits	Chewable candies	Yes	11.2	0.00	63574	6.4
Skittles sours lollies large bag	Chewable candies	Yes	9.8	0.00	21771	2.2
Food additives (highest to lowest)						
Gel colour super white	White	Yes	238570	23.9	558295	55.8
Gel colour neon blue	Blue	Yes	47386	4.74	769346	76.9
Gel colour neon yellow	Yellow	Yes	45584	4.56	524497	52.4
Gel colour neon orange	Orange	Yes	44743	4.47	632202	63.2
Toothpastes and related (highest to lowest)						
Macleans protect fresh mint	Toothpastes	Yes	6349	0.63	28860	2.9
Mouth fresh cool mint toothpaste	Toothpastes	Yes	4775	0.48	24692	2.5
Sensodyne rapid relief	Toothpastes	Yes	4229	0.42	20834	2.1
Oral-B 3D white	Toothpastes	Yes	1870	0.19	7767	0.8
Steradent active plus denture paste	Toothpastes	Yes	1693	0.17	4455	0.4
Colgate sensitive whitening	Toothpastes	Yes	1192	0.12	5543	0.6
Kids mild mint flavour toothpaste (manufacturer redacted)**	Toothpastes	No	922	0.09	4305	0.4
Pronamel gentle whitening fresh mint	Toothpastes	Yes	19.9	0.00	100	0.0

Note that some of the samples, including E171 in ash estimates, are vulnerable to large errors when the ash weight is very low; this effect was particularly evident in the hard candies. For two of these, the E171 in ash estimate exceeded 100% (which is not possible in reality). These are shown with an asterisk (*) to indicate the low reliability of those two estimates.

** The identity of the manufacturer is redacted due to a mismatch where some E171 was present though not listed in the product labelling. These are being referred to the applicable regulator. In all other cases, E171 detection was either consistent with the labelling, or (in 7 cases) E171 was not present despite being listed on the product labelling.

5.3.2 E171 concentrations

Where identified, E171 concentrations ranged from a minimum of 9.75 mg/kg (just under 0.001%) in a chewable candy (**Table 5.2**), to a maximum of 239000 mg/kg (23.9%) in a liquid food colourant (**Table 5.3**; see also **Table 5.6**).

5.3.2.1 Food colourings, cake coatings, decorations, and fillings

Food colourings had the highest E171 levels overall, and notably these were highest in white products: the range was from 44740 mg/kg (4.5%) in gel colour neon orange to 23.9% in gel colour super white (**Table 5.3**, **Appendix 5.2**). These products are concentrates, which are diluted before use. Ready-made white cake icing was found to contain E171 at 2086 mg/kg (**Appendix 5.2**) and is a good example of a product where one of these colourings would be present. The concentration of E171 in the icing was therefore just under 1% (0.87%) of the concentration in the white food colouring, which is the respective concentrate (presumably representative of the type used in the icing).

Previous research by Bucher et al. (2024) examined a range of cake decoration products, including cupcake icings, creamy icings, sugar paste icings, decorative pearls, and other mixes, and reported E171 concentrations ranging from 2.5 mg/kg in football-themed decorations to 11440 mg/kg in super paste gold and vanilla-flavoured icing. These findings highlight the variability in E171 content across decorative applications.

Beyond cake decorations, E171 levels in coatings and fillings (excluding fruit-based fillings) also show significant variation. For example, Clayton-Cuch (2023) reported 1260 mg/kg in a decorative 'gold dust' spray, while da Silveira Estevão et al. (2023) found 950 mg/kg in similar products. He et al. (2022) observed a narrower range of 3.2–301 mg/kg across various coatings. Verleysen et al. (2022b) contributed multiple datasets, reporting 354–2840 mg/kg in general decorative items and 217–6730 mg/kg specifically in decorative pearls. Additional studies supporting these findings include Nkenda et al. (2023) who reported 325 mg/kg, and Sungur et al. (2020) who found concentrations ranging from 213–2370 mg/kg in similar decorative applications. Data in this study clearly fall within this broad spectrum for cake decorations and related products and provide further insight into the approximate magnitude of dilution relative to E171 in white food colouring (which could be considered an index concentrate). The highest concentration reported for a food product in the literature discussed above (11440 mg/kg) is approximately 5% (4.8%) of the concentration in white food colouring (239000 mg/kg).

5.3.2.2 Sugar-based and chocolate confectionery

Across the confectionery group, 125 samples were analysed, of which 36 showed non-detectable levels of Ti.

Among candies and chewing gums, Peak chewing gum stood out at 2223 mg/kg, followed closely by M&Ms Chocolate Crispy (2076 mg/kg) and Swirly Heart Pops Raspberry Flavoured Hard Candy (1797 mg/kg). Other notable products include M&Ms Sweets Cookie Dough (1572 mg/kg), Unicorn Spinner Lollipop (1387 mg/kg), and Woolworths Lollies Milk Bottles Chewable Candy (1256 mg/kg) (**Appendix 5.2**).

The range of E171 found for chewing gums in this study was 2–2223 mg/kg, which aligns with several previous findings. For instance, He et al. (2022) reported a range of 6.7–1337 mg/kg, and Namhoon Kim et al. (2018) observed concentrations between 20.4–75.9 mg/kg. Similarly, Putra et al. (2022) reported values from 20–836 mg/kg, and Sungur et al. (2020) documented a range of 195–1057 mg/kg. Verleysen et al. (2022b) presented a broader range of 18.7–2878 mg/kg, which largely overlaps with our results. Some previous studies also reported higher concentrations at the top end of their surveyed ranges. For example, Dudefoi et al. (2018) observed a wide range of 500–12100 mg/kg, while Periasamy et al. (2015) reported values between 2990 and 3854 mg/kg. Individual findings from Nkenda et al. (2023), Reed et al. (2015), and Fiordaliso et al. (2018) were 3423 mg/kg, 5122 mg/kg, and 250–7530 mg/kg, respectively. More recent data from Cao et al. (2024) and Bastardo-Fernández et al. (2024), reported 4.6 mg/kg and 7.52 mg/kg, respectively, both of which fall near the lower end of our observed range. Collectively, these comparisons suggest that our findings on the E171 concentration range are broadly consistent with those previously reported in the literature and capture the variability across different studies.

Chocolate-containing products showed wide variation in Ti concentrations (**Appendix 5.2**), as reported in the broader literature, though relatively few contained it as E171. Specifically, Ti was detected in 39 of the 53 (74%) chocolate products tested, with an overall range from <0.05 mg/kg to 2076 mg/kg in M&Ms Chocolate Crispy (**Appendix 5.2**). However, only 5 of the 53 samples (9%) met the threshold tests used to indicate the likely presence of E171 (**Table 5.2**). All 5 of these E171-positive samples were chocolate-containing sweets. Mean [E171] in this subset was 1230 mg/kg (**Table 5.2**). This value aligns with findings from Espada-Bernabé et al. (2024), who reported a mean E171 concentration of 1219 mg/kg in coloured chocolate candies. M&Ms Milk contained E171 at a concentration of 704 mg/kg, while Darrell Lea Minty Crunchy Balls had 474 mg/kg. Snack-bars – Strawberry flavoured thick shake bar (manufacturer redacted) and Tasti Milkies Choc Vanilla Bars – contained [E171] at 467 mg/kg and 391 mg/kg, respectively, with sour lollies showing 311 mg/kg (**Appendix 5.2**).

These values fall within or slightly below the ranges reported in other studies. For example, Weir et al. (2012) found E171 levels between 2.15–8.41 mg/kg in general chocolates, while Bastardo-Fernández et al. (2024) reported a broader range of 1–272 mg/kg. Cao et al. (2024) documented a notably high concentration of 4680 mg/kg. In Smarties and M&Ms, Lomer et al. (2000) reported 460 mg/kg,

Verleysen et al. (2022b) found 1451–2265 mg/kg, and Weir et al. (2012) observed 1400–2085 mg/kg. Reed et al. (2015) reported 1735 mg/kg, while Bucher et al. (2024) identified a wide range of 2.54–6940 mg/kg in Junior Mints and 3.1–5502 mg/kg in M&Ms. Abd-ElHamid et al. (2023) reported exceptionally high levels of 600–16200 mg/kg in M&Ms. Other studies such as Kim et al. (2018), Lim et al. (2018), and Liu et al. (2022), reported ranges from 38.5 to 2750 mg/kg. Compared to these findings, our data generally falls within the mid-to-lower end of the reported spectrum, suggesting variability across product types, manufacturing batches, and (possibly) regional formulations.

5.3.2.3 Toothpastes

Toothpastes (**Table 5.3**) have also shown significant levels of E171, with considerable variation across brands and formulations. Among the 10 samples analysed, [TiO_2] equivalents ranged from undetectable (<0.69 mg/kg) in Red Seal Kid's Toothpaste Gel to 6349 mg/kg in Macleans Protect Freshmint (**Appendix 5.2**). E171 was detected in 9 of the 10 toothpastes. Three of the 10 samples contained undetectable or low levels of TiO_2 equivalents or E171 (the <0.69 mg/kg noted above, 8 mg/kg in Colgate Advanced Whitening, and 19.9 mg/kg in Pronamel Gentle Whitening Freshmint), whereas the other seven toothpastes showed moderate to relatively high levels of E171 (from 922-6349 mg/kg), mean 3004 mg/kg, standard deviation 2100 mg/kg. Adelantado et al. (2020) reported E171 concentrations ranging from 833–6013 mg/kg in Elmex Sensitive Plus Gum Care toothpaste, indicating substantial variability even within a single product line. In Colgate formulations, several studies have documented elevated levels including Asfaw and Wibetoe (2004) reported 7841 mg/kg, Correia et al. (2018) found 8676 mg/kg, and De la Calle et al. (2017) observed a wide range from 90.1–12346 mg/kg. Peters et al. (2014) reported concentrations between 4740 and 8201 mg/kg, while Schwab et al. (2012) identified levels ranging from 45–8700 mg/kg. Some Sensodyne products are also reported to contain significant E171. Wasim et al. (2023) reported a range of 6.0 to 9623 mg/kg, Verleysen et al. (2022b) found 951 mg/kg, and Weir et al. (2012) documented 9343 mg/kg in Sensodyne and 1168 mg/kg in Colgate. In comparison, this study identified 8.0 mg/kg in Colgate Advanced Whitening and 4229 mg/kg in Sensodyne Rapid Relief (**Appendix 5.2**). These findings suggest that while some toothpaste products contain high levels of E171, others, particularly recent formulations, may reflect efforts to reduce its concentrations.

5.3.2.4 Flour or cereal-based confectionery

Sixteen products in this category were tested. E171 was detected in only two of these, both of which were chewable bars (**Table 5.3**). Concentrations were not particularly high (391 mg/kg) in a Tasti milkies choc vanilla snack size bar, and 467 mg/kg in a Strawberry flavoured thick shake bar (manufacturer redacted) (**Appendix 5.2**). The relative prevalence of E171 is further discussed in **Section 5.3.3**.

5.3.2.5 Dairy and related products

Eleven products in this category were tested. E171 was detected in only one of these (an imported product: Coconut ice cream bites 6 pieces (manufacturer redacted), **Appendix 5.2**) at a relatively low concentration of 160 mg/kg (**Table 5.4**). The relative prevalence of E171 is further discussed in **Section 5.3.3**.

5.3.2.6 Other items

In addition to the items discussed above, 28 other products were tested, from the following categories (with the number of products in brackets): infant foods (13), non-dairy drinks and drink additives (12), pharmaceuticals/nutraceuticals (2), and grain-based foods (1). E171 was not detected (to a level that met the threshold tests for E171) in any of these (**Table 5.4**). The highest Ti concentration across all 28 of these other products was only 5 mg/kg, found in one of the pharmaceutical tablets. The mean and highest Ti concentrations detected across the 13 samples of infant foods were 0.25 mg/kg and 0.79 mg/kg, respectively, which are low enough to reflect natural Ti. The maximum Ti determined for any of the 12 (non-dairy) drinks or drink additives was also a low figure (0.61 mg/kg), and more likely to be natural Ti than E171.

5.3.2.7 Overall

For items in which E171 was detected, the concentrations found in this study were 'in keeping with' those reported previously. Part of the picture is that some product categories show large variations in E171 between individual products, for example, E171 in 10 toothpastes ranged from <0.69 mg/kg to 6349 mg/kg. However, the upper ends of the ranges reported in this study are consistent with those previously reported in overseas studies. In some of the targeted food categories – including infant foods – levels of Ti detected were very low, and most likely reflected natural Ti rather than any presence of E171.

5.3.3 E171 prevalence and the accuracy of labelling

Table 5.4A provides percentages of the 163 consumed food or chewed food items below and above set thresholds for [Ti] and [TiO_2] equivalents; and **Table 5.4B** shows percentiles for the same set. **Table 5.5** presents summary statistics for samples that met the decision thresholds for the presence of E171 (see **Section 5.3.1**), across all 180 (both food and non-food) samples, and how these relate to food labelling. **Table 5.7** (on the following page) lists products where either E171 was declared on the label but not detected, or E171 was detected in the product but not listed on the label.

Table 5.7 Identities of apparently mis-labelled food products and related analytical data.

Type of mislabelling	Product identity	mgTi/kg	mgTiO_2 /kg equivalents	Manufacturer	Type
E171 listed on the label but not detected	Weight watchers choc coconut delight bar	0.58	0.97	Tasti	Chocolate-containing bar
	Donut factory 12 mini-iced	0.66	1.10	The Donut Factory	Biscuits
	LCMs cereal bars unicorn	1.96	3.26	Kelloggs	Biscuits (chewable bar)
	Sprinkle medley eyes baby 80g	<0.19	<0.32	Sweet moments	Cake decorations
	Berries and cream	<0.25	<0.40	the CareFillery	Chewable candy
	Extra white gum	1.21	2.02	Mars Wrigley	Chewing gum
	Crystal sticks cotton candy flavoured sticks	<0.33	<0.56	Candy showcase	Hard candy
E171 detected but not listed on the label	Strawberry flavoured thick shake bar (manufacturer redacted)*	280	467	----------	Biscuits (chewable bar)
	Coconut ice cream bites 6 pieces (manufacturer redacted)*	96	160	----------	Ice cream biscuits
	Kids mild mint flavour toothpaste (manufacturer redacted)*	553	922	----------	Toothpaste

* The identity of the manufacturer is redacted due to a mismatch where some E171 was present though not listed in the product labelling. These are being referred to the applicable regulator. In all other cases, E171 detection was either consistent with the labelling, or (in 7 cases) E171 was not present despite being listed on the product labelling.

The study set out in this chapter was designed to target foods more likely to contain E171. Despite this, over half (54%) of the food items contained less than 0.5 mgTi/kg (**Table 5.4A**), and most detected concentrations were towards the lower end of the possible range. Detections above 5 mgTi/kg were more likely reflecting the presence of E171 (TiO_2). In these units ($mgTiO_2$ /kg), only 19% of the food samples contained more than 5 mg/kg, 11% more than 50 mg/kg, and 6% more than 500 mg/kg, and 0.6% (only one product) more than 2000 mg/kg (**Table 5.4A**).

Overall, E171 was detected in 38 of the 180 samples (21.1%). Among the samples, 42 (23.3%) were labelled as containing E171, and within this group, E171 presence was confirmed in 35 samples (83% of the labelled set). However, seven labelled samples (17% of that set) did not contain detectable levels of E171, while three samples tested positive for E171 despite lacking labelling.

This data highlights two possible sources of discrepancy in the detection of E171: inconsistent labelling practices or limitations in the experimental testing procedure.

While most of the 42 products labelled as containing E171 did test positive, seven did not (**Table 5.7**):

- For some of these samples, it is possible that E171 had been intentionally incorporated in the product, but only at a trace level. This is considered unlikely because trace-level use of E171 would be inconsistent with its known uses.
- It seems more likely that some products have been reformulated to exclude E171, but their packaging has not been updated accordingly. Listing E171 on a product label (where none is present) would present a low risk to a manufacturer working through a stock of old packaging. The higher regulatory risk would be using E171 without recording it on the product label.

Conversely, three products with no indication of E171 or titanium dioxide on the labelling were found to contain it at readily detectable concentrations: 160 mg/kg, 467 mg/kg, and 922 mg/kg (**Table 5.7**). These levels appear to be higher than could be accounted for by trace contamination or cross-contact during manufacturing and are likely cases of mislabelling. One of the three products is a toothpaste (Kids mild mint flavour toothpaste; manufacturer redacted), and the other two are highly processed foods (thick shake bars and ice-cream bites). It might be the case that, for highly processed foods, manufacturers may be unaware of the presence of E171 in one or more ingredients, and/or that levels are low enough not to require a label for that product in its country of origin.

5.4 Dietary intake estimates for habitual consumers

In **Chapter 4,** it was determined that the natural intakes of Ti in New Zealanders are lower than 1 mg/day (as ingested). Age- and gender-specific groups aged 11 years and older are estimated to consume 500–750 µg/day. In younger age groups, intakes are even lower, reflecting lower food consumption. Expressed as a dose, adults averaged 7.5 µg/kg/day (**Table 4.10**, **Section 4.3**). This created a significant mismatch between estimated TiO_2 intakes reported in previous studies (**Table 4.1**) and those found in this study. Even the low end of the range reported by EFSA (2016) was 25 times higher than natural intakes estimated in this study (**Section 4.3**). The difference was attributed to the proportion of total foods likely to contain added E171.

In this chapter, targeting 180 products previously reported to contain significant E171, there were definite positives in **Table 5.5**. Where detected in samples across a given group, E171 was also present in the same concentration ranges as previously reported. However, the prevalence of E171 (21% of samples) appears lower than implied by previous overseas research. While this may reflect unique aspects of some products (such as confectionery) sold in NZ, it seems more likely that a genuine change in E171 prevalence has occurred in response to restrictions in overseas markets. Either way, this outcome makes it difficult to provide an average or range for E171 intakes among New Zealanders, because determining such a range would require detailed knowledge of every food product people routinely eat and the E171 status of all these foods. In a situation where E171 is present in only a small subset of confectioneries, even to the extent that it is present in some types of M&Ms but not others, intakes are going to become more idiosyncratic.

This part of the thesis explores potential intakes among people who habitually consume a preferred product that contains E171, building on the E171 concentration and product data shown in **Table 5.6**. To undertake these estimates, assumptions must be made about the amount of E171-containing product being consumed, and how often this is, over a given time period. Such estimates are necessarily indicative of possibilities but serve to bridge the gap between the natural Ti intakes and the magnitudes of possible intakes when the E171-containing product is habitually consumed.

Data relating to the subset of products containing E171, assumed weight-per-serving, servings per fortnight, and proportion ingested; and resulting E171 intakes, are provided in **Table 5.8**. The origin of each portion-size weight selected in **Table 5.8** is set out in **Appendix 5.3**. Inclusion of one composite group comprising chewable candy, chocolate-containing sweets, and hard candy is intended to allow some switching between similar products within these groups, which may contain E171.

Table 5.9 sets out these potential intakes on a Ti dose basis for 10 of the 11 age and gender groups (the infant 6–12 months category is excluded, because the exposure assumptions set out in **Table 5.8**

are unrealistic for that group). **Table 5.10** presents the ratios of doses received relative to natural doses (**Table 4.10**).

Table 5.8 Indicative dietary intakes of E171 (TiO_2) based on consumption of food products containing E171.
(Infants are excluded as assumptions in **Table 5.8** are not applicable).

Data relating to the subset of products found to contain E171	Mean E171 (mg/kg = µg/g)	Weight per serving (g)	Servings per 14 days	Weight per 14 days (g)	Proportion ingested	E171 ingested	
						µg/14 d	µg/d
Ice cream biscuits (N=1)	160	26	4	104	1.0	16640	1189
Chewable candies (N=8)	214	180	4	720	1.0	154080	11006
Biscuits (chewable bars) (N=2)	429	20	4	80	1.0	34320	2451
Hard candies (N=3)	1108	23	4	92	1.0	101936	7281
Chocolate-containing sweets (N=5)	1231	130	4	520	1.0	640120	45723
Cake icings (N=2)	1431	40	2	80	1.0	114480	8177
Maxima for chewable candies (1256), chocolate-containing sweets (2076), and hard candies (1797) (N=3)	1710	111	4	444	1.0	759240	54231
Chewing gums (N=1)	2223	28	4	112	0.2	49795.2	3557
Toothpastes (N=8)	2631	2.8	14	39.2	0.1	10314	737

Table 5.9 Potential Ti intakes (as doses) for people habitually consuming a product containing E171, for 10 of the 11 age and gender groups.
(Infants are excluded as assumptions in **Table 5.8** are not applicable).

Data relating to the subset of products found to contain E171	Mean E171 (mg/kg = µg/g)	Ti ingested									
		As ingested	Dose per kg body weight µg/kg/d								
		µg/d	Males 19 - 24 yrs	Males >25 yrs	Females >25 yrs	Pacific Females >15 yrs	Pacific Males >15 yrs	Boys (11-14 yrs)	Girls (11 - 14 yrs)	Children (5 - 6 yrs)	Pre-school (1-3 yrs)*
Ice cream biscuits (N=1)	160	712	9	8	10	8	7	13	13	31	55
Chewable candies (N=8)	214	6596	83	76	90	75	67	122	122	287	507
Biscuits (chewable bars) (N=2)	429	1469	18	17	20	17	15	27	27	64	113
Hard candies (N=3)	1108	4364	55	50	60	50	44	81	81	190	336
Chocolate-containing sweets (N=5)	1231	27402	345	316	374	311	279	507	507	1191	2108
Cake icings (N=2)	1431	4901	62	57	67	56	50	91	91	213	377
Maxima for chewable candies (1256), chocolate-containing sweets (2076), and hard candies (1797) (N=3)	1710	32501	409	375	443	369	331	602	602	1413	2500
Chewing gums (N=1)	2223	2132	27	25	29	24	22	39	39	93	164
Toothpastes (N=8)	2631	442	6	5	6	5	5	8	8	19	34

Table 5.10 Ratios of potential Ti intake from consuming a product containing E171 (see Table 5.9) compared with natural intakes (see Table 4.10).

Data relating to the subset of products found to contain E171	Intake ratios: Ti from ingested E171 / estimated natural Ti								
	Males 19 - 24 yrs	Males >25 yrs	Females >25 yrs	Pacific Females >15 yrs	Pacific Males >15 yrs	Boys (11-14 yrs)	Girls (11 - 14 yrs)	Children (5 - 6 yrs)	Pre-school (1-3 yrs)*
Ice cream biscuits (N=1)	1	1	1	1	1	1	1	2	2
Chewable candies (N=8)	9	10	13	12	9	11	13	15	18
Biscuits (chewable bars) (N=2)	2	2	3	3	2	2	3	3	4
Hard candies (N=3)	6	7	9	8	6	7	9	10	12
Chocolate-containing sweets (N=5)	39	42	53	49	36	46	56	61	76
Cake icings (N=2)	7	8	10	9	6	8	10	11	14
Maxima for chewable candies (1256), chocolate-containing sweets (2076), and hard candies (1797) (N=3)	46	50	63	58	43	54	66	73	91
Chewing gums (N=1)	3	3	4	4	3	4	4	5	6
Toothpastes (N=8)	1	1	1	1	1	1	1	1	1

Results demonstrate that routine consumption of a product containing E171 can easily bridge the gap between natural Ti intakes and those estimated in previous surveys (**Table 4.1**). For example, a 30-year-old female who eats two 130 g packs of a specific chocolate sweet each week, which happens to contain E171 (at 1231 mg/kg, **Table 5.8**), would ingest the equivalent of 27.4 mgTi/day (**Table 5.9**), increasing their equivalent daily dose of Ti by a factor of 63 times (**Table 5.10**).

Similarly, Ti intakes in preschoolers could potentially reach a dose equivalent of 2.5 mg/kg/day (**Table 5.9**), or 4.2 mg/kg/day expressed as TiO_2.

The assumptions in **Table 5.8** can clearly be varied. Still, the overall picture will always be that the routine consumption of even one type of food product containing E171 can significantly increase a person's overall Ti intake, in these estimates by between approximately 1 and 100 times (**Table 5.10**) compared with natural intakes. Two packs per week of an E171-containing product in the composite confectionery group (a typical E171-containing chewable candy, chocolate-containing sweet, or hard candy) would be sufficient to deliver the equivalent of 54 mg E171 per day (**Table 5.8**), and a dose range of 0.55–4.2 mg/kg/day (from Pacific males >15 yrs to pre-school children) (**Table 5.9**).

Closing the loop, there is now close correspondence between these indicative estimates for habitual consumers of E171-containing items and reported E171 intakes from previous studies (**Table 4.1**). For example, EFSA (2016) reported ranges of 0.3–4.0 mg/kg/day for adults, and 0.5-3.7 mg/kg/day for children (**Table 4.1**). What appears to have changed is that most previous estimates seem to represent (or are presented as) actual intake ranges across the study population, presumably because E171 was more prevalent than it is today, or in NZ in 2024. By contrast, the estimates in this section are best seen as possible idiosyncratic intakes in particular individuals who (for one reason or another) continue to consume a specific product that happens to contain E171.

The other finding from this hypothetical analysis is that intakes from E171-containing chewing gums or toothpastes may be relatively modest, compared with those from food items. Using the assumptions shown in **Table 5.8**, each of these product categories may work to approximately double E171 intakes relative to their natural levels (**Table 5.10**), which is not a substantive increase. Note, however, that for these products the estimates are sensitive to assumptions about the proportions ingested, assumed to be 5% for chewing gum and 10% for toothpaste. For all other items, the ingested portion was assumed to be 100%.

Finally, it is worth reiterating that not all products in each category were found to contain E171 in this survey. Therefore, these estimates relate only to the idiosyncratic exposures of habitual consumers of a product in a given category (e.g., a chewing gum) that actually contains it.

5.5 Discussion and summary – key findings

5.5.1 Prevalence and use of E171

The focus of this survey was on products sold in NZ that are most likely to contain E171, based primarily on findings from previous research (**Table 5.1**) and product labelling. A total of 180 products were tested, 163 of which were foods. E171 was deemed to be present when a product contained [Ti] at both >5.0 mg/kg in the product and >100 mg/kg in the ash.

Applying these criteria, E171 was detected in 21% (38) of the 180 samples. 23% (42) of the 180 samples had labelling indicating the presence of E171. In seven of these, however, E171 was not present despite the labelling. Conversely, three products were found to contain E171, but it was not listed on the product label.

Discussion relating to E171 concentrations by product type has been presented in **Section 5.3.2**. It will not be repeated here, except to note that in products where E171 was detected, its concentration was in the usual range reported for that product type in previous literature. The more novel findings in this survey relate more to the prevalence of E171 use and labelling.

Considered together, these three factors –

1. A relatively low apparent prevalence: only one-fifth (21%) of the products contained E171 despite the survey being designed to target products where it has been most commonly used. This follows on from E171 only being detected in one product across the composite food survey study (**Chapter 4**);
2. A significant subset (17%) of cases where E171-labelled products did not actually contain E171; and
3. E171 concentrations are in their expected range in products where they were detected.

This suggests that the proportion of products using E171 has decreased, mainly by moving product lines to E171-free versions rather than a gradual decrease in concentrations.

This finding is regarded as probable rather than definitive, because there is no previous NZ survey data to compare the survey results with.

However, Factors 1 and 2 are consistent with declining use. The finding that 17% of products labelled as containing E171 do not actually contain it (Factor 2) suggests that food manufacturers who have substituted to an equivalent product that does not contain E171 (to meet overseas market requirements) may be working through old stock of packaging or may have yet to update product labels.

Factor 3 suggests that any decrease is likely achieved by moving each product to an E171-free production chain (from presence to absence), rather than by reducing the concentration of E171 in individual products.

5.5.2 Possible intakes for habitual consumers

Results of basic intake modelling demonstrate that habitual consumption of a product containing E171 can easily bridge the gap between natural Ti intakes (approximately 7.5 µg/kg/day for adult New Zealanders, **Chapter 4**) and those estimated in most previous surveys (for example, EFSA's estimate of 0.3–4.0 mg/kg/day for adults). Routine consumption of even one type of food product containing E171 can significantly increase a person's overall Ti intake by approximately 1–100 times compared with natural intakes.

Results also confirm that previous intake estimates from other jurisdictions closely track E171 as the sole Ti or TiO_2 source. This was reasonable under circumstances where E171 was prevalent and difficult to avoid in the diet, because under those circumstances, it would quickly come to dominate Ti intake. The current study (and some more recent literature) suggests that such intake estimates would now be out of date, especially in EU countries.

Assuming E171 prevalence in food has been decreasing, these factors suggest that NZ intakes would probably now fall into two distinct bands:

- Most people for whom intakes of Ti would be close to (perhaps within 2-3 times of) those attributable to the intake of natural Ti from foods (**Chapter 4**);
- Some people who habitually consume a preferred food (e.g., a specific confectionery), or a long-term pharmaceutical medication, that contains E171, whose intakes of Ti (and TiO_2) could easily be 50 or more times higher (**Section 5.3.2**).

Taking the precautionary view that higher doses of E171 may cause health effects over the longer term, the best outcome would be for the (apparent) trend of E171 being gradually phased out across an increasing number of product lines to continue.

In this study (**Section 5.3.2**), it was also found that E171 intakes from toothpaste ingestion, or routine use of a chewing gum containing E171, may be relatively low compared with those obtainable from ingestion of E171-containing confectionery or other food products. In this case, the proportion ingested is one of the moderating assumptions (**Table 5.8**), and testing this could be a valuable focus for future research (see below).

Finally, in this study, only two pharmaceutical/nutraceutical products were tested. Neither contained E171 (**Table 5.3**); however, some long-term medications do contain E171, and restrictions on its use

have not yet extended to this area. For example, a search of product data sheets for perindopril (a daily-dose ACE inhibitor used to lower blood pressure) and atorvastatin (a daily-dose statin) reveals that both contain E171 in the film coating. Formulations may vary, and this tablet formulation information is not provided in NZ Data sheets for either drug (provided by Medsafe), but does appear in data sheets, labels, and product monographs from the UK, US, Canada, and South Africa (EMC, 2025; Medsafe, 2025; SAHPRA, 2025; Servier Canada Inc, 2016; USFDA, 2024). Some people taking long-term medications could therefore fall into category two above, due to ongoing use of E171 in some tablets.

5.5.3 Suggestions for future research

Four avenues of potentially useful future NZ research in this area are as follows:

- A repeat of the product survey at a future date (say 2034) to establish whether the prevalence of E171 has declined between then and 2024, and whether the potential higher-dose exposures are likely to have declined;
- A future survey to better characterise consumption patterns for products that contain E171, which people or groups are most likely to eat a given product routinely;
- Work to characterise better the proportions of E171 ingested from chewing gum and toothpastes (the 'proportion ingested' in **Table 5.8**), to set intakes from those sources in the context of the natural baseline from foods; and
- Characterisation of E171 in the most common long-term tablet medications (e.g., perindopril for blood pressure and atorvastatin for blood lipids), to determine whether these might lead to significant daily intakes, and the possible significance of such exposures for such patient groups.

CHAPTER 6: Cytotoxicity of titanium dioxide (E171 and P21) in an oleic acid-induced steatosis in HepG2 cells

6.1 Introduction

The increasing use of TiO_2 NPs, particularly in food-grade applications, has raised concerns regarding their potential health impacts (Younes et al., 2021). As these particles interact with biological systems, their physicochemical properties play a pivotal role in determining their behaviour, distribution, and toxicity. Previous studies evaluating the toxicity and potential adverse effects of E171/TiO_2 NPs have emphasised the importance of thorough physicochemical characterisation. Parameters such as particle size, shape, surface charge, and crystalline structure significantly influence their biological interactions and toxicokinetic behaviour (**Appendices 2.1** and **2.2**). Several tools, including X-ray photoelectron spectroscopy (XPS), Scanning Electron Microscopy (SEM), Transmission Electron Microscopy (TEM), X-ray Diffraction (XRD), Graphite Furnace Atomic Absorption Spectroscopy (GFAAS), and DLS, are robust and practical tools for the detection, characterisation, and quantification of TiO_2 (Yang et al., 2014).

The liver's function in filtering and processing foreign substances makes it particularly susceptible to nanoparticle-induced toxicity (Sun et al., 2021). Hepatocytes play an important role in detoxification, metabolism, protein synthesis, and innate immunity (Zhou et al., 2016). One of the key pathological outcomes of liver dysfunction is hepatic steatosis, which is the first step in MASLD, a condition linked to obesity and dyslipidaemia. Moreover, both environmental and dietary factors also contribute to the development and progression of MASLD (Girish & John, 2025). In humans, hepatic steatosis is characterised by the accumulation of triglycerides in the liver, with monounsaturated fatty acids, including OA, being disproportionately elevated in patients with hepatic steatosis (Araya et al., 2004; Guo et al., 2022). The OA-induced steatotic HepG2 cell model exhibits morphological characteristics similar to those of hepatocytes in patients with hepatic steatosis and has therefore been widely utilised as an *in vitro* model of steatosis (see **Table 2.2**). Establishing a human cell model of steatosis is of significant value for understanding the early mechanisms of MASLD.

Previous studies have demonstrated that TiO_2 can induce dose-dependent cytotoxic effects *in vitro* (for details, see **Appendix 2.2**). These effects include reduced cell viability, oxidative stress, and membrane damage across various cell lines (**Appendix 2.2**). To investigate early-stage changes in MASLD, it is essential to determine the cytotoxic dose range of E171/TiO_2 NPs. Establishing an optimal concentration will enable meaningful correlation between exposure to E171/TiO_2 NPs and cellular responses in the steatotic cell model.

The aims of the study set out in this chapter are:

1. To establish the HepG2 cell model to be used for the rest of this study.
2. To characterise E171 and P21 nanoparticles.
3. To optimise an OA-induced steatotic model.
4. To evaluate the cytotoxic effects of TiO_2 on HepG2 cells.
5. To determine the effect of oleic acid (OA) treatment on the cytotoxicity of TiO_2 in HepG2 cells.
6. To investigate whether TiO_2 exposure promotes lipid accumulation in HepG2 cells.
7. To assess whether co-treatment with TiO_2 enhances OA-induced lipid accumulation in HepG2 cells.

The overall aim was to establish a physiologically relevant *in vitro* platform to evaluate the impact of TiO_2 (E171 and P21) exposure on HepG2 cells, focusing on their physicochemical properties, cytotoxicity, and effects on lipid metabolism in a steatotic model.

6.2 Methods

6.2.1 Physicochemical characterisation

To evaluate the potential variability in the physicochemical properties of E171, three samples (labelled E171 A, E171 B, and E171 C) were initially sourced from different suppliers. Comparative analysis showed no significant differences among E171 samples (A, B, C), and therefore E171 B was selected as a representative bulk material for further experimentation. In parallel, commercially available P21 nanoparticles (Sigma-Aldrich) were included to provide a defined nanoscale comparator. The rationale for this selection was:

I. E171 represents the bulk TiO_2 particles to which humans are commonly exposed through diet.

II. P21 represents engineered nanoparticles (<100 nm), which are frequently reported in the literature as the predominant form of TiO_2 assessed in previous studies (**Appendices 2.1** and **2.2**).

Using both materials allowed us to determine whether bulk E171 and nanoscale P21 exhibit distinct physicochemical properties and biological effects, thereby addressing the gap between real-world human exposure and nanoparticle-focused research.

6.2.2 SEM and TEM characterisation

SEM and TEM were utilised to study the morphology of TiO_2 (E171 and P21). E171 was analysed by SEM at 150,000-300,000x magnification with 10 kV acceleration, using water suspensions sonicated

and air-dried on stubs without coating. TEM examined P21 at 200 kV and 100,000x magnification, prepared in ethanol, dropped onto carbon-coated copper grids, air-dried, plasma-coated, and imaged with a digital camera. At least six images per sample for SEM and ten images for TEM were processed, and ImageJ was used to determine particle size distributions. See **Section 3.8** for a detailed description of the SEM and TEM procedures.

6.2.3 Powder X-ray diffraction spectroscopy (XRD)

Crystalline phases of TiO_2 samples were analysed using X-ray powder diffractometry on a Rigaku Spider diffractometer equipped with a rotating anode generator (Cu α radiation, 1.54180 Å), multilayer mirror optics, and a curved image plate detector. Powdered samples were pressed onto specimen holders to achieve uniform thickness, and the resulting data were processed in Microsoft Excel. XRD is described in more detail in **Section 3.8**.

6.2.4 Energy-dispersive X-ray spectroscopy (EDX) and energy dispersive spectroscopy (EDS)

Elemental composition of TiO_2 (E171 and P21) was analysed using SEM/EDX and TEM/EDS. For E171, a FEI Quanta 200 SEM in EDX mode was used to quantify major elements; samples were mounted on carbon tape and analysed by point analysis and elemental mapping. For P21, high-resolution elemental mapping was performed using a JEOL TEM with a silicon drift detector at x600K magnification. Spectra and elemental maps from both instruments were processed to interpret composition and spatial distribution. See **Section 3.8.3** for a more detailed description of the EDX and EDS procedures.

6.2.5 Dynamic light scattering (DLS)

Hydrodynamic diameter, zeta potential, and polydispersity index of TiO_2 (E171 and P21) were measured using a Malvern Zetasizer (ZEN 3600). Samples (0.05%) were prepared from stock, sonicated for 30 min in DI water or DMEM, and analysed. Three independent experiments were conducted, with pH and refractive index of the media recorded before analysis. See **Section 3.8.4** for a more detailed description of the DLS procedure.

6.2.6 Induction of steatosis

HepG2 cells were seeded at a density of 8×10^5/well in 6-well plates for 24 hours. Cells were subjected to serum starvation for 6 hours to enhance OA uptake. Cells were then treated with OA at varying concentrations (0–1 mM) for 48 hours to induce lipid accumulation.

The degree of steatosis was then evaluated by microscopic examination of ORO and haematoxylin-stained cells. The extent of steatosis was quantified spectrophotometrically through ORO dye uptake. See **Section 3.10** for a more detailed description of this procedure and **Section 3.10.2** for a description of the preparation of OA.

6.2.7 Oil red O (ORO) staining for evaluation of steatosis

HepG2 cells were seeded in 24-well plates and treated with varying concentrations of OA (0–1 mM) for 48 hours to induce steatosis. After treatment, cells were fixed with 10% formalin, rinsed, and stained with ORO and haematoxylin to assess lipid accumulation. Stained cells were imaged by light microscopy, and retained dye was eluted with isopropanol for spectrophotometric quantification at 500 nm, using isopropanol blanks for correction. Cells were examined at 20× magnification using a light microscope with an EP50 digital camera. Images were captured under uniform exposure settings and analysed with EP50 imaging software version 4.0. See **Section 3.11** for a more detailed description of ORO staining.

6.2.8 Cell viability assays

MTT assay was performed to assess cell viability. HepG2 cells (1×10^4/well) were seeded in 96-well plates and treated with varying OA concentrations (0–1 mM) for 48 h. After washing, cells were incubated with MTT for 4 hours, and DMSO was added to dissolve the formazan crystals. Plates were shaken for 15 min, and absorbance was measured at 570 nm using a microplate reader. See **Section 3.10.3** for a more detailed description of the MTT assay method.

The trypan blue exclusion assay was used to evaluate HepG2 cell viability after treatment with TiO_2 (E171 and P21) ± OA. Cells (8×10^5/well) were seeded in 6-well plates, treated with varying TiO_2 concentrations (0–200 µg/mL) for 48 hours, then harvested by trypsinisation and centrifugation. Cell suspensions were mixed 1:1 with 0.4% trypan blue, incubated briefly, and counted using a haemocytometer under a light microscope. Viable cells excluded the dye, while non-viable cells appeared blue. All assays were performed in triplicate. See **Section 3.10.3** for a more detailed description of the trypan blue exclusion assay.

The NRU assay was used to assess the cytotoxicity of TiO_2 (E171 and P21) ± OA in HepG2 cells. Cells ($2x10^4$ cells/well) were seeded in 96-well plates, treated with varying TiO_2 concentrations (0–200 µg/mL) for 48 hours, then incubated with neutral red solution to evaluate lysosomal integrity. After dye uptake, cells were washed, and the dye was extracted with destain solution. Absorbance was measured at 540 nm using a microplate reader. All assays were performed in triplicate. See **Section 3.10.3** for a more detailed description of the NRU assay.

6.2.9 Measurement of E171 and P21 cellular uptake in HepG2 cells

Cellular uptake of TiO_2 (E171 and P21) in HepG2 cells was assessed by exposing cells (± 0.25 mM OA) to TiO_2 concentrations (0–50 µg/mL) for 3 h. After thorough PBS washing and centrifugation to remove unbound particles, cell pellets were incinerated in a muffle furnace, digested in concentrated sulfuric acid, and diluted with DI water.

Each standard (0–50 µg/mL) was run in duplicate, and blank correction was performed by subtracting the blank reading from all standard values. Sulfuric acid served as a negative control. A standard curve (410 nm) was generated using E171 (**Figure 6.1**) and P21 (**Figure 6.2**) standards, and a straight line was obtained with its corresponding equation. The TiO_2 recovered content was obtained from the equation of the standard curve. See **Section 3.19** for a more detailed description of the measurement of cellular uptake of TiO_2.

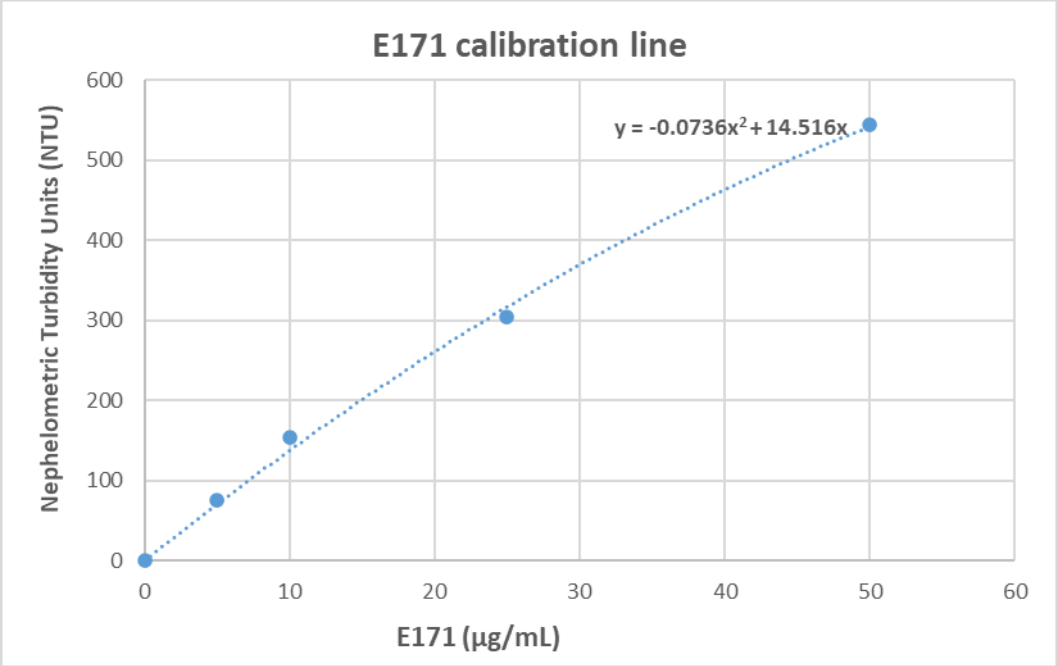

Figure 6.1 Representative standard curve of E171 concentration versus absorbance.

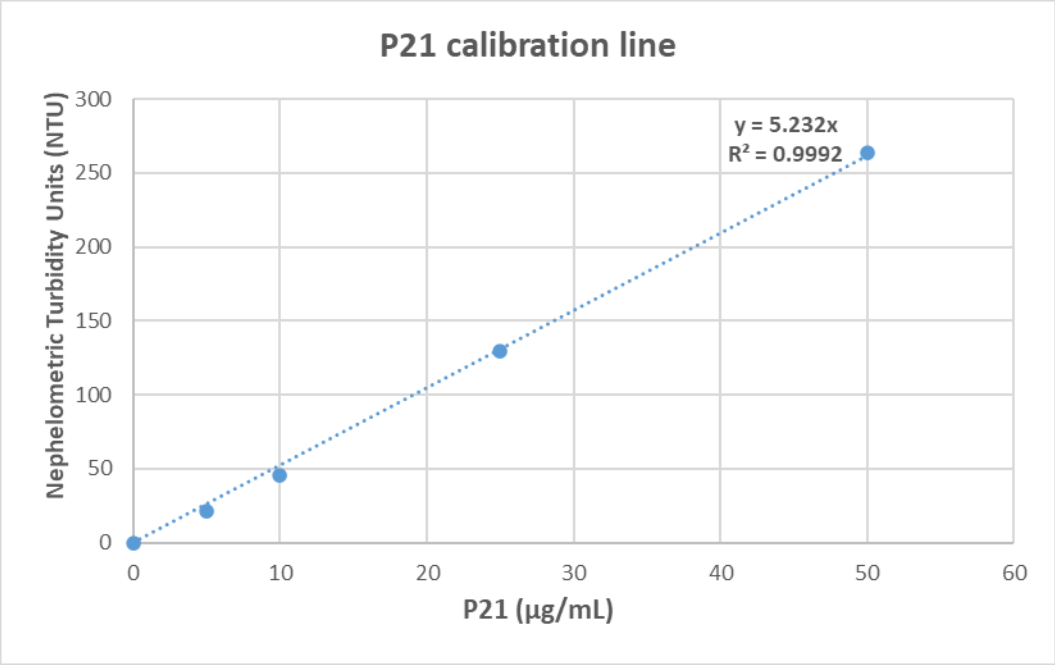

Figure 6.2 Representative standard curve of P21 concentration versus absorbance.

6.2.10 Statistical analysis

All experiments were conducted in at least triplicate, and data are expressed as mean ± SEM unless otherwise specified. Group differences were assessed using one-way ANOVA when a single variable was tested, or two-way ANOVA when two variables were evaluated, followed by Tukey's post hoc test for multiple comparisons. Statistical analyses were performed using GraphPad Prism version 10.6.1 (GraphPad Software, La Jolla, CA, USA).

6.3 Results

6.3.1 SEM and TEM characterisation

SEM analysis revealed that the E171 powder comprised particles with a range of sizes and primarily slightly rounded morphologies (**Figure 6.3**).

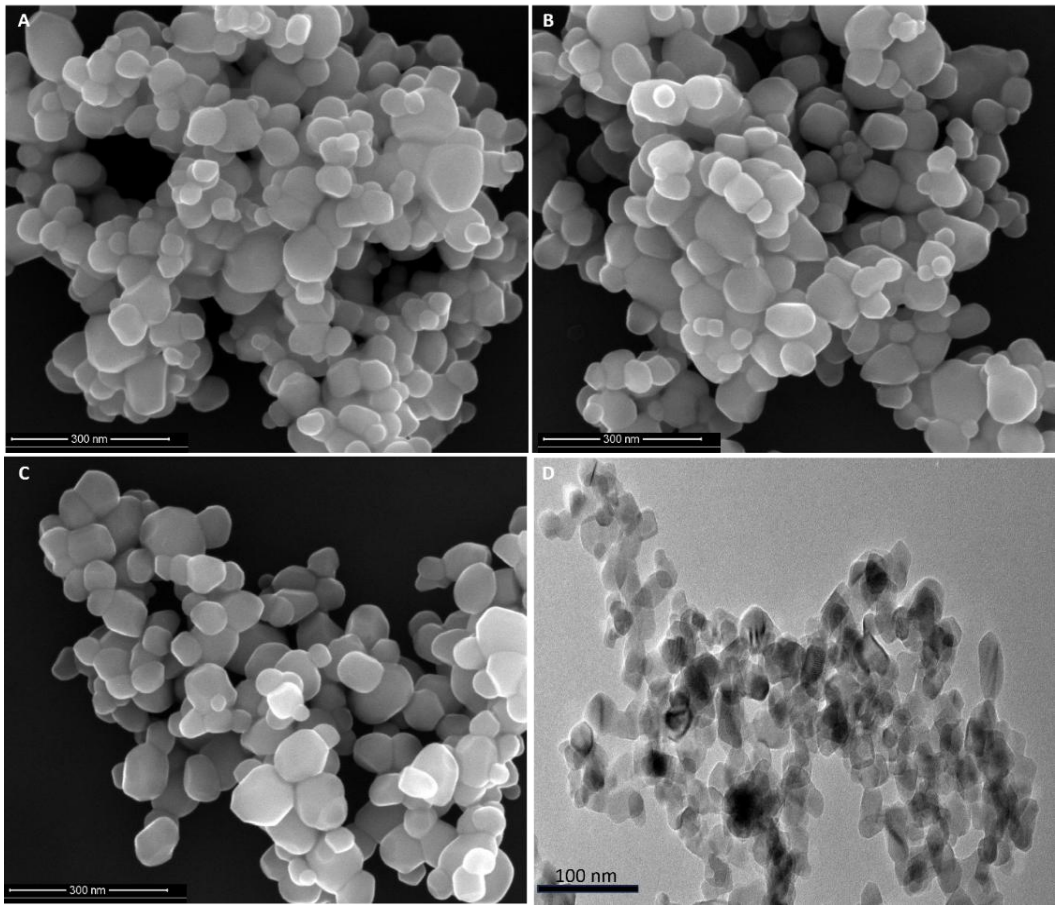

Figure 6.3 Representative images of primary size and shape of E171 analysed by SEM and P21 by TEM.

(A) E171 A, (B) E171 B, (C) E171 C, (D) P21. (A-C) Imaging conditions: accelerating voltage (HV) =10.00 kV; detector=TLD; magnification=300,000×; spot size=3.0; working distance (WD)=5.6 mm; scale bar=300 nm. (D) accelerating voltage (HV) =200kV; magnification=x100K

Analysis of representative SEM images indicated that size ranges were 39.3–326.2 nm (mean 130.1 ± 53.20) for E171 A, 28.8–351.4 nm (mean 133.6 ± 58.07) for E171 B, and 43.7–324.6 nm (mean 139.5± 59.61) for E171 C. However, nanoparticles with diameters less than 100 nm constituted 35%, 34%, and 34% of the total particle population in samples E171 A, E171 B, and E171 C, respectively. The average particle sizes for each sample are summarised in **Table 6.1**. These findings suggest that in E171 samples, less than 35% of particles were nanoscale particles (**Figure 6.4**).

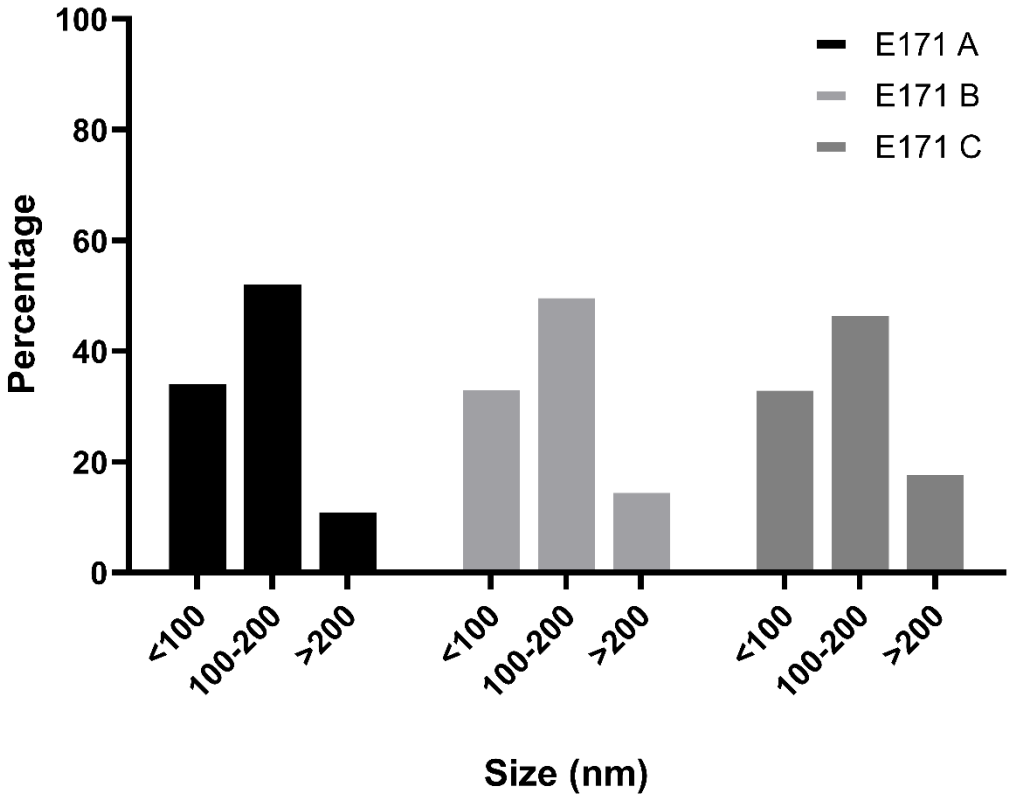

Figure 6.4 Quantitative analysis of E171 A, E171 B, and E171 C.
Histograms showing the particle size distributions for (A) E171 A, (B) E171 B, and (C) E171 C. Each graph shows the percentage of particles as a function of particle size, illustrating variation in particle size across the different samples. A minimum of six representative SEM images were analysed per sample, with at least 400 particles measured per sample for average size estimation.

TEM characterisation of the P21 powder demonstrated a heterogeneous particle size distribution (12.1–30.6 nm; mean 20.79 ± 4.47), with slightly rounded to near-spherical morphologies. The relative distribution of particle sizes is shown in **Figure 6.5**. These results indicate that, in the P21 sample, most particles were ultrafine nanoparticles with diameters below 21 nm.

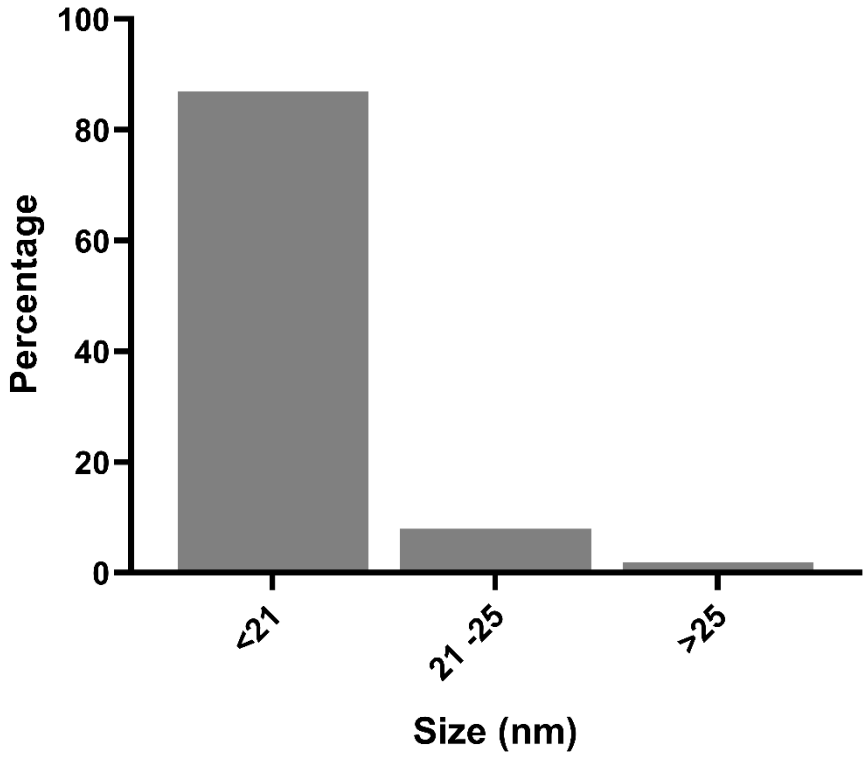

Figure 6.5 Quantitative analysis of P21.
Histogram showing the particle-size distribution for P21. The graph represents the percentage of particles as a function of their size. A minimum of 10 representative TEM images were analysed per sample, with at least 400 particles measured to estimate average size.

6.3.2 X-ray powder diffraction (XRD)

The XRD patterns of the E171 (A, B, C) samples provide information on their crystalline phase composition and purity. The most prominent peaks appear at approximately 25.36°, which is characteristic of the anatase form of TiO_2, specifically corresponding to the (101) crystallographic plane (**Figure 6.6**). Additional peaks at 38.06°, 48.36°, and 55.06° support the presence of anatase and align with known reflections for this phase. No significant peaks are observed at 27.45° or 41.26°, which are typically associated with the rutile phase of TiO_2. This absence demonstrates that the E171 sample is phase-pure anatase. The sharpness and intensity of the peaks suggest a high degree of crystallinity. This analysis confirms that E171 consists predominantly of anatase TiO_2.

The XRD analysis of the P21 sample shows a series of sharp, well-defined peaks, indicating a highly crystalline structure. Prominent diffraction peaks were observed at 28.22°, 38.96°, 44.12°, 64.16°, and 77.26°, which correspond to the rutile phase of TiO_2. These reflections correspond to the (110), (101), (111), (211), and (301) crystallographic planes, respectively. The results suggest that the P21 sample consists of rutile TiO_2.

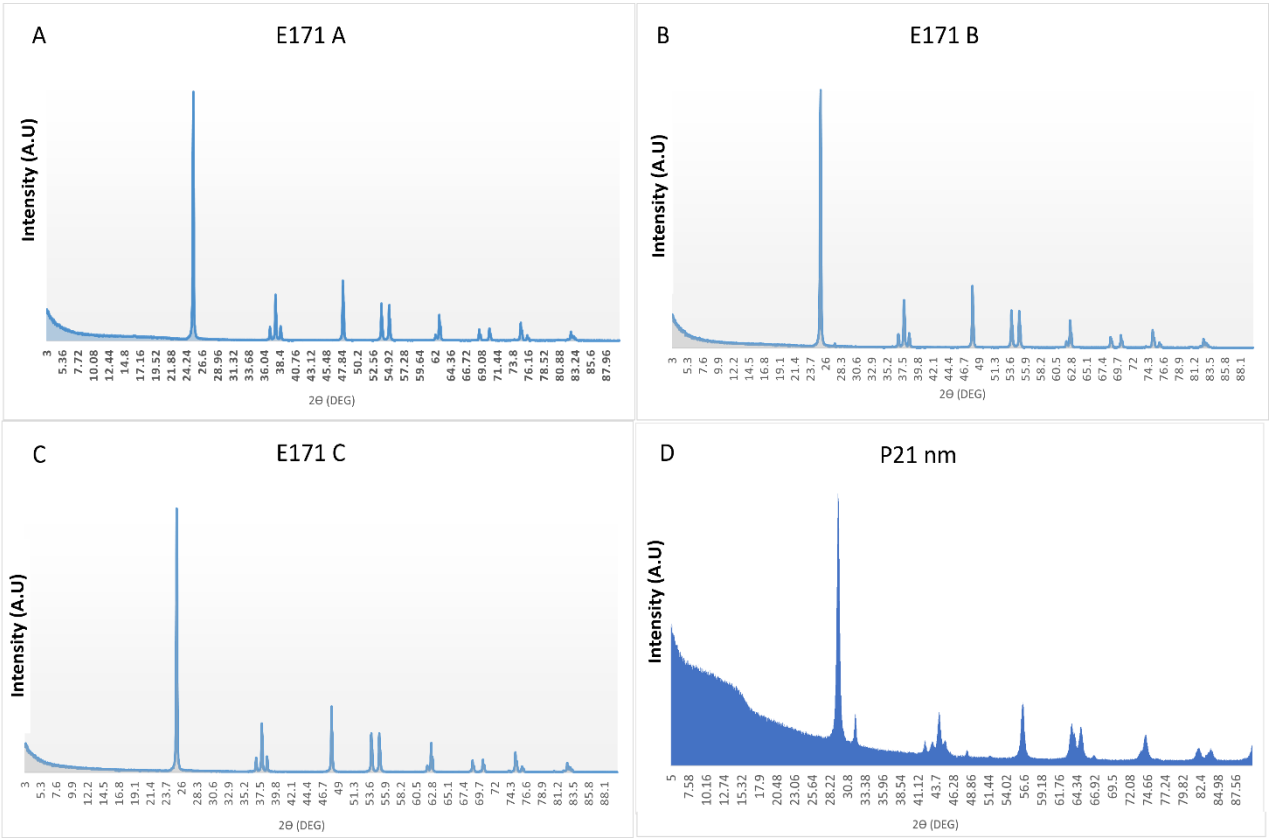

Figure 6.6 X-ray powder diffraction analysis (XRD) of E171 and P21.
(A) E171 A, (B) E171 B, (C) E171 C (D) P21.

6.3.3 Energy dispersive X-ray analysis (EDX)

SEM/EDX results for E171 (A, B, C) (**Figure 6.7 A, B, C**) show firm peaks for the presence of Ti and O (oxygen), and with indication of some impurities. Together with the SEM/EDX and XRD results, these findings indicate that the three food-grade E171 samples are likely to be relatively pure TiO_2 in the anatase form. Moreover, TEM/EDS for P21 also shows peaks for Ti and O as major elements (**Figure 6.7D**). The presence of carbon in the EDX and EDS spectra is attributed to the conductive graphite coating applied to the samples before imaging.

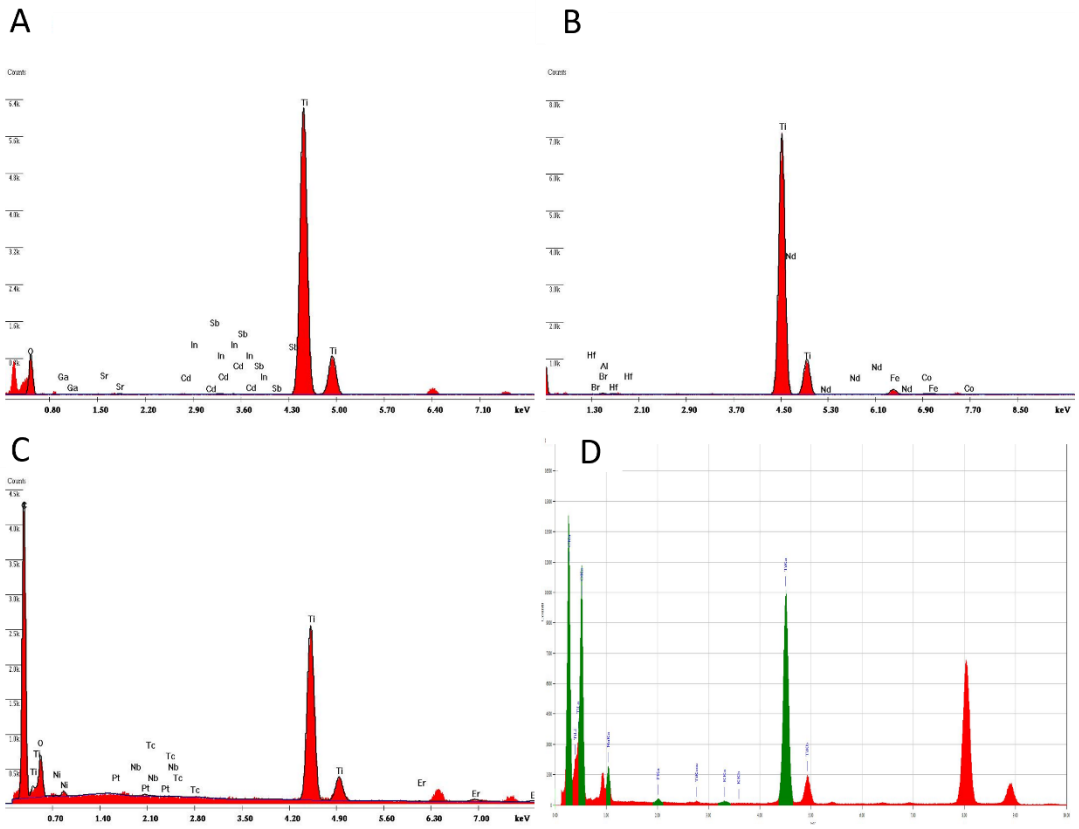

Figure 6.7 Energy dispersive X-ray (EDX) analysis of E171 and EDS of P21.
(A) E171 A, (B) E171 B, (C) E171 C (D) P21

6.3.4 Hydrodynamic size, zeta potential, and polydispersity index

The hydrodynamic particle size, zeta potential, polydispersity index (PDI), and pH values of three E171 samples (A, B, and C) and P21 were assessed in both DI water and DMEM.

DLS measures the hydrodynamic size and distribution of nanoparticles in suspension. DLS measurements showed larger hydrodynamic sizes in DMEM (766.3 ± 42.1 nm for E171 A, 838.5 ± 45.1 nm for E171 B, 819.4 ± 115.5 nm for E171 C and 1265.5 ± 331.5 for P21) compared to DI water (372.1 ± 10.4 nm for E171 A, 407.3 ± 9.7 nm for E171 B, 364 ± 18 nm for E171 C and 637.4 ± 49.3 for P21), likely due to protein corona formation or particle aggregation.

Zeta potential is a measure of the surface charge of particles, reflecting their stability in suspension. Zeta potential measurements in DI water revealed near-neutral surface charges (−0.22 ± 0.92 mV for E171 A, −0.27 ± 0.50 mV for E171 B, −0.31 ± 0.16 mV for E171 C, and -34.7 ± 11.6 mV for P21). In contrast, in DMEM, the values were more negative (−9.82 ± 1.18 mV for E171 A, −9.52 ± 0.67 mV for E171 B, −10.15 ± 0.78 mV for E171 C, and 0.507 ± 0.32 for P21), suggesting increased colloidal stability in biological media.

The polydispersity index (PDI) measures the uniformity of particle size distribution within a sample. The PDI values in DI water ranged from 0.24 to 0.30 (0.25 ± 0.02 for E171 A, 0.29 ± 0.02 for E171 B, 0.24 ± 0.02 for E171 C, and 0.30 ± 0.07 for P21), indicating moderate monodispersity, while in DMEM, higher PDI values (0.55 ± 0.16 for E171 A, 0.54 ± 0.02 for E171 B, 0.66 ± 0.13 for E171 C, and 0.507 ± 0.32 for P21), suggested broader size distributions.

The pH of the suspensions (E171 A, E171 B, E171 C, P21) remained slightly basic in both media, ranging from 7.60–8.06 in DI water and 7.82–7.93 in DMEM. This suggests that the particles do not significantly alter the pH of their environment, suggesting chemical inertness.

The physicochemical characteristics of E171 (A, B, C) and P21, including primary particle size, crystalline phase, purity, and supplier information, are summarised in **Table 6.1**.

Table 6.1 Summary of physicochemical properties of E171 (A, B, C) and P21.

Sample		**E171 (A)**	**E171 (B)**	**E171 (C)**	**P21 nm**
Source		Cake Warehouse, (NZ)	Sensient Technologies (USA)	Jiangsu Hushen Titanium White Technology (China)	Sigma-Aldrich
Shape		Slightly rounded	Slightly rounded	Slightly rounded	Slightly rounded
Average particle size (nm)		130	133	139	21
<100 nm Particles (%)		35	34	34	100
Elemental Composition (Major elements)		Ti and O	Ti and O	Ti and O	Ti and O
Crystallographic Form		Anatase	Anatase	Anatase	Anatase and rutile
pH	**DI Water**	7.92	7.60	8.06	7.10
	DMEM	7.82	7.93	7.91	7.84
Zeta Potential [mV]	**DI Water**	-0.22 ± 0.92	-0.27 ± 0.50	-0.31 ± 0.16	-34.7 ± 11.6
	DMEM	-9.82 ± 1.18	-9.52 ± 0.67	-10.15 ± 0.78	-9.5 ± 1.6
Polydispersity Index (PdI)	**DI Water**	0.25 ± 0.02	0.29 ± 0.02	0.24 ± 0.02	0.30 ± 0.07
	DMEM	0.55 ± 0.16	0.54 ± 0.02	0.66 ± 0.13	0.507 ± 0.32
Dynamic Size [nm]	**DI Water**	372.1 ± 10.40	407.3 ± 9.70	364 ± 18	637.4 ± 49.3
	DMEM	766.3 ± 42.1	838.5 ± 45.1	819.4 ± 115.5	1265.5 ± 331.5

Since the physicochemical properties of E171 samples (A, B, C) were comparable, sample B was selected for subsequent experiments. This choice was based on its representative characteristics and consistency with the overall profile of the E171 group.

6.3.5 Optimisation of a steatotic model in HepG2 cells

To establish an *in vitro* model of steatosis, HepG2 cells were treated with increasing concentrations of OA (0.1–1 mM) for 48 hours. Lipid accumulation was assessed using ORO staining, with haematoxylin counterstaining.

Following treatment with OA, ORO staining in the untreated control group (no OA) (**Figure 6.8 A**) demonstrated a minor presence of intracellular lipid. Lipid droplets in HepG2 cells are shown in red. However, treated HepG2 cells showed increasing intracellular lipid accumulation as OA concentration increased, as demonstrated by increasing intensity of ORO staining followed by haematoxylin counterstaining (**Figure 6.8 B–F**). The most pronounced lipid deposition was noted at 1 mM OA. Overall, these findings confirm that OA induces dose-dependent steatosis in HepG2 cells, with higher OA concentrations resulting in progressively larger and more abundant intracellular lipid droplets. This morphological change indicated lipid accumulation and confirmed the establishment of a steatotic model.

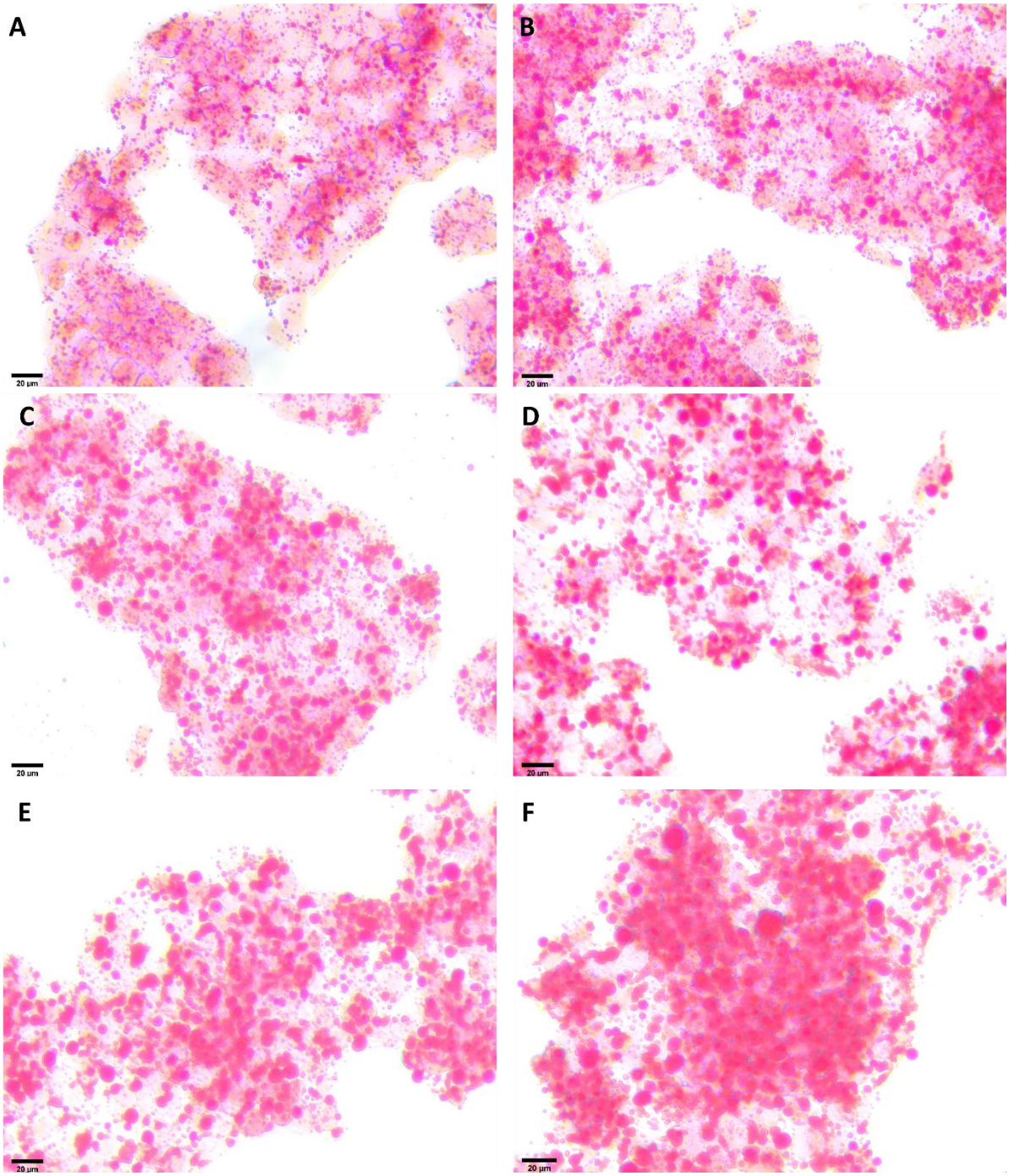

Figure 6.8 OA-induced steatosis in HepG2 cells.
Representative images of HepG2 cells treated with OA at the concentrations of 0.1, 0.25, 0.5, 0.75, and 1 mM for 48 hours. Cells were stained with ORO to visualize intracellular neutral lipid droplets (red) and counterstained with haematoxylin (A) Control (0 mM) (B) 0.1 mM (C) 0.25 mM (D) 0.5 mM (E) 0.75 mM (F) 1 mM. All images were obtained under 20x magnification. Scale bars represent 20 µm.

6.3.6 Quantification of lipid accumulation via Oil Red O (ORO) assay

To quantify intracellular lipid accumulation, ORO staining was measured spectrophotometrically. Following 48 hours of treatment with OA (0–1 mM), there was a significant increase in lipid

accumulation with all doses of OA above 0.25 mM, as reflected by ORO absorbance values when compared with the untreated control group (**Figure 6.9**). Although lipid accumulation peaked at 0.5 mM, 0.25 mM was selected for subsequent experiments as it induces moderate steatosis, to allow for both increases and decreases in lipid accumulation to be detected in future experiments.

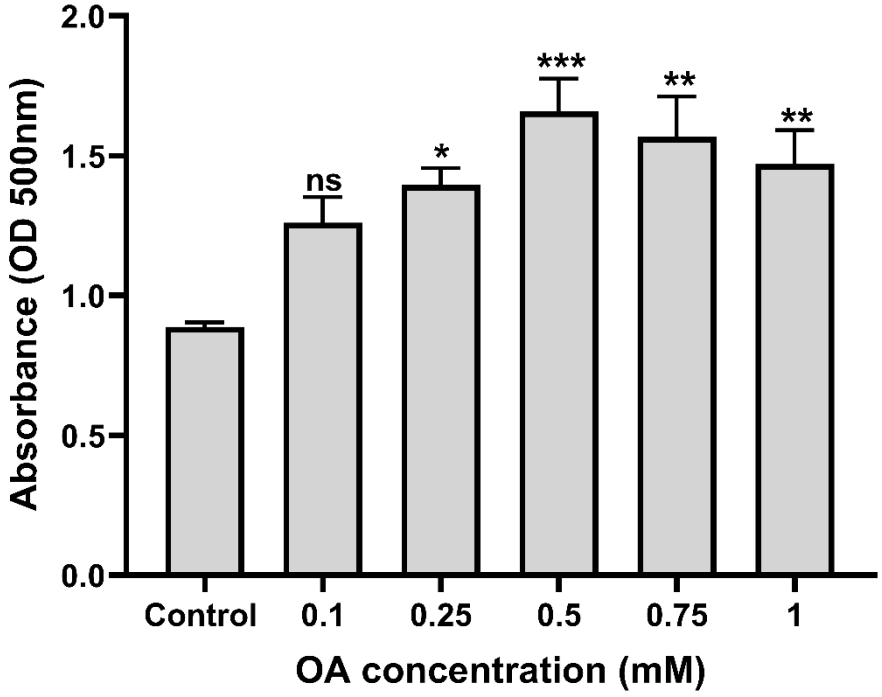

Figure 6.9 Quantification of intracellular lipid accumulation in response to OA treatment using Oil Red O assay.

Cells were treated with increasing concentrations of OA: control (0), 0.1, 0.25, 0.5, 0.75, and 1 mM. Lipid accumulation was quantified by measuring ORO absorbance at 500 nm. Values are mean ± SEM. *p<0.05, **p<0.01, ***p<0.001 vs control. Each experiment was performed in triplicate (n=3).

6.3.7 Cytotoxicity of oleic acid in HepG2 cells

To evaluate the cytotoxic effect of OA on HepG2 cells, cell viability was quantified via MTT assay. As shown in **Figure 6.10**, no significant differences in viability were observed among the treatment groups compared with the control (p>0.05). This data suggests OA exposure did not induce significant cytotoxicity in HepG2 cells across the tested concentration range and validates OA as a non-lethal inducer of steatosis.

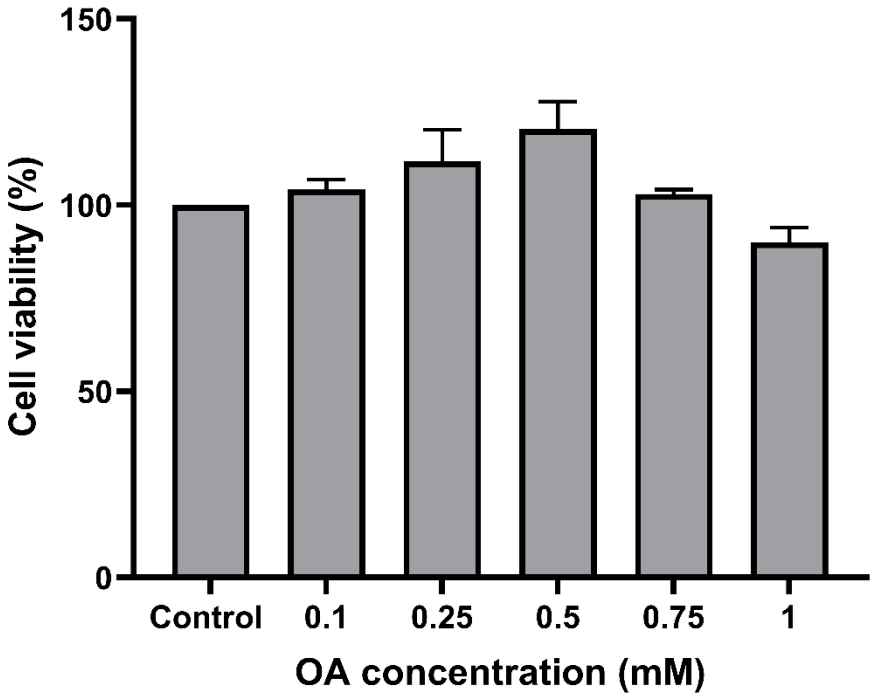

Figure 6.10 Effect of OA on HepG2 cell viability.
(A) The dose-dependent effect of OA (0.1, 0.25, 0.5, 0.75, and 1 mM) on cytotoxicity in HepG2 cells. Values are mean ± SEM. Each experiment was performed in triplicate (n = 3).

6.3.8 Morphological evaluation of E171 treated steatotic and non-steatotic HepG2 cells

To visualise the morphological changes induced by E171 and P21, HepG2 cells were treated with varying concentrations (0, 5, 50, 100, and 200 µg/mL) of E171 and P21, both in the presence and absence of OA (0.25 mM). Following 48 hours of treatment, cellular morphology and lipid accumulation were examined microscopically using ORO staining and haematoxylin counterstaining.

Microscopic evaluation of HepG2 cells treated with E171 revealed distinct dose-dependent morphological changes under both steatotic (+OA) and non-steatotic (-OA) conditions. Untreated control cells exhibited normal morphology with minimal lipid deposition (**Figure 6.11A, Figure 6.12A**). Steatosis was successfully induced with 0.25 mM OA, as shown in **Figure 6.8C**, which showed prominent lipid droplet accumulation.

At higher concentrations (100 and 200 µg/mL), E171 induced morphological alterations both under steatotic and non-steatotic conditions. Cells displayed reduced membrane definition, increased clustering, and signs of cytoplasmic condensation. These findings indicate that elevated E171 exposure may disrupt cellular architecture at higher doses (100–200 µg/mL) [**Figure 6.11 (D, E); Figure 6.12 (D, E)**].

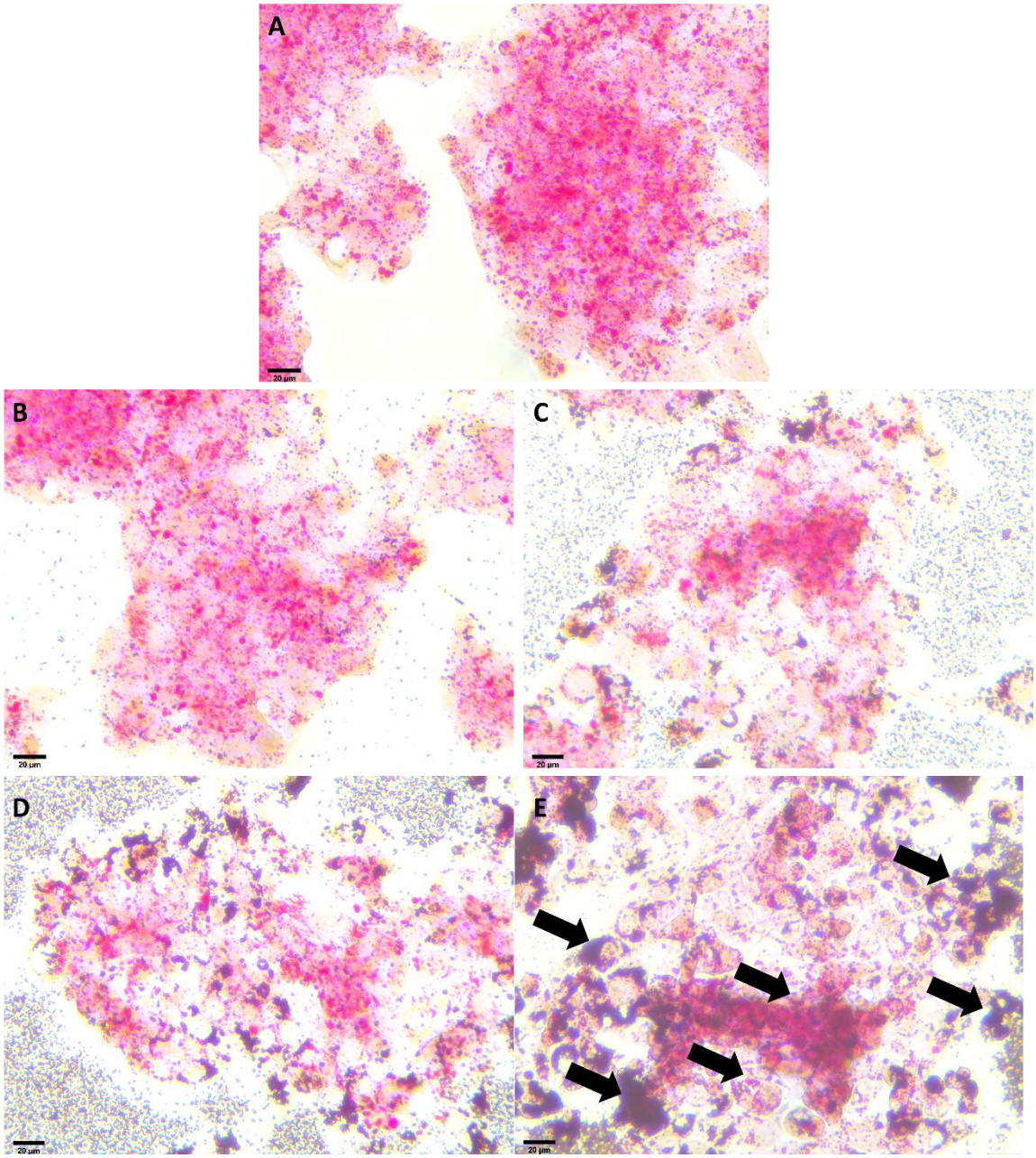

Figure 6.11 Effect of E171 on HepG2 cell morphology and lipid content under non-steatotic conditions.

HepG2 cells were treated with various concentrations of E171 for 48 hours: (A) Control, (B) 5 µg/mL, (C) 50 µg/mL, (D) 100 µg/mL, (E) 200 µg/mL. Arrows show reduced membrane definition, increased clustering, and signs of cytoplasmic condensation. Cells stained with ORO and haematoxylin were visualised under a microscope at 20x magnification. Scale bar=20 µm.

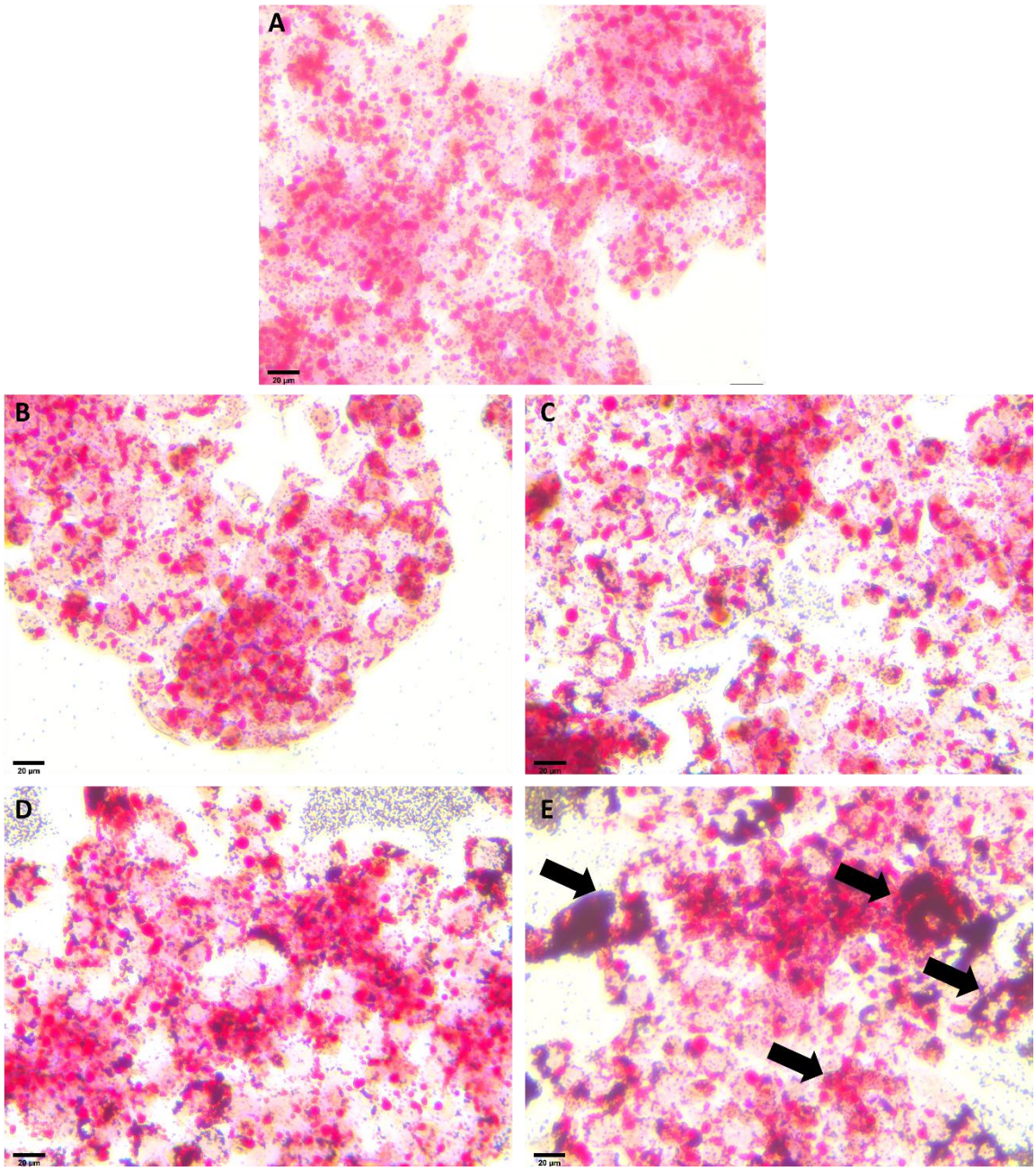

Figure 6.12 Effect of E171 on HepG2 cell morphology and lipid content under steatotic conditions. HepG2 cells were treated with various concentrations of E171 for 48 hours: (A) Control, (B) 5 µg/mL, (C) 50 µg/mL, (D) 100 µg/mL, (E) 200 µg/mL. Arrows show reduced membrane definition, increased clustering, and signs of cytoplasmic condensation. Cells stained with ORO and haematoxylin were visualised under a microscope at 20x magnification. Scale bar=20 µm.

6.3.9 Morphological evaluation of P21 treated steatotic and non-steatotic HepG2 cells

Microscopic evaluation of HepG2 cells treated with P21 revealed dose-dependent morphological changes under both steatotic and non-steatotic conditions.

In untreated controls, HepG2 cells retained their morphology, with well-defined membranes and minimal lipid deposition (**Figure 6.13A, Figure 6.14A**). Following induction of steatosis with 0.25 mM

OA, cells exhibited pronounced intracellular lipid droplet accumulation, confirming the successful establishment of the steatotic model (**Figure 6.14C**).

Interestingly, particle visualisation under the microscope revealed differences in appearance between E171 and P21. E171 particles appeared grey (**Figure 6.11, 6.12**), whereas P21 particles exhibited a yellow hue (**Figure 6.13, Figure 6.14**), suggesting potential differences in optical properties or aggregation behaviour.

At lower P21 concentrations (≤50 µg/mL), HepG2 cells largely maintained their morphology, with only subtle changes in membrane definition and lipid droplet distribution. However, at higher concentrations (100 and 200 µg/mL), pronounced morphological disruptions were evident in both steatotic and non-steatotic conditions. Cells displayed reduced membrane integrity, increased clustering, and cytoplasmic condensation [**Figure 6.13 (D, E), Figure 6.14 (D, E)]**.

Collectively, these findings demonstrate that P21 exposure exerts dose-dependent effects on HepG2 cell morphology. While low concentrations produced minimal alterations, higher doses (100–200 µg/mL) disrupted cellular architecture, reduced membrane definition, and promoted clustering.

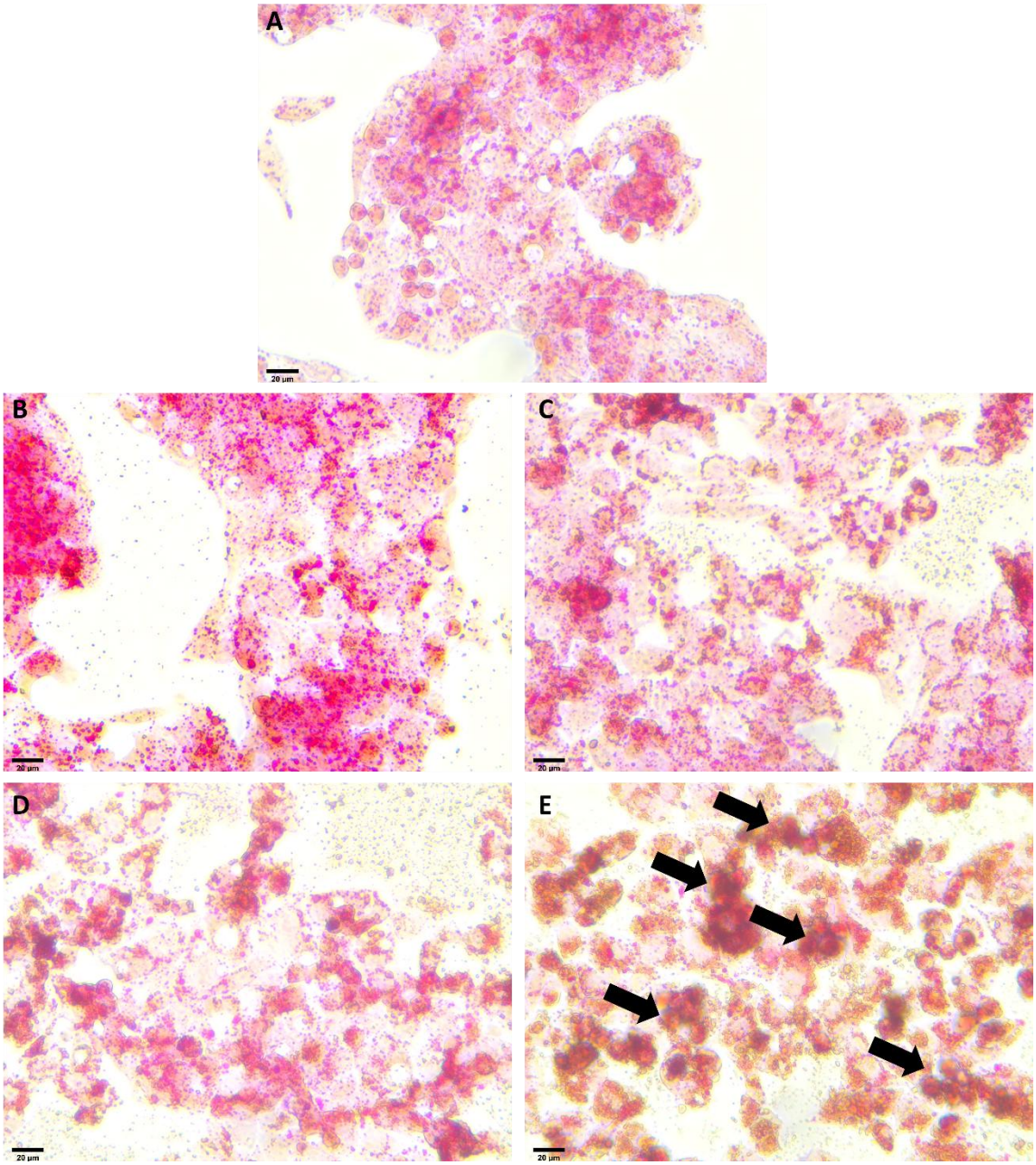

Figure 6.13 Effect of P21 on HepG2 cell morphology and lipid content under non-steatotic conditions. HepG2 cells were treated with various concentrations of P21 for 48 hours: (A) Control, (B) 5 µg/mL, (C) 50 µg/mL, (D) 100 µg/mL, (E) 200 µg/mL. Arrows show reduced membrane definition, increased clustering, and signs of cytoplasmic condensation. Cells stained with ORO and haematoxylin were visualised under a microscope at 20x magnification. Scale bar=20 µm.

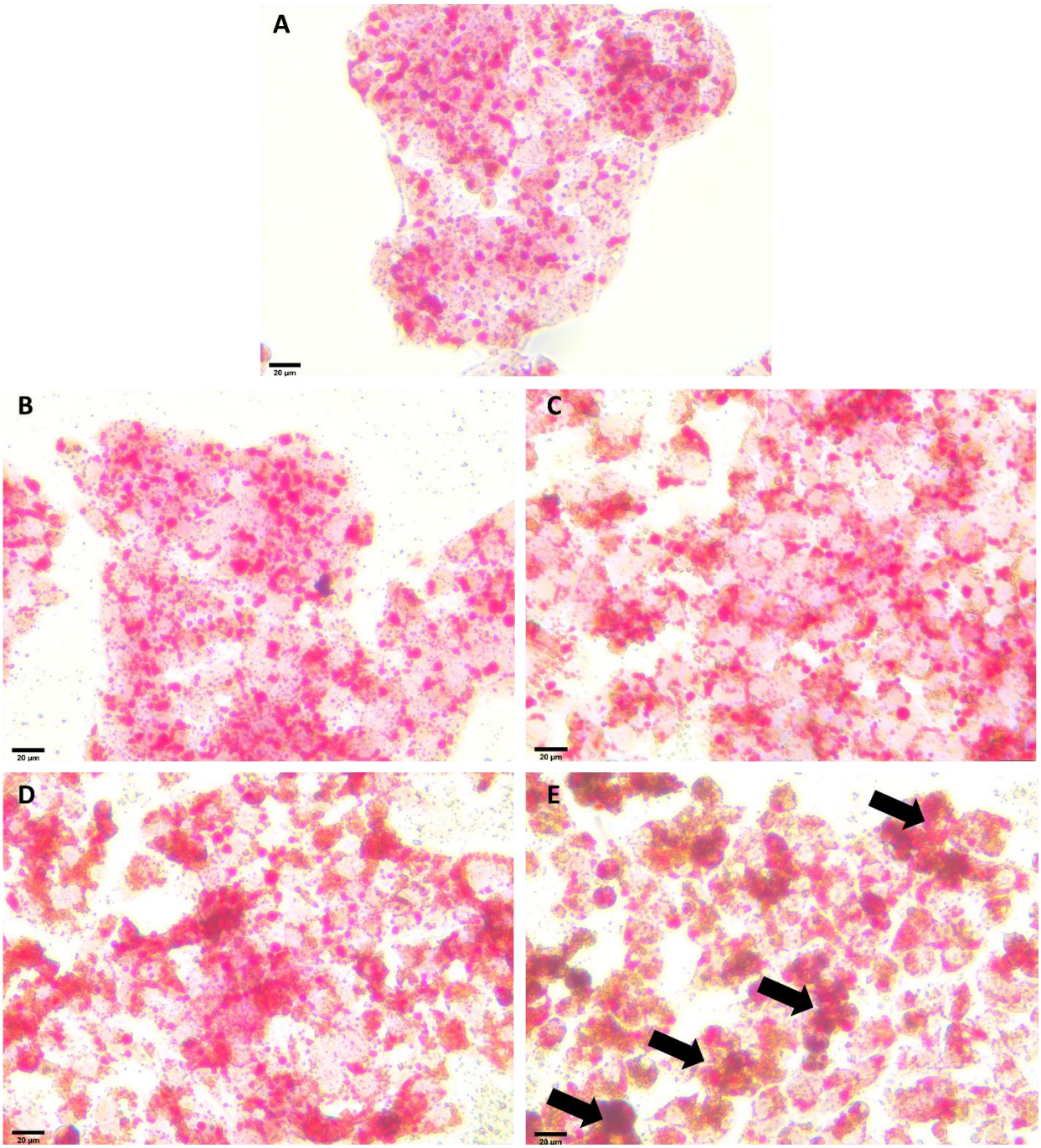

Figure 6.14 Effects of P21 on HepG2 cell morphology and lipid content under steatotic conditions. HepG2 cells were treated with various concentrations of **P21** for 48 hours: (A) Control, (B) 5 µg/mL, (C) 50 µg/mL, (D) 100 µg/mL, (E) 200 µg/mL. Arrows show reduced membrane definition, increased clustering, and signs of cytoplasmic condensation. Cells stained with ORO and haematoxylin were visualised under a microscope at 20x magnification. Scale bar=20 µm.

6.3.10 Cell viability assessment by haemocytometry

The effect of TiO_2 on cell number was assessed by cell counting using a haemocytometer following 48-hour treatment with E171 and P21 at concentrations of 0, 5, 50, 100, and 200 µg/mL, both in the

presence and absence of OA (0.25 mM). Trypan blue exclusion was used to distinguish live cells (unstained) from dead cells (blue-stained cytoplasm).

In non-steatotic HepG2 cells, treatment with E171 did not result in statistically significant changes in cell number or cell viability (%) at any tested concentration compared with untreated controls (**Figure 6.15A, B**).

However, in E171-treated steatotic cells (treated with OA), exposure to the highest concentration (200 µg/mL) led to a small but significant reduction in cell number ($p=0.0035$) and in the percentage of viable cells ($p=0.0015$) (**Figure 6.15 A, B**), suggesting enhanced cytotoxicity under high lipid-loaded conditions.

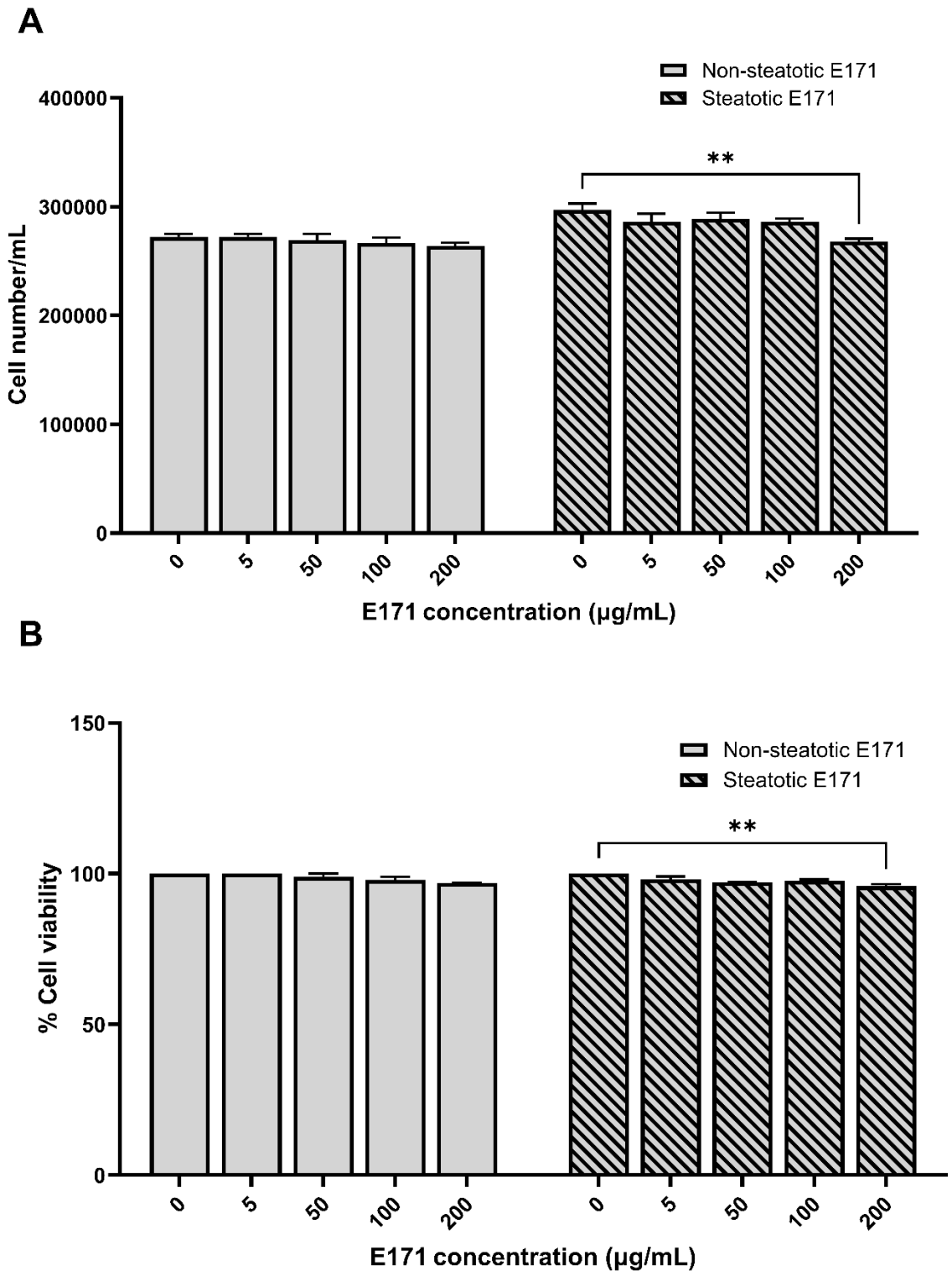

Figure 6.15 Cell viability of steatotic and non-steatotic HepG2 cells following treatment with E171. (A) Cell numbers expressed as number of cells /mL (B) Percentage cell viability normalised to untreated controls. Cells were treated with increasing concentrations of E171: 0, 5, 50, 100, and 200 µg/mL. Cell viability was assessed using trypan blue exclusion via haemocytometry. Values are mean ± SEM, (**p<0.01, * represents vs. 0 µg/mL control). Each experiment was performed in triplicate (n=3).

Similarly, **Figure 6.16** demonstrates that in non-steatotic HepG2 cells, treatment with P21 at all tested concentrations did not result in significant changes in cell number and cell viability (%) compared to respective controls. In contrast, in P21-treated steatotic cells, exposure to the highest concentration (200 µg/mL) led to a significant reduction in cell number ($p=0.0037$) and % cell viability ($p=0.0246$) (**Figure 6.16 A, B**).

These findings suggest that lipid accumulation may enhance HepG2 cells' susceptibility to TiO_2-induced cytotoxicity, with both E171 and P21 exhibiting pronounced effects at high concentrations under steatotic conditions.

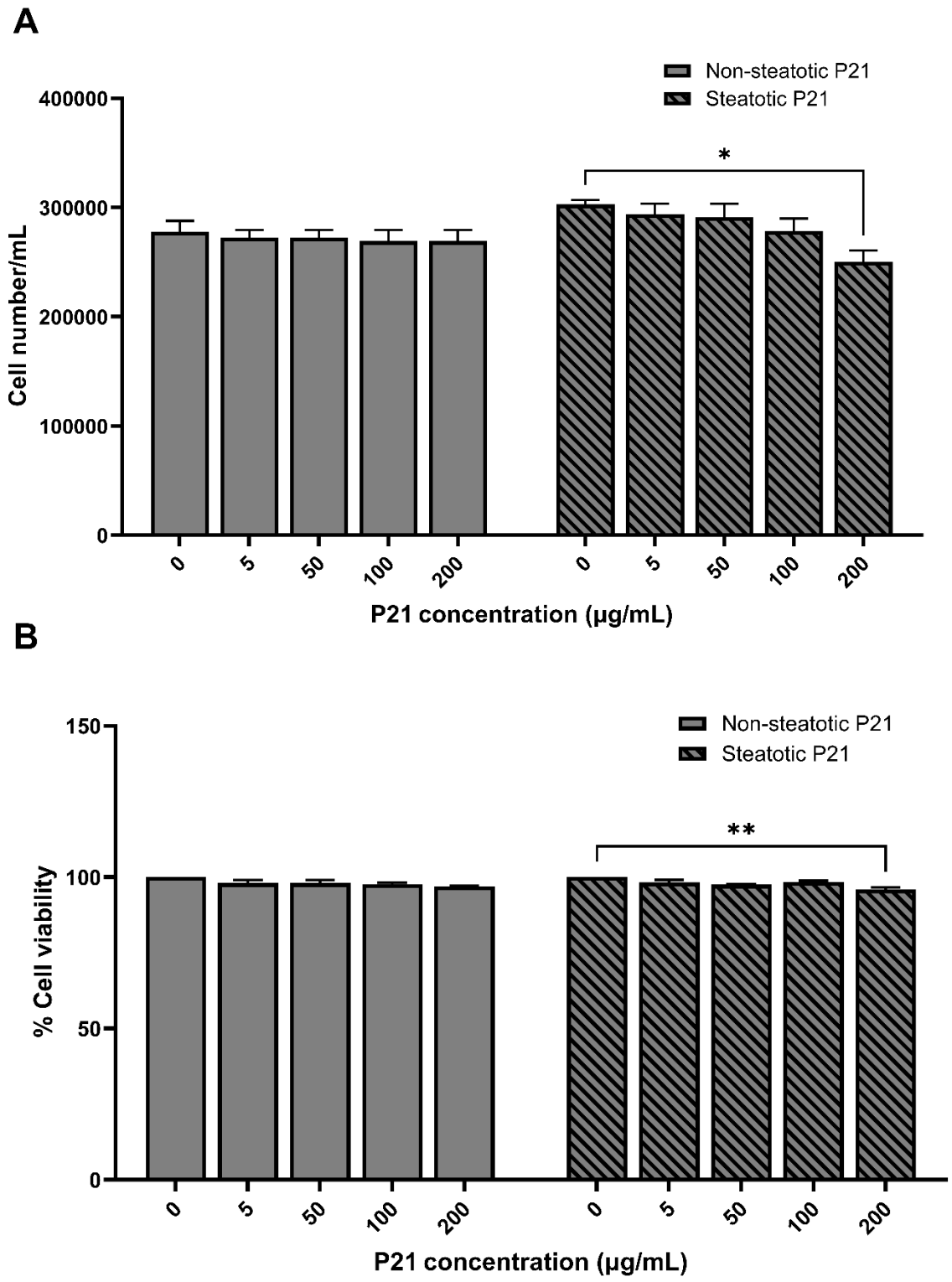

Figure 6.16 Cell number and cell viability of steatotic and non-steatotic HepG2 cells following treatment with P21.

(A) Cell numbers expressed as number of cells /mL (B) Percentage cell viability normalised to untreated controls. Cells were treated with increasing concentrations of P21: 0, 5, 50, 100, and 200 µg/mL. Cell viability was assessed using trypan blue exclusion via haemocytometry. Values are mean ± SEM, (*$p<0.05$, **$p<0.01$ * represents comparison vs. 0 µg/mL control). Each experiment was performed in triplicate (n=3).

6.3.11 Cytotoxicity assessment by neutral red uptake assay

The cytotoxicity of TiO_2 in HepG2 cells was evaluated using the neutral red uptake assay following 48-hour treatment with E171 and P21 at concentrations of 0, 5, 50, 100, and 200 µg/mL, in both steatotic (OA-treated) and non-steatotic (in the absence of OA) cells. To assess cytotoxicity, the uptake of neutral red dye by untreated control cells was taken as 100% viability, and a reduction in this uptake was taken as a cytotoxic response to TiO_2 exposure. In non-steatotic cells, treatment with E171 did not result in significant changes in cell viability when compared to the respective control (p=0.545). In contrast, E171-treated steatotic cells show lower viability at higher doses (200 µg/mL) (p=0.0036). This suggests that E171 exposure at higher doses may significantly compromise HepG2 cell viability (**Figure 6.17**).

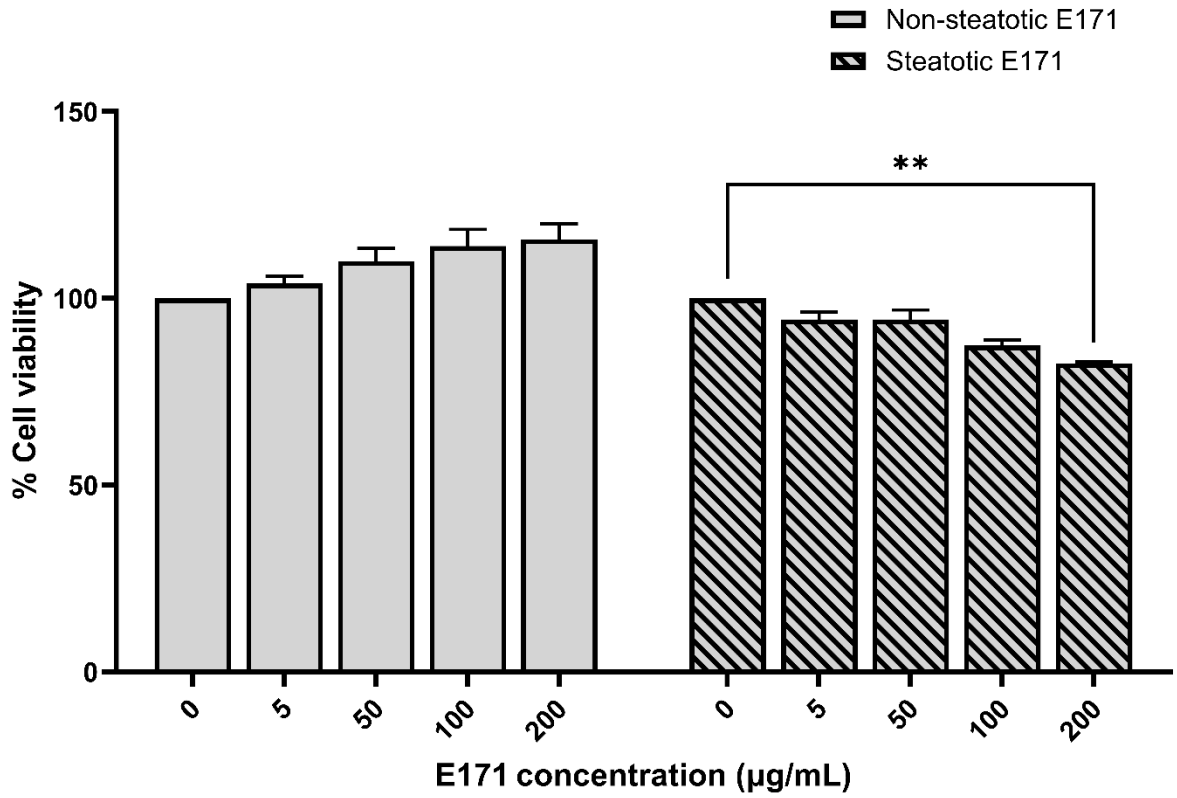

Figure 6.17 Cytotoxicity of E171 in steatotic and non-steatotic HepG2 cells, assessed by neutral red uptake assay.

HepG2 cells were treated with E171 at concentrations of 0, 5, 50, 100, and 200 µg/mL for 48 hours, with and without OA (0.25 mM). Cytotoxicity was determined by a decrease in the uptake and retention of the neutral red dye within lysosomes of viable cells compared to untreated controls. Values are mean ± SEM, (**p<0.01 * represents comparison vs. 0 µg/mL control). Each experiment was performed in triplicate (n=3).

Non-steatotic HepG2 cells treated with P21 did not show statistically significant changes in cell viability compared to the respective untreated controls (**Figure 6.18**). Similarly, steatotic cells exposed to P21 across all tested concentrations showed no significant reduction in viability. These findings indicate

that P21 exposure, even at the highest concentration tested, does not significantly compromise HepG2 cell viability under either non-steatotic or steatotic conditions (**Figure 6.18**).

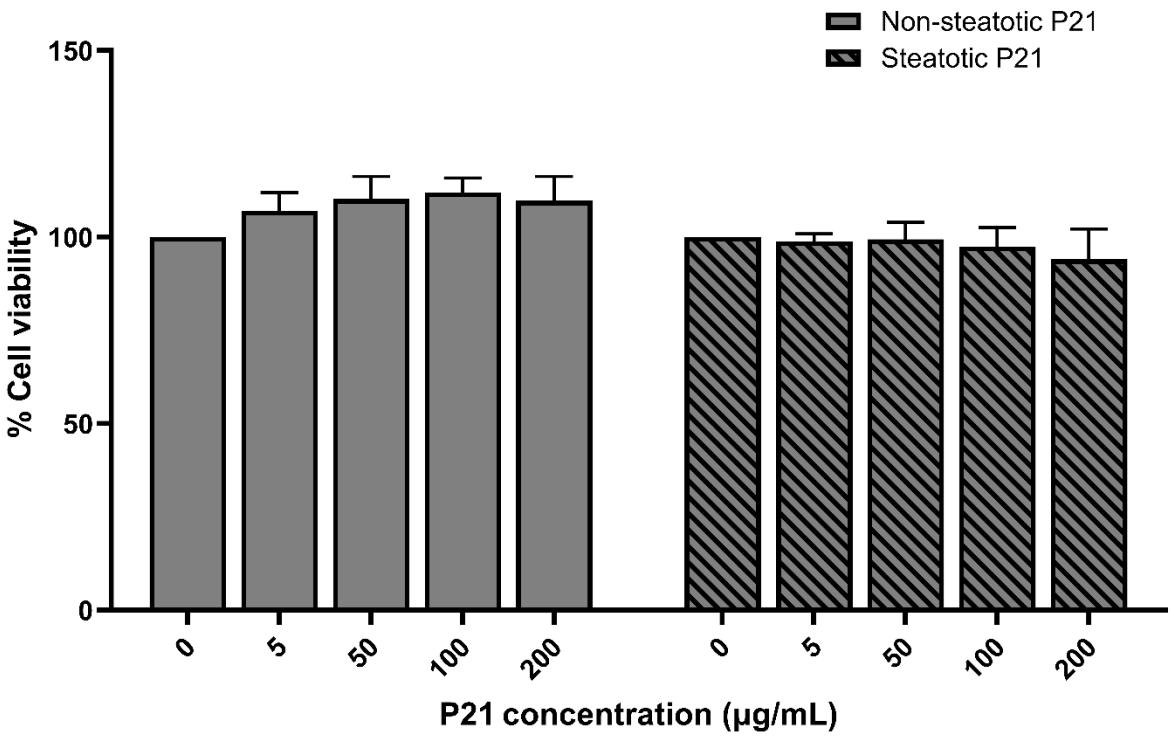

Figure 6.18 Cytotoxicity of P21 in steatotic and non-steatotic HepG2 cells, assessed by neutral red uptake assay.
HepG2 cells were treated with P21 at concentrations of 0, 5, 50, 100, and 200 µg/mL for 48 hours, with and without OA (0.25 mM). Cytotoxicity was determined by a decrease in the uptake and retention of the neutral red dye within lysosomes of viable cells compared to untreated controls. Values are mean ± SEM. Each experiment was performed in triplicate (n=3).

The overall pattern for both E171 and P21 is therefore quite similar, but variability was greater in the P21 experiments. This suggests that the observed effects are minor, and whether they reach statistical significance may depend on the degree of experimental variability.

6.3.12 Cellular uptake of E171 and P21

The cellular uptake of E171 and P21 was quantified in HepG2 cells under steatotic and non-steatotic conditions following 48 hours of exposure at 10 µg/mL and 50 µg/mL. Uptake was expressed as the percentage of TiO_2 recovered from cell lysates.

At both tested concentrations, E171 exhibited a higher uptake under non-steatotic conditions (**Figure 6.19**). At 10 µg/mL, non-steatotic E171-treated cells showed the highest recovery (~32%), representing a significant increase ($p<0.0001$) compared to the untreated control. At 50 µg/mL, non-steatotic E171 again demonstrated elevated uptake (~19%), which was significantly greater ($p<0.0011$) than the control (0 µg/mL). These findings confirm that E171 is more readily internalised/sorbed in

non-steatotic HepG2 cells. In contrast, under steatotic conditions, no significant differences in uptake were observed between 0, 10, and 50 µg/mL treatments. This suggests that lipid accumulation may attenuate or mask E171's uptake capacity, thereby reducing the influence of concentration on sorption in steatotic cells.

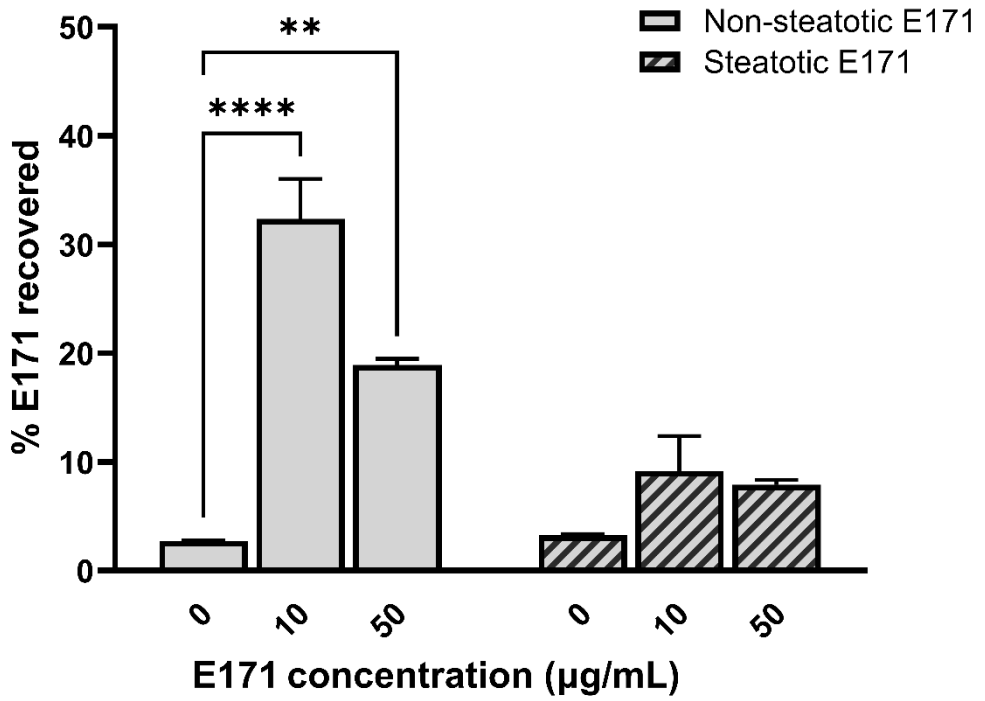

Figure 6.19 Cellular uptake of E171 in steatotic and non-steatotic HepG2 cells.
HepG2 cells were treated with E171 at 10 µg/mL and 50 µg/mL for 48 hours, with or without OA (0.25 mM). The percentage of E171 recovered from cell lysates was quantified to assess cellular uptake. Values are mean ± SEM. (**p<0.01, ****p<0.0001 * represents comparison w.r.t control). Each experiment was performed in triplicate (n=3).

For P21, uptake was higher under steatotic conditions (**Figure 6.20**). At 50 µg/mL, steatotic P21-treated cells showed the highest recovery (~25%), representing a significant increase compared to the untreated control (p<0.0001). In contrast, no significant differences in uptake were observed across concentrations in non-steatotic cells. These findings confirm that P21 is more readily internalised/sorbed in steatotic HepG2 cells. This suggests that lipid accumulation enhances the cellular uptake of P21, indicating that steatotic conditions may facilitate particle internalisation compared to non-steatotic states.

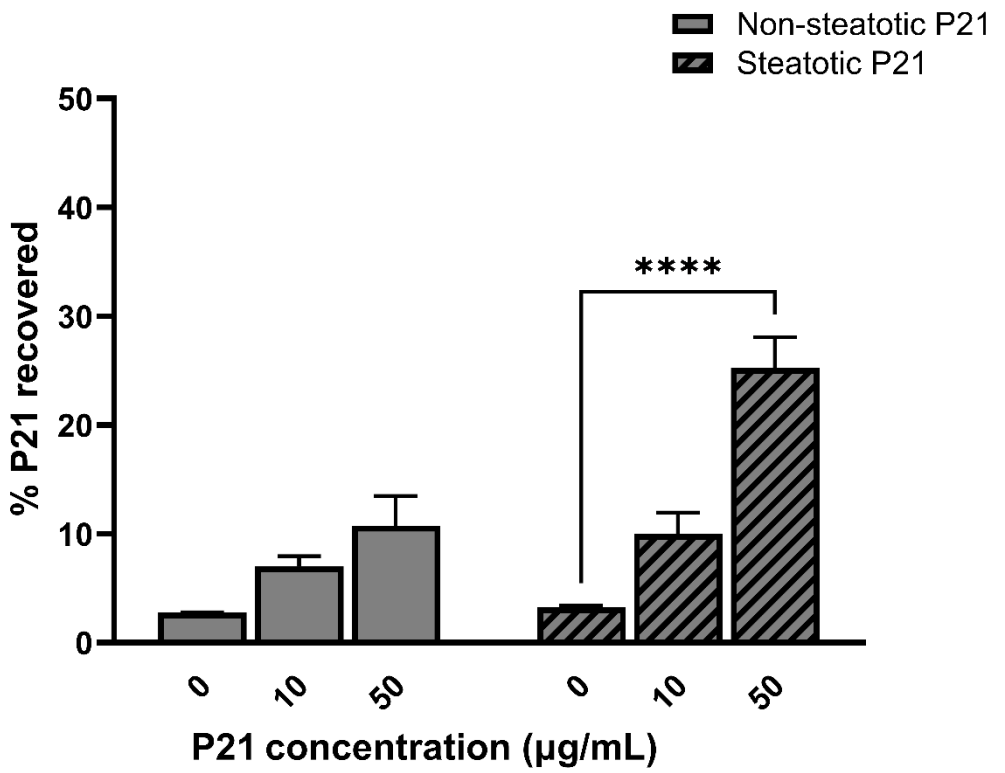

Figure 6.20 Cellular uptake of P21 in steatotic and non-steatotic HepG2 cells.
HepG2 cells were treated with P21 at 10 µg/mL and 50 µg/mL for 48 hours, with or without OA (0.25 mM). The percentage of P21 recovered from cell lysates was quantified to assess cellular uptake. Values are mean ± SEM. (****p<0.0001 * represents comparison w.r.t control). Each experiment was performed in triplicate (n=3).

6.4 Discussion

The physicochemical characterisation of E171 and P21 highlights the role of particle properties in shaping biological outcomes. In this study, to ensure relevance and comparability, three independent E171 samples (A, B, and C) were initially sourced from different suppliers. As comparative analysis revealed no significant differences among them, E171 B was selected as a representative bulk material for subsequent experimentation. In parallel, the commercially available P21 nanoparticles were included to provide a defined nanoscale comparator. The heterogeneous size distribution of E171, with approximately one-third of particles below the nanoscale threshold, highlights its dual identity as both a bulk pigment and a source of nanosized fractions. This is toxicologically significant, as particles <100 nm are known to exhibit enhanced cellular uptake, systemic translocation, and higher surface reactivity, thereby increasing the likelihood of biological interactions (Younes et al., 2021). The consistency of the physicochemical findings from this study with multiple independent reports (Dudefoi et al., 2018; Faust et al., 2016; Peters et al., 2014; Verleysen et al., 2020; Warheit, 2024; Weir et al., 2012; Yang et al., 2008; Yusoff et al., 2018) strengthens confidence that the E171 samples tested

in this study are representative of food-grade TiO_2. The predominantly anatase crystalline phase further aligns with regulatory specifications and prior research.

The observed differences in particle size distribution between E171 and P21 highlight an important consideration. Although E171 is often described as micro-sized TiO_2, a non-negligible nano-fraction is consistently present across commercial batches, which may contribute disproportionately to adverse biological effects (Proquin et al., 2017). In contrast, the much higher proportion and smaller absolute size of NPs in P21 explain its frequent use as a worst-case nano-TiO_2 benchmark. This provides a valuable comparative framework as E171 reflects the complexity of consumer exposure, while P21 serves as a controlled reference for mechanistic studies (Jovanović, 2014; Ropers et al., 2017).

The XRD analysis confirming anatase phase purity in all E171 samples is consistent with the manufacturing specifications of food-grade TiO_2. In contrast, the XRD pattern of P21 displayed sharp, well-resolved peaks of the rutile polymorph. This clear distinction in crystalline phase composition between E171 and P21 provides a mechanistic basis for their comparative use in toxicological studies. Previous *in vitro* and *in vivo* studies suggest that anatase and rutile TiO_2 can elicit different inflammatory and cytotoxic responses, with some evidence pointing to greater pro-inflammatory potential of anatase-rich materials at equivalent mass doses (De Matteis et al., 2016; Johnston et al., 2009; Simon-Deckers et al., 2008; Warheit et al., 2007). These findings highlight that crystalline phase composition is not just a physicochemical descriptor but an important determinant of biological outcomes.

Energy-dispersive X-ray spectroscopy (EDX/EDS) performed in conjunction with SEM and TEM provided evidence of the elemental composition and overall purity of the investigated TiO_2 (E171 (A, B, C) and P21). SEM/EDX analysis of the three food-grade E171 consistently revealed strong characteristic peaks for titanium and oxygen with atomic ratios close to the expected 1:2 stoichiometry for TiO_2. Only minor traces of other elements were detected in some samples (e.g., low-intensity signals for Ga, Sr, Cd, In, Sb, Co, Ni, Pt), most likely originating from residual processing aids or minor contamination during manufacturing. No evidence of heavy-metal impurities or significant phosphate/silicate coatings commonly used in pigment-grade TiO_2 was observed. Combined with the XRD data demonstrating phase-pure anatase, these results confirm that the E171 samples used in this study were of high chemical purity and fully representative of typical food-grade titanium dioxide. Similarly, TEM/EDS analysis of the P21 reference nanomaterial showed intense Ti and O peaks as the dominant elemental signals. The prominent carbon peak present in all EDX/EDS spectra was attributed to the thin conductive graphite layer routinely applied to non-conductive powder samples before electron microscopy, and possibly to residual carbon from the TEM grid. Our findings align with previous studies, which reported the predominant presence of Ti and O in TiO_2 samples (Bouzakher-Ghomrasni

et al., 2021; Wells et al., 2024). The high elemental purity observed across all tested materials is toxicologically relevant, as it largely excludes confounding effects from surface coatings that could otherwise contribute to biological responses independently of the TiO_2. This high purity strengthens the validity of our findings and enhances the relevance of the data to real-world dietary exposure scenarios involving commercial E171.

Dynamic light scattering (DLS) analysis revealed considerable differences in the hydrodynamic diameter (Z-average) and degree of dispersion of the TiO_2 (E171 and P21) when suspended in DI water versus complete cell culture medium (DMEM +10% FBS), highlighting the influence of the dispersion medium on particle behaviour under biologically relevant conditions. In DI water, all E171 samples exhibited moderate hydrodynamic sizes ranging from 364 ± 18 nm to 407.3 ± 9.7 nm, whereas P21 showed a larger Z-average of 637.4 ± 49.3 nm. These values are considerably larger than the primary particle sizes determined by electron microscopy (SEM/TEM), confirming the presence of agglomerates even in low-ionic-strength conditions. The higher hydrodynamic diameter of P21 in water is consistent with its smaller primary particle size (~21 nm) and higher surface area, which promote stronger interparticle attraction and more extensive agglomeration in the absence of sufficient electrostatic or steric stabilisation. Upon dispersion in DMEM supplemented with 10 % foetal bovine serum, a marked increase in hydrodynamic diameter was observed for all materials, with Z-average values rising to 766–838 nm for the E171 samples and reaching 1265.5 ± 331.5 nm for P21. This pronounced medium-dependent agglomeration is a well-documented phenomenon for TiO_2 and is primarily attributable to the high ionic strength of DMEM (~150 mM), which compresses the electrical double layer and reduces electrostatic repulsion, and to partial shielding or bridging effects exerted by adsorbed serum proteins. Our findings align with previous studies, which reported that the hydrodynamic size of particles increases in water and DMEM compared to the primary particle sizes measured by SEM/TEM. Under aqueous conditions, the particles were observed in agglomerated or aggregated forms, with Z-average sizes of TiO_2 particles in a range of 127–504 nm (Yang et al., 2014) and 285.30 ± 6.68–345.27 ± 4.45 nm (Hwang et al., 2019).

In DI water, all tested materials exhibited PDI values between 0.24 and 0.30 (E171: 0.24–0.29; P21: 0.30). While values below 0.3 are often interpreted as indicative of narrow size distributions in DLS, such apparent uniformity requires cautious interpretation. The PDI obtained from DLS reflects the breadth of the intensity-weighted hydrodynamic size distribution and is inherently biased toward larger particles or agglomerates. Our findings are consistent with previous reports: Dorier et al. (2019) observed a PDI of 0.48 ± 0.07 for E171 in water, while Talbot et al. (2018) reported a lower value of 0.18. More recently, Kunc et al. (2025) described a broader range of PDI values (0.14–0.56), further underscoring the variability in dispersion behaviour across studies. In complete cell culture medium

(DMEM supplemented with 10% FBS), PDI values increased substantially (E171: 0.54–0.66; P21: 0.51), reflecting broader and more heterogeneous size distributions. The exceptionally high variability observed for both E171 and P21 in DMEM highlights their susceptibility to uncontrolled agglomeration in complex biological environments. Notably, the PDI values obtained in our study were considerably higher than those reported previously. For example, Uribe-García et al. (2025) reported PDI values of 0.20–0.33 for E171 in Minimum Essential Medium (MEM), suggesting more homogeneous size distributions. Similarly, much lower PDI values have been reported in other media, such as 0.18 in 4-(2-hydroxyethyl)-1-piperazineethanesulfonic acid (HEPES) saline solution (Herrera-Rodríguez et al., 2023), 0.19 (Bischoff et al., 2020) and 0.16 in Roswell Park Memorial Institute Medium (RPMI)/F-12K (Kaighn's Modification of Ham's F-12 Medium) to 0.17 in Williams + 10% FCS (Lankoff et al., 2012). These discrepancies emphasise that PDI is highly dependent on the dispersion medium and experimental conditions.

Zeta potential provides an essential measure of particle surface charge and, by extension, their stability in suspension. In our study, E171 exhibited near-neutral zeta potentials in DI water (−0.22 to −0.31 mV), consistent with poor electrostatic stabilisation and a tendency to agglomerate. P21, by contrast, showed a distinctly negative charge (−34.7 mV), suggesting greater intrinsic stability in aqueous suspension. However, when dispersed in DMEM supplemented with 10% FBS, the zeta potentials of E171 shifted to moderately negative values (−9.5 to −10.2 mV), while P21 approached neutrality (0.5 mV). These medium-dependent changes highlight the role of biomolecule adsorption and protein corona formation in modulating particle surface charge and colloidal behaviour. Our findings differ from previous reports. For example, Bischoff et al. (2020) reported −31.4 mV for E171, and Verleysen et al. (2020) observed values as low as −45 mV, both indicating substantially greater stabilisation than observed in our DMEM dispersions. Similarly, Hwang et al. (2019) reported values between −36.7 and −42.2 mV for E171, again more negative than our findings. In contrast, Uribe-García et al. (2025) reported values of −7.0 to −8.7 mV for E171 in MEM, which are closer to the range we observed in DMEM. Taken together, these comparisons emphasise that zeta potential values are dependent on the dispersion medium. While strongly negative values in buffered saline or simpler culture media suggest robust electrostatic stabilisation, our results in DMEM supplemented with serum proteins indicate a more moderate level of stabilisation, likely reflecting complex biomolecular interactions.

Across all samples, suspension pH remained mildly basic (7.6–8.1) in both DI water and DMEM, with no systematic or substantial deviation from the baseline pH of the respective media. This stability indicates negligible dissolution of TiO_2 or release of acidic/basic surface species under physiological conditions, consistent with its extremely low aqueous solubility. The absence of measurable pH shifts supports the chemical inertness of both anatase (E171) and rutile (P21) polymorphs in biological

environments. It effectively rules out pH-mediated cytotoxicity as a confounding mechanism in subsequent *in vitro* assays. The slightly higher pH observed in DI water suspensions (up to 8.06) is typical of oxide nanoparticle dispersions and can be attributed to minor surface deprotonation or adsorption of hydroxyl ions (OH^-) at the TiO_2 water interface. Importantly, these modest increases are not toxicologically relevant and do not compromise the interpretation of biological assays.

The establishment of a reproducible steatotic HepG2 model using OA provides a key foundation for interpreting the subsequent TiO_2 exposure experiments. The dose-dependent lipid accumulation observed by ORO and haematoxylin staining, coupled with preserved cell viability, confirms that OA acts as a non-lethal inducer of steatosis within the tested concentration range. The selection of 0.25 mM OA as a moderate inducer is particularly relevant, as it balances robust lipid loading with no cytotoxicity, thereby recapitulating the initial reversible stage of simple hepatic steatosis characteristic of MASLD (Girish & John, 2025; Krahmer et al., 2025). This distinction is important because it allows the study of TiO_2 interactions under conditions that mimic metabolic stress without confounding effects from cell death or apoptosis. Unlike saturated fatty acids such as palmitic acid, which trigger endoplasmic reticulum stress and lipoapoptosis at comparable concentrations, OA primarily promotes neutral lipid storage in the form of triglyceride-filled droplets (Eynaudi et al., 2021; Moliterni et al., 2024), recapitulating the early reversible stage of simple hepatic steatosis observed in MASLD (Carli et al., 2024). This reproducible, non-cytotoxic lipid-loading phenotype not only validates HepG2 cells as a robust *in vitro* platform for investigating the role of TiO_2 in hepatic steatosis but also strengthens confidence in the biological relevance of our subsequent findings with TiO_2 (E171 and P21). Consistency with previous reports (see **Table 2.3**) further validates the reliability of this model. The agreement across independent studies demonstrates that OA-induced steatosis in HepG2 cells is a well-established and reproducible phenomenon, thereby enhancing confidence in the biological relevance of these findings. Importantly, the dose-dependent induction of steatosis provides a controlled system in which the effects of TiO_2 can be evaluated against a background of lipid overload, allowing investigation into how TiO_2 exposure interacts with pre-existing metabolic stress. Taken together, the OA-induced HepG2 model represents a physiologically relevant in vitro system for investigating TiO_2-mediated effects in hepatic steatosis. By mimicking the early stages of MASLD without introducing confounding cytotoxicity, this model provides a reliable framework for interpreting the biological responses to TiO_2 (E171 and P21).

The morphological alterations observed in HepG2 cells exposed to TiO_2 are consistent with established hallmarks of cytotoxicity reported in the literature. Previous studies have demonstrated that high concentrations of TiO_2 can induce cell shrinkage, nuclear condensation, apoptosis, and micronucleus formation in hepatic and other cell types (Abbasi-Oshaghi et al., 2019; Li et al., 2020; Sha et al., 2011;

Shukla et al., 2013; Xia et al., 2018). These findings collectively support the interpretation that TiO_2, particularly at higher doses, compromises cellular integrity through mechanisms associated with early apoptotic processes and genotoxic stress. Importantly, this study extends these observations by demonstrating that morphological damage is not confined to non-steatotic HepG2 cells but also occurs in OA-induced steatotic cells. This suggests that lipid accumulation does not mitigate TiO_2-induced cytotoxicity; instead, the presence of steatosis may exacerbate susceptibility to morphological disruption. Steatotic cells, already burdened by altered lipid metabolism and organelle stress, may be less resilient to additional insults such as TiO_2 exposure. This synergistic vulnerability highlights the relevance of TiO_2 toxicity in metabolically compromised environments, such as those encountered in early stages of MASLD, where hepatocytes are already lipid-loaded (Girish & John, 2025; Krahmer et al., 2025). These findings highlight the importance of considering underlying metabolic states when evaluating TiO_2 toxicity.

The combined haemocytometry and NRU assays results provide important insight into the differential cytotoxicity of TiO_2 in non-steatotic versus steatotic HepG2 cells. In non-steatotic cells, neither E171 nor P21 induced statistically significant reductions in viability across the tested concentration range, consistent with the general view that TiO_2 exerts no cytotoxicity under basal conditions. However, in steatotic cells, exposure to the highest concentration (200 μg/mL) of either E171 or P21 resulted in a significant reduction in viability, highlighting the enhanced vulnerability of lipid-loaded hepatocytes to TiO_2 stress. This finding is particularly relevant given the increasing prevalence of MASLD, where hepatocytes are chronically burdened by lipid accumulation. The NRU assay revealed a dose-dependent cytotoxic effect of E171 in steatotic cells, with significant reduction in viability at the highest concentration tested. Interestingly, while haemocytometry revealed an impact of P21 in the presence of OA, the NRU assay did not detect measurable changes in viability under either non-steatotic or steatotic conditions. This discrepancy likely reflects differences in assay sensitivity and the cellular parameters being measured. Haemocytometry directly assesses cell number, whereas NRU quantifies lysosomal activity as a proxy for viability (Madorran et al., 2024). The divergence suggests that P21 may induce subtle alterations in cell growth or division under steatotic conditions, without accompanying lysosomal dysfunction. This distinction between E171 and P21 may reflect differences in particle size distribution, crystalline phase, or agglomeration behaviour, all of which influence cellular uptake and intracellular stress responses. The absence of measurable toxicity for P21 in this study is consistent with previous reports (Jalili et al., 2018; Kirkland et al., 2024; Kunc et al., 2025), which similarly found no evidence of cytotoxicity in HepG2 cells. Together, these studies support the interpretation that steatotic hepatocytes are more susceptible to TiO_2-induced cytotoxicity, and that metabolic stress amplifies the toxic potential of otherwise inert particles. These findings feature the

importance of incorporating metabolically relevant models into TiO_2 risk assessment. Traditional assays in healthy cells may underestimate toxicity, whereas steatotic models reveal heightened vulnerability.

Quantification of cellular uptake highlights important distinctions in how E171 and P21 interact with hepatocytes under different metabolic conditions. The observation that E171 was more readily internalised under non-steatotic conditions suggests that its physicochemical characteristics, larger primary particle size, heterogeneous distribution, and anatase crystalline phase may facilitate stronger interactions with cell membranes in the absence of lipid accumulation. This pattern is consistent with the notion that bulk food-grade TiO_2 can be taken up by hepatocytes even without metabolic stress, potentially contributing to baseline cytotoxicity at higher concentrations. In contrast, P21 displayed comparatively lower uptake in non-steatotic cells but was significantly more internalised under steatotic conditions. This enhanced uptake in lipid-loaded hepatocytes may reflect the altered cellular environment associated with steatosis, such as changes in membrane composition, endocytic activity, and intracellular trafficking. Lipid accumulation can modify membrane fluidity and receptor availability, thereby influencing nanoparticle internalisation pathways (Sunshine & Iruela-Arispe, 2017). The apparent contradiction between E171's higher uptake in non-steatotic cells and P21's enhanced uptake in steatotic cells highlights the complex interplay between particle physicochemical properties and cellular metabolic state. These findings align with previous reports demonstrating concentration-dependent uptake of TiO_2 in HepG2 cells (Brandão et al., 2020), reinforcing the sensitivity of these cells to nanoparticle exposure across a broad dose range. However, the differential uptake patterns observed here extend the literature by showing that metabolic stress can modulate nanoparticle internalisation in a particle-specific manner. This suggests that risk assessment of TiO_2 should not only consider concentration and particle properties but also the metabolic status of target cells, as populations with hepatic steatosis may exhibit altered susceptibility to nanoparticle accumulation.

An interesting qualitative distinction was observed in the visual appearance of the E171 and P21 under bright-field illumination. E171 aggregates appeared greyish, whereas P21 aggregates displayed a distinctive yellowish hue. This difference can be attributed to variations in primary particle size and crystalline phase, both of which strongly influence light scattering and absorption behaviour. The larger primary particles and anatase structure of E171 favour Mie scattering in the visible range, producing a whitish-grey appearance (Rastar et al., 2017). In contrast, the rutile-dominant P21 particles fall within the Rayleigh scattering regime and exhibit a slight yellowish tint (Elim et al., 2009). Our findings are consistent with Verleysen et al. (2020), who similarly noted optical differences and observed different undertones among commercial brands of E171. Although these colour distinctions do not directly

inform toxicity mechanisms, they provide a useful internal marker to confirm identity during experiments.

Collectively, comprehensive physicochemical characterisation of TiO_2 (E171 A, B, C and P21) established their aggregated morphologies, crystalline phase composition, elemental purity, and medium-dependent dispersion behaviour, with DLS and zeta potential analyses confirming pronounced agglomeration and variable stability across biological media. These findings, together with the establishment of a steatotic HepG2 cell model and initial assessments of particle uptake and viability, provide a robust foundation for advancing toward biochemical assays to investigate the role of TiO_2 in lipid accumulation and oxidative stress under both normal and steatotic conditions.

CHAPTER 7: Effect of titanium dioxide (E171 and P21) on steatosis and oxidative stress in HepG2 cells

7.1 Introduction

Hepatic steatosis is characterised by excessive lipid accumulation within hepatocytes and is a defining feature of MASLD (Mayén et al., 2024). MASLD is increasingly recognised as a global health burden, progressing from simple steatosis to steatohepatitis, fibrosis, and cirrhosis (Younossi et al., 2025). Steatosis occurs when the balance between lipid uptake, synthesis, and clearance is disrupted, leading to triglyceride accumulation and lipotoxicity. In parallel, oxidative stress, an imbalance between ROS production and the antioxidant defence system, plays a key role in driving lipid peroxidation, inflammatory signalling, hepatocellular injury, thereby accelerating MASLD progression (Chen et al., 2025; Zhang et al., 2025).

In hepatocytes, TiO_2 exposure has been linked to alterations in lipid droplet formation, triglyceride storage, and ROS generation (**Chapter 2**), especially under steatotic conditions where cells are metabolically stressed. Major pathological features shared by MASLD and TiO_2 NPs induced toxicity are summarised in **Table 2.2**. These similarities suggest a possible link between TiO_2 and hepatic steatosis, and a potential role in the pathogenesis of MASLD.

This chapter investigates the effects of TiO_2 on lipid accumulation, cholesterol and triglyceride metabolism, ROS production, antioxidant capacity, and markers of oxidative damage under both steatotic and non-steatotic conditions.

The aims of the study set out in this chapter are as follows:

1. To investigate the effects of E171 and P21 on lipid accumulation in steatotic and non-steatotic HepG2 cells.
2. To evaluate the oxidative stress response induced by E171 and P21 in steatotic and non-steatotic HepG2 cells.

The overall aim was to investigate the roles of E171 and P21 in inducing and promoting steatosis and oxidative stress, thereby contributing to understanding the mechanisms underlying the onset and progression of MASLD.

7.2 Methods

To investigate the effects of E171 and P21 on lipid accumulation and oxidative stress in steatotic and non-steatotic HepG2 cells, steatosis was induced using 0.25 mM OA, followed by exposure to E171 or P21.

Following treatment, intracellular lipid accumulation was assessed using ORO staining to quantify lipid deposition in HepG2 cells. Biochemical quantification of triglycerides (TG) and total cholesterol (TCHO) was conducted using commercially available colourimetric/fluorometric assay kits. To evaluate the effects of E171 and P21 on oxidative stress, intracellular ROS levels were determined using the ROS detection kit, total antioxidant capacity (TAC) was assessed to determine the overall ability of cellular antioxidants to neutralise free radicals, nitric oxide (NO) levels were quantified as an indicator of nitrosative stress, and lipid peroxidation was evaluated by measuring malondialdehyde (MDA) levels. All assays were performed according to the manufacturers' protocols using commercially available kits, as detailed in **Chapter 3**.

7.2.1 Triglyceride quantification assay

Triglyceride levels in HepG2 cells treated with TiO_2 (E171 or P21) were quantified using the Abcam Triglyceride Quantification Kit, following the manufacturer's protocol. Cells were seeded, treated for 48 h with or without OA, harvested, and homogenised in 5% Nonidet P-40 before heating and centrifugation. Supernatants were diluted and added to 96-well plates containing cholesterol esterase/lipase, which hydrolyses triglycerides into glycerol and free fatty acids. The samples were then incubated with an assay master mix containing Enzyme Mix VI, which oxidises the glycerol to generate a product that reacts with the OxiRed™ probe. Each standard was run in duplicate, and blank correction was performed by subtracting the blank reading from all standard values. A fluorometric standard curve (Ex/Em=544/590−10 nm) was generated using triglyceride standards (0–1 nmol/well), and a line of best fit and its corresponding equation were generated by Microsoft Excel, as shown in **Figure 7.1**. Triglyceride concentrations (mM) were calculated according to the formula (B/V) × D, where B represents the amount derived from the standard curve, V is the sample volume, and D is the dilution factor. See **Section 3.13** for a more detailed description of the Triglyceride quantification assay.

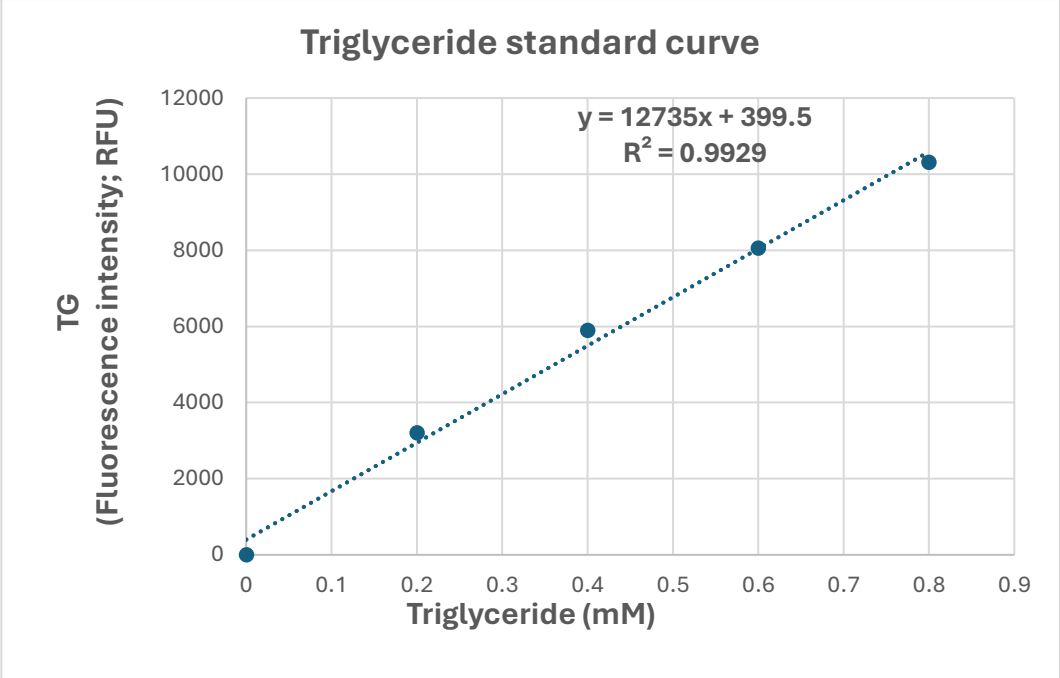

Figure 7.1 Representative standard curve of triglyceride concentration versus fluorescence.

7.2.2 Total cholesterol (TCHO) quantification assay

Total intracellular cholesterol levels in HepG2 cells treated with TiO_2 (E171 or P21) were quantified using the Abcam Total Cholesterol Assay Kit, following the manufacturer's instructions. Cells were seeded, treated with or without OA for 48 hours, harvested, and lysed using a chloroform:isopropanol: NP-40 mixture. Lysates were centrifuged, organic solvents removed, and dried lipid pellets dissolved in assay buffer. Samples were diluted and incubated with fluorometric reaction mix in 96-well plates at 37 °C for 60 min. Each standard was run in duplicate, and blank correction was performed by subtracting the blank reading from all standard values. A fluorometric standard curve (Ex/Em= 544/590−10 nm) was generated using cholesterol standards (0–0.5 µg/well), and a line of best fit and its corresponding equation were generated by Microsoft Excel, as shown in **Figure 7.2**. Sample values were determined using this equation after blank correction. Cholesterol concentrations (µM) were calculated using the formula (A/V) × D, where A is the absorbance at the standard curve, V is the sample volume, and D is the dilution factor. See **Section 3.14** for a more detailed description of the TCHO quantification assay.

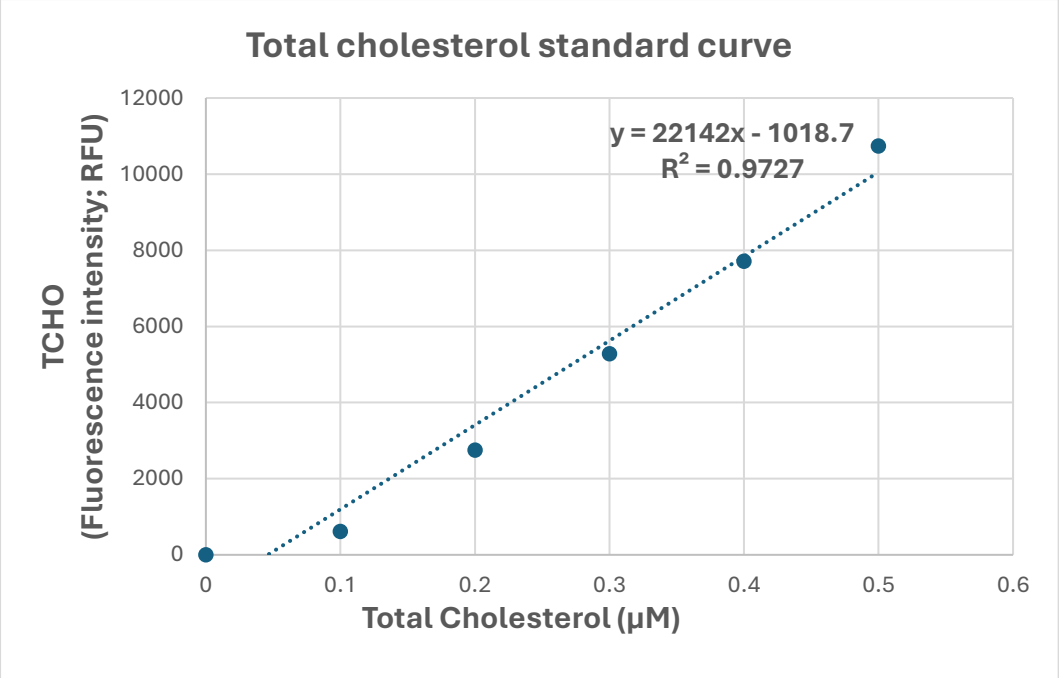

Figure 7.2 Representative standard curve of total cholesterol concentration versus fluorescence.

7.2.3 Reactive oxygen species (ROS) detection

ROS generation in HepG2 cells was quantified using the peroxide-sensitive fluorescent probe H_2DCFDA (Thermo Fisher Scientific). Cells were seeded in 96-well plates, pre-incubated with H_2DCFDA for 1 hour at 37 °C and then treated with TiO_2 (E171 or P21, 5 or 50 µg/mL) with or without OA for 5 hours. After washing, intracellular fluorescence of dichlorofluorescein (DCF), a marker of ROS levels, was measured using a microplate reader at Ex/Em = 485/535 nm. Different concentrations of Hydrogen peroxide were tested to identify an appropriate positive control for ROS induction. A concentration of 1050 µM was selected as the positive control (**Figure 7.3**). Absorbance values were corrected by subtracting blanks containing DMEM and TiO_2, and results were expressed as fluorescence intensity. See **Section 3.15** for further details on the ROS detection.

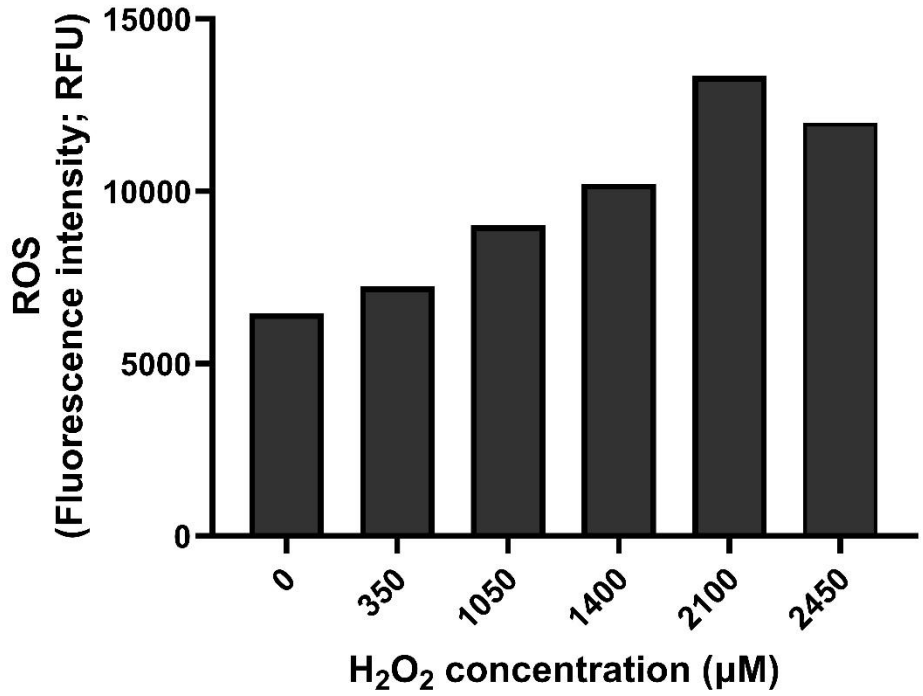

Figure 7.3 Representative bar graph of various hydrogen peroxide concentrations versus fluorescence.
The graph shows fluorescence intensity measured at different hydrogen peroxide concentrations, illustrating the dose-dependent induction of reactive oxygen species (ROS). Values are ± SEM.

7.2.4 Total antioxidant capacity (TAC) assay

TAC in HepG2 cells treated with TiO_2 (E171 or P21) was measured using the Abcam TAC Assay Kit, following the manufacturer's protocol. Cells were seeded, treated for 48 hours with or without OA, harvested, and homogenised in ddH_2O. Homogenates were centrifuged to remove debris, and supernatants were collected for analysis. Aliquots of lysates were mixed with a protein mask to inhibit protein-based antioxidant activity, allowing selective measurement of small-molecule antioxidants. Samples and standards were incubated with Cu^{2+} working solution for 90 min at RT in the dark.

Each standard was run in duplicate, and blank correction was performed by subtracting the blank reading from all standard values. A colourimetric standard curve (570 nm) was generated using Trolox standards (0–20 nmol/well), and a line of best fit and its corresponding equation were generated by Microsoft Excel, as shown in **Figure 7.4**. TAC values (mM) were calculated using the formula (B/V) × D, where B is the value derived from the standard curve, V is the sample volume, and D is the dilution factor. Results were expressed as nmol/µL. See **Section 3.16** for further details on TAC assay.

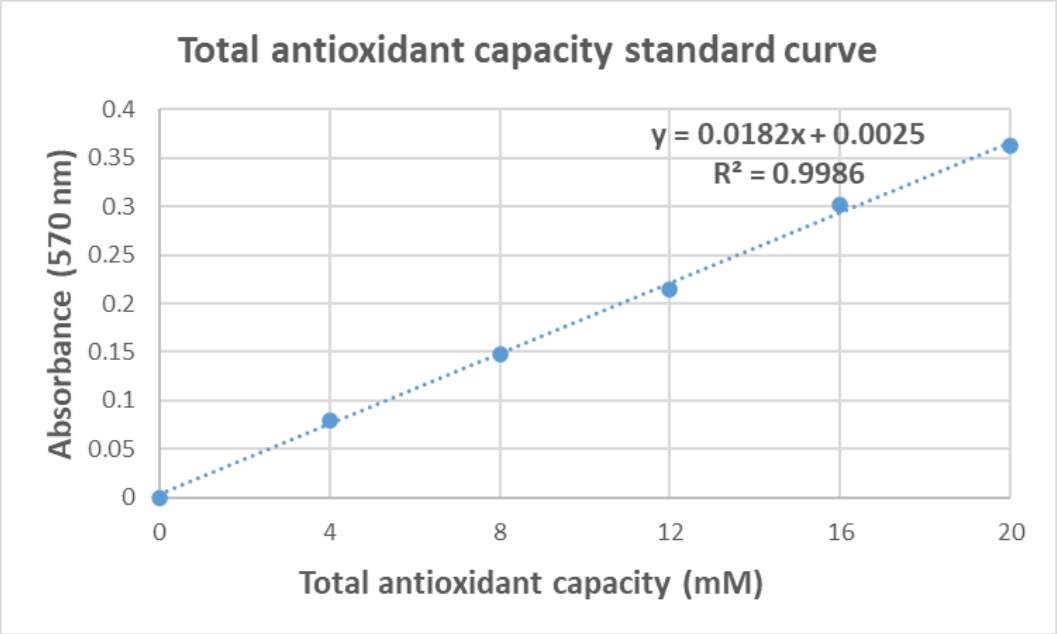

Figure 7.4 Representative standard curve of total antioxidant capacity versus absorbance.

7.2.5 Nitric oxide (NO) quantification assay

Nitric oxide (NO) levels in HepG2 cells treated with TiO_2 (E171 or P21) were quantified using the Sigma-Aldrich Nitric Oxide Assay Kit, following the manufacturer's instructions. Cells were seeded, treated with or without OA for 48 hours, harvested, and culture supernatants collected. Supernatants were deproteinised using Zinc sulfate and sodium hydroxide, followed by centrifugation to remove precipitated proteins. Clear supernatants were mixed with Griess reagents in 96-well plates and incubated at 37 °C for 60 min. Each standard was run in duplicate, and blank correction was performed by subtracting the blank reading from all standard values. A colourimetric standard curve (540 nm) was generated using nitrite standards (0–100 µmol/well), and a line of best fit and its corresponding equation were generated by Microsoft Excel, as shown in **Figure 7.5**. Sample values were determined using this equation after blank correction. Nitrite concentrations (µM) were calculated using the corrected absorbance (corrected absorbance/ slope) × DF, where DF is the dilution factor. See **Section 3.17** for further details on NO assay.

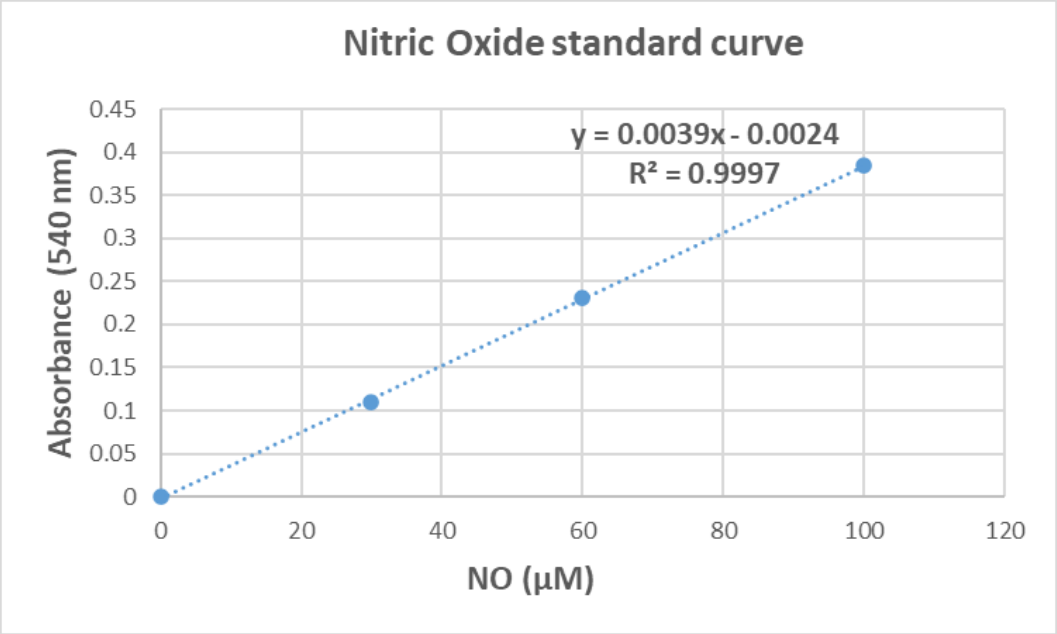

Figure 7.5 Representative standard curve of NO concentration versus absorbance.

7.2.6 Lipid peroxidation (malondialdehyde, MDA) assay

Lipid peroxidation in HepG2 cells treated with TiO_2 (E171 or P21) with or without OA was quantified using the Abcam Lipid Peroxidation (MDA) Assay Kit. Cells were seeded, treated for 48 hours, harvested, lysed with kit lysis buffer, and homogenised and sonicated. Lysates were centrifuged to remove debris, and supernatants were collected for analysis. Aliquots of lysates were incubated with developer mix at 95 °C for 60 min, cooled, and centrifuged to remove precipitates. Each standard was run in duplicate, and blank correction was performed by subtracting the blank reading from all standard values. MDA concentrations (µM) were calculated from a fluorometric standard curve (Ex/Em=544/590-10 nm) using MDA standards (0–0.5 nmol/well), and a line of best fit and its corresponding equation were generated in Microsoft Excel, as shown in **Figure 7.6**. See **Section 3.18** for further details on the lipid peroxidation assay.

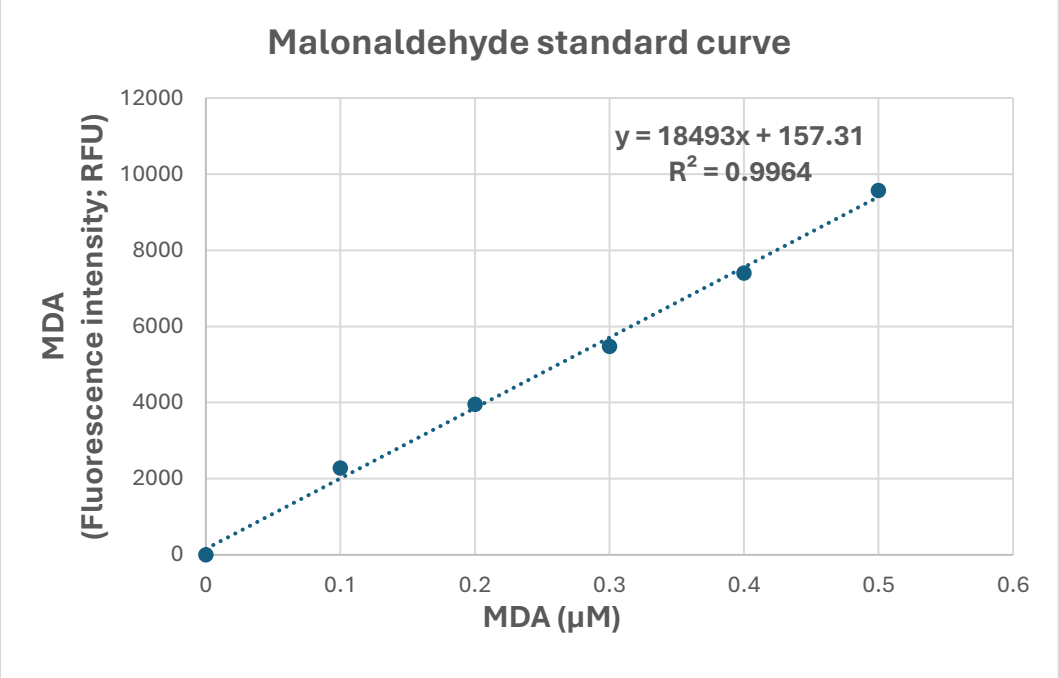

Figure 7.6 Representative standard curve of MDA concentration versus fluorescence.

7.2.7 Statistical analysis

Statistical analysis was performed using a two-way ANOVA and Tukey's multiple-comparison test, with a significance level set at $p<0.05$. Statistical analysis was performed using GraphPad Prism (GraphPad Software, version 10.6.1, La Jolla, California, USA).

7.3 Results

7.3.1 Lipid accumulation in HepG2 cells following exposure to E171 and P21 via ORO staining

Intracellular lipid storage is a characteristic of steatosis, and quantification of lipid accumulation provides a direct indicator of disrupted lipid metabolism (Pei et al., 2020). To determine the effect of E171 and P21 on lipid accumulation, HepG2 cells were treated with increasing concentrations (0, 5, 10, and 50 µg/mL) of E171 or P21, both in the presence and absence of OA (0.25 mM). Lipid accumulation was quantified using ORO staining, and absorbance was measured spectrophotometrically. Statistical analysis was performed using two-way ANOVA followed by Tukey's multiple comparisons test.

Under non-steatotic conditions (no OA treatment), E171-treated cells exhibited minimal lipid accumulation, as demonstrated by a low absorbance when the ORO staining was quantified. There was no increase in lipid accumulation in the presence of E171 at any tested concentration (**Figure 7.7**). Under steatotic conditions (in the absence of E171), lipid accumulation increased markedly, confirming the induction of steatosis. However, there was no further increase observed with any dose of E171 (**Figure 7.7**).

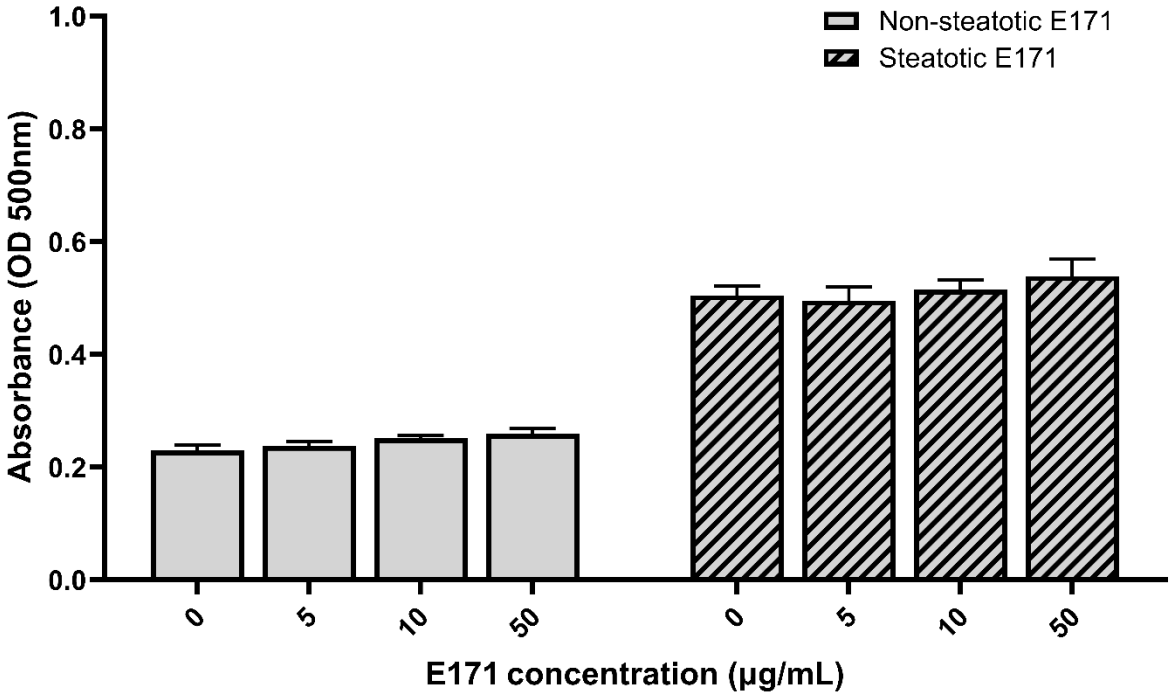

Figure 7.7 Quantification of lipid accumulation in HepG2 cells following exposure to E171 in steatotic and non-steatotic conditions.

HepG2 cells were treated with E171 at concentrations of 0, 5, 10, and 50 µg/mL, both in the presence and absence of OA (0.25 mM). Lipid accumulation was assessed using ORO staining, and absorbance was measured spectrophotometrically. Values are mean ± SEM. Each experiment was performed in triplicate (n=3).

Figure 7.8 shows the lipid accumulation in HepG2 cells treated with P21 under both non-steatotic and steatotic conditions. P21-treated cells exhibited minimal lipid accumulation across all tested concentrations under non-steatotic conditions (**Figure 7.8**). Under steatotic conditions (in the absence of P21), lipid accumulation increased, confirming the induction of steatosis. However, no further increase in lipid accumulation was observed with any dose of P21 (**Figure 7.8**).

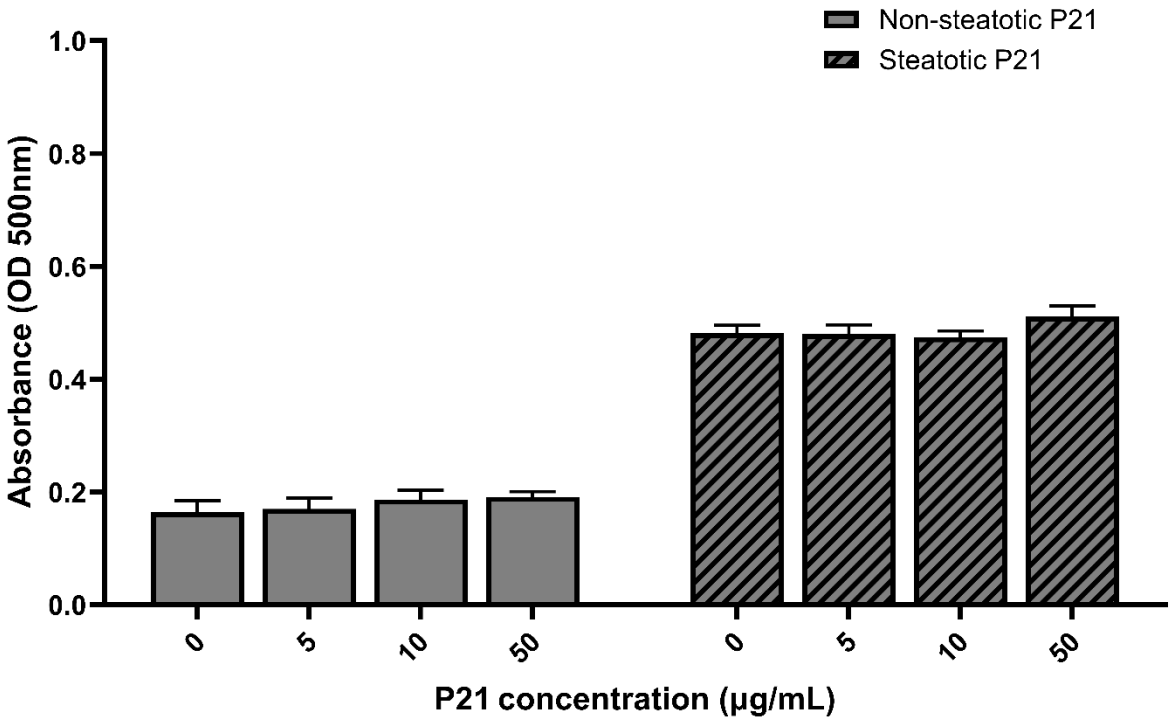

Figure 7.8 Quantification of lipid accumulation in HepG2 cells following exposure to P21 in steatotic and non-steatotic conditions.

HepG2 cells were treated with P21 at concentrations of 0, 5, 10, and 50 µg/mL, both in the presence and absence of OA (0.25 mM). Lipid accumulation was assessed using ORO staining, and absorbance was measured spectrophotometrically. Values are mean ± SEM. Each experiment was performed in triplicate (n=3).

Overall, these results demonstrate that neither E171 nor P21 exerted a significant effect on lipid accumulation in HepG2 cells, regardless of steatotic (presence of OA) or non-steatotic (absence of OA) conditions.

7.3.2 Quantification of triglycerides in HepG2 Cells following exposure to E171 and P21

Intracellular triglyceride accumulation is a characteristic of steatosis, and quantifying triglycerides provides a direct indicator of lipid storage dysregulation and metabolic disturbance (Heeren & Scheja, 2021). Although neither form of TiO_2 had an apparent effect on overall lipid accumulation, we considered the possibility that it might affect lipid distribution, so we investigated intracellular triglycerides and total cholesterol. To investigate the impact of TiO_2 on intracellular triglycerides, HepG2 cells were treated with increasing concentrations (0, 5, and 50 µg/mL) of E171 or P21, both in the presence and absence of OA (0.25 mM). Triglyceride content was quantified, and statistical analysis was performed using two-way ANOVA with Tukey's multiple comparisons test.

In non-steatotic conditions, E171 treatment did not induce any significant changes in intracellular triglycerides compared with the control (0 µg/mL) at either 5 or 50 µg/mL (**Figure 7.9**).

In contrast, steatotic E171-treated cells showed a significant increase (mean values rising from (1.4 ± 0.1) mM to (1.7 ± 0.1) mM in intracellular triglycerides at the higher tested concentration (50 µg/mL) compared with the control (p=0.0230) (**Figure 7.9**).

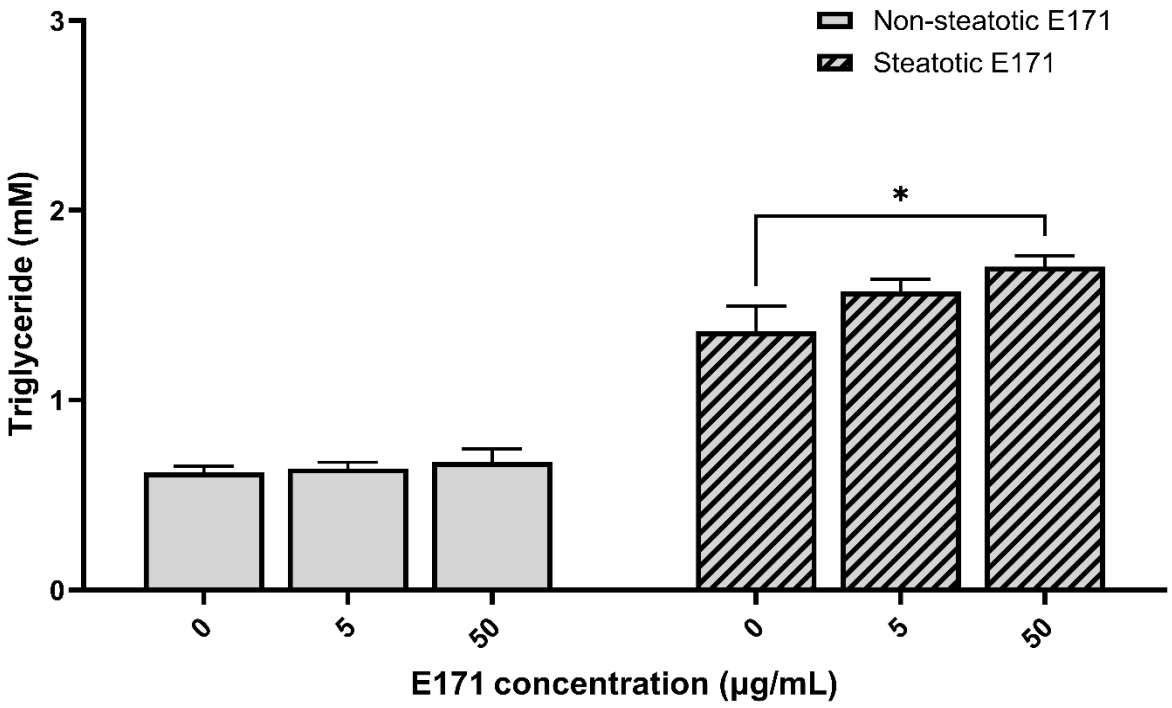

Figure 7.9 Quantification of intracellular triglyceride levels in HepG2 cells treated with E171 under non-steatotic and steatotic conditions.
HepG2 cells were treated with E171 at concentrations of 0, 5, and 50 µg/mL, both in the presence and absence of OA (0.25 mM). Triglyceride levels were measured using the Triglyceride Quantification Kit. Values are mean ± SEM. Each experiment was performed in duplicate (n = 4). Significantly different from control (∗ p ≤ 0.05).

Similarly, under non-steatotic conditions, P21 treatment did not produce significant changes in lipid accumulation compared with the control (0 µg/mL) at any tested concentration (**Figure 7.10**). However, steatotic P21-treated cells showed a significant increase in lipid accumulation (mean values rising from (1.3 ± 0.1) mM to (1.8 ± 0.1) mM at 50 µg/mL compared with the control (p=0.0354). This suggests that P21 increased intracellular triglycerides under steatotic conditions at a higher concentration (50 µg/mL).

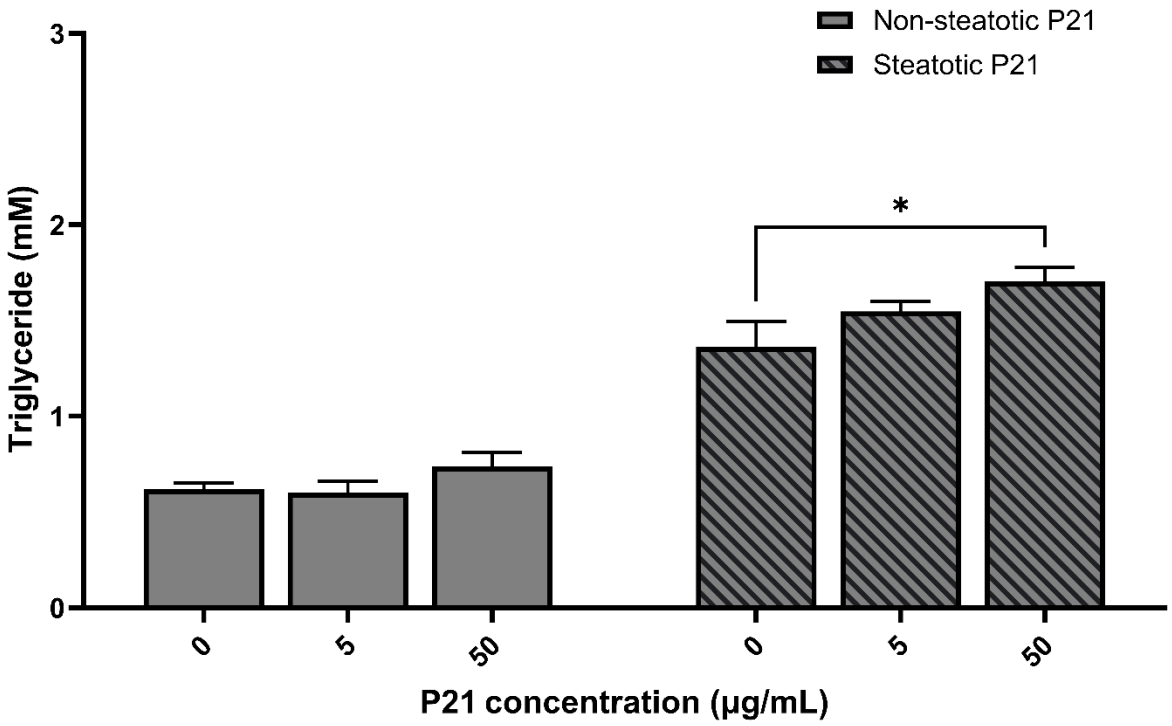

Figure 7.10 Quantification of intracellular triglyceride levels in HepG2 cells treated with P21 under non-steatotic and steatotic conditions.

HepG2 cells were treated with P21 at concentrations of 0, 5 and 50 µg/mL, both in the presence and absence of OA (0.25 mM). Triglyceride levels were measured using the Triglyceride Quantification Kit. Values are mean ± SEM. Each experiment was performed in duplicate (n = 4). Significantly different from control (∗ p≤0.05).

Collectively, these findings demonstrate that while P21 and E171 do not significantly alter lipid accumulation under basal (non-steatotic) conditions, both enhance lipid deposition at higher concentrations (50 µg/mL) under steatotic conditions.

7.3.3 Quantification of total cholesterol in HepG2 cells following exposure to E171 and P21

Cholesterol accumulation is also a characteristic of steatosis, and quantification of cholesterol levels provides insight into lipid homeostasis and membrane integrity (Cui et al., 2025). To determine the effect of E171 and P21 on intracellular cholesterol levels, HepG2 cells were treated with 0, 5, and 50 µg/mL of each particle type, both in the presence and absence of OA (0.25 mM). Total cholesterol was quantified using the Cholesterol Assay Kit, and statistical analysis was performed using two-way ANOVA with Tukey's multiple comparisons test.

Quantification of total cholesterol revealed no significant differences in HepG2 cells treated with E171, with or without OA, at 5 or 50 µg/mL compared to control (**Figure 7.11**).

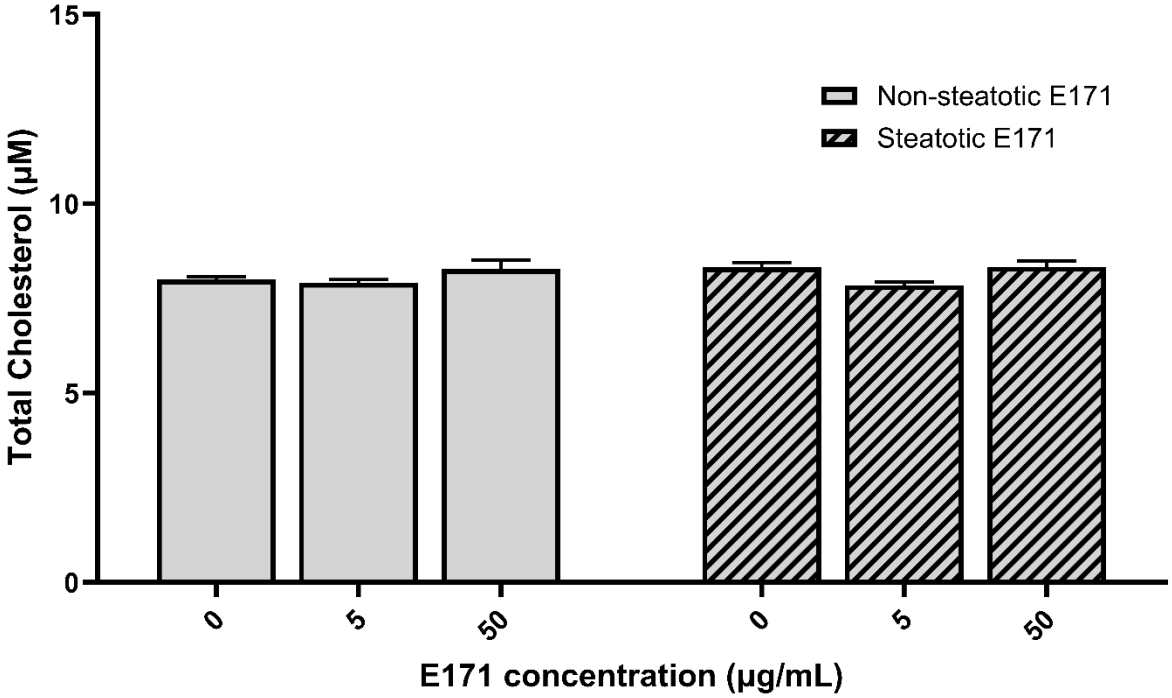

Figure 7.11 Total cholesterol levels in HepG2 cells following exposure to E171 under steatotic and non-steatotic conditions.
HepG2 cells were treated with E171 at concentrations of 0, 5, and 50 µg/mL, both in the presence and absence of OA (0.25 mM). Values are mean ± SEM. Each experiment was performed in duplicate (n=4).

Quantification of total cholesterol in HepG2 cells treated with P21 revealed no significant differences under non-steatotic conditions. Across all tested concentrations (0, 5, and 50 µg/mL), cholesterol levels remained stable. Similarly, in steatotic cells, P21 did not significantly alter cholesterol levels compared with controls (**Figure 7.12**).

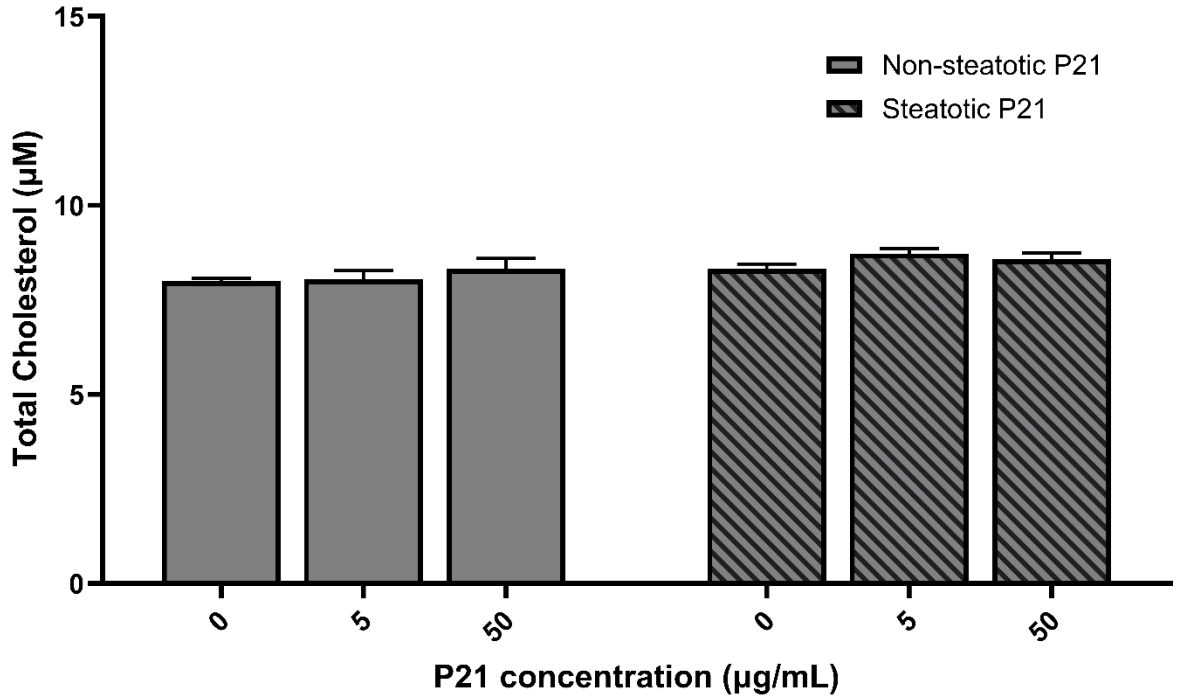

Figure 7.12 Total cholesterol levels in HepG2 cells following exposure to P21 under steatotic and non-steatotic conditions.
HepG2 cells were treated with P21 at concentrations of 0, 5, and 50 µg/mL, both in the presence and absence of OA (0.25 mM). Values are mean ± SEM. Each experiment was performed in duplicate (n=4).

Collectively, these results demonstrate that TiO_2 exposure does not influence total cholesterol levels in HepG2 cells, regardless of steatotic or non-steatotic conditions.

7.3.4 Quantification of ROS in HepG2 Cells following exposure to E171 and P21

Elevated levels of ROS are a critical indicator of oxidative stress and cellular damage (Chandimali et al., 2025). To determine the effect of E171 and P21 on intracellular ROS generation, HepG2 cells were treated with 0, 5, and 50 µg/mL of each particle type, both in the presence and absence of OA (0.25 mM). ROS levels were quantified using a ROS detection kit, and statistical analysis was performed using two-way ANOVA with Tukey's multiple comparisons test.

Quantification of ROS in HepG2 cells following exposure to E171 showed no significant differences under non-steatotic conditions. In contrast, steatotic cells exhibited a modest but significant increase (mean value rising from (2525 ± 93.9) RFU to (2996 ± 71.7) RFU in ROS levels at 50 µg/mL compared with the control (p=0.0167) (**Figure 7.13**).

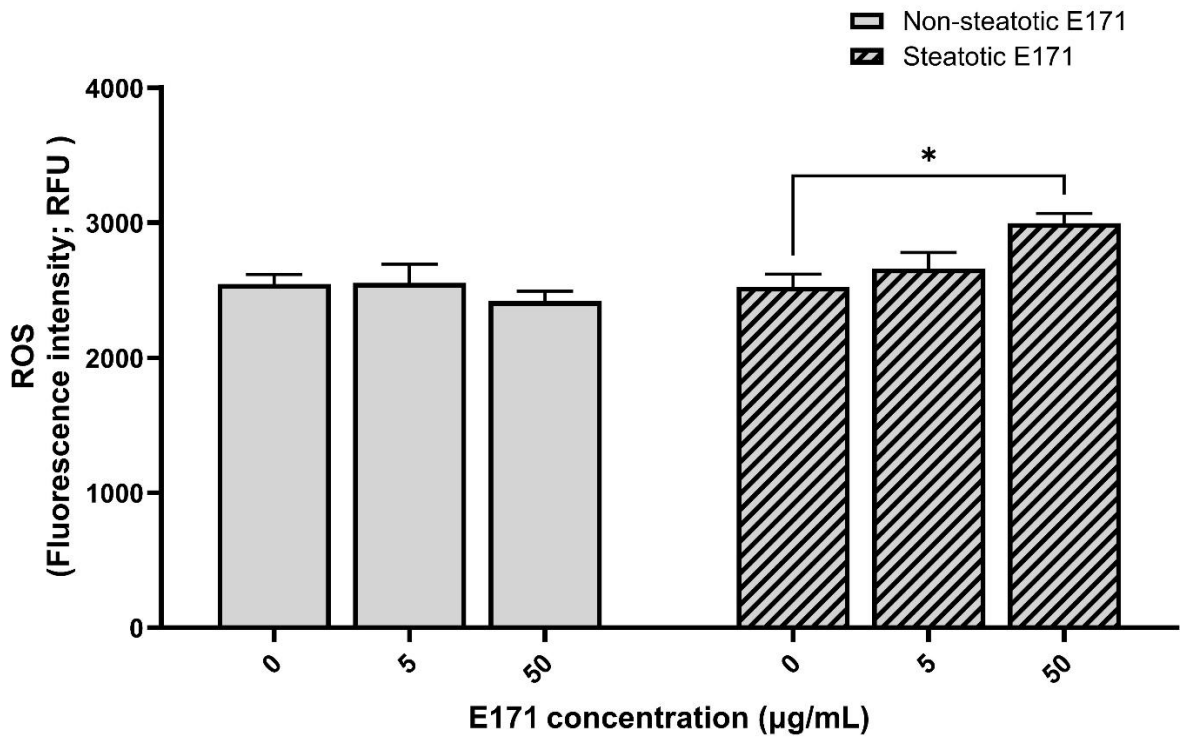

Figure 7.13 Intracellular ROS levels in HepG2 cells following exposure to E171 under steatotic and non-steatotic conditions.

HepG2 cells were treated with E171 at concentrations of 0, 5, and 50 µg/mL, both in the presence and absence of OA (0.25 mM). ROS levels were quantified using a commercial ROS detection kit. Values are mean ± SEM. Each experiment was performed in triplicate (n=3). Significantly different from control (∗ p≤0.05).

Quantification of ROS in HepG2 cells following exposure to P21 showed no significant differences under non-steatotic conditions. Across all tested concentrations, ROS levels remained stable. In contrast, steatotic HepG2 cells exhibited a modest but statistically significant increase in ROS levels at 50 µg/mL compared with the steatotic control (p=0.0029). Furthermore, ROS levels at 50 µg/mL were significantly elevated compared with those at 5 µg/mL (p=0.0438). Quantitatively, mean values increased from 2525 nm ± 93.9 in the control to 2999 nm ± 79.4 at 50 µg/mL, reflecting enhanced oxidative stress under steatotic conditions (**Figure 7.14**).

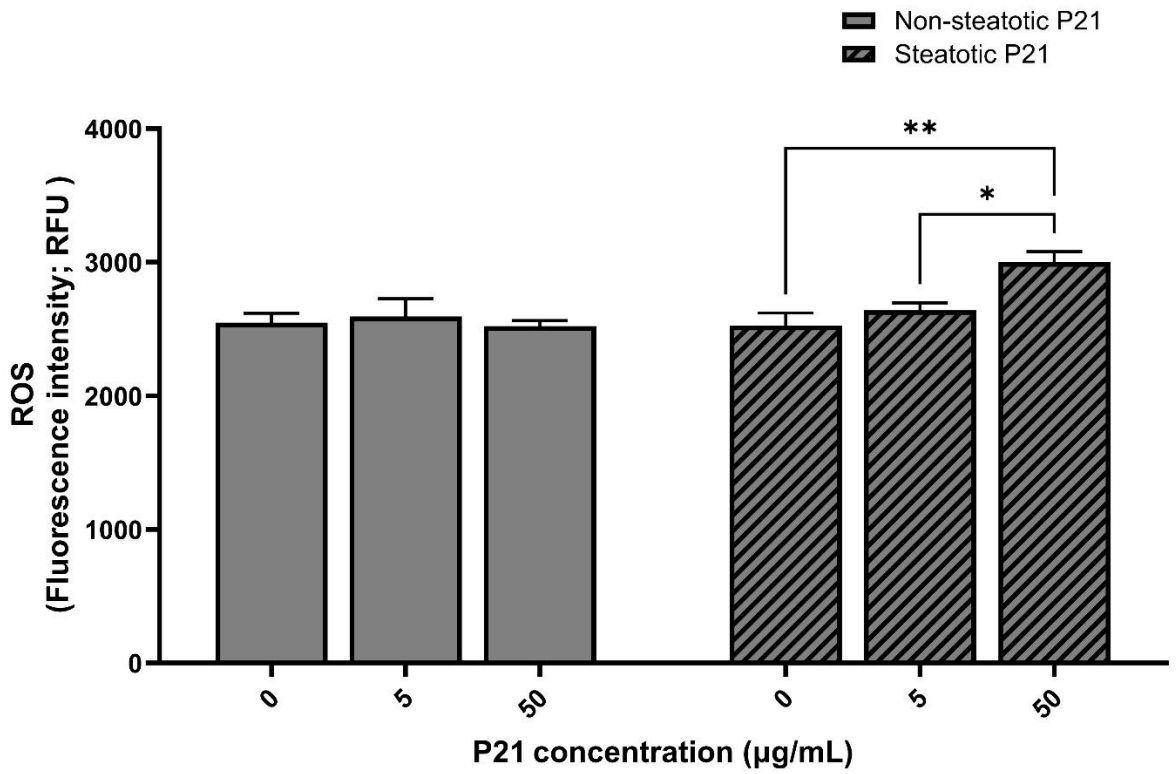

Figure 7.14 Intracellular ROS levels in HepG2 cells following exposure to P21 under steatotic and non-steatotic conditions.

HepG2 cells were treated with P21 at concentrations of 0, 5, and 50 µg/mL, both in the presence and absence of OA (0.25 mM). ROS levels were quantified using a commercial ROS detection kit. Values are mean ± SEM. Each experiment was performed in triplicate (n=3). Significantly different from control (∗ p≤0.05; ∗∗ p≤0.001).

These findings suggest that while E171 and P21 do not influence ROS production in non-steatotic HepG2 cells at tested concentrations, higher concentrations (50 µg/mL) of both enhance oxidative stress under steatotic conditions.

7.3.5 Quantification of NO levels in HepG2 cells following exposure to E171 and P21

NO is an important marker of redox balance and inflammatory signalling, since altered NO levels reflect oxidative stress and potential cellular damage (Chen et al., 2020). To determine the effect of E171 and P21 on NO activity, HepG2 cells were treated with 0, 5, and 50 µg/mL of each particle type, both in the presence and absence of OA (0.25 mM). NO levels were quantified using a commercial assay kit. Statistical analysis was performed using two-way ANOVA with Tukey's multiple comparisons test.

Under non-steatotic conditions, E171-treated HepG2 cells exhibited stable NO activity across all tested concentrations. No statistically significant variation was observed compared with the untreated control, indicating that E171 exposure did not alter basal NO production. In steatotic cells, overall NO

activity remained within a narrow range (0.48 µM–0.51 µM). However, statistical analysis revealed a modest but significant difference between the 0 µg/mL and 50 µg/mL groups (p=0.0299) (**Figure 7.15**).

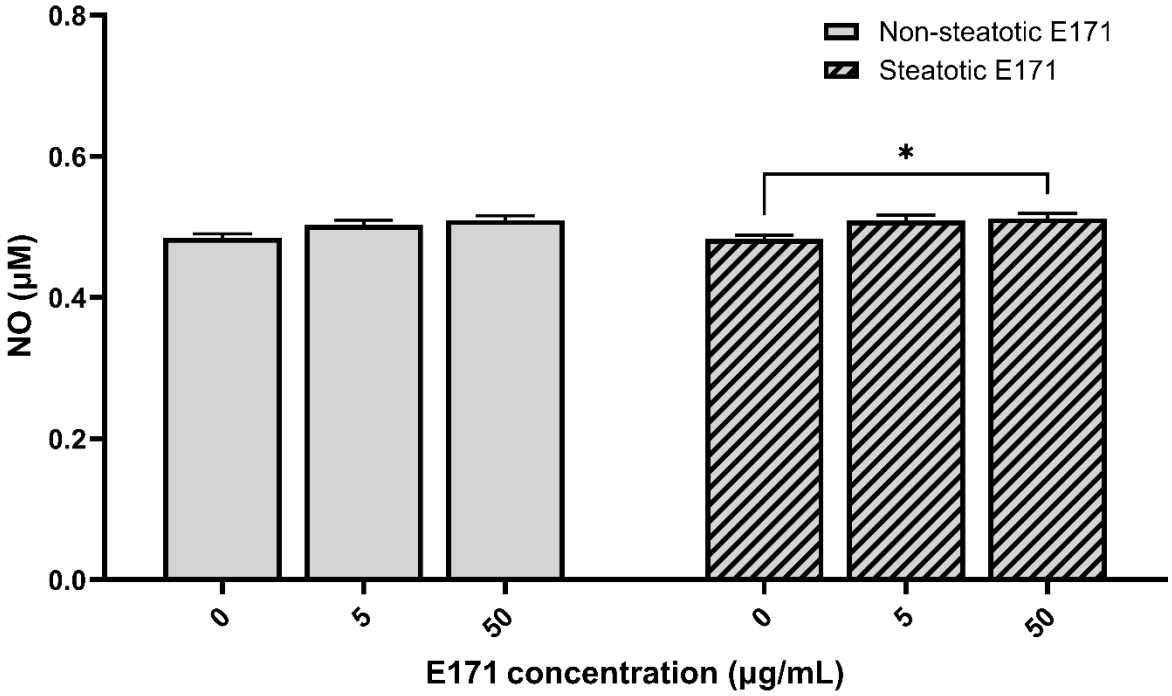

Figure 7.15 Quantification of NO activity in HepG2 cells exposed to E171.
HepG2 cells were treated with E171 at concentrations of 0, 5, and 50 µg/mL, with or without OA (0.25 mM). NO activity was measured using a commercial NO assay kit. Values are mean ± SEM. Each experiment was performed in duplicate (n=4). Significantly different from control (∗ p≤0.05).

A comparable pattern was observed for P21. Under non-steatotic conditions, NO activity remained steady with no significant differences relative to controls. Similarly, in steatotic HepG2 cells, P21 treatment indicated no impact on NO production (**Figure 7.16**).

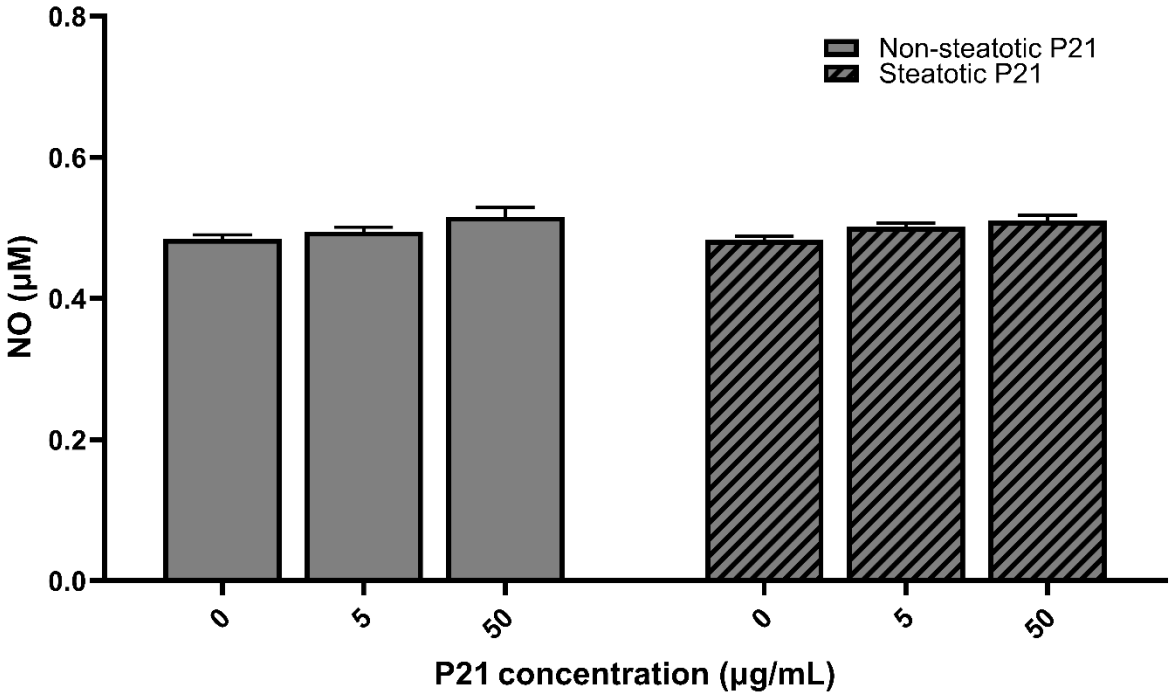

Figure 7.16 Quantification of NO activity in HepG2 cells exposed to P21.

HepG2 cells were treated with P21 at concentrations of 0, 5, and 50 µg/mL, with or without OA (0.25 mM). NO activity was measured using a commercial NO assay kit. Values are mean ± SEM. Each experiment was performed in duplicate (n=4).

Collectively, the data indicate that P21 treatment does not exert any measurable effect on NO activity under either non-steatotic or steatotic conditions. In contrast, E171 exposure shows statistically significant effect at the highest tested concentration (50 µg/mL) under steatotic conditions.

7.3.6 Total antioxidant capacity in HepG2 cells following exposure to E171 and P21

Total antioxidant defences are important for maintaining redox balance and protection against cellular damage (El-Sehrawy et al., 2025). To investigate the effect of E171 and P21 on total antioxidant capacity, HepG2 cells were treated with 0, 5, and 50 µg/mL of each particle type, both in the presence and absence of OA (0.25 mM). Antioxidant levels were quantified using a commercial kit, and statistical analysis was performed using two-way ANOVA with Tukey's multiple comparisons test.

In non-steatotic HepG2 cells, treatment with E171 did not produce significant changes in TAC compared with the untreated control, indicating that basal antioxidant status was unaffected by E171 exposure. Similarly, in steatotic HepG2 cells co-treated with OA, E171 did not induce significant changes in antioxidant capacity at any of the tested concentrations (**Figure 7.17**).

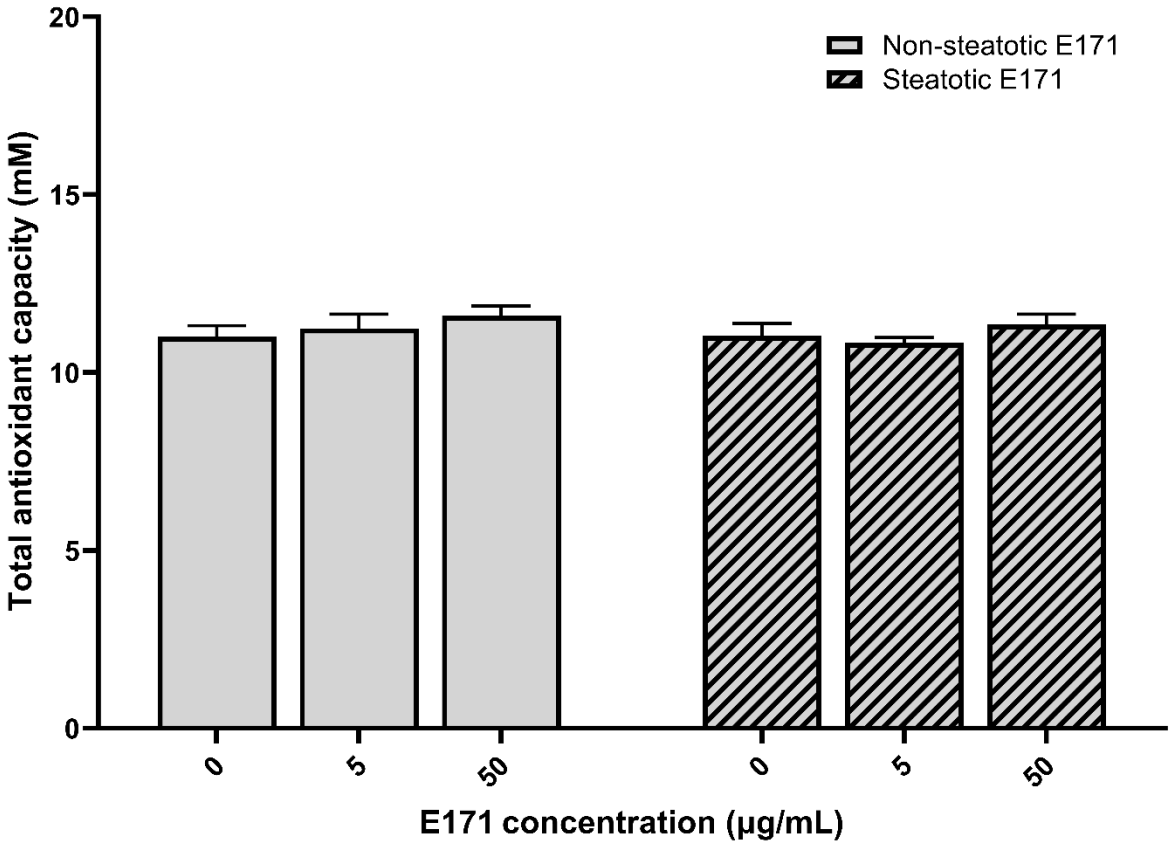

Figure 7.17 Quantification of total antioxidant capacity in HepG2 cells exposed to E171 under steatotic and non-steatotic conditions.

HepG2 cells were treated with E171 at concentrations of 0, 5, and 50 µg/mL, with or without OA (0.25 mM). Total antioxidant capacity was measured using a commercial assay kit. Values are mean ± SEM. Each experiment was performed in duplicate (n=4).

Under non-steatotic conditions, P21 treatment did not significantly alter total antioxidant capacity compared with the control. Similarly, in steatotic HepG2 cells, co-treatment with OA and P21 also failed to produce significant changes in antioxidant capacity (**Figure 7.18**).

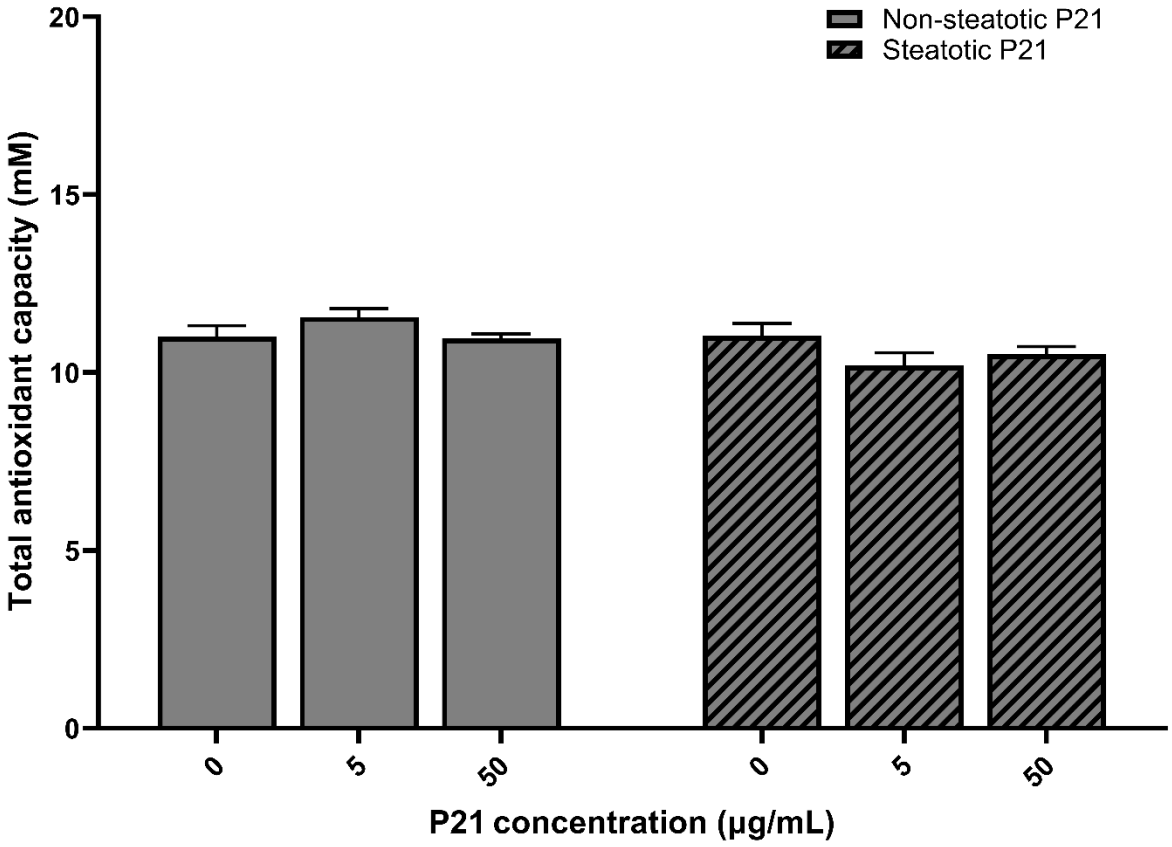

Figure 7.18 Quantification of total antioxidant capacity in HepG2 cells exposed to P21 under steatotic and non-steatotic conditions.
HepG2 cells were treated with P21 at concentrations of 0, 5, and 50 µg/mL, with or without OA (0.25 mM). Total antioxidant capacity was measured using a commercial assay kit. Values are mean ± SEM. Each experiment was performed in duplicate (n=4).

Taken together, the data indicate that neither E171 nor P21 significantly modulate the total antioxidant capacity of HepG2 cells and even in the presence of OA induced steatosis, antioxidant status remained stable.

7.3.7 Quantification of lipid peroxidation (MDA) in HepG2 Cells following exposure to E171 and P21

MDA is a stable end-product that serves as a key marker of oxidative damage to cellular membranes (Zelber-Sagi et al., 2020). To investigate the effect of E171 and P21 on lipid peroxidation, HepG2 cells were treated with 0, 5, and 50 µg/mL of each particle type, both in the presence and absence of OA (0.25 mM). MDA levels were quantified using a commercial kit, and statistical analysis was performed using two-way ANOVA with Tukey's multiple comparisons test.

In non-steatotic cells, treatment with E171 did not produce significant changes in lipid peroxidation compared with the control at any concentration tested. Similarly, in steatotic cells, E171 did not induce significant alterations in lipid peroxidation across the tested concentrations. Although a slight

increasing trend was observed at the higher concentration of E171 (50 µg/mL) in both non-steatotic and steatotic conditions, this increase did not reach statistical significance (**Figure 7.19**).

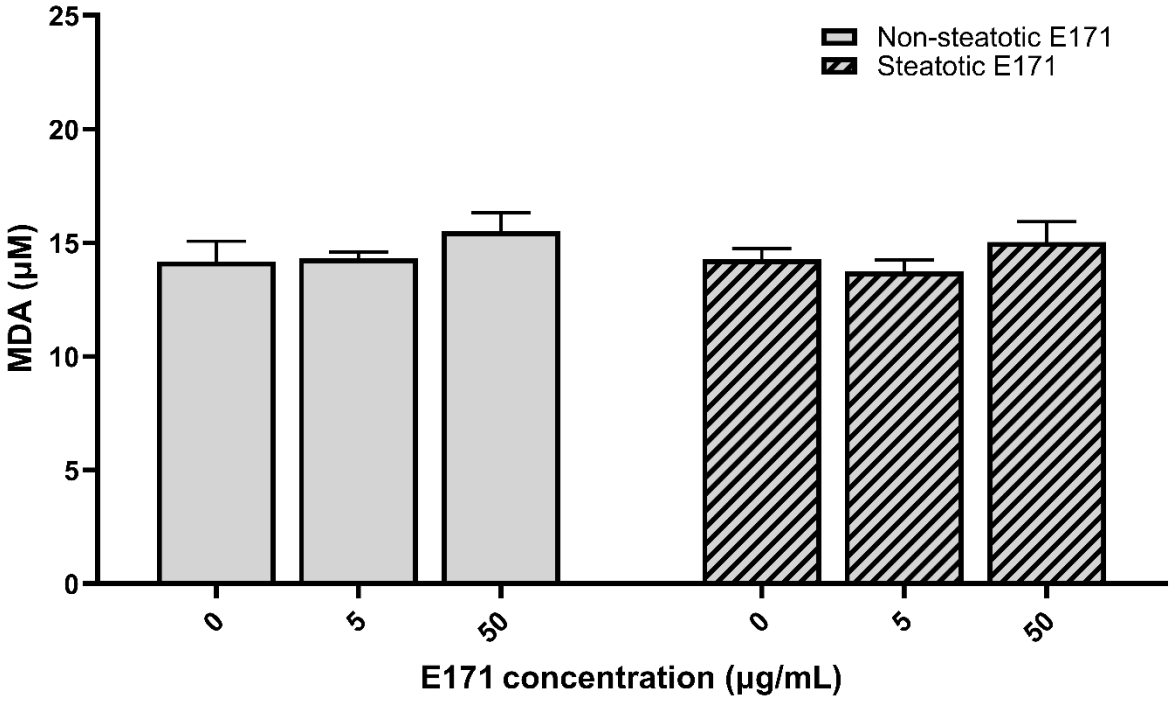

Figure 7.19 Quantification of MDA in HepG2 cells exposed to E171 under steatotic and non-steatotic conditions.

HepG2 cells were treated with E171 at concentrations of 0, 5, and 50 µg/mL, with or without OA (0.25 mM). MDA was measured using a commercial assay kit. Values are mean ± SEM. Each experiment was performed in duplicate (n=4).

In non-steatotic cells, treatment with P21 did not produce significant changes in lipid peroxidation compared with the control at any of the concentrations tested. Similarly, in steatotic HepG2 cells cotreated with OA, P21 did not induce significant alterations in lipid peroxidation. Although a slight upward trend was observed at the highest P21 concentration (50 µg/mL) under both non-steatotic and steatotic conditions, this increase did not reach statistical significance (**Figure 7.20**).

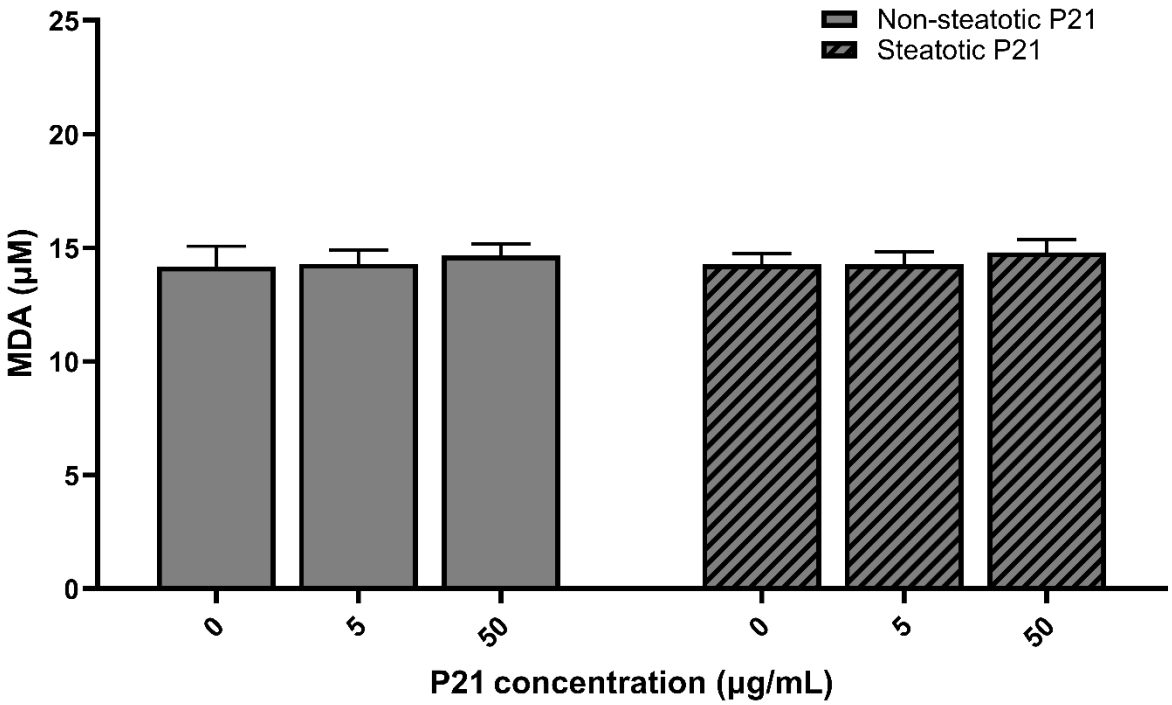

Figure 7.20 Quantification of MDA in HepG2 cells exposed to P21 under steatotic and non-steatotic conditions.

HepG2 cells were treated with P21 at concentrations of 0, 5, and 50 µg/mL, with or without OA (0.25 mM). MDA was measured using a commercial assay kit. Values are mean ± SEM. Each experiment was performed in duplicate (n=4).

Collectively, these findings suggest that exposure to E171 and P21 does not significantly modulate MDA levels in HepG2 cells.

7.4 Discussion

In this chapter, the effects of E171 and P21 on lipid accumulation and oxidative stress in HepG2 cells were investigated. The study aimed to demonstrate the role of E171 and P21 in inducing and promoting steatosis and oxidative stress, thereby contributing to the onset and progression of MASLD phenotype *in vitro*.

ORO staining showed that E171 or P21 had no significant effect on lipid accumulation in HepG2 cells under either steatotic or non-steatotic conditions. Although a slight increase in absorbance was observed in both E171- and P21-treated steatotic and non-steatotic cells, statistical analysis revealed that these differences were not significant within the same treatment group. This indicates that, while steatosis itself markedly increased lipid accumulation, increasing the E171 or P21 dose did not further enhance lipid accumulation in either condition. Biochemical quantification of triglycerides demonstrated marginal effects. Under steatotic conditions, both E171 and P21 at the highest concentration tested (50 µg/mL) increased triglyceride accumulation compared with controls. This effect was not observed in non-steatotic cells, highlighting that the presence of OA induced steatosis

may sensitise cells to TiO_2 exposure. The discrepancy between ORO staining and triglyceride quantification suggests that, while overall lipid droplet accumulation may not be visibly altered, specific lipid fractions, such as triglycerides, can be selectively affected under metabolic stress. Additionally, quantification of total cholesterol showed no significant changes across treatments, regardless of steatotic status. This finding indicates that cholesterol metabolism remains stable in HepG2 cells exposed to E171 and P21, and that alterations in cholesterol storage do not accompany the observed triglyceride changes. This selective influence on triglycerides rather than cholesterol is consistent with several previous reports. For example, Zhang et al. (2021) observed only marginal, non-significant elevations of both triglycerides and cholesterol in HepG2 cells at low-dose TiO_2 exposure (4 µg/mL). Another study by Chen et al. (2022b) reported steatosis in rat hepatocytes following exposure to TiO_2 NPs at 50 mg/kg, while Yu et al. (2025) demonstrated significant upregulation of specific triacylglycerol (TAG) and diacylglycerol (DAG) in rat liver, accompanied by altered DAG transport. Similarly, metabolomic studies in Human bronchial epithelial cells immortalized with an adenovirus 12–SV40 hybrid virus (BEAS2B) (TiO_2 NPs 0–100 µg/mL) (Zhang et al., 2022) and dietary exposure in mice (Perez et al., 2021) revealed changes in lipid metabolic pathways and circulating TAG levels. In contrast, IV administration in rats increased LDL cholesterol without affecting TAG (Su et al., 2018). Taken together, these findings suggest that TiO_2 can perturb lipid metabolism across both *in vitro* and *in vivo* systems. However, the specific lipid classes affected whether triglycerides, DAGs, or cholesterol appear, depending on exposure conditions, cell type, and physiological context. In summary, while E171 and P21 did not significantly drive lipid droplet formation or cholesterol storage in HepG2 cells, a subtle, steatosis-dependent elevation of triglycerides was detected at higher doses. These findings contribute to a growing body of evidence that TiO_2 can interfere with lipid metabolic pathways in a context-specific manner, with triglyceride homeostasis appearing more vulnerable than cholesterol homeostasis under conditions of pre-existing metabolic stress.

ROS measurements revealed no significant changes in non-steatotic cells across all concentrations of E171 and P21. Our findings were consistent with those of Kunc et al. (2025), who reported no change in ROS production in response to TiO_2 exposure when assessed using the H_2DCFDA assay in normal HepG2 cells. However, in steatotic cells, both E171 and P21 induced a dose-dependent increase in ROS, with a significant effect observed at the highest concentration tested (50 µg/mL) compared with controls. This indicates that steatosis enhances cellular susceptibility to TiO_2-induced oxidative stress. Notably, the ROS increase was modest and concentration dependent, suggesting that oxidative stress is triggered only under conditions of lipid overload and higher TiO_2 exposure. These findings align with earlier research showing that TiO_2 NPs significantly elevated ROS levels in HepG2 cells in a dose-dependent manner (Abbasi-Oshaghi et al., 2019; Li et al., 2020).

In our study, NO activity remained unchanged in HepG2 cells exposed to E171 or P21 (5–50 µg/mL), regardless of steatotic status, suggesting that TiO_2 did not activate inflammatory signalling via NO within the tested dosage range. This contrasts with Shajari et al. (2021), who observed elevated NO levels in HepG2 cells after repeated passages at higher concentrations (125–250 µg/mL), and with *in vivo* studies reporting significant NO increases in rat liver following TiO_2 NPs exposure at 10–200 mg/kg (Abbasi-Oshaghi et al., 2019; Grissa et al., 2020). The discrepancy may reflect differences in exposure duration, cumulative passage effects, or the higher doses used in those studies compared with our experimental design. It also highlights the importance of cellular context and experimental conditions in shaping inflammatory responses to TiO_2. Taken together, while *in vivo* evidence points to NO elevation as a marker of TiO_2-induced- inflammation, our *in vitro* data suggest that under controlled conditions and within the tested concentration range, HepG2 cells do not exhibit this response.

In our study, quantification of MDA revealed no significant changes in either non-steatotic or steatotic HepG2 cells treated with E171 or P21, indicating that although ROS levels increased under steatotic conditions, they did not progress to measurable lipid peroxidation, consistent with the stable TAC results. This outcome contrasts with several *in vivo* investigations reporting elevated MDA following TiO_2 NPs exposure. For example, Kandeil et al. (2020) observed increased MDA in rat liver after 14 days of gavage at 500 mg/kg, while Hu et al. (2015) reported significant MDA elevation in both serum and liver at 64 and 320 mg/kg after 14 weeks. Similarly, Gurr et al. (2005) demonstrated that TiO_2 NPs induced MDA formation in BEAS-2B cells, but only at smaller anatase particle sizes (10–20 nm), with larger anatase and rutile particles showing no effect. Taken together, these comparisons suggest that MDA induction by TiO_2 is highly dependent on particle size, dose, exposure duration, and biological context. Our findings, therefore, highlight that, under the tested in vitro conditions, TiO_2 exposure did not trigger lipid peroxidation in HepG2 cells, despite increased ROS, reinforcing the importance of considering both oxidative stress markers and downstream lipid damage when evaluating TiO_2 toxicity.

Overall, our findings demonstrate that TiO_2 (E171 and P21) exposure in HepG2 cells exerts only modest and context-dependent effects, with triglyceride accumulation and ROS generation becoming evident primarily under steatotic conditions. At the same time, cholesterol metabolism, NO activity, and MDA levels remained stable across all treatments at the tested concentrations (5–50 µg/mL). These results suggest that lipid overload may sensitise HepG2 cells to TiO_2-induced oxidative stress, yet the absence of significant inflammatory signalling (NO) or lipid peroxidation (MDA) levels indicates that the cellular response is limited in scope under the tested *in vitro* conditions. When considered alongside *in vivo* studies reporting more pronounced alterations in MDA, oxidative stress, and inflammatory markers, our data highlight the importance of dose, particle characteristics, exposure duration, and physiological context in shaping TiO_2 toxicity.

CHAPTER 8: Discussion

8.1 Significance

This thesis is organised into two parts: the first (**Chapters 4–5**) characterising prevalence and dietary exposure of E171 in the NZ food supply, and the second (**Chapters 6–7**) investigating the role of TiO_2 in steatosis and oxidative stress in HepG2 cells that are key initiating events in MASLD pathogenesis.

TiO_2 has recently attracted international scrutiny following the safety re-evaluation of E171 by EFSA. EFSA concluded that concern about genotoxicity could not be ruled out, prompting France (2019) and, subsequently, the entire European Union (2022) to prohibit its use as a food additive. Despite these regulatory shifts, E171 remains authorised to be used as a food additive in NZ, Australia, the US, and many other countries (Warheit, 2024). Real-world dietary exposure to E171 varies significantly across countries due to differences in food manufacturing practices, labelling requirements, and consumer preferences.

Food consumption surveys are an important tool for estimating real-world exposure to food additives such as E171 and for informing risk assessments. Before the present study, no data were available on dietary intake of Ti or E171 in the NZ population. Although TiO_2-containing foods and consumer products remain widely available on NZ supermarket shelves, neither the periodic NZTDS, the most comprehensive national dietary survey, nor any other systematic survey had previously included Ti among the analytes. The first part of this thesis, therefore, fills an important evidence gap by providing the first estimates of E171 prevalence in the NZ food supply, providing locally relevant evidence on both the presence and dietary intake of TiO_2 as the intentional food additive E171 and naturally occurring Ti in foods. By analysing 180 market-representative food samples and combining these occurrence data with national food consumption surveys across ten age groups, this food survey delivers the first comprehensive estimate of habitual E171 exposure for the NZ population, including identification of major contributing food categories and high-exposure subgroups (e.g., children and adolescents).

MASLD is one of the most prevalent chronic liver diseases worldwide (Chan et al., 2023). Previous studies have shown that TiO_2 induces oxidative stress, inflammation, and dysregulated lipid metabolism (early events in MASLD pathogenesis) (**Table 2.2**). The second part of this thesis aimed to investigate the role of TiO_2 on key MASLD-related endpoints in HepG2 cells, including cytotoxicity, steatosis, and oxidative stress.

This study addressed four key objectives: first, we identified that natural dietary Ti intakes in NZ are consistently low, with background contributions from plant, dairy, eggs, meats, dried fruits, and teas, while high-dose exposures arise from residual E171 use in confectionery and personal care products,

particularly toothpaste, confirming **Objective 1**. Second, the estimated population intake of E171 is 0.5–0.75 mg/day, indicating that while baseline exposure is modest, frequent consumers of E171-containing confectionery may reach substantially higher levels, fulfilling **Objective 2**. Third, *in vitro* HepG2 models demonstrated that E171 and P21 selectively exacerbate triglyceride accumulation under lipid overload without altering cholesterol storage or lipid droplet formation, addressing **Objective 3**. Finally, **Objective 4** was met by showing that E171 and P21 increase ROS levels in steatotic cells, indicating oxidative stress.

8.2 General discussion

8.2.1 Ti in NZ foods and estimated dietary intakes

In this study, the wide variation in Ti concentrations across the 43 food composites (**Table 4.2**) reflects the heterogeneous distribution of Ti in NZ foods.

8.2.1.1 Concentrations in foods

The highest Ti concentration observed in this study was in the eggs composite (1.17 mg/kg). These findings merit particular attention, as eggs are not expected to contain added E171. Ti in eggs is most likely derived from soil-derived TiO_2 ingested by hens *via* feed, dust, or grit. Similar natural Ti accumulation has been reported in free-range and conventional egg production systems internationally, with soil and feed contamination identified as primary pathways (FSA, 2020; Giannenas et al., 2009). Free-range and barn systems, which are common in NZ, allow greater soil and dust ingestion by hens compared with the cage systems that predominated in many European studies (Majewski et al., 2024). The concentration of Ti measured in the current NZ egg composite, therefore, likely represents natural background accumulation rather than additive use and highlights the importance of country-specific data when estimating dietary Ti exposure.

The detection of Ti in fresh meats, beef (0.815 mg/kg), pork (0.854 mg/kg), and chicken (0.765 mg/kg) further provides evidence of a natural background contribution across animal-derived foods. Notably, these levels cannot be attributed to the intentional addition of E171, which is not permitted as an additive in raw meat in NZ (MPI, 2017). The most important mechanism that accounts for this background contribution is direct soil ingestion. Naturally occurring TiO_2 minerals in soils may exist in various crystalline forms, such as rutile and anatase, and minerals such as ilmenite (mixed iron-TiO_2 mineral). Dairy cows can ingest approximately 0.5 kg of soil per day, and indeed, Ti is used to measure soil ingestion by cattle (Fries et al., 1982; Healy, 1968; Mayland et al., 1975). Chickens also ingest significant amounts of soil (Grace & MacFarlane, 2016; Jurjanz et al., 2014). As noted by Jurjanz et al. (2014), soil ingestion is recognised as the primary source of environmental contaminants in food-producing animals reared outdoors. One conventional pathway for many chemical contaminants is

soil-to-plant-to-animal transfer, where the substance is taken into the food of grazing or feed-ing livestock. Another secondary source is inhalation of Ti-rich dusts in intensive farming environments, where wind-blown soil particles, barn dust, and road dust may contain between 0.5–6% TiO_2 by weight (Mugudamani, 2022). In addition, unintentional introduction can occur during feed formulation, as mineral premixes, limestone carriers, or phosphate supplements often contain trace Ti impurities (Younes et al., 2021). Finally, minor contamination during slaughter and primary processing, through contact with knives, conveyor belts, or water supplies, may contribute to Ti residues that are analytically indistinguishable from tissue-incorporated Ti.

Across the major plant- and dairy-based food groups, Ti concentrations remained low and closely aligned with expected natural background levels. Fruit and vegetable composites ranged from <0.15 to 0.686 mg/kg, grain and cereal-based products (rice, pasta, breakfast cereals, biscuits, cakes) from <0.36 to 0.673 mg/kg, and fluid milk (Composite 27) was below 0.1 mg/kg. The single notable outlier was Composite 29 (“Milk products 2”), which returned 14.8 mg/kg due to a single mochi-style coconut ice-cream product containing 96.1 mg/kg Ti, almost certainly added E171. Notably, despite the high concentration, the product was not declared or labelled as containing E171. This may raise important questions about compliance with labelling regulations and highlight the potential for undeclared TiO_2 use in certain processed foods.

The detection of Ti in dried fruits, berries, and dry tea leaves (4.77 mg/kg) (in the range normally expected for dried plant leaves) provides further support for a natural, plant-mediated background contribution to dietary Ti exposure. This pattern is consistent with the known phytoavailability of soil-borne TiO_2. Plant roots with fine root hairs or mycorrhizal associations can take up Ti from the rhizosphere. Once absorbed, Ti tends to translocate poorly to edible portions in most species but accumulates favourably in leaf tissues and in the epidermal layers of fruits, structures that become concentrated upon dehydration (Wang et al., 2023). The impact of drying is significant as the removal of water concentrates analytes when expressed on a dry-weight basis. Fresh berries and fruits usually contain 85–92% moisture, while tea leaves are reduced to less than 5% moisture during drying. As a result, even relatively low Ti levels in fresh material (for example, 0.2–0.6 mg/kg fresh weight) can translate into several milligrams per kilogram in the dried product, without any external source of contamination (It should be noted, however, that tea drinking would not be a significant source of dietary Ti, because there is both substantial dilution, and incomplete extraction).

As none of the dried fruit, berry, or tea samples analysed in the present study declared E171 on the label, so the detection of Ti therefore cannot be attributed to intentional addition of the E171 and must reflect soil-derived TiO_2 taken up during plant growth.

8.2.1.2 Intakes in New Zealanders

The estimated total dietary Ti intakes derived from this food survey, approximately 500 – 750 µg/day across all age and gender groups ≥11 yrs fall toward the lower end of values reported internationally (**Table 4.1**). This relatively modest exposure is documented by the low concentrations of E171 in the surveyed foods. The contribution profile (**Table 4.12**, **Figure 4.3**) reveals that more than half (56%) of total dietary Ti arises from just two broad food groups, high-protein foods (28%, predominantly fresh meat, poultry, fish, and eggs) and grain and cereal-based products (28%, mainly bread, breakfast cereals, rice, and pasta). The remaining exposure is distributed almost evenly across vegetables, fungi, dairy products, and fruits (≈11–12% each). This pattern diverges markedly from pre-ban European and North American assessments, in which confectionery, chewing gum, cakes/pastries, and white sauces collectively contributed 50–80% of total Ti intake due to heavy reliance on E171 as a whitener (Sprong et al., 2016; Weir et al., 2012; Younes et al., 2021). The present distribution, therefore, reflects the underlying natural background sources discussed earlier: soil-to-plant transfer in cereals and vegetables, animal tissue accumulation in meat and dairy, and concentration effects in dried fruits and tea.

8.2.1.3 Relationship to other trace elements

A secondary finding of this study was that natural concentrations of Ti in foods and baseline dietary intakes of Ti were about halfway between those of Cr (at the low end) and Zn (at the high end). Ti and Cr seem to show a particularly strong correlation, which could be the subject of future research. The existence of such relationships further supports the conclusion that the dietary survey results were likely to reflect natural Ti rather than predominantly anthropogenic inputs.

Three important points arise from this study:

1) Due to the lower-than-expected prevalence of E171 as a food additive, the findings across all 43 food composites showed that only one product contained added Ti. This indicates that, in the absence of E171, dietary Ti exposure in the NZ population is likely to be minimal. Apart from Composite 29, which contained added Ti in one item (mochi-style coconut ice-cream), this leaves a persistent baseline exposure of ~500–750 µg/day. Most of this presumably derives from natural sources, though in some foods a contribution from agricultural sources or commercial processing cannot be ruled out.

2) Populations consuming diets rich in whole grains, legumes, leafy vegetables, tea, and meats (often considered healthy dietary patterns) may also receive higher natural Ti intakes than those consuming highly processed, formerly E171-containing foods. However, intakes for both

groups are relatively low, and routine use of even one food containing E171 is sufficient to increase those substantially (see **Section 8.2.2**)

3) The virtual absence of E171 simplifies interpretation but does not eliminate all sources of incidental anthropogenic Ti (e.g., processing equipment wear, phosphate supplements in animal feed, or nano-TiO_2 in agricultural amendments). The intake estimates should therefore be regarded as a practical minimum baseline rather than an absolute natural-only value.

In conclusion, this food survey offers a timely snapshot of dietary Ti exposure where E171 remains legally authorised under the Australia New Zealand Food Standards Code (FSANZ, 2022), unlike the EU, where E171 has been banned since August 2022 (Regulation (EU) 2022/63). The estimated mean intake of approximately 500–750 µg/day (0.5–0.75 mg/day) across adolescents and adults is markedly lower than historical pre-ban European estimates, and even below recent North American figures (**Section 8.2**). This low exposure level, derived from over 43 food composites, could be seen to represent a “permitted but potentially declining" E171 landscape, where the near absence of the additive suggests industry’s proactive changes rather than regulatory enforcement. In NZ, where FSANZ reaffirmed E171's safety in 2022 based on no genotoxicity concerns at typical exposures (FSANZ, 2022), this small detected amount may thus signal a *de facto* reduction in usage.

8.2.2 Levels of E171 in food suspected to contain E171 and its estimated habitual exposure in NZ population

In parallel with the estimation of E171 exposure from the nationally representative total diet survey (**Chapter 4**), a targeted sample of 180 individual retail food items was deliberately selected based on:

I. explicit declaration of E171 (INS 171/TiO_2) on the ingredient list,

II. historical or literature-based evidence of frequent E171 use in that product category, or

III. visual appearance strongly suggestive of TiO_2 whitening.

Among the products analysed, professional and retail food colourings, particularly white and super-white gels, exhibited by far the highest E171 concentrations in this study, reaching 239000 mg/kg (23.9% w/w) in a gel colour labelled “Super White” and 44740 mg/kg even in a neon-orange variant that uses TiO_2 as an opacifying base (**Table 5.3**, **Appendix 5.2**). These values are orders of magnitude above those typically reported in finished consumer foods, placing concentrated food colourings in a unique category. They effectively represent near-pure or minimally diluted E171 suspensions marketed as ingredients rather than ready-to-eat products. Previous studies have also reported a wide range of TiO_2 in decorative applications (Bucher et al., 2024; Clayton-Cuch, 2023; He et al., 2022; Nkenda et al., 2023; Sungur et al., 2020; Verleysen et al., 2022a). Although colourants are used in small quantities

(typically 0.1–2 g/kg of icing or fondant), the extreme starting concentration means that even low addition rates may yield finished decorations containing several thousand mg/kg. Thus, highly decorated celebration cakes, cupcakes, and children's novelty confectionery remain a significant, often overlooked route of very high bolus exposure to TiO_2. For instance, a decorated children's cake containing 500 g of icing at 4000 mg/kg Ti would deliver ≈2000 µg Ti in total. Assuming the cake is divided into 10 slices, each slice would provide about 200 µg Ti, equivalent to roughly half a day of average background intake from the entire diet.

Within the confectionery subgroup (n=125 samples), 36 items (29%) returned non-detectable or background Ti levels (<1 mg/kg). However, the remaining 89 products exhibited a strikingly heavy-tailed distribution, with several globally recognised children's and family-share products containing E171 at concentrations exceeding 1000–2200 mg/kg, levels comparable to or higher than many pre-bans European reports (**Appendix 5.2**). Previous studies have also reported a wide range of TiO_2 in confectionery groups (Abd-ElHamid et al., 2023; Bucher et al., 2024; Cao et al., 2024; Kim et al., 2018; Lim et al., 2018; Liu et al., 2021; Lomer et al., 2000; Reed et al., 2015; Verleysen et al., 2022a; Weir et al., 2012). For instance, a single 45 g bag of M&M's Crispy or a few pieces of Peak gum can deliver 80–100 mg of TiO_2, equivalent to 15–20% of an adult's total weekly background intake in one sitting. In the 53 chocolate-based products analysed, Ti content varied widely, from less than 0.05 mg/kg in some samples to as high as 2076 mg/kg. The highest concentration was found in the M&M's Crispy Share Pack, underscoring the substantial heterogeneity in Ti levels across products. Overall, Ti was detected in 39 of the 53 samples (74%) (**Appendix 5.2**). The presence of several hundred mg/kg of E171 in mainstream snack bars (Strawberry flavoured thick shake bar; manufacturer redacted) is particularly noteworthy, as these items are marketed as lunchbox-friendly options and are regularly consumed by school-aged children in NZ and Australia. Unlike cakes or icing, these items are retained in the mouth for prolonged periods, which increases oral mucosal contact and potential for direct translocation across buccal tissues or inadvertent swallowing of the snack bar.

Although the primary focus of this survey was dietary Ti exposure, the inclusion of personal care products (toothpaste) (**Table 5.3, Appendix 5.2**) provides a valuable context for total (dietary + oral) exposure. The results reveal that toothpastes remain one of the most concentrated intentional sources of E171 in everyday consumer products, with TiO_2 equivalents ranging from undetectable (<0.69 mg/kg) in a children's gel formulation to 6349 mg/kg (0.63% w/w) in Macleans Protect Freshmint. Seven of the ten samples contained moderate-to-high E171, confirming that TiO_2 is still routinely used as a whitening and opacifying agent in mainstream adult dentifrices sold in NZ in 2024–2025. The mean level of E171 in the highest toothpaste (6349 mg/kg) is 2–3 times higher than the most concentrated confectionery or icing products analysed in this study and 50–100 times higher than

typical residual E171 in coated chocolates. Toothpaste, therefore, represents the single most intense daily point source of TiO_2 for the NZ population. Unlike dietary TiO_2, which is dispersed within food matrices and undergoes gastrointestinal dilution with very low absorption (<0.1–1%), toothpaste presents a different exposure pathway. Applied directly to the oral mucosa twice daily and retained for 1–2 min, it allows potential interaction and limited absorption across the oral mucosa before swallowing. In addition, a fraction of the toothpaste (estimated 5–20% of the loaded amount, or 2–20 mg per brushing) is inadvertently ingested (EFSA, 2016, 2019), delivering a concentrated bolus into the upper gastrointestinal tract. This differs from dietary intake because the exposure occurs outside the protective context of food matrices, salivary dilution, gastric processing, and microbiome modulation, resulting in a more direct and potentially higher local dose. Using conservative swallowing estimates (5 mg toothpaste per brushing, 10% swallowed, twice daily), regular use of a 3,000 mg/kg toothpaste delivers ≈0.6 mg TiO_2 per day, comparable to or exceeding the entire mean dietary intake (0.5–0.75 mg/day) identified in this composite food survey (**Chapter 4**). For users of the highest-concentration product (6349 mg/kg), the swallowed intake from toothpaste alone approaches 1.3 mg/day. In summary, toothpastes also represent a significant source of bioaccessible TiO_2.

The representative composite survey (**Chapter 4**) established a consistent background dietary Ti intake of approximately 500–750 µg/day (0.5–0.75 mg/day) for New Zealanders aged ≥11 years, attributable to natural and incidental environmental sources. However, the targeted analysis of 180 items (**Chapter 5**) revealed that some products deliver E171 at concentrations of several hundred to several thousand mg/kg. When these residual products are habitually consumed, even in moderate amounts, they can raise the natural baseline and exceed higher exposure levels. For instance, eating two 130 g share-packs per week of a coated chocolate sweet containing 1231 mg/kg E171 (a value typical of several M&M's and similar products) receives an additional 320 mg Ti per week, equivalent to 45.7 mg/day when averaged over the week. Adding this to the baseline ~0.6 mg/day increases total intake by a factor of ~76 (from 0.6–46.3 mg/day). An adolescent (15 years, 60 kg-bw) who chews one pack (14 g) weekly of Peak gum containing 2223 mg/kg E171 may ingest an extra 4.4 mg Ti/day. A preschooler (4 yrs, 16 kg-bw) allowed one 45 g bag of residual E171-coated chocolate (1500 mg/kg) three times per week receives an additional 202 mg Ti/week or ~29 mg/day on average, pushing total intake to approximately 2.5 mg/kg-bw/day (4.2 mg/kg-bw per day expressed as TiO_2). This is 30–50 times the natural background for that age group, as concluded from adult data.

Interestingly, among the products analysed, E171 was detected in 38 (21.1%). Of the 42 products labelled as containing E171, 35 tested positive, while seven did not, and three unlabelled products contained E171. These differences are best explained by industry reformulation without updated packaging, rather than trace-level use or analytical error. Using outdated labels poses minimal

regulatory risk, whereas undeclared use presents a higher compliance concern, consistent with the small number of unlabelled positives observed. Overall, the findings demonstrate broader industry trends following EFSA's 2021–2022 safety concerns and subsequent EU bans, with manufacturers increasingly reformulating to eliminate E171 ahead of packaging updates.

8.2.3 Evaluation of cell viability, cytotoxicity, and morphological changes following exposure to TiO_2

In **Chapter 6**, physicochemical characterisation, optimisation of OA-induced steatosis, and assessment of cytotoxicity and morphological effects of E171 and P21 were performed. Comprehensive analyses revealed that E171 consisted of aggregated particles with heterogeneous sizes and morphologies, with less than 35% in the nanoscale range (<100 nm), whereas P21 displayed a higher proportion of ultrafine particles (88% <21 nm). All E171 samples were phase-pure anatase, and P21 was rutile; both materials exhibited high chemical purity. Pronounced agglomeration was observed in both aqueous and culture media, with particle sizes substantially exceeding their primary dimensions (for details, see **Chapter 6**).

Notably, the PDI data provided insight into the dispersion behaviour of TiO_2 under different conditions. While values below 0.3 are often interpreted as indicating narrow size distributions, these results highlight the need for caution in interpretation. Because DLS is intensity-weighted, the PDI is inherently biased toward larger particles and agglomerates, meaning that apparently uniform distributions may still conceal significant nanoscale heterogeneity. The values obtained for E171 and P21 in DI water (0.24–0.30) fall within the range reported in previous studies, yet the variability across the literature (Dorier et al., 2019; Kunc et al., 2025; Talbot et al., 2018) underscores the sensitivity of PDI measurements to differences in dispersion protocols and particle handling. The increase in PDI observed in complete cell culture medium (DMEM + 10% FBS) illustrates the influence of biological environments on particle behaviour. Values exceeding 0.5 indicate broad, heterogeneous size distributions, consistent with uncontrolled agglomeration driven by higher ionic strength and protein adsorption. This variability is toxicologically relevant, as it affects particle sedimentation, diffusion, and cellular interactions, thereby influencing the effective concentration delivered *in vitro*. The higher PDI values observed in this study compared with those reported in other media (e.g., MEM, HEPES saline, RPMI, Williams medium) emphasise that dispersion stability is highly medium-dependent (Bischoff et al., 2025; Herrera-Rodríguez et al., 2023; Kunc et al., 2025; Lankoff et al., 2012; Uribe-García et al., 2025). Differences in ionic composition, buffering capacity, and protein content can either stabilise or destabilise suspensions, leading to divergent outcomes across studies. These findings reinforce the need to interpret PDI in conjunction with hydrodynamic size, zeta potential, and medium composition.

These results demonstrate that TiO_2 particles are highly susceptible to agglomeration in complex biological environments, and this instability must be accounted for when extrapolating *in vitro* results.

The OA-induced HepG2 model provided a reproducible and physiologically relevant system for TiO_2 exposure studies. Dose-dependent lipid accumulation with preserved viability confirmed OA as a non-lethal inducer of steatosis, with 0.25 mM selected as a moderate inducer (Girish & John, 2025; Krahmer et al., 2025). Morphological alterations in TiO_2-exposed HepG2 cells were consistent with cytotoxic characteristics such as shrinkage, nuclear condensation, apoptosis, and micronucleus formation (Abbasi-Oshaghi et al., 2019; Li et al., 2020; Sha et al., 2011; Shukla et al., 2013; Xia et al., 2018). Importantly, damage was also evident in steatotic cells, suggesting lipid accumulation exacerbates susceptibility rather than mitigating toxicity. Haemocytometry and NRU assays showed no significant cytotoxicity in non-steatotic cells, supporting the view that TiO_2 is inert under basal conditions. In steatotic cells, however, higher concentrations of E171 or P21 reduced viability, with E171 showing dose-dependent effects (Jalili et al., 2018; Kirkland et al., 2024; Kunc et al., 2025). Cellular uptake studies revealed that E171 was more readily internalised under non-steatotic conditions. By contrast, P21 uptake was significantly enhanced in steatotic cells, likely reflecting altered membrane composition and trafficking in lipid-loaded hepatocytes (Sunshine & Iruela-Arispe, 2017).

The effects of TiO_2 on cytotoxicity, cellular uptake, and its role in inducing steatosis and oxidative stress in HepG2 cells are summarised in **Table 8.1**.

Table 8.1 Summary of parameters measured in HepG2 cells under steatotic (+OA) and non-steatotic (-OA) conditions, showing the observed effects of E171 and P21.

"Yes" denotes a significant effect under the specified condition, whereas "No" indicates no effect. The arrows indicate direction: ↑ suggests an increase in the impact, while ↓ indicates a decrease.

Parameters measured	Effect of E171		Effect of P21	
	Steatotic (+OA)	Non-steatotic (-OA)	Steatotic (+OA)	Non-steatotic (-OA)
Cell viability	Yes (↓)	No	Yes (↓)	No
Cytotoxicity by neutral red uptake assay	Yes (↑)	No	No	No
Cellular uptake	No	Yes (↑)	Yes (↑)	No
Lipid accumulation via ORO	No	No	No	No
Levels of triglycerides	Yes (↑)	No	Yes (↑)	No
Levels of TCHO	No	No	No	No
Levels of ROS	Yes (↑)	No	Yes (↑)	No
Levels of NO	Yes (↑)	No	No	No
Levels of TAC	No	No	No	No
Levels of MDA	No	No	No	No

8.2.4 Role of TiO_2 in promoting hepatic lipid accumulation and oxidative stress

In this study, the role of TiO_2 in hepatic lipid accumulation and oxidative stress under different metabolic states in HepG2 cells was investigated. The summary **Table 8.1** highlights the differential effects of E171 and P21 in steatotic versus non-steatotic HepG2 cells. E171 exerted greater cytotoxicity under steatotic conditions, reducing viability and neutral red uptake, while elevating triglyceride, ROS, and NO levels. In contrast, P21 showed comparatively lower toxicity, with uptake enhanced in steatotic cells but without measurable effects on viability in non-steatotic cells. Both materials failed to alter lipid accumulation, cholesterol, antioxidant capacity, or MDA levels, indicating that their primary impact lies in modulating cell viability, oxidative stress, and triglyceride metabolism in metabolically stressed hepatocytes.

The absence of significant changes in lipid droplet accumulation by ORO staining suggests that neither E171 nor P21 directly drives steatosis in HepG2 cells, regardless of OA treatment. However, the biochemical assays revealed a more subtle effect. Under steatotic conditions, both E171 and P21 induced a modest but measurable increase in triglyceride levels at higher concentrations, whereas cholesterol metabolism remained unaffected. Although ORO staining is widely used to visualise neutral lipid droplets, it is a relatively blunt tool. Even when quantified spectrophotometrically, ORO primarily reflects bulk droplet accumulation and cannot resolve subtle changes in specific lipid fractions (Feldhaus & Piskobulu, 2024). In contrast, biochemical assays provide more sensitive and targeted measurements of triglycerides and cholesterol. This discrepancy between staining and biochemical quantification highlights the importance of using complementary methods, as lipid droplet accumulation may mask selective perturbations in specific lipid fractions. In MASLD, triglycerides drive hepatic steatosis by accumulating in lipid droplets, while cholesterol dysregulation contributes to lipotoxicity, and progression toward inflammation, liver injury, and fibrosis (Iturbe-Rey et al., 2025; Krahmer et al., 2025). The selective elevation of triglycerides without parallel changes in cholesterol points to a targeted disruption of lipid homeostasis, consistent with previous reports that TiO_2 exposure can alter triacylglycerol and diacylglycerol metabolism *in vitro* and *in vivo*. For example, Zhang et al. (2021) observed only non-significant elevations of triglycerides and cholesterol in HepG2 cells at low-dose TiO_2 exposure, while Chen et al. (2019) reported steatosis in rat hepatocytes following TiO_2 exposure. Yu et al. (2025) further demonstrated significant up-regulation of specific TAG and DAG species in rat liver, accompanied by altered DAG transport. Similarly, metabolomic studies in BEAS-2B cells (Zhang et al., 2022) and dietary exposure in mice (Perez et al., 2021) revealed changes in lipid metabolic pathways and circulating TAG levels, whereas intravenous administration in rats produced increases in LDL cholesterol without significant effects on TAG (Su et al., 2018). Taken together, these findings suggest that TiO_2 can perturb lipid metabolism across both *in vitro* and *in vivo* systems.

In summary, while E171 and P21 did not significantly drive lipid droplet formation or cholesterol storage in HepG2 cells, a subtle, steatosis-dependent elevation of triglycerides was detected at higher doses. These findings contribute to evidence that TiO_2 can interfere with lipid metabolic pathways in a context-specific manner, with triglyceride homeostasis appearing more vulnerable than cholesterol homeostasis under conditions of pre-existing metabolic stress. This highlights the importance of distinguishing between triglyceride storage (a marker of steatosis) and cholesterol dysregulation (a driver of progression) (Hagström et al., 2024; Syed-Abdul, 2023).

The present study demonstrates a clear contrast in the oxidative stress response of HepG2 hepatocytes to TiO_2, depending on the cells' metabolic state. In non-steatotic HepG2 cells, neither form of TiO_2 induced measurable ROS production across a wide concentration range (0–50 µg/mL), confirming the relative inertness of TiO_2 particles in metabolically competent liver cells under basal conditions. This finding is entirely consistent with a previous finding using the same cell line and H_2DCFDA methodology (Kunc et al., 2025) and reinforces the growing consensus that short-term, cytotoxic exposures to TiO_2 do not trigger oxidative stress in healthy hepatic models. Such observations align with the broader toxicological profile of TiO_2, which has historically been classified as poorly soluble, low-toxicity particulate matter by regulatory agencies (Younes et al., 2021). In contrast, steatotic HepG2 cells, induced here by OA loading, exhibited dose-dependent ROS elevation when treated with either E171 or P21, reaching statistical significance at 50 µg/mL. This indicated that pre-existing lipid accumulation can act as a decisive susceptibility factor for TiO_2-induced oxidative stress in human hepatocytes. The result aligns with emerging evidence that metabolic dysfunction may alter particle-cell interactions. Excess intracellular lipids are known to impair mitochondrial function, deplete glutathione pools, and shift redox homeostasis toward a pro-oxidant state (Awashra & Młynarz, 2023; Sukhorukov & Orekhov, 2024).

The absence of NO induction in both non-steatotic and steatotic HepG2 cells following 48 h exposure to TiO_2 (E171 or P21) at concentrations up to 50 µg/mL represents a notable finding that merits careful consideration. Nitric oxide, produced primarily by inducible iNOS in response to pro-inflammatory stimuli, is a key effector and signalling molecule in particle-induced liver inflammation (Jin et al., 2023; Kamboj et al., 2024; Sharma et al., 2007). Several *in vivo* rodent studies have consistently reported marked upregulation of hepatic iNOS expression and elevated NO metabolites (nitrite/nitrate) after oral or systemic administration of TiO_2, typically at cumulative doses orders of magnitude higher than those achievable *via* dietary exposure (**Appendix 2.1**). These effects are frequently accompanied by histological inflammatory infiltrates, NF-κB activation, and elevations in circulating pro-inflammatory cytokines, supporting a classical particle-driven inflammatory cascade in the intact liver (e.g., 10–200 mg/kg body weight daily for weeks (Abbasi-Oshaghi et al., 2019; Grissa et al., 2020). However, *in vitro*

evidence for direct NO induction in hepatocytes by TiO_2 is far less consistent. The only positive report in HepG2 cells comes from Shajari et al. (2021), who observed increased NO after prolonged culture (multiple passages) in the continuous presence of relatively high concentrations of TiO_2 NPs (250 mg/kg). Several biological and methodological factors likely explain this apparent *in vitro–in vivo* contradiction. First, hepatic NO production during TiO_2 challenge *in vivo* is predominantly driven by Kupffer cells (resident liver macrophages) rather than hepatocytes themselves (Maeda et al., 2022; Shiratori et al., 1998). The HepG2 model, being a pure hepatocytic line devoid of immune-competent cells, inherently lacks macrophage–hepatocyte crosstalk that amplifies iNOS expression *via* paracrine cytokine networks (TNF-α, IL-1β, IFN-γ) ((Maeda et al., 2022; Russwurm et al., 2002). Second, iNOS is a highly inducible enzyme that requires sustained transcriptional activation (Farahani et al., 2025); the transient 24-48 h exposure window used in most *in vitro* studies may be insufficient to trigger measurable NO output even if slight signalling events are initiated. Third, the doses used in many positive *in vivo* studies produce liver Ti burdens (hundreds of µg/g tissue) that far exceed those reported in human autopsy samples after lifelong dietary exposure (Heringa et al., 2018), raising questions about human relevance.

The absence of lipid peroxidation, as measured by MDA levels in both non-steatotic and steatotic HepG2 cells exposed to E171 or P21, despite clear ROS elevation in the steatotic model, represents an important dissociation between early oxidative stress and downstream macromolecular damage. This finding is consistent with the unchanged total antioxidant capacity observed in the same experiments and, collectively, indicates that the magnitude and/or duration of ROS generation were insufficient to initiate cellular repair and antioxidant defence within the 48-h timeframe. ROS induction is a sensitive but non-specific endpoint, whereas lipid peroxidation requires a higher threshold of sustained oxidative insult (Ayala et al., 2014; Zheng et al., 2024). Several factors likely contributed to the lack of MDA accumulation in this study. First, HepG2 cells retain substantial expression of antioxidant enzymes (SOD, catalase, GPx) and phase II systems (GST, Nrf2-regulated genes) even after oleic/palmitic acid-induced steatosis (Bołdys et al., 2024; García-Pérez et al., 2021). These defences appear capable of neutralising the modest, dose-dependent ROS increase elicited by TiO_2 at ≤50 µg/mL. Second, the primary ROS species under cell culture conditions are often superoxide and hydroxyl radicals (Manke et al., 2013; Skipitari et al., 2023), which have relatively short half-lives and limited susceptibility to initiate chain-propagating lipid peroxidation. Third, the polyunsaturated fatty acid content of cellular membranes in steatotic HepG2 cells, while increased, may remain lower than in primary hepatocytes or *in vivo* MASLD liver, potentially reducing the availability of substrate for propagation of lipid peroxidation (Teixeira et al., 2023).

Studies reporting hepatic MDA elevation typically employed repeated high-doses (50–1200 mg/kg/day for weeks to months), reviewed by Khan et al. (2024) that produce cumulative liver Ti burdens 10–100-fold higher than those documented in human autopsy livers from high-exposure populations (Heringa et al., 2018). Chronic dosing also triggers secondary inflammatory cascades involving Kupffer cell-derived cytokines and sustained iNOS activity, generating peroxynitrite and other potent initiators of lipid peroxidation that are absent in monoculture hepatocyte models (Abbasi-Oshaghi et al., 2019; Ayala et al., 2014). Thus, the *in vivo* MDA signal is frequently a downstream consequence of prolonged inflammation rather than a direct reflection of TiO_2-induced ROS.

Overall, findings from this study contribute to the growing understanding that TiO_2 toxicity is highly context-dependent, shaped by both physicochemical properties and the metabolic state of the exposed cells. The study demonstrates that while TiO_2 (E171 and P21) exerts minimal effects in healthy, non-steatotic hepatocytes, its impact becomes more pronounced under conditions of lipid overload, where steatotic cells show increased susceptibility to oxidative stress, modest triglyceride dysregulation, and reduced viability. This context-specific vulnerability reflects the pathophysiological environment of MASLD, suggesting that individuals with pre-existing metabolic stress may be disproportionately affected by TiO_2 exposure. Notably, the selective influence on triglycerides rather than cholesterol, the modest ROS increases without progression to lipid peroxidation, and the absence of NO activation under controlled conditions all highlight that TiO_2 effects are indirect and multifactorial. These insights highlight the need to evaluate TiO_2 safety not only in standard cell models but also in metabolically compromised systems, as such conditions reveal hidden susceptibilities that are highly relevant to real-world populations.

8.3 Future directions and limitations

This study reports the results of screening 43 food composites and 180 individual food products available on the NZ market. All samples were digested and analysed using graphite furnace atomic absorption spectroscopy (GFAAS) to assess the presence of TiO_2 and quantify its total content where detected. The dataset provides a unique and novel contribution, offering real-world evidence of the occurrence and use levels of the food additive E171 in NZ products. To our knowledge, this is the first study to generate experimental data for estimating actual dietary exposure to E171 in the NZ population. Nevertheless, several limitations were observed. The study was restricted to a finite sample size, which may not fully capture the diversity of the national food supply. While sensitive, reliance on GFAAS may yield detection limits that underestimate trace-level TiO_2 concentrations compared to more advanced techniques such as ICP-MS. However, the latter's sensitivity is matrix dependent. GFAAS measures total Ti after digestion, so (like conventional ICP-MS), it cannot distinguish between nano-sized TiO_2 (the form of regulatory concern in the EU), micro-sized TiO_2, and naturally

occurring Ti or Ti from contamination. Additionally, the sampling was cross-sectional, reflecting a single time point, and therefore may not account for ongoing reformulation trends or seasonal variations in product availability. Some Ti in food can come from natural sources (soil, minerals) or contamination, not just the intentional additive E171. Without complementary techniques (e.g., SEM-EDX, spICP-MS, or electron microscopy), it is not possible to confirm that the detected Ti is from E171 as an additive. Moreover, many foods in NZ are imported (mainly from Australia, the EU, and Asia). The presence/absence of E171 may reflect the regulations of the country of manufacture more than NZ-specific use.

To refine exposure assessments for the NZ population, a repeat survey, ideally in approximately 10 years (e.g., 2034–2035), would allow direct comparison with the current dataset. This would establish whether the prevalence and concentration of E171 in foodstuffs have declined in response to international regulatory pressure and voluntary phase-out by manufacturers, especially in high-exposure categories such as confectionery, chewing gum, and sauces. Moreover, current exposure estimates rely on general food consumption surveys. Targeted investigations focusing on products confirmed to contain E171 are needed to identify population subgroups with habitual high intake (e.g., children and adolescents who frequently consume sweets and chewing gum). Such data would significantly improve the accuracy of high-percentile exposure estimates. A substantial proportion of E171 in chewing gum and most toothpastes is not swallowed. Experimental studies determining the bioaccessible/ingested fraction under realistic use conditions would allow more accurate inclusion or exclusion of these sources in dietary exposure assessments and better contextualisation against natural background Ti intake from food. Furthermore, many widely prescribed solid-dose pharmaceuticals (e.g., perindopril, atorvastatin, metformin, and certain supplements) use E171 as a coating or opacifier (Hancock et al., 2024). Systematic screening of the most dispensed tablet/capsule medications in NZ, combined with typical daily dosing regimens, would clarify whether chronic pharmaceutical exposure represents a significant additional source of E171, particularly for older adults and patients with cardiovascular or metabolic conditions.

New Zealand's multicultural population, with diverse dietary patterns, underscores the need for an ethnicity-stratified national survey of TiO_2-containing products to better assess subgroup-specific exposures and protect vulnerable communities. Diabetes, obesity, and liver cancer are disproportionately higher among Māori and Pacific people (Health New Zealand, 2023), placing them at greater risk of MASLD and related outcomes.

Addressing these knowledge gaps would further strengthen the evidence base for future risk-management decisions in NZ and provide a more complete picture of total E171 exposure across the lifespan and across different exposure routes.

The second section of this study demonstrates that TiO_2 properties, including crystalline phase, size distribution, zeta potential, and dispersion behaviour, play a critical role in determining cellular uptake and toxicity. E171 and P21 exhibited distinct patterns of interaction with HepG2 cells, indicating that the two forms can exert different biological effects. These differences may arise from any of the physicochemical factors noted above, each of which influences how particles are internalised and how they trigger intracellular stress responses. Importantly, this variability highlights the limitations of extrapolating from rodent studies alone when assessing human risk. Rodent models often fail to capture the complexity of human metabolic states and particle–cell interactions, meaning that *in vitro* systems such as HepG2 steatotic models provide complementary insight into human-relevant outcomes.

Although the present study offers significant insight into the context-dependent oxidative stress elicited by TiO_2 in human hepatocytes, several important limitations must be considered when placing these findings in the broader toxicological landscape. The reliance on a 2D monoculture of HepG2 cells, while convenient and human-relevant, inherently excludes the immune-competent compartment, particularly Kupffer cells, which drive much of the nitric oxide production and sustained lipid peroxidation observed *in vivo* after TiO_2 exposure. The consistently negative NO and MDA results in this study almost certainly reflect the absence of macrophage–hepatocyte crosstalk rather than a complete lack of TiO_2's inflammatory potential. Furthermore, the acute 48-hour exposure protocol and moderate concentration range (≤50 µg/mL) do not capture the chronic, low-dose, repeated ingestion scenario that characterises lifelong dietary exposure to food-grade TiO_2. Many of the positive *in vivo* findings that we contrast against employed cumulative doses orders of magnitude higher and over weeks to months, conditions under which secondary inflammation and progressive antioxidant depletion readily translate transient ROS into measurable macromolecular damage. The OA-induced steatosis model, although effective in sensitising cells to ROS, remains a simplified early-stage MASLD phenotype and lacks the systemic insulin resistance, advanced fibrosis, and chronic inflammatory setting present in patients with MASH or cirrhosis.

Looking forward, future research should expand to chronic, low-dose exposure models that better mimic real-world scenarios, and incorporate advanced liver systems such as 3D spheroids, organoids, or co-cultures with Kupffer and stellate cells to capture the complexity of hepatic responses (Caddeo et al., 2024; Ma et al., 2023). Mechanistic studies focusing on ROS generation, mitochondrial dysfunction, ER stress, and inflammatory signalling would provide greater clarity on how TiO_2 interacts with metabolically compromised hepatocytes. Extending investigations to other metabolic states, such as insulin resistance or fibrosis, would broaden the relevance to MASLD progression. *In vivo* validation using animal models of steatosis (diet-induced rodent models high-fat diet, Western diet, high-fructose

diet) (Cui et al., 2025; Fu et al., 2024) could bridge the gap between *in vitro* findings and human risk assessment. Validation in diet-induced MASLD or MASH animal models using human-relevant oral doses, coupled with accurate measurement of hepatic Ti burdens, will be important to bridge the *in vitro–in vivo* gap. Finally, integrating high-content omics approaches with functional endpoints (mitochondrial respiration, DNA damage, cytokine profiling) and, ultimately, human biomonitoring studies correlating liver Ti accumulation with metabolic liver disease severity will be required to determine whether food-grade TiO_2 truly represents a variable co-factor in MASLD pathogenesis in susceptible populations.

In conclusion, while this study convincingly demonstrates that metabolic status is a main susceptibility factor for TiO_2-induced oxidative stress in human hepatocytes, the absence of downstream lipid peroxidation pathways under acute conditions should not be interpreted as proof of safety in chronic or immunocompetent settings. Only by moving toward more physiologically relevant, long-term, and multicellular models will we be able to definitively assess whether dietary TiO_2 represents a meaningful co-factor in the progression of metabolic liver disease in susceptible individuals.

References

Abbasi-Oshaghi, E., Mirzaei, F., & Pourjafar, M. (2019). NLRP3 inflammasome, oxidative stress, and apoptosis induced in the intestine and liver of rats treated with titanium dioxide nanoparticles: in vivo and in vitro study. *International journal of nanomedicine*, *14*, 1919.

Abd-Elhakim, Y. M., Hashem, M. M. M., Abo-El-Sooud, K., Mousa, M. R., Soliman, A. M., Mouneir, S. M., Ismail, S. H., Hassan, B. A., & El-Nour, H. H. M. (2023). Interactive effects of cadmium and titanium dioxide nanoparticles on hepatic tissue in rats: Ameliorative role of coenzyme 10 via modulation of the NF-κB and TNFα pathway. *Food Chem Toxicol*, *182*, 114191. https://doi.org/10.1016/j.fct.2023.114191

Abd-ElHamid, G. H., El-Darder, O. M., Ibrahim, A. K., Abdel-Salam, R. A., Hadad, G., Abdelshakour, M. A., & Abdel Hameed, E. A. (2023). A Novel Approach for the Analysis of Titanium Dioxide Content by Simple Digestion System in Foodstuffs from the Egyptian Market Using ICP-OES and ICP-MS. *Records of Pharmaceutical and Biomedical Sciences*, *7*(1), 1-9.

Abdel-Wahhab, M. A., El-Nekeety, A. A., Mohammed, H. E., El-Messery, T. M., Roby, M. H., Abdel-Aziem, S. H., & Hassan, N. S. (2021b). Synthesis of encapsulated fish oil using whey protein isolate to prevent the oxidative damage and cytotoxicity of titanium dioxide nanoparticles in rats. *Heliyon*, *7*(11), e08456.

Abdel-Wahhab, M. A., El-Nekeety, A. A., Mohammed, H. E., Elshafey, O. I., Abdel-Aziem, S. H., & Hassan, N. S. (2021a). Elimination of oxidative stress and genotoxicity of biosynthesized titanium dioxide nanoparticles in rats via supplementation with whey protein-coated thyme essential oil. *Environmental Science and Pollution Research*, *28*(41), 57640-57656. https://doi.org/10.1007/s11356-021-14723-7

Acar, M., Bulut, Z., Ateş, A., Nami, B., Koçak, N., & Yıldız, B. (2015). Titanium dioxide nanoparticles induce cytotoxicity and reduce mitotic index in human amniotic fluid-derived cells. *Human & Experimental Toxicology*, *34*(1), 74-82.

Adams, L. A., Roberts, S. K., Strasser, S. I., Mahady, S. E., Powell, E., Estes, C., Razavi, H., & George, J. (2020). Nonalcoholic fatty liver disease burden: Australia, 2019-2030. *J Gastroenterol Hepatol*, *35*(9), 1628-1635. https://doi.org/10.1111/jgh.15009

Additives, E. P. o. F., & Food, N. S. a. t. (2016). Re-evaluation of titanium dioxide (E 171) as a food additive. *Efsa Journal*, *14*(9), e04545.

Adelantado, C., Ríos, Á., & Zougagh, M. (2020). A new nanometrological strategy for titanium dioxide nanoparticles screening and confirmation in personal care products by CE-spICP-MS. *Talanta*, *219*, 121385.

Ali, S. A., Rizk, M. Z., Hamed, M. A., Aboul-Ela, E. I., El-Rigal, N. S., Aly, H. F., & Abdel-Hamid, A. Z. (2019). Assessment of titanium dioxide nanoparticles toxicity via oral exposure in mice: effect of dose and particle size. *Biomarkers*, *24*(5), 492-498. https://doi.org/10.1080/1354750x.2019.1620336

Alshawsh, M. A., Alsalahi, A., Alshehade, S. A., Saghir, S. A. M., Ahmeda, A. F., Al Zarzour, R. H., & Mahmoud, A. M. (2022). A Comparison of the Gene Expression Profiles of Non-Alcoholic Fatty Liver Disease between Animal Models of a High-Fat Diet and Methionine-Choline-Deficient Diet. *MOLECULES*, *27*(3). https://doi.org/10.3390/molecules27030858

Altun, S. K., Paksoy, N., Dinç, H., & Durmaz, H. (2019). Determination of 17 elements in free-range hen eggs with ICP-MS. *Applied Ecology & Environmental Research*, *17*(4).

An, J.-M., Hur, S. H., Kim, H., Lee, J. H., Kim, Y.-K., Sim, K. S., Lee, S.-E., & Kim, H. J. (2024). Determination of the geographical origin of chicken (breast and drumstick) using ICP-OES and ICP-MS: Chemometric analysis. *FOOD CHEMISTRY*, *437*, 137836.

Anderson, R. A., Bryden, N. A., & Polansky, M. M. (1992). Dietary chromium intake: Freely chosen diets, institutional diets, and indidual foods. *Biological Trace Element Research*, *32*(1), 117-121.

Anderson, R. A., Bryden, N. A., & Polansky, M. M. (1993). Dietary intake of calcium, chromium, copper, iron, magnesium, manganese, and zinc: duplicate plate values corrected using derived nutrient intake. *Journal of the American Dietetic Association*, *93*(4), 462-465.

Araya, J., Rodrigo, R., Videla, L. A., Thielemann, L., Orellana, M., Pettinelli, P., & Poniachik, J. (2004). Increase in long-chain polyunsaturated fatty acid n - 6/n - 3 ratio in relation to hepatic steatosis in patients with non-alcoholic fatty liver disease. *Clin Sci (Lond)*, *106*(6), 635-643. https://doi.org/10.1042/cs20030326

Arumugam, M. K., Gopal, T., Kalari Kandy, R. R., Boopathy, L. K., Perumal, S. K., Ganesan, M., Rasineni, K., Donohue Jr, T. M., Osna, N. A., & Kharbanda, K. K. (2023). Mitochondrial dysfunction-associated mechanisms in the development of chronic liver diseases. *Biology*, *12*(10), 1311.

Arzumanian, V. A., Kiseleva, O. I., & Poverennaya, E. V. (2021). The Curious Case of the HepG2 Cell Line: 40 Years of Expertise. *Int J Mol Sci*, *22*(23). https://doi.org/10.3390/ijms222313135

Asfaw, A., & Wibetoe, G. (2004). Freon (CHF3)-assisted atomization for the determination of titanium using ultrasonic slurry sampling–graphite furnace atomic absorption spectrometry (USS–GFAAS): a simple and advantageous method for solid samples. *Analytical and Bioanalytical Chemistry*, *379*(3), 526-531.

Awashra, M., & Młynarz, P. (2023). The toxicity of nanoparticles and their interaction with cells: an in vitro metabolomic perspective. *Nanoscale Advances*, *5*(10), 2674-2723.

Ayala, A., Muñoz, M. F., & Argüelles, S. (2014). Lipid peroxidation: production, metabolism, and signaling mechanisms of malondialdehyde and 4-hydroxy-2-nonenal. *Oxidative Medicine and Cellular Longevity*, *2014*(1), 360438.

Azim, S. A., Darwish, H. A., Rizk, M. Z., Ali, S. A., & Kadry, M. O. (2015). Amelioration of titanium dioxide nanoparticles-induced liver injury in mice: possible role of some antioxidants. *Exp Toxicol Pathol*, *67*(4), 305-314. https://doi.org/10.1016/j.etp.2015.02.001

Bachler, G., von Goetz, N., & Hungerbuhler, K. (2015). Using physiologically based pharmacokinetic (PBPK) modeling for dietary risk assessment of titanium dioxide (TiO_2) nanoparticles. *Nanotoxicology*, *9*(3), 373-380. https://doi.org/10.3109/17435390.2014.940404

Bakour, M., Hammas, N., Laaroussi, H., Ousaaid, D., Fatemi, H. E., Aboulghazi, A., Soulo, N., & Lyoussi, B. (2021). Moroccan bee bread improves biochemical and histological changes of the brain, liver, and kidneys induced by titanium dioxide nanoparticles. *BioMed Research International*, *2021*.

Bakshi, M., Liné, C., Bedolla, D. E., Stein, R. J., Kaegi, R., Sarret, G., Del Real, A. E. P., Castillo-Michel, H., Abhilash, P., & Larue, C. (2019). Assessing the impacts of sewage sludge amendment containing nano-TiO_2 on tomato plants: A life cycle study. *Journal of Hazardous Materials*, *369*, 191-198.

Baranowska-Wójcik, E., Szwajgier, D., & Winiarska-Mieczan, A. (2022). A review of research on the impact of E171/TiO(2) NPs on the digestive tract. *J Trace Elem Med Biol*, *72*, 126988. https://doi.org/10.1016/j.jtemb.2022.126988

Barbero-Becerra, V. J., Giraudi, P. J., Chávez-Tapia, N. C., Uribe, M., Tiribelli, C., & Rosso, N. (2015). The interplay between hepatic stellate cells and hepatocytes in an in vitro model of NASH. *Toxicol In Vitro*, *29*(7), 1753-1758. https://doi.org/10.1016/j.tiv.2015.07.010

Barkhade, T., Mahapatra, S. K., & Banerjee, I. (2021). A protein and membrane integrity study of TiO_2 nanoparticles-induced mitochondrial dysfunction and prevention by iron incorporation. *The Journal of Membrane Biology*, *254*(2), 217-237.

Barreau, F., Tisseyre, C., Menard, S., Ferrand, A., & Carriere, M. (2021). Titanium dioxide particles from the diet: involvement in the genesis of inflammatory bowel diseases and colorectal cancer. *Particle and fibre toxicology*, *18*(1), Article 26. https://doi.org/10.1186/s12989-021-00421-2

Başak, F., Kuşat, T., Ersan, Y., & Kahraman, T. (2025). Titanium dioxide-induced fibrotic liver model and the therapeutic effect of resveratrol by modulation of α-SMA and 8-oHdG expressions, oxidative stress, and inflammation. *Tissue Cell*, *93*, 102748. https://doi.org/10.1016/j.tice.2025.102748

Bastardo-Fernández, I., Chekri, R., Noireaux, J., Givelet, L., Lambeng, N., Delvallée, A., Loeschner, K., Fisicaro, P., & Jitaru, P. (2024). Characterisation of titanium dioxide (nano) particles in foodstuffs and E171 additives by single particle inductively coupled plasma-tandem mass spectrometry using a highly efficient sample introduction system. *Food Additives & Contaminants: Part A*, *41*(8), 867-884.

Bautista-Pérez, R., Cano-Martínez, A., Herrera-Rodríguez, M. A., Ramos-Godinez, M. D. P., Pérez Reyes, O. L., Chirino, Y. I., Rodríguez Serrano, Z. J., & López-Marure, R. (2024). Oral Exposure to Titanium Dioxide E171 and Zinc Oxide Nanoparticles Induces Multi-Organ Damage in Rats: Role of Ceramide. *Int J Mol Sci*, *25*(11). https://doi.org/10.3390/ijms25115881

Begriche, K., Massart, J., Robin, M. A., Bonnet, F., & Fromenty, B. (2013). Mitochondrial adaptations and dysfunctions in nonalcoholic fatty liver disease. *Hepatology*, *58*(4), 1497-1507.

Behzadi, S., Serpooshan, V., Tao, W., Hamaly, M. A., Alkawareek, M. Y., Dreaden, E. C., ... & Mahmoudi, M. (2017). Cellular uptake of nanoparticles: Journey inside the cell. Chemical Society Reviews, 46(14), 4218–4244. https://doi.org/10.1039/C6CS00636A

Bermudez, E., Mangum, J. B., Asgharian, B., Wong, B. A., Reverdy, E. E., Janszen, D. B., Hext, P. M., Warheit, D. B., & Everitt, J. I. (2002). Long-term pulmonary responses of three laboratory rodent species to subchronic inhalation of pigmentary titanium dioxide particles. *Toxicological Sciences*, *70*(1), 86-97.

Bhattacharya, K., Davoren, M., Boertz, J., Schins, R. P., Hoffmann, E., & Dopp, E. (2009). Titanium dioxide nanoparticles induce oxidative stress and DNA-adduct formation but not DNA-breakage in human lung cells. *Particle and Fibre Toxicology, 6*, Article 17. https://doi.org/10.1186/1743-8977-6-17

Bischoff, M., Biriukov, D., Předota, M., Roke, S., & Marchioro, A. (2020). Surface Potential and Interfacial Water Order at the Amorphous TiO2 Nanoparticle/Aqueous Interface. *The Journal of Physical Chemistry C*, *124*(20), 10961-10974. https://doi.org/10.1021/acs.jpcc.0c01158

Bischoff, N. S., Bussi, M. R., Van Breda, S. G., Jolani, S., Sijm, D. T., de Kok, T. M., & Briedé, J. J. (2025). Food-grade titanium dioxide exposure between age groups and in global regions: a systematic review and meta-analysis. *CRITICAL REVIEWS IN FOOD SCIENCE AND NUTRITION*, 1-11.

Bischoff, N. S., de Kok, T. M., Sijm, D. T. H. M., van Breda, S. G., Briedé, J. J., Castenmiller, J. J. M., Opperhuizen, A., Chirino, Y. I., Dirven, H., Gott, D., Houdeau, E., Oomen, A. G., Poulsen, M., Rogler, G., & van Loveren, H. (2021). Possible Adverse Effects of Food Additive E171 (Titanium Dioxide) Related to Particle Specific Human Toxicity, Including the Immune System.

International Journal of Molecular Sciences, *22*(1), 207. https://www.mdpi.com/1422-0067/22/1/207

Blaznik, U., Krušič, S., Hribar, M., Kušar, A., Žmitek, K., & Pravst, I. (2021). Use of Food Additive Titanium Dioxide (E171) before the Introduction of Regulatory Restrictions Due to Concern for Genotoxicity. *Foods*, *10*(8). https://doi.org/10.3390/foods10081910

Bockmann, J., Lahl, H., Eckhert, T., & Unterhalt, B. (2000). Blood levels of titanium before and after oral administration of titanium dioxide. *Pharmazie*, *55*(2), 140-143.

Bołdys, A., Bułdak, Ł., Skudrzyk, E., Machnik, G., & Okopień, B. (2024). The impact of glucagon and exenatide on oxidative stress levels and antioxidative enzyme expression in in vitro induced steatosis in HepG2 cell culture. *Endokrynologia Polska*, *75*(4), 419-427.

Boutillier, S., Fourmentin, S., & Laperche, B. (2021). History of titanium dioxide regulation as a food additive: a review. *Environmental Chemistry Letters*, 1-17.

Boutillier, S., Fourmentin, S., & Laperche, B. (2022). History of titanium dioxide regulation as a food additive: a review. *Environmental Chemistry Letters*, *20*(2), 1017-1033. https://doi.org/10.1007/s10311-021-01360-2

Bouzakher-Ghomrasni, N., Taché, O., Leroy, J., Feltin, N., Testard, F., & Chivas-Joly, C. (2021). Dimensional measurement of TiO2 (Nano) particles by SAXS and SEM in powder form. *Talanta*, *234*, 122619. https://doi.org/https://doi.org/10.1016/j.talanta.2021.122619

Boyer, R. R. (2010). Attributes, characteristics, and applications of titanium and its alloys. *JOM*, *62*(5), 21-24. https://doi.org/10.1007/s11837-010-0071-1

Brandão, F., Fernández-Bertólez, N., Rosário, F., Bessa, M. J., Fraga, S., Pásaro, E., Teixeira, J. P., Laffon, B., Valdiglesias, V., & Costa, C. (2020). Genotoxicity of TiO_2 nanoparticles in four different human cell lines (A549, HEPG2, A172 and SH-SY5Y). *Nanomaterials*, *10*(3), 412.

Brandão, F., Fernández-Bertólez, N., Rosário, F., Bessa, M. J., Fraga, S., Pásaro, E., ... & Costa, C. (2020). Genotoxicity of TiO_2 nanoparticles in four different human cell lines (A549, HepG2, A172 and SH-SY5Y). *Nanomaterials, 10*(3), Article 412. https://doi.org/10.3390/nano10030412

Briñas, R., Dessipri, E., Srinivasan, J. R., & Walch, S. (2024). Titanium dioxide. In *97th JECFA – Chemical and Technical Assessment (CTA)*. Food and Agriculture Organization of the United Nations.

Bucher, G., El Hadri, H., Asensio, O., Auger, F., Barrero, J., & Rosec, J.-P. (2024). Large-scale screening of E171 food additive (TiO_2) on the French market from 2018 to 2022: Occurrence and particle size distribution in various food categories. *Food Control*, *155*, 110102.

Buettner, K. M., & Valentine, A. M. (2012). Bioinorganic chemistry of titanium [Review]. *Chemical reviews*, *112*(3), 1863-1881. https://doi.org/10.1021/cr1002886

Caddeo, A., Maurotti, S., Kovooru, L., & Romeo, S. (2024). 3D culture models to study pathophysiology of steatotic liver disease. *Atherosclerosis*, *393*, 117544. https://doi.org/10.1016/j.atherosclerosis.2024.117544

Canli, E. G., Ila, H. B., & Canli, M. (2019). Response of the antioxidant enzymes of rats following oral administration of metal-oxide nanoparticles (Al2O3, CuO, TiO_2). *Environmental Science and Pollution Research*, *26*(1), 938-945.

Cao, Y. N., Yue, S. S., Wang, A. Y., Xu, L., Hu, Y. T., Qiao, X., Wu, T. Y., Ye, M., Wu, Y. C., & Qi, R. (2022). Antrodia cinnamomea and its compound dehydroeburicoic acid attenuate nonalcoholic fatty liver disease by upregulating ALDH2 activity. *J Ethnopharmacol*, *292*, 115146. https://doi.org/10.1016/j.jep.2022.115146

Cao, Y., Long, J., Liu, L., He, T., Jiang, L., Zhao, C., & Li, Z. (2017). A review of endoplasmic reticulum (ER) stress and nanoparticle (NP) exposure. *Life Sciences*, *186*, 33-42.

Cao, Y., Wang, H., Liang, C., Liu, Q., Ou, T., Yong, L., Xiao, X., Sui, H., Jiang, D., & Liu, Z. (2024). Characterization of Food-Additive Titanium Dioxide and Dietary Exposure to Titanium Dioxide Nanoparticles among the Chinese Population. *Nanomaterials*, *14*(17), 1427.

Carli, F., Della Pepa, G., Sabatini, S., Puig, A. V., & Gastaldelli, A. (2024). Lipid metabolism in MASLD and MASH: From mechanism to the clinic. *JHEP Reports*, *6*(12), 101185.

Chakrabarti, S., Goyary, D., Karmakar, S., & Chattopadhyay, P. (2019). Exploration of cytotoxic and genotoxic endpoints following sub-chronic oral exposure to titanium dioxide nanoparticles. *Toxicology and Industrial Health*, *35*(9), 577-592.

Chakravarthy, M. V., Pan, Z., Zhu, Y., Tordjman, K., Schneider, J. G., Coleman, T., Turk, J., & Semenkovich, C. F. (2005). "New" hepatic fat activates PPARα to maintain glucose, lipid, and cholesterol homeostasis. *Cell metabolism*, *1*(5), 309-322.

Chalasani, N., Younossi, Z., Lavine, J. E., Diehl, A. M., Brunt, E. M., Cusi, K., Charlton, M., & Sanyal, A. J. (2012). The diagnosis and management of non-alcoholic fatty liver disease: practice guideline by the American Gastroenterological Association, American Association for the Study of Liver Diseases, and American College of Gastroenterology. *Gastroenterology*, *142*(7), 1592-1609. https://doi.org/10.1053/j.gastro.2012.04.001

Chan, W.-K., Chuah, K.-H., Rajaram, R. B., Lim, L.-L., Ratnasingam, J., & Vethakkan, S. R. (2023). Metabolic dysfunction-associated steatotic liver disease (MASLD): a state-of-the-art review. *Journal of obesity & metabolic syndrome*, *32*(3), 197.

Chandimali, N., Bak, S. G., Park, E. H., Lim, H.-J., Won, Y.-S., Kim, E.-K., Park, S.-I., & Lee, S. J. (2025). Free radicals and their impact on health and antioxidant defenses: a review. *Cell Death Discovery*, *11*(1), 19. https://doi.org/10.1038/s41420-024-02278-8

Chang, H., Li, L., Deng, Y., Song, G., & Wang, Y. (2023). Protective effects of lycopene on TiO(2) nanoparticle-induced damage in the liver of mice. *J Appl Toxicol*, *43*(6), 913-928. https://doi.org/10.1002/jat.4433

Charlton, M., Sreekumar, R., Rasmussen, D., Lindor, K., & Nair, K. S. (2002). Apolipoprotein synthesis in nonalcoholic steatohepatitis. *Hepatology*, *35*(4), 898-904.

Chen, H. W., Su, S. F., Chien, C. T., Lin, W. H., Yu, S. L., Chou, C. C., Chen, J. J. W., & Yang, P. C. (2006). Titanium dioxide nanoparticles induce emphysema-like lung injury in mice [Article]. *FASEB Journal*, *20*(13), E1732-E1741. https://doi.org/10.1096/fj.06-6485fje

Chen, J., Dong, X., Zhao, J., & Tang, G. (2009). In vivo acute toxicity of titanium dioxide nanoparticles to mice after intraperitioneal injection. *J Appl Toxicol*, *29*(4), 330-337. https://doi.org/10.1002/jat.1414

Chen, J., Zhang, J., Cao, J., Xia, Z., & Gan, J. (2016). Inflammatory MAPK and NF-κB signaling pathways differentiated hepatitis potential of two agglomerated titanium dioxide particles. *Journal of Hazardous Materials*, *304*, 370-378.

Chen, Q., Wang, N., Zhu, M., Lu, J., Zhong, H., Xue, X., Guo, S., Li, M., Wei, X., & Tao, Y. (2018). TiO_2 nanoparticles cause mitochondrial dysfunction, activate inflammatory responses, and attenuate phagocytosis in macrophages: A proteomic and metabolomic insight. *Redox Biology*, *15*, 266-276.

Chen, X. X., Cheng, B., Yang, Y. X., Cao, A., Liu, J. H., Du, L. J., Liu, Y., Zhao, Y., & Wang, H. (2013). Characterization and preliminary toxicity assay of nano-titanium dioxide additive in sugar-coated chewing gum. *Small*, *9*(9-10), 1765-1774.

Chen, X., & Mao, S. S. (2007). Titanium dioxide nanomaterials: synthesis, properties, modifications, and applications. *Chemical reviews*, *107*(7), 2891-2959.

Chen, Y., Lei, K., Liu, Y., Liu, J., Wei, K., Guo, J., & Su, Z. (2025). Metabolic Dysfunction-Associated Steatotic Liver Disease: From a Very Low-Density Lipoprotein Perspective. *Biomolecules*, *15*(7). https://doi.org/10.3390/biom15070990

Chen, Z. J., Han, S., Zhou, S. P., Feng, H. M., Liu, Y., & Jia, G. (2020). Review article Review of health safety aspects of titanium dioxide nanoparticles in food application. *NanoImpact*, *18*, Article 100224. https://doi.org/10.1016/j.impact.2020.100224

Chen, Z. J., Zheng, P., Han, S., Zhang, J. H., Li, Z. J., Zhou, S. P., & Jia, G. (2020). Tissue-specific oxidative stress and element distribution after oral exposure to titanium dioxide nanoparticles in rats. *Nanoscale*, *12*(38), 20033-20046. https://doi.org/10.1039/d0nr05591c

Chen, Z., Han, S., Zheng, P., Zhang, J., Zhou, S., & Jia, G. (2022b). Landscape of lipidomic metabolites in gut-liver axis of Sprague-Dawley rats after oral exposure to titanium dioxide nanoparticles. *Part Fibre Toxicol*, *19*(1), 53. https://doi.org/10.1186/s12989-022-00484-9

Chen, Z., Tian, R., She, Z., Cai, J., & Li, H. (2020). Role of oxidative stress in the pathogenesis of nonalcoholic fatty liver disease. *Free Radic Biol Med*, *152*, 116-141. https://doi.org/10.1016/j.freeradbiomed.2020.02.025

Chen, Z., Zhou, D., Han, S., Zhou, S., & Jia, G. (2019). Hepatotoxicity and the role of the gut-liver axis in rats after oral administration of titanium dioxide nanoparticles. *Particle and fibre toxicology*, *16*(1), 48.

Cho, W. S., Kang, B. C., Lee, J. K., Jeong, J., Che, J. H., & Seok, S. H. (2013). Comparative absorption, distribution, and excretion of titanium dioxide and zinc oxide nanoparticles after repeated oral administration. *Part Fibre Toxicol*, *10*, 9. https://doi.org/10.1186/1743-8977-10-9

Christensen, F. M., Johnston, H. J., Stone, V., Aitken, R. J., Hankin, S., Peters, S., & Aschberger, K. (2011). Nano-TiO_2 –feasibility and challenges for human health risk assessment based on open literature. *Nanotoxicology*, *5*(2), 110-124.

Christie, A. B., & Brathwaite, R. L. (1998). Mineral commodity report 16 – Titanium. *New Zealand Mining, 23*, 15–25.

Chung, I.-M., Kim, J.-K., Lee, K.-J., Park, S.-K., Lee, J.-H., Son, N.-Y., Jin, Y.-I., & Kim, S.-H. (2018). Geographic authentication of Asian rice (Oryza sativa L.) using multi-elemental and stable isotopic data combined with multivariate analysis. *FOOD CHEMISTRY*, *240*, 840-849.

Cihlar, J., Tinoco Navarro, L. K., Kasparek, V., Michalicka, J., Cihlar, J., Kastyl, J., Castkova, K., & Celko, L. (2021). Influence of LA/Ti molar ratio on the complex synthesis of anatase/brookite nanoparticles and their hydrogen production. *International Journal of Hydrogen Energy*, *46*(12), 8578-8593. https://doi.org/https://doi.org/10.1016/j.ijhydene.2020.12.080

Clare, K., Dillon, J. F., & Brennan, P. N. (2022). Reactive oxygen species and oxidative stress in the pathogenesis of MAFLD. *Journal of Clinical and Translational Hepatology*, *10*(5), 939.

Clayton-Cuch, D. (2023). *ICP-OES analysis of titanium dioxide in foods prepared with a one-step digestion. Agilent Technologies, Inc.*

Coccini, T., Grandi, S., Lonati, D., Locatelli, C., & De Simone, U. (2015). Comparative cellular toxicity of titanium dioxide nanoparticles on human astrocyte and neuronal cells after acute and prolonged exposure. *Neurotoxicology*, *48*, 77-89.

Coelho, S. G., Patri, A. K., Wokovich, A. M., McNeil, S. E., Howard, P. C., & Miller, S. A. (2016). Repetitive application of sunscreen containing titanium dioxide nanoparticles on human skin. *JAMA dermatology*, *152*(4), 470-472.

Cominguez, D. C., Park, Y. J., Kang, Y. M., Nugroho, A., Kim, S., & An, H. J. (2022). Clitorin ameliorates western diet-induced hepatic steatosis by regulating lipogenesis and fatty acid oxidation in vivo and in vitro. *Sci Rep*, *12*(1), 4154. https://doi.org/10.1038/s41598-022-07937-3

Commission Regulation EU. (2012). Commission Regulation (EU) No 231/2012 of 9 March 2012 laying down specifications for food additives listed in Annexes II and III to Regulation (EC) No 1333/2008 of the European Parliament and of the Council Text with EEA relevance. *Official Journal of the European Union*. http://data.europa.eu/eli/reg/2012/231/oj

Conde de la Rosa, L., Goicoechea, L., Torres, S., Garcia-Ruiz, C., & Fernandez-Checa, J. C. (2022). Role of oxidative stress in liver disorders. *Livers*, *2*(4), 283-314.

Correia, M., Uusimäki, T., Philippe, A., & Loeschner, K. (2018). Challenges in determining the size distribution of nanoparticles in consumer products by asymmetric flow field-flow fractionation coupled to inductively coupled plasma-mass spectrometry: the example of Al2O3, TiO_2 , and SiO2 nanoparticles in toothpaste. *Separations*, *5*(4), 56.

Crosera, M., Prodi, A., Mauro, M., Pelin, M., Florio, C., Bellomo, F., Adami, G., Apostoli, P., De Palma, G., & Bovenzi, M. (2015). Titanium dioxide nanoparticle penetration into the skin and effects on HaCaT cells. *International Journal of Environmental Research and Public Health*, *12*(8), 9282-9297.

Cui, X. S., Li, H. Z., Li, L., Xie, C. Z., Gao, J. M., Chen, Y. Y., Zhang, H. Y., Hao, W., Fu, J. H., & Guo, H. (2025). Rodent model of metabolic dysfunction-associated fatty liver disease: a systematic review. *J Gastroenterol Hepatol*, *40*(1), 48-66. https://doi.org/10.1111/jgh.16749

Cui, Y. L., Gong, X. L., Duan, Y. M., Li, N., Hu, R. P., Liu, H. T., Hong, M. M., Zhou, M., Wang, L., Wang, H., & Hong, F. S. (2010). Hepatocyte apoptosis and its molecular mechanisms in mice caused by titanium dioxide nanoparticles. *Journal of Hazardous Materials*, *183*(1-3), 874-880. https://doi.org/10.1016/j.jhazmat.2010.07.109

Cui, Y. L., Liu, H. T., Zhou, M., Duan, Y. M., Li, N., Gong, X. L., Hu, R. P., Hong, M. M., & Hong, F. S. (2011). Signaling pathway of inflammatory responses in the mouse liver caused by TiO_2 nanoparticles. *Journal of Biomedical Materials Research Part A*, *96A*(1), 221-229. https://doi.org/10.1002/jbm.a.32976

Cui, Y., Gong, X., Duan, Y., Li, N., Hu, R., Liu, H., Hong, M., Zhou, M., Wang, L., & Wang, H. (2010). Hepatocyte apoptosis and its molecular mechanisms in mice caused by titanium dioxide nanoparticles. *Journal of Hazardous Materials*, *183*(1-3), 874-880.

Cui, Y., Liu, H., Zhou, M., Duan, Y., Li, N., Gong, X., Hu, R., Hong, M., & Hong, F. (2011). Signaling pathway of inflammatory responses in the mouse liver caused by TiO2 nanoparticles. *Journal of Biomedical Materials Research Part A*, *96*(1), 221-229.

da Silveira Estevão, P. L., Lemes, L. F. R., Soares, F. L. F., & Nagata, N. (2023). Raman mapping for determination of TiO_2 in different solid food samples by multivariate curve resolution with alternating least squares. *Analytical and Bioanalytical Chemistry*, *415*(21), 5235-5245.

Dar, G. I., Saeed, M., & Wu, A. (2020). Toxicity of TiO_2 Nanoparticles. In *TiO_2 Nanoparticles* (pp. 67-103). https://doi.org/https://doi.org/10.1002/9783527825431.ch2

De la Calle, I., Menta, M., Klein, M., & Séby, F. (2017). Screening of TiO_2 and Au nanoparticles in cosmetics and determination of elemental impurities by multiple techniques (DLS, SP-ICP-MS, ICP-MS and ICP-OES). *Talanta*, *171*, 291-306.

De La Cruz, L. N. P., Giorgione, R., Marini, F., & Astolfi, M. L. (2024). Rice sample preparation method for ICP-MS and CV-AFS analysis: Elemental levels and estimated intakes. *FOOD CHEMISTRY*, *461*, 140831.

De Matteis, V., Rojas, M., Cascione, M., Mazzotta, S., Di Sansebastiano, G. P., & Rinaldi, R. (2021). Physico-Chemical Properties of Inorganic NPs Influence the Absorption Rate of Aquatic Mosses Reducing Cytotoxicity on Intestinal Epithelial Barrier Model. *MOLECULES*, *26*(10). https://doi.org/10.3390/molecules26102885

Demir, F., Kipcak, A. S., Dere Ozdemir, O., & Moroydor Derun, E. (2020). Determination of essential and non-essential element concentrations and health risk assessment of some commercial fruit juices in Turkey. *Journal of Food Science and Technology*, *57*(12), 4432-4442.

Dhupal, M., Oh, J.-M., Tripathy, D. R., Kim, S.-K., Koh, S. B., & Park, K.-S. (2018). Immunotoxicity of titanium dioxide nanoparticles via simultaneous induction of apoptosis and multiple toll-like receptors signaling through ROS-dependent SAPK/JNK and p38 MAPK activation. *International journal of nanomedicine*, 6735-6750.

Di Bucchianico, S., Cappellini, F., Le Bihanic, F., Zhang, Y., Dreij, K., & Karlsson, H. L. (2017). Genotoxicity of TiO_2 nanoparticles assessed by mini-gel comet assay and micronucleus scoring with flow cytometry. *Mutagenesis, 32*(1), 127–137. https://doi.org/10.1093/mutage/gew030

Diabetes NZ. (2024). *New diabetes data confirms 'worst case' predictions*. Retrieved 09 December from https://www.diabetes.org.nz/news-and-update/worst-case-predictions

Diebold, U. (2003). The surface science of titanium dioxide. *Surface science reports*, *48*(5-8), 53-229.

Dikalov, S., Panov, A., & Dikalova, A. (2024). Critical role of mitochondrial fatty acid metabolism in normal cell function and pathological conditions. *International Journal of Molecular Sciences*, *25*(12), 6498.

Diraison, F., Moulin, P., & Beylot, M. (2003). Contribution of hepatic de novo lipogenesis and reesterification of plasma non esterified fatty acids to plasma triglyceride synthesis during non-alcoholic fatty liver disease. *Diabetes & metabolism*, *29*(5), 478-485.

Committee on Toxicity of Chemicals in Food, Consumer Products and the Environment (COT). (2024). *Statement on the safety of titanium dioxide (E171) as a food additive: Exposure assessment*. https://cot.food.gov.uk/Exposure%20Assessment%20%20%28E171%29%20Executive%20Summary

Dobrzański, Z., Chojnacka, K., Trziszka, T., Opaliński, S., Bobak, Ł., Konkol, D., & Korczyński, M. (2020). The effect of dietary humic preparations on the content of essential and non-essential chemical elements in hen eggs. *Animals*, *10*(8), 1252.

Donato, M. T., Tolosa, L., & Gómez-Lechón, M. J. (2015). Culture and Functional Characterization of Human Hepatoma HepG2 Cells. *Methods Mol Biol*, *1250*, 77-93. https://doi.org/10.1007/978-1-4939-2074-7_5

Donnelly, K. L., Smith, C. I., Schwarzenberg, S. J., Jessurun, J., Boldt, M. D., & Parks, E. J. (2005). Sources of fatty acids stored in liver and secreted via lipoproteins in patients with nonalcoholic fatty liver disease. *The Journal of clinical investigation*, *115*(5), 1343-1351.

Dorier, M., Tisseyre, C., Dussert, F., Béal, D., Arnal, M. E., Douki, T., Valdiglesias, V., Laffon, B., Fraga, S., Brandão, F., Herlin-Boime, N., Barreau, F., Rabilloud, T., & Carriere, M. (2019). Toxicological impact of acute exposure to E171 food additive and TiO(2) nanoparticles on a co-culture of Caco-2 and HT29-MTX intestinal cells. *Mutat Res Genet Toxicol Environ Mutagen*, *845*, 402980. https://doi.org/10.1016/j.mrgentox.2018.11.004

Dreno, B., Alexis, A., Chuberre, B., & Marinovich, M. (2019). Safety of titanium dioxide nanoparticles in cosmetics. *JOURNAL OF THE EUROPEAN ACADEMY OF DERMATOLOGY AND VENEREOLOGY*, *33*, 34-46. https://doi.org/10.1111/jdv.15943

Du, J., Zhao, L., Kang, Q., He, Y., & Bi, Y. (2023). An optimized method for Oil Red O staining with the salicylic acid ethanol solution. *Adipocyte*, *12*(1), 2179334.

Dua, A., Kumari, R., Singh, M., Kumar, R., Pradeep, S., Ojesina, A. I., & Kumar, R. (2025). Metabolic Dysfunction-Associated Steatotic Liver Disease (MASLD): the interplay of gut microbiome, insulin resistance, and diabetes. *Front Med (Lausanne)*, *12*, 1618275. https://doi.org/10.3389/fmed.2025.1618275

Duan, Y., Liu, J., Ma, L., Li, N., Liu, H., Wang, J., Zheng, L., Liu, C., Wang, X., Zhao, X., Yan, J., Wang, S., Wang, H., Zhang, X., & Hong, F. (2010). Toxicological characteristics of nanoparticulate anatase titanium dioxide in mice. *Biomaterials*, *31*(5), 894-899. https://doi.org/10.1016/j.biomaterials.2009.10.003

Dudefoi, W., Terrisse, H., Popa, A. F., Gautron, E., Humbert, B., & Ropers, M.-H. (2018). Evaluation of the content of TiO_2 nanoparticles in the coatings of chewing gums. *Food Additives & Contaminants: Part A*, *35*(2), 211-221.

Dumon, J., & Ernst, W. (1988). Titanium in plants. *Journal of Plant Physiology*, *133*(2), 203-209.

Eberlé, D., Hegarty, B., Bossard, P., Ferré, P., & Foufelle, F. (2004). SREBP transcription factors: master regulators of lipid homeostasis. *Biochimie*, *86*(11), 839-848.

Edgar, E., & Mateparae, J. (2020). *The economic and social cost of type 2 diabetes*. PwC New Zealand. https://healthierlives.co.nz/wp-content/uploads/Economic-and-Social-Cost-of-Type-2-Diabetes-FINAL-REPORT.pdf

EFSA, N. (2017). Panel (EFSA Panel on Dietetic Products, Nutrition and Allergies), Turck, D., Bresson, J. *L., Burlingame, B., Dean, T., Fairweather-Tait, S., Heinonen, M., et al*.

EFSA. (2006). *Tolerable upper intake levels for vitamins and minerals. European Food Safety Authority.* https://en.wikipedia.org/wiki/Chromium_deficiency#cite_note-13

EFSA. (2016). Re-evaluation of titanium dioxide (E 171) as a food additive. *Efsa Journal*, *14*(9), e04545.

EFSA. (2019). EFSA statement on the review of the risks related to the exposure to the food additive titanium dioxide (E 171) performed by the French Agency for Food, Environmental and Occupational Health and Safety (ANSES). *Efsa Journal*, *17*(6), e05714.

Eguchi, N., Vaziri, N. D., Dafoe, D. C., & Ichii, H. (2021). The Role of Oxidative Stress in Pancreatic β Cell Dysfunction in Diabetes. *Int J Mol Sci*, *22*(4). https://doi.org/10.3390/ijms22041509

El Hosry, L., Sok, N., Richa, R., Al Mashtoub, L., Cayot, P., & Bou-Maroun, E. (2023). Sample preparation and analytical techniques in the determination of trace elements in food: A review. *Foods*, *12*(4), 895.

Elim, H. I., Cai, B., Kurata, Y., Sugihara, O., Kaino, T., Adschiri, T., Chu, A. L., & Kambe, N. (2009). Refractive index control and Rayleigh scattering properties of transparent TiO2 nanohybrid polymer. *J Phys Chem B*, *113*(30), 10143-10148. https://doi.org/10.1021/jp902598f

El-Sehrawy, A., Mohammed, A. N., Gupta, J., Mohammed, J. S., Roopashree, R., Kashyap, A., Janney, J. B., Sahoo, S., Al-Hasnaawei, S., & Nasr, Y. M. (2025). Combating oxidative stress in non-alcoholic fatty liver disease: From mechanisms to therapeutic strategies. *Pathol Res Pract*, *272*, 156053. https://doi.org/10.1016/j.prp.2025.156053

EMC. (2025). *Package leaflet: Information for Lipitor (10 mg. 20 mg, 40 mg, 80 mg) and Coversyl Arginine plus 5mg/1.25 mg film-coated tablets.* Retrieved 17 Nov from https://www.medicines.org.uk/emc/files/pil.6223.pdf and https://www.medicines.org.uk/emc/files/pil.1059.pdf

Emsley, J. (2011). *Nature's building blocks: an AZ guide to the elements*. Oxford University Press.

Espada-Bernabé, E., Moreno-Martín, G., Gómez-Gómez, B., & Madrid, Y. (2024). Assesing the behaviour of particulate/nanoparticulate form of E171 (TiO_2) food additive in colored chocolate candies before and after in vitro oral ingestion by spICP-MS, TEM and cellular in vitro models. *FOOD CHEMISTRY*, *432*, 137201.

Eynaudi, A., Díaz-Castro, F., Bórquez, J. C., Bravo-Sagua, R., Parra, V., & Troncoso, R. (2021). Differential Effects of Oleic and Palmitic Acids on Lipid Droplet-Mitochondria Interaction in the Hepatic Cell Line HepG2. *Front Nutr*, *8*, 775382. https://doi.org/10.3389/fnut.2021.775382

Fabbrini, E., Mohammed, B. S., Magkos, F., Korenblat, K. M., Patterson, B. W., & Klein, S. (2008). Alterations in adipose tissue and hepatic lipid kinetics in obese men and women with nonalcoholic fatty liver disease. *Gastroenterology*, *134*(2), 424-431.

Fabian, E., Landsiedel, R., Ma-Hock, L., Wiench, K., Wohlleben, W., & van Ravenzwaay, B. (2008). Tissue distribution and toxicity of intravenously administered titanium dioxide nanoparticles in rats. *Arch Toxicol*, *82*(3), 151-157. https://doi.org/10.1007/s00204-007-0253-y

Fadda, L. M., Hagar, H., Mohamed, A. M., & Ali, H. M. (2018). Quercetin and idebenone ameliorate oxidative stress, inflammation, DNA damage, and apoptosis induced by titanium dioxide nanoparticles in rat liver. *Dose-Response*, *16*(4), 1559325818812188.

Faddah, L., Abdel Baky, N., Al-Rasheed, N. M., & Al-Rasheed, N. M. (2013). Biochemical responses of nanosize titanium dioxide in the heart of rats following administration of idepenone and quercetin. *Afr J Pharm Pharmacol*, *7*(38), 2639-2651.

Fagan, R., Synnott, D. W., McCormack, D. E., & Pillai, S. C. (2016). An effective method for the preparation of high temperature stable anatase TiO_2 photocatalysts. *Applied Surface Science*, *371*, 447-452.

Farahani, A., Farahani, A., Kashfi, K., & Ghasemi, A. (2025). Inducible nitric oxide synthase (iNOS): More than an inducible enzyme? Rethinking the classification of NOS isoforms. *Pharmacological research*, 107781.

Fatma, Ü., KORKMAZ, F. D., Suludere, Z., Özlem, E., & YÜZBAŞIOĞLU, D. (2021). Genotoxicity of two nanoparticles: titanium dioxide and zinc oxide. *Gazi University Journal of Science*, *34*(4), 948-958.

Faust, J. J., Doudrick, K., Yang, Y., Capco, D. G., & Westerhoff, P. (2016). A Facile Method for Separating and Enriching Nano and Submicron Particles from Titanium Dioxide Found in Food and Pharmaceutical Products. *PLoS One*, *11*(10), Article e0164712. https://doi.org/10.1371/journal.pone.0164712

FDA. (2024). *Titanium Dioxide as a Color Additive in Foods*. Retrieved 01 DEC from https://www.fda.gov/industry/color-additives/titanium-dioxide-color-additive-foods

Feldhaus, C., & Piskobulu, V. (2024). A low bias method for quantification of Oil Red O staining. *BioRxiv*, 2024.2006. 2018.599611.

Filippi, C., Pryde, A., Cowan, P., Lee, T., Hayes, P., Donaldson, K., Plevris, J., & Stone, V. (2015). Toxicology of ZnO and TiO_2 nanoparticles on hepatocytes: impact on metabolism and bioenergetics. *Nanotoxicology*, *9*(1), 126-134.

Filippi, C., Pryde, A., Cowan, P., Lee, T., Hayes, P., Donaldson, K., Plevris, J., & Stone, V. (2015). Toxicology of ZnO and TiO2 nanoparticles on hepatocytes: impact on metabolism and bioenergetics. *Nanotoxicology*, *9*(1), 126-134.

Filippini, T., Cilloni, S., Malavolti, M., Violi, F., Malagoli, C., Tesauro, M., Bottecchi, I., Ferrari, A., Vescovi, L., & Vinceti, M. (2018). Dietary intake of cadmium, chromium, copper, manganese, selenium

and zinc in a Northern Italy community. *Journal of Trace Elements in Medicine and Biology*, *50*, 508-517.

Filippini, T., Cilloni, S., Malavolti, M., Violi, F., Malagoli, C., Tesauro, M., Bottecchi, I., Ferrari, A., Vescovi, L., & Vinceti, M. (2018). Dietary intake of cadmium, chromium, copper, manganese, selenium and zinc in a Northern Italy community. *Journal of Trace Elements in Medicine and Biology*, *50*, 508-517.

Fiordaliso, F., Bigini, P., Salmona, M., & Diomede, L. (2022). Toxicological impact of titanium dioxide nanoparticles and food-grade titanium dioxide (E171) on human and environmental health [10.1039/D1EN00833A]. *Environmental Science: Nano*, *9*(4), 1199-1211. https://doi.org/10.1039/D1EN00833A

Fiordaliso, F., Foray, C., Salio, M., Salmona, M., & Diomede, L. (2018). Realistic evaluation of titanium dioxide nanoparticle exposure in chewing gum. *Journal of agricultural and food chemistry*, *66*(26), 6860-6868.

Food Standards Australia New Zealand. (2016). Titanium dioxide as a food additive: Assessment report. https://www.foodstandards.gov.au/consumer/foodtech/Documents/FSANZ_TiO_2_Assessment_report.pdf

Food Standards Australia New Zealand. (2021). Titanium dioxide (INS 171) as a food additive. https://www.foodstandards.gov.au/

Food Standards Australia New Zealand. (2022). Titanium dioxide. https://www.foodstandards.gov.au/

Fridlyand, L., & Philipson, L. (2006). Reactive species and early manifestation of insulin resistance in type 2 diabetes. *Diabetes, Obesity and Metabolism*, *8*(2), 136-145.

Fries, G., Marrow, G., & Snow, P. (1982). Soil ingestion by dairy cattle. *Journal of Dairy Science*, *65*(4), 611-618.

FSA, F. S. A. (2020). *Total Diet Study of metals and other elements in food from the 2014-2016 UK Total Diet Study. FSA, UK*. https://www.food.gov.uk/sites/default/files/media/document/total-diet-study-of-metals-and-other-elements-in-food_0.pdf

Fu, Y., Hua, Y., Alam, N., & Liu, E. (2024). Progress in the Study of Animal Models of Metabolic Dysfunction-Associated Steatotic Liver Disease. *Nutrients*, *16*(18). https://doi.org/10.3390/nu16183120

García-Pérez, E., Ryu, D., Lee, C., & Lee, H. J. (2021). Ochratoxin A induces oxidative stress in HepG2 Cells by impairing the gene expression of antioxidant enzymes. *Toxins*, *13*(4), 271.

Gázquez, M. J., Bolívar, J. P., Garcia-Tenorio, R., & Vaca, F. (2014). A review of the production cycle of titanium dioxide pigment. *Materials Sciences and Applications*, *2014*. https://doi.org/10.4236/msa.2014.57048

Genchi, G., Lauria, G., Catalano, A., Carocci, A., & Sinicropi, M. S. (2023). Prevalence of cobalt in the environment and its role in biological processes. *Biology*, *12*(10), 1335.

Geraets, L., Oomen, A. G., Krystek, P., Jacobsen, N. R., Wallin, H., Laurentie, M., Verharen, H. W., Brandon, E. F., & de Jong, W. H. (2014). Tissue distribution and elimination after oral and intravenous administration of different titanium dioxide nanoparticles in rats. *Particle and fibre toxicology*, *11*(1), 30.

Ghasemi, M., Turnbull, T., Sebastian, S., & Kempson, I. (2021). The MTT assay: utility, limitations, pitfalls, and interpretation in bulk and single-cell analysis. *International Journal of Molecular Sciences*, *22*(23), 12827.

Giannenas, I., Nisianakis, P., Gavriil, A., Kontopidis, G., & Kyriazakis, I. (2009). Trace mineral content of conventional, organic and courtyard eggs analysed by inductively coupled plasma mass spectrometry (ICP-MS). *FOOD CHEMISTRY*, *114*(2), 706-711.

Gilbert, J. D., Neubauer, K., & Byard, R. W. (2021). Macroscopic identification of visceral titanium pigment in an intravenous drug user. *Journal of Forensic Sciences*, *66*(5), 2024-2028.

Girish, V., & John, S. (2025). Metabolic Dysfunction-Associated Steatotic Liver Disease (MASLD). In *StatPearls*. StatPearls Publishing

Grace, E. J., & MacFarlane, G. R. (2016). Assessment of the bioaccumulation of metals to chicken eggs from residential backyards. *Science of the Total Environment*, *563*, 256-260.

Grand View Research. (2024). *Titanium Dioxide Market (2024 - 2030)*. https://www.grandviewresearch.com/industry-analysis/titanium-dioxide-industry

Grassian, V. H., Adamcakova-Dodd, A., Pettibone, J. M., O'Shaughnessy, P. T., & Thorne, P. S. (2007). Inflammatory response of mice to manufactured titanium dioxide nanoparticles: Comparison of size effects through different exposure routes. *Nanotoxicology*, *1*(3), 211-226. https://doi.org/10.1080/17435390701694295

Green, C. J., Johnson, D., Amin, H. D., Sivathondan, P., Silva, M. A., Wang, L. M., Stevanato, L., McNeil, C. A., Miljan, E. A., Sinden, J. D., Morten, K. J., & Hodson, L. (2015). Characterization of lipid metabolism in a novel immortalized human hepatocyte cell line. *Am J Physiol Endocrinol Metab*, *309*(6), E511-522. https://doi.org/10.1152/ajpendo.00594.2014

Green, C. J., Parry, S. A., Gunn, P. J., Ceresa, C. D. L., Rosqvist, F., Piché, M. E., & Hodson, L. (2018). Studying non-alcoholic fatty liver disease: the ins and outs of in vivo, ex vivo and in vitro human models. *Horm Mol Biol Clin Investig*, *41*(1). https://doi.org/10.1515/hmbci-2018-0038

Grissa, I., ElGhoul, J., Mrimi, R., El Mir, L., Ben Cheikh, H., & Horcajada, P. (2020). In deep evaluation of the neurotoxicity of orally administered TiO2 nanoparticles. *Brain Research Bulletin*, *155*, 119-128. https://doi.org/10.1016/j.brainresbull.2019.10.005

Grohmann, M., Wiede, F., Dodd, G. T., Gurzov, E. N., Ooi, G. J., Butt, T., Rasmiena, A. A., Kaur, S., Gulati, T., & Goh, P. K. (2018). Obesity drives STAT-1-dependent NASH and STAT-3-dependent HCC. *Cell*, *175*(5), 1289-1306. e1220.

Gu, N., Hu, H. L., Guo, Q., Jin, S. L., Wang, C. L., Oh, Y. R., Feng, Y. J., & Wu, Q. (2015). Effects of oral administration of titanium dioxide fine-sized particles on plasma glucose in mice. *Food and Chemical Toxicology*, *86*, 124-131. https://doi.org/10.1016/j.fct.2015.10.003

Gunn, P. J., Green, C. J., Pramfalk, C., & Hodson, L. (2017). In vitro cellular models of human hepatic fatty acid metabolism: differences between Huh7 and HepG2 cell lines in human and fetal bovine culturing serum. *Physiol Rep*, *5*(24). https://doi.org/10.14814/phy2.13532

Guo, X., Yin, X., Liu, Z., & Wang, J. (2022). Non-Alcoholic Fatty Liver Disease (NAFLD) Pathogenesis and Natural Products for Prevention and Treatment. *Int J Mol Sci*, *23*(24). https://doi.org/10.3390/ijms232415489

Gurr, J.-R., Wang, A. S., Chen, C.-H., & Jan, K.-Y. (2005). Ultrafine titanium dioxide particles in the absence of photoactivation can induce oxidative damage to human bronchial epithelial cells. *Toxicology*, *213*(1-2), 66-73.

Hagström, H., Shang, Y., Hegmar, H., & Nasr, P. (2024). Natural history and progression of metabolic dysfunction-associated steatotic liver disease. *The lancet Gastroenterology & hepatology*, *9*(10), 944-956.

Halawa, A. A., Elshopakey, G., El-Adl, M., Lashen, S., Shalaby, N., Rezk, S., Elmetwally, O., Eldomany, E., Farghali, A., & Elmetwally, M. (2025). Chitosan attenuates titanium dioxide nanoparticles

induced hepatic and renal toxicities. *Sci Rep*, *15*(1), 18983. https://doi.org/10.1038/s41598-025-01736-2

Hamilton, L. E. (2013). Titanium Pigment Deposition in an Intravenous Drug User. *Academic Forensic Pathology*, *3*(4), 486-489.

Hancock, B., Harris, D., Kaye, J., Meehan, L., Melnick, J., Tobyn, M., Gibbard, B., Grou, J., Guarino, C. T., & Halota, M. (2024). Titanium Dioxide (E171 Grade) and the search for replacement opacifiers and colorants: supplier readiness survey, case studies and regulatory perspective. *JOURNAL OF PHARMACEUTICAL SCIENCES*, *113*(5), 1285-1298.

Hassanein, K. M. A., & El-Amir, Y. O. (2017). Protective effects of thymoquinone and avenanthramides on titanium dioxide nanoparticles induced toxicity in Sprague-Dawley rats [Article]. *Pathology Research and Practice*, *213*(1), 13-22. https://doi.org/10.1016/j.prp.2016.08.002

Hassanein, K. M. A., & El-Amir, Y. O. (2018). Ameliorative effects of thymoquinone on titanium dioxide nanoparticles induced acute toxicity in rats. *International journal of veterinary science and medicine*, *6*(1), 16-21. https://doi.org/10.1016/j.ijvsm.2018.02.002

He, L., Wang, H., Duan, S., Gao, Y., Lyu, L., Ou, X., Yu, N., Zhang, Y., Zheng, L., & Wang, Y. (2022). Characterization of titanium dioxide nanoparticles in confectionary products and estimation of dietary exposure level among the Chinese population. *NanoImpact*, *28*, 100435.

Health New Zealand. (2023). *Health Status Report* https://www.tewhatuora.govt.nz/assets/Publications/Health-status-reports/HNZ-TWO-Health-Status-Report_FULL.pdf

Healy, W. (1968). Ingestion of soil by dairy cows. *New Zealand journal of agricultural research*, *11*(2), 487-499.

Heeren, J., & Scheja, L. (2021). Metabolic-associated fatty liver disease and lipoprotein metabolism. *Mol Metab*, *50*, 101238. https://doi.org/10.1016/j.molmet.2021.101238

Heringa, M. B., Geraets, L., van Eijkeren, J. C. H., Vandebriel, R. J., de Jong, W. H., & Oomen, A. G. (2016). Risk assessment of titanium dioxide nanoparticles via oral exposure, including toxicokinetic considerations [Article]. *Nanotoxicology*, *10*(10), 1515-1525. https://doi.org/10.1080/17435390.2016.1238113

Heringa, M. B., Peters, R. J. B., Bleys, R., van der Lee, M. K., Tromp, P. C., van Kesteren, P. C. E., van Eijkeren, J. C. H., Undas, A. K., Oomen, A. G., & Bouwmeester, H. (2018). Detection of titanium particles in human liver and spleen and possible health implications. *Part Fibre Toxicol*, *15*(1), 15. https://doi.org/10.1186/s12989-018-0251-7

Hernández-Gea, V., Hilscher, M., Rozenfeld, R., Lim, M. P., Nieto, N., Werner, S., Devi, L. A., & Friedman, S. L. (2013). Endoplasmic reticulum stress induces fibrogenic activity in hepatic stellate cells through autophagy. *Journal of hepatology*, *59*(1), 98-104.

Herrera-Rodríguez, M. A., Del Pilar Ramos-Godinez, M., Cano-Martínez, A., Segura, F. C., Ruiz-Ramírez, A., Pavón, N., Lira-Silva, E., Bautista-Pérez, R., Thomas, R. S., Delgado-Buenrostro, N. L., Chirino, Y. I., & López-Marure, R. (2023). Food-grade titanium dioxide and zinc oxide nanoparticles induce toxicity and cardiac damage after oral exposure in rats. *Part Fibre Toxicol*, *20*(1), 43. https://doi.org/10.1186/s12989-023-00553-7

Hext, P. M., Tomenson, J. A., & Thompson, P. (2005). Titanium dioxide: inhalation toxicology and epidemiology. *Annals of Occupational Hygiene*, *49*(6), 461-472.

Higashimoto, S. (2019). Titanium-dioxide-based visible-light-sensitive photocatalysis: Mechanistic insight and applications. *Catalysts*, *9*(2), 201.

Hoenig, M. (2001). Preparation steps in environmental trace element analysis—facts and traps. *Talanta*, *54*(6), 1021-1038.

Hong, F., Ji, J., Ze, X., Zhou, Y., & Ze, Y. (2020). Liver inflammation and fibrosis induced by long-term exposure to nano titanium dioxide (TiO_2) nanoparticles in mice and its molecular mechanism. *Journal of biomedical nanotechnology*, *16*(5), 616-625.

Hong, J., Wang, L., Zhao, X. Y., Yu, X. H., Sheng, L., Xu, B. Q., Liu, D., Zhu, Y. T., Long, Y., & Hong, F. S. (2014). Th2 Factors May Be Involved in TiO2 NP-Induced Hepatic Inflammation. *Journal of agricultural and food chemistry*, *62*(28), 6871-6878. https://doi.org/10.1021/jf501428w

Horton, J. D., Shimano, H., Hamilton, R. L., Brown, M. S., & Goldstein, J. L. (1999). Disruption of LDL receptor gene in transgenic SREBP-1a mice unmasks hyperlipidemia resulting from production of lipid-rich VLDL. *The Journal of clinical investigation*, *103*(7), 1067-1076.

Howell, J., Majumdar, A., Fink, M., Byrne, M., McCaughan, G., Strasser, S. I., Crawford, M., Hodgkinson, P., Stuart, K. A., & Tallis, C. (2022). The hidden epidemic: the prevalence and impact of concurrent liver diseases in patients undergoing liver transplantation in Australia and New Zealand. *Transplantation direct*, *8*(8), e1345.

Howes, M. T., King, J., & Rosengren, R. J. (2025). Effects of Fructose on Features of Steatotic Liver Disease in HepG2 Cells. *Nutrients*, *17*(17). https://doi.org/10.3390/nu17172762

Hsiang, J. C., Bai, W. W., Raos, Z., Stableforth, W., Upton, A., Selvaratnam, S., Gane, E. J., & Gerred, S. J. (2015). Epidemiology, disease burden and outcomes of cirrhosis in a large secondary care hospital in South Auckland, New Zealand. *Intern Med J*, *45*(2), 160-169. https://doi.org/10.1111/imj.12624

Hu, H., Guo, Q., Wang, C., Ma, X., He, H., Oh, Y., Feng, Y., Wu, Q., & Gu, N. (2015). Titanium dioxide nanoparticles increase plasma glucose via reactive oxygen species-induced insulin resistance in mice. *J Appl Toxicol*, *35*(10), 1122-1132. https://doi.org/10.1002/jat.3150

Hu, H., Li, L., Guo, Q., Jin, S., Zhou, Y., Oh, Y., Feng, Y., Wu, Q., & Gu, N. (2016). A mechanistic study to increase understanding of titanium dioxide nanoparticles-increased plasma glucose in mice. *Food Chem Toxicol*, *95*, 175-187. https://doi.org/10.1016/j.fct.2016.07.010

Hu, H., Zhang, B., Li, L., Guo, Q., Yang, D., Wei, X., Fan, X., Liu, J., Wu, Q., Oh, Y., Feng, Y., Chen, K., Wang, C., Hou, L., & Gu, N. (2020). The toxic effects of titanium dioxide nanoparticles on plasma glucose metabolism are more severe in developing mice than in adult mice. *Environ Toxicol*, *35*(4), 443-456. https://doi.org/10.1002/tox.22880

Hu, R. P., Zheng, L., Zhang, T., Gao, G. D., Cui, Y. L., Cheng, Z., Cheng, J., Hong, M. M., Tang, M., & Hong, F. S. (2011). Molecular mechanism of hippocampal apoptosis of mice following exposure to titanium dioxide nanoparticles. *Journal of Hazardous Materials*, *191*(1-3), 32-40. https://doi.org/10.1016/j.jhazmat.2011.04.027

Hu, R., Gong, X., Duan, Y., Li, N., Che, Y., Cui, Y., Zhou, M., Liu, C., Wang, H., & Hong, F. (2010). Neurotoxicological effects and the impairment of spatial recognition memory in mice caused by exposure to TiO_2 nanoparticles. *Biomaterials*, *31*(31), 8043-8050.

Hu, R., Gong, X., Duan, Y., Li, N., Che, Y., Cui, Y., Zhou, M., Liu, C., Wang, H., & Hong, F. (2010). Neurotoxicological effects and the impairment of spatial recognition memory in mice caused by exposure to TiO2 nanoparticles. *Biomaterials*, *31*(31), 8043-8050.

Huang, Z., Li, L., Dudley, K., Xiao, L., Huang, G., Subramaniam, V. N., Chen, C., Crawford, R., & Xiao, Y. (2025). Three-Dimensional Dynamic Cell Models for Metabolic Dysfunction-Associated Steatotic Liver Disease Progression. *BME Front*, *6*, 0181. https://doi.org/10.34133/bmef.0181

Huggins, C. B., & Froehlich, J. P. (1966). High concentration of injected titanium dioxide in abdominal lymph nodes. *J Exp Med*, *124*(6), 1099-1106. https://doi.org/10.1084/jem.124.6.1099

Hwang, J. S., Yu, J., Kim, H. M., Oh, J. M., & Choi, S. J. (2019). Food Additive Titanium Dioxide and Its Fate in Commercial Foods. *Nanomaterials (Basel)*, *9*(8). https://doi.org/10.3390/nano9081175

IARC. (2010). *Carbon black, titanium dioxide, and talc* (Vol. 93). IARC Press, International Agency for Research on Cancer.

Inc., S. C. (2016). *Product monograph for perindopril arginine film-coated tablets 2.5 mg, 5 mg and 10 mg and perindopril arginine orodispersible tablets 2.5 mg, 5 mg and 10 mg.* Retrieved 17 Nov from https://pdf.hres.ca/dpd_pm/00037213.PDF

Ipsen, D. H., Lykkesfeldt, J., & Tveden-Nyborg, P. (2018). Molecular mechanisms of hepatic lipid accumulation in non-alcoholic fatty liver disease. *Cellular and Molecular Life Sciences*, *75*, 3313-3327.

Iturbe-Rey, S., Maccali, C., Arrese, M., Aspichueta, P., Oliveira, C. P., Castro, R. E., Lapitz, A., Izquierdo-Sanchez, L., Bujanda, L., & Perugorria, M. J. (2025). Lipotoxicity-driven metabolic dysfunction-associated steatotic liver disease (MASLD). *Atherosclerosis*, *400*, 119053.

Jacobs, J. J., Skipor, A. K., Black, J., Urban, R., & Galante, J. O. (1991). Release and excretion of metal in patients who have a total hip-replacement component made of titanium-base alloy. *J Bone Joint Surg Am*, *73*(10), 1475-1486.

Jafari, A., Rasmi, Y., Hajaghazadeh, M., & Karimipour, M. (2018). Hepatoprotective effect of thymol against subchronic toxicity of titanium dioxide nanoparticles: biochemical and histological evidences. *Environmental Toxicology and Pharmacology*, *58*, 29-36.

Jalili, P., Gueniche, N., Lanceleur, R., Burel, A., Lavault, M. T., Sieg, H., Bohmert, L., Meyer, T., Krause, B. C., Lampen, A., Estrela-Lopis, I., Laux, P., Luch, A., Hogeveen, K., & Fessard, V. (2018). Investigation of the in vitro genotoxicity of two rutile TiO2 nanomaterials in human intestinal and hepatic cells and evaluation of their interference with toxicity assays. *NanoImpact*, *11*, 69-81. https://doi.org/10.1016/j.impact.2018.02.004

Jeejeebhoy, K. N. (1999). The role of chromium in nutrition and therapeutics and as a potential toxin. *Nutrition reviews*, *57*(11), 329-335.

Jeon, H., Shin, H., Lee, J., Kim, J., Biswas, S., Lee, J., & Yun, J. (2025). Welfare characteristics of laying hens in aviary and cage systems. *Poultry Science*, *104*(5), 104987.

Jia, X. C., Wang, S., Zhou, L., & Sun, L. (2017). The Potential Liver, Brain, and Embryo Toxicity of Titanium Dioxide Nanoparticles on Mice. *Nanoscale research letters*, *12*, Article 478. https://doi.org/10.1186/s11671-017-2242-2

Jiménez-González, C., Alonso-Peña, M., Argos Vélez, P., Crespo, J., & Iruzubieta, P. (2025). Unraveling MASLD: The Role of Gut Microbiota, Dietary Modulation, and AI-Driven Lifestyle Interventions. *Nutrients*, *17*(9), 1580.

Jin, G., Yao, X., Liu, D., Zhang, J., Zhang, X., Yang, Y., Bi, Y., Zhang, H., Dong, G., & Tang, H. (2023). Inducible nitric oxide synthase accelerates nonalcoholic fatty liver disease progression by regulating macrophage autophagy. *Immunity, Inflammation and Disease*, *11*(12), e1114.

Jin, T., Costa, M., & Chen, X. (2022). Titanium. In *Handbook on the Toxicology of Metals* (pp. 857-868). Elsevier.

Jing, L., Zhou, W., Tian, G., & Fu, H. (2013). Surface tuning for oxide-based nanomaterials as efficient photocatalysts. *Chem Soc Rev*, *42*(24), 9509-9549. https://doi.org/10.1039/c3cs60176e

Johnston, H. J., Hutchison, G. R., Christensen, F. M., Peters, S., Hankin, S., & Stone, V. (2009). Identification of the mechanisms that drive the toxicity of TiO(2)particulates: the contribution of physicochemical characteristics. *Part Fibre Toxicol*, *6*, 33. https://doi.org/10.1186/1743-8977-6-33

Jovanović, B. (2014). Critical review of public health regulations of titanium dioxide, a human food additive. *Integrated Environmental Assessment and Management*, *11*(1), 10-20. https://doi.org/10.1002/ieam.1571

Jugan, M.-L., Barillet, S., Simon-Deckers, A., Herlin-Boime, N., Sauvaigo, S., Douki, T., & Carriere, M. (2012). Titanium dioxide nanoparticles exhibit genotoxicity and impair DNA repair activity in A549 cells. *Nanotoxicology*, *6*(5), 501-513.

Jurjanz, S., Germain, K., Dziurla, M., Juin, H., & Jondreville, C. (2014). Use of acid-insoluble ash and n-alkanes as markers of soil and plant ingestion by chickens. *ANIMAL FEED SCIENCE AND TECHNOLOGY*, *188*, 92-101.

Kaewklin, P., Siripatrawan, U., Suwanagul, A., & Lee, Y. S. (2018). Active packaging from chitosan-titanium dioxide nanocomposite film for prolonging storage life of tomato fruit. *International Journal of Biological Macromolecules*, *112*, 523-529.

Kaim, W., Schwederski, B., & Klein, A. (2013). *Bioinorganic Chemistry--Inorganic Elements in the Chemistry of Life: An Introduction and Guide*. John Wiley & Sons.

Kalra, A., Yetiskul, E., Wehrle, C. J., & Tuma, F. (2025). Physiology, Liver. In *StatPearls*. StatPearls Publishing

Kamboj, P., Goyal, R. K., Yadav, R., Banerjee, S. K., & Mahajan, D. (2024). Role of Inducible Nitric Oxide Synthase (iNOS) in the Pathogenesis and Progression of Metabolic Dysfunction-Associated Steatotic Liver Disease in a Choline-Deficient High-Fat Diet Model. *Journal of Clinical and Experimental Hepatology*, *14*.

Kandeil, M. A., Mohammed, E. T., Hashem, K. S., Aleya, L., & Abdel-Daim, M. M. (2020). Moringa seed extract alleviates titanium oxide nanoparticles (TiO2-NPs)-induced cerebral oxidative damage, and increases cerebral mitochondrial viability. *Environmental Science and Pollution Research*, *27*(16), 19169-19184.

Keller, A. A., McFerran, S., Lazareva, A., & Suh, S. (2013). Global life cycle releases of engineered nanomaterials. *Journal of nanoparticle research*, *15*(6), 1-17.

Keller, C. A., Frost, A., Cagle, P. T., & Abraham, J. L. (1995). Pulmonary alveolar proteinosis in a painter with elevated pulmonary concentrations of titanium. *Chest*, *108*(1), 277-280.

Kermanizadeh, A., Gaiser, B. K., Hutchison, G. R., & Stone, V. (2012). An in vitro liver model-assessing oxidative stress and genotoxicity following exposure of hepatocytes to a panel of engineered nanomaterials. *Particle and fibre toxicology*, *9*(1), 1-13.

Kersten, S., & Stienstra, R. (2017). The role and regulation of the peroxisome proliferator activated receptor alpha in human liver. *Biochimie*, *136*, 75-84.

Khalifa, O., Al-Akl, N. S., Errafii, K., & Arredouani, A. (2022). Exendin-4 alleviates steatosis in an in vitro cell model by lowering FABP1 and FOXA1 expression via the Wnt/-catenin signaling pathway. *Sci Rep*, *12*(1), 2226. https://doi.org/10.1038/s41598-022-06143-5

Khamphaya, T., Chukijrungroat, N., Saengsirisuwan, V., Mitchell-Richards, K. A., Robert, M. E., Mennone, A., Ananthanarayanan, M., Nathanson, M. H., & Weerachayaphorn, J. (2018). Nonalcoholic fatty liver disease impairs expression of the type II inositol 1,4,5-trisphosphate receptor. *Hepatology*, *67*(2), 560-574. https://doi.org/10.1002/hep.29588

Khan, J., Kim, N. D., Bromhead, C., Truman, P., Kruger, M. C., & Mallard, B. L. (2024). Hepatotoxicity of titanium dioxide nanoparticles. *Journal of applied toxicology*.

Khan, M. A. B., Hashim, M. J., King, J. K., Govender, R. D., Mustafa, H., & Al Kaabi, J. (2020). Epidemiology of type 2 diabetes–global burden of disease and forecasted trends. *Journal of epidemiology and global health*, *10*(1), 107.

Khorsandi, L., Orazizadeh, M., Mansori, E., & Fakhredini, F. (2015). Glycyrrhizic acid attenuated lipid peroxidation induced by titanium dioxide nanoparticles in rat liver. *Bratislavske Lekarske Listy*, *116*(6), 383-388.

Kim, N., Kim, C., Jung, S., Park, Y., Lee, Y., Jo, J., Hong, M., Lee, S., Oh, Y., & Jung, K. (2018). Determination and identification of titanium dioxide nanoparticles in confectionery foods, marketed in South Korea, using inductively coupled plasma optical emission spectrometry and transmission electron microscopy. *Food Addit Contam Part A Chem Anal Control Expo Risk Assess*, *35*(7), 1238-1246. https://doi.org/10.1080/19440049.2018.1482011

King, N., Thomas, K., & Gautam, A. (2024). *Emerging Risk Identification System (ERIS), Annual Report, Year Three (March 2023–February 2024). Prepared for the New Zealand Food Safety Science & Research Centre by the Institute of Environmental Science and Research (ESR) Ltd. ESR report number CSC24004.* https://www.nzfssrc.org.nz/assets/ERIS/ERIS-Annual-Report-Y3-Mar2024-V1.1.pdf

Kirkland, D., Burzlaff, A., Czich, A., Doak, S. H., Fowler, P., Pfuhler, S., & Stankowski, L. F. (2024). Updated assessment of the genotoxic potential of titanium dioxide based on reviews of in vitro comet, mode of action and cellular uptake studies, and recent publications. *Regulatory Toxicology and Pharmacology*, *154*, 105734. https://doi.org/https://doi.org/10.1016/j.yrtph.2024.105734

Klein, D. H., & Russell, P. (1973). Heavy metals. Fallout around a power plant. *Environmental Science & Technology*, *7*(4), 357-358.

Kohen, R., & Nyska, A. (2002). Oxidation of biological systems: oxidative stress phenomena, antioxidants, redox reactions, and methods for their quantification. *Toxicol Pathol*, *30*(6), 620-650. https://doi.org/10.1080/01926230290166724

Koliaki, C., Dalamaga, M., Kakounis, K., & Liatis, S. (2025). Metabolically Healthy Obesity and Metabolic Dysfunction-Associated Steatotic Liver Disease (MASLD): Navigating the Controversies in Disease Development and Progression. *Current Obesity Reports*, *14*(1), 46.

Kollander, B., Rodushkin, I., & Sundström, B. (2023). Multi-element assessment of potentially toxic and essential elements in new and traditional food varieties in Sweden. *Foods*, *12*(9), 1831.

Koo, S.-H. (2013). Nonalcoholic fatty liver disease: molecular mechanisms for the hepatic steatosis. *Clinical and molecular hepatology*, *19*(3), 210.

Korotcenkov, G. (2020a). Current trends in nanomaterials for metal oxide-based conductometric gas sensors: Advantages and limitations. part 1: 1D and 2D nanostructures. *Nanomaterials*, *10*(7), 1392.

Korotcenkov, G. (2020b). *Titanium Dioxide (TiO2) and Its Applications*. Elsevier.

Krahmer, N., Walther, T. C., & Farese, R. V., Jr. (2025). The pathogenesis of hepatic steatosis in MASLD: a lipid droplet perspective. *J Clin Invest*, *135*(18). https://doi.org/10.1172/jci198334

Kreyling, W. G., Holzwarth, U., Haberl, N., Kozempel, J., Hirn, S., Wenk, A., Schleh, C., Schäffler, M., Lipka, J., Semmler-Behnke, M., & Gibson, N. (2017). Quantitative biokinetics of titanium dioxide nanoparticles after intravenous injection in rats: Part 1. *Nanotoxicology*, *11*(4), 434-442. https://doi.org/10.1080/17435390.2017.1306892

Kreyling, W. G., Holzwarth, U., Schleh, C., Kozempel, J., Wenk, A., Haberl, N., Hirn, S., Schäffler, M., Lipka, J., Semmler-Behnke, M., & Gibson, N. (2017). Quantitative biokinetics of titanium dioxide nanoparticles after oral application in rats: Part 2. *Nanotoxicology*, *11*(4), 443-453. https://doi.org/10.1080/17435390.2017.1306893

Kreyling, W. G., Semmler, M., Erbe, F., Mayer, P., Takenaka, S., Schulz, H., Oberdörster, G., & Ziesenis, A. (2002). Translocation of ultrafine insoluble iridium particles from lung epithelium to extrapulmonary organs is size dependent but very low. *J Toxicol Environ Health A*, *65*(20), 1513-1530. https://doi.org/10.1080/00984100290071649

Kunc, F., Du, X., Zborowski, A., Johnston, L. J., & Kennedy, D. C. (2025). Titanium dioxide nanoparticles - physicochemical characterization and cytotoxic risk. *NanoImpact*, *37*, 100543. https://doi.org/10.1016/j.impact.2025.100543

La Maestra, S., D'Agostini, F., Sanguineti, E., Yus González, A., Annis, S., Militello, G. M., Parisi, G., Scuderi, A., & Gaggero, L. (2021). Dispersion of Natural Airborne TiO(2) Fibres in Excavation Activity as a Potential Environmental and Human Health Risk. *Int J Environ Res Public Health*, *18*(12). https://doi.org/10.3390/ijerph18126587

Lala, V., Zubair, M., & Minter, D. (2023). Liver function tests. *StatPearls*.

Lammel, T., Mackevica, A., Johansson, B. R., & Sturve, J. (2019). Endocytosis, intracellular fate, accumulation, and agglomeration of titanium dioxide (TiO_2) nanoparticles in the rainbow trout liver cell line RTL-W1. *Environmental Science and Pollution Research, 26*(15), 15354–15372. https://doi.org/10.1007/s11356-019-04841-6

Lankoff, A., Sandberg, W. J., Wegierek-Ciuk, A., Lisowska, H., Refsnes, M., Sartowska, B., Schwarze, P. E., Męczyńska-Wielgosz, S., Wojewódzka, M., & Kruszewski, M. (2012). The effect of agglomeration state of silver and titanium dioxide nanoparticles on cellular response of HepG2, A549 and THP-1 cells. *Toxicology Letters, 208*(3), 197–213. https://doi.org/10.1007/s11356-019-04856-1

Lankoff, A., Sandberg, W. J., Wegierek-Ciuk, A., Lisowska, H., Refsnes, M., Sartowska, B., Schwarze, P. E., Meczynska-Wielgosz, S., Wojewodzka, M., & Kruszewski, M. (2012). The effect of agglomeration state of silver and titanium dioxide nanoparticles on cellular response of HepG2, A549 and THP-1 cells. *Toxicol Lett*, *208*(3), 197-213. https://doi.org/10.1016/j.toxlet.2011.11.006

Leone, J. L. (1973). Collaborative study of the quantitative determination of titanium dioxide in cheese. *Journal of the Association of Official Analytical Chemists*, *56*(3), 535-537.

Li, C., & Tang, M. (2024). The toxicological effects of nano titanium dioxide on target organs and mechanisms of toxicity. *J Appl Toxicol*, *44*(2), 152-164. https://doi.org/10.1002/jat.4534

Li, Q., Fu, Y., Liu, C., Zhang, R., Zhang, Z., & McClements, D. J. (2018). Impact of Titanium Dioxide on the Bioaccessibility of β-Carotene in Emulsions with Different Particle Sizes. *J Agric Food Chem*, *66*(35), 9318-9325. https://doi.org/10.1021/acs.jafc.8b02025

Li, T., Wang, H., Dong, S., Liang, M., Ma, J., Jiang, X., & Yu, W. (2022). Protective effects of maslinic acid on high fat diet-induced liver injury in mice. *Life Sci*, *301*, 120634. https://doi.org/10.1016/j.lfs.2022.120634

Li, Y., Yang, P., Ye, J., Xu, Q., Wu, J., & Wang, Y. (2024). Updated mechanisms of MASLD pathogenesis. *Lipids in health and disease*, *23*(1), 117.

Li, Z. Z., Berk, M., McIntyre, T. M., & Feldstein, A. E. (2009). Hepatic lipid partitioning and liver damage in nonalcoholic fatty liver disease: role of stearoyl-CoA desaturase. *Journal of Biological Chemistry*, *284*(9), 5637-5644.

Li, Z., Fan, X., Gao, F., Pan, S., Ma, X., Cheng, H., Nakatsukasa, H., Zhang, W., & Zhang, D. (2025). Fructose metabolism and its roles in metabolic diseases, inflammatory diseases, and cancer. *Molecular Biomedicine*, *6*(1), 43.

Li, Z., He, J., Li, B., Zhang, J., He, K., Duan, X., Huang, R., Wu, Z., & Xiang, G. (2020). Titanium dioxide nanoparticles induce endoplasmic reticulum stress-mediated apoptotic cell death in liver cancer cells. *Journal of International Medical Research*, *48*(4), 0300060520903652.

Liang, G., Pu, Y., Yin, L., Liu, R., Ye, B., Su, Y., & Li, Y. (2009). Influence of different sizes of titanium dioxide nanoparticles on hepatic and renal functions in rats with correlation to oxidative stress. *J Toxicol Environ Health A*, *72*(11-12), 740-745. https://doi.org/10.1080/15287390902841516

Lim, C. M., Carey, M., Williams, P. N., & Koidis, A. (2021). Rapid classification of commercial teas according to their origin and type using elemental content with X-ray fluorescence (XRF) spectroscopy. *Current Research in Food Science*, *4*, 45-52.

Lim, J. H., Bae, D., & Fong, A. (2018). Titanium Dioxide in Food Products: Quantitative Analysis Using ICP-MS and Raman Spectroscopy. *J Agric Food Chem*, *66*(51), 13533-13540. https://doi.org/10.1021/acs.jafc.8b06571

Lima, M. A. d., Santos, V. M. d., Demachki, S., & Lazo, J. (2004). Titanium pigment in tissues of drug addicts: report of 5 necropsied cases. *Revista do Hospital das Clínicas*, *59*, 86-88.

Listenberger, L. L., Han, X., Lewis, S. E., Cases, S., Farese Jr, R. V., Ory, D. S., & Schaffer, J. E. (2003). Triglyceride accumulation protects against fatty acid-induced lipotoxicity. *Proceedings of the National Academy of Sciences*, *100*(6), 3077-3082.

Liu, H., Ma, L., Liu, J., Zhao, J., Yan, J., & Hong, F. (2010). Toxicity of nano-anatase TiO_2 to mice: Liver injury, oxidative stress [Article]. *TOXICOLOGICAL AND ENVIRONMENTAL CHEMISTRY*, *92*(1), 175-186. https://doi.org/10.1080/02772240902732530

Liu, X., Li, D., Liang, Y., Lin, Y., Liu, Z., Niu, H., & Xu, Y. (2021). Establishment of anti-oxidation platform based on few-layer molybdenum disulfide nanosheet-coated titanium dioxide nanobelt nanocomposite. *J Colloid Interface Sci*, *601*, 167-176. https://doi.org/10.1016/j.jcis.2021.05.056

Liu, Y., Huang, Y., Cao, Y., Hu, X., Li, S., Dai, J., Lee, K., & Qin, W. (2022). Characterization and assessment of potential risks of titanium dioxide nanoparticles isolated from gummy candies. *JOURNAL OF CLEANER PRODUCTION*, *373*, 133829.

Liu, Z., Lv, Y., Zhao, N., Guan, G., & Wang, J. (2015). Protein kinase R-like ER kinase and its role in endoplasmic reticulum stress-decided cell fate. *Cell death & disease*, *6*(7), e1822-e1822.

Lobstein, T., Brinsden, H., & Neveux, M. (2022). *World obesity atlas 2022*. World Obesity. https://s3-eu-west-1.amazonaws.com/wof-files/World_Obesity_Atlas_2022.pdf

Lomer, M. C., Thompson, R. P., Commisso, J., Keen, C. L., & Powell, J. J. (2000). Determination of titanium dioxide in foods using inductively coupled plasma optical emission spectrometry. *Analyst*, *125*(12), 2339-2343. https://doi.org/10.1039/b006285p

Lonardo, A., Lugari, S., Ballestri, S., Nascimbeni, F., Baldelli, E., & Maurantonio, M. (2019). A round trip from nonalcoholic fatty liver disease to diabetes: molecular targets to the rescue? *Acta diabetologica*, *56*(4), 385-396.

Long, T. C., Tajuba, J., Sama, P., Saleh, N., Swartz, C., Parker, J., Hester, S., Lowry, G. V., & Veronesi, B. (2007). Nanosize titanium dioxide stimulates reactive oxygen species in brain microglia and damages neurons in vitro. *Environmental health perspectives*, *115*(11), 1631-1637.

Loomba, R., & Chalasani, N. (2015). The hierarchical model of NAFLD: prognostic significance of histologic features in NASH. *Gastroenterology*, *149*(2), 278-281.

Loomba, R., Schork, N., Chen, C.-H., Bettencourt, R., Bhatt, A., Ang, B., Nguyen, P., Hernandez, C., Richards, L., & Salotti, J. (2015). Heritability of hepatic fibrosis and steatosis based on a prospective twin study. *Gastroenterology*, *149*(7), 1784-1793.

Lucaciu, R. L., Coste, S. C., Hangan, A. C., Iancu, M., Orășan, O. H., Cozma, A., Gog Bogdan, S., & Procopciuc, L. M. (2025). Pathogenesis and Clinical Management of Metabolic Dysfunction-Associated Steatotic Liver Disease. *International Journal of Molecular Sciences*, *26*(12), 5717.

Luo, Z., Li, Z., Xie, Z., Sokolova, I. M., Song, L., Peijnenburg, W., Hu, M., & Wang, Y. (2020). Rethinking Nano-TiO(2) Safety: Overview of Toxic Effects in Humans and Aquatic Animals. *Small*, *16*(36), e2002019. https://doi.org/10.1002/smll.202002019

Lyu, S., Wei, X., Chen, J., Wang, C., Wang, X., & Pan, D. (2017). Titanium as a beneficial element for crop production. *FRONTIERS IN PLANT SCIENCE*, *8*, 597.

Ma, L., Zhao, J., Wang, J., Liu, J., Duan, Y., Liu, H., Li, N., Yan, J., Ruan, J., & Wang, H. (2009). The acute liver injury in mice caused by nano-anatase TiO_2 . *Nanoscale research letters*, *4*(11), 1275.

Ma, X., Huang, T., Chen, X., Li, Q., Liao, M., Fu, L., Huang, J., Yuan, K., Wang, Z., & Zeng, Y. (2025). Molecular mechanisms in liver repair and regeneration: from physiology to therapeutics. *Signal Transduction and Targeted Therapy*, *10*(1), 63.

Ma, Y., Guo, Y., Ye, H., Huang, K., Lv, Z., & Ke, Y. (2019). Different effects of titanium dioxide nanoparticles instillation in young and adult mice on DNA methylation related with lung inflammation and fibrosis. *Ecotoxicology and Environmental Safety*, *176*, 1-10.

Ma, Y., Yu, N., Lu, H., Shi, J., Zhang, Y., Chen, Z., & Jia, G. (2023). Titanium dioxide nanoparticles: revealing the mechanisms underlying hepatotoxicity and effects in the gut microbiota. *Arch Toxicol*, *97*(8), 2051-2067. https://doi.org/10.1007/s00204-023-03536-x

Madorran, E., Ambrož, M., Knez, J., & Sobočan, M. (2024). An Overview of the Current State of Cell Viability Assessment Methods Using OECD Classification. *Int J Mol Sci*, *26*(1). https://doi.org/10.3390/ijms26010220

Maeda, H., Ishima, Y., Saruwatari, J., Mizuta, Y., Minayoshi, Y., Ichimizu, S., Yanagisawa, H., Nagasaki, T., Yasuda, K., & Oshiro, S. (2022). Nitric oxide facilitates the targeting Kupffer cells of a nano-antioxidant for the treatment of NASH. *Journal of Controlled Release*, *341*, 457-474.

Magkos, F., Fabbrini, E., Mohammed, B. S., Patterson, B. W., & Klein, S. (2010). Increased whole-body adiposity without a concomitant increase in liver fat is not associated with augmented metabolic dysfunction. *Obesity*, *18*(8), 1510-1515.

Ma-Hock, L., Burkhardt, S., Strauss, V., Gamer, A. O., Wiench, K., van Ravenzwaay, B., & Landsiedel, R. (2009). Development of a short-term inhalation test in the rat using nano-titanium dioxide as a model substance. *Inhalation toxicology*, *21*(2), 102-118.

Majewski, E., Potori, N., Sulewski, P., Wąs, A., Mórawska, M., Gębska, M., Malak-Rawlikowska, A., Grontkowska, A., Szili, V., & Erdős, A. (2024). End of the Cage age? a study on the impacts of the transition from cages on the EU laying hen sector. *Agriculture*, *14*(1), 111.

Maldybayev, G., Korabayev, A., Sharipov, R., Al Azzam, K. M., Negim, E. S., Baigenzhenov, O., ... & Shayakhmetova, R. (2024). Processing of titanium-containing ores for the production of titanium products: A comprehensive review. *Heliyon, 10*(3), Article e25312. https://doi.org/10.1016/j.heliyon.2024.e24966

Malekpour-Dehkordi, Z., Nourbakhsh, M., Shahidi, M., Sarraf, N., & Sharifi, R. (2022). Silymarin diminishes oleic acid-induced lipid accumulation in HepG2 cells by modulating the expression of endoplasmic reticulum stress markers. *Journal of Herbal Medicine*, *33*, 100565.

Manivannan, J., Banerjee, R., & Mukherjee, A. (2020). Genotoxicity analysis of rutile titanium dioxide nanoparticles in mice after 28 days of repeated oral administration. *The Nucleus*, *63*(1), 17-24.

Manke, A., Wang, L., & Rojanasakul, Y. (2013). Mechanisms of nanoparticle-induced oxidative stress and toxicity. *BioMed Research International*, *2013*(1), 942916.

Mantovani, A., Scorletti, E., Mosca, A., Alisi, A., Byrne, C. D., & Targher, G. (2020). Complications, morbidity and mortality of nonalcoholic fatty liver disease. *Metabolism*, *111*, 154170.

Mao, J., DeMayo, F. J., Li, H., Abu-Elheiga, L., Gu, Z., Shaikenov, T. E., Kordari, P., Chirala, S. S., Heird, W. C., & Wakil, S. J. (2006). Liver-specific deletion of acetyl-CoA carboxylase 1 reduces hepatic triglyceride accumulation without affecting glucose homeostasis. *Proceedings of the National Academy of Sciences*, *103*(22), 8552-8557.

Marjot, T., Moolla, A., Cobbold, J. F., Hodson, L., & Tomlinson, J. W. (2020). Nonalcoholic Fatty Liver Disease in Adults: Current Concepts in Etiology, Outcomes, and Management. *Endocr Rev*, *41*(1). https://doi.org/10.1210/endrev/bnz009

Martins Jr, A. d. C., Azevedo, L. F., de Souza Rocha, C. C., Carneiro, M. F. H., Venancio, V. P., de Almeida, M. R., Antunes, L. M. G., de Carvalho Hott, R., Rodrigues, J. L., & Ogunjimi, A. T. (2017). Evaluation of distribution, redox parameters, and genotoxicity in Wistar rats co-exposed to silver and titanium dioxide nanoparticles. *Journal of Toxicology and Environmental Health, Part A*, *80*(19-21), 1156-1165.

Mashek, D. G. (2013). Hepatic fatty acid trafficking: multiple forks in the road. *Advances in nutrition*, *4*(6), 697-710.

Mayén, A. L., Sabra, M., Aglago, E. K., Perlemuter, G., Voican, C., Ramos, I., Debras, C., Blanco, J., Viallon, V., Ferrari, P., Olsen, A., Tjønneland, A., Langmann, F., Dahm, C. C., Rothwell, J., Laouali, N., Marques, C., Schulze, M. B., Katzke, V., Kaaks, R., Palli, D., Macciotta, A., Panico, S., Tumino, R., Agnoli, C., Farràs, M., Molina-Montes, E., Amiano, P., Chirlaque, M. D., Castilla, J., Werner, M., Bodén, S., Heath, A. K., Tsilidis, K., Aune, D., Weiderpass, E., Freisling, H., Gunter, M. J., & Jenab, M. (2024). Hepatic steatosis, metabolic dysfunction and risk of mortality: findings from a multinational prospective cohort study. *BMC Med*, *22*(1), 221. https://doi.org/10.1186/s12916-024-03366-3

Mayland, H., Florence, A., Rosenau, R., Lazar, V., & Turner, H. (1975). Soil ingestion by cattle on semiarid range as reflected by titanium analysis of feces. *Rangeland Ecology & Management/Journal of Range Management Archives*, *28*(6), 448-452.

McNulty, G. S. (2007). Production of titanium dioxide. Plenary lecture presented at the NORM V International Conference

Medina-Reyes, E. I., Delgado-Buenrostro, N. L., Diaz-Urbina, D., Rodriguez-Ibarra, C., Deciga-Alcaraz, A., Gonzalez, M. I., Reyes, J. L., Villamar-Duque, T. E., Lo Flores-Sanchez, M., Hernandez-Pando, R., Mancilla-Diaz, J. M., Chirino, Y. I., & Pedraza-Chaverri, J. (2020). Food-grade titanium dioxide (E171) induces anxiety, adenomas in colon and goblet cells hyperplasia in a regular diet model and microvesicular steatosis in a high fat diet model. *Food and Chemical Toxicology*, *146*, Article 111786. https://doi.org/10.1016/j.fct.2020.111786

Medsafe. (2025). *Consumer Medical Information for Atorvastatin 10mg, 20mg, 40mg & 80mg film-coated tablets and New Zealand Data Sheet for Coversyl (2 mg, 4 mg, 8 mg tablets).* Retrieved 17 Nov from https://www.medsafe.govt.nz/consumers/cmi/a/atorvastatin.pdf and https://www.medsafe.govt.nz/profs/datasheet/c/Coversyltab.pdf

Mehndiratta, M., Agarwal, P., Tatke, M., & Krishnamurthy, M. (2002). Neurological mitochondrial cytopathies. *Neurology India*, *50*(2), 162.

Merian, E., Anke, M., Ihnat, M., & Stoeppler, M. (2004). *Elements and their compounds in the environment: occurrence, analysis and biological relevance*. Wiley-VCH Verlag GmbH & Co. KGaA.

Ministry of Health. (2018). *Living well with diabetes: A plan for people at high risk of or living with diabetes 2015-2020*. https://www.health.govt.nz/publication/living-well-diabetes

Mohamed, H. R. H., El-Shamy, S., Abdelgayed, S. S., Albash, R., & El-Shorbagy, H. (2024). Modulation efficiency of clove oil nano-emulsion against genotoxic, oxidative stress, and histological injuries induced via titanium dioxide nanoparticles in mice. *Sci Rep*, *14*(1), 7715. https://doi.org/10.1038/s41598-024-57728-1

Mohammadinejad, R., Moosavi, M. A., Tavakol, S., Vardar, D. Ö., Hosseini, A., Rahmati, M., Dini, L., Hussain, S., Mandegary, A., & Klionsky, D. J. (2019). Necrotic, apoptotic and autophagic cell fates triggered by nanoparticles. *Autophagy*, *15*(1), 4-33.

Mohammed, E. T., & Safwat, G. M. (2020). Grape Seed Proanthocyanidin Extract Mitigates Titanium Dioxide Nanoparticle (TiO(2)-NPs)-Induced Hepatotoxicity Through TLR-4/NF-κB Signaling Pathway. *Biol Trace Elem Res*, *196*(2), 579-589. https://doi.org/10.1007/s12011-019-01955-5

Moliterni, C., Vari, F., Schifano, E., Tacconi, S., Stanca, E., Friuli, M., Longo, S., Conte, M., Salvioli, S., Gnocchi, D., Mazzocca, A., Uccelletti, D., Vergara, D., Dini, L., & Giudetti, A. M. (2024). Lipotoxicity of palmitic acid is associated with DGAT1 downregulation and abolished by PPARα activation in liver cells. *J Lipid Res*, *65*(12), 100692. https://doi.org/10.1016/j.jlr.2024.100692

Moradi, A., Ziamajidi, N., Ghafourikhosroshahi, A., & Abbasalipourkabir, R. (2019). Effects of vitamin A and vitamin E on attenuation of titanium dioxide nanoparticles-induced toxicity in the liver of male Wistar rats. *Molecular biology reports*, *46*(3), 2919-2932.

Moretti, V., Romeo, S., & Valenti, L. (2024). The contribution of genetics and epigenetics to MAFLD susceptibility. *Hepatology International*, *18*(Suppl 2), 848-860.

Morgan, A., Ibrahim, M. A., Galal, M. K., Ogaly, H. A., & Abd-Elsalam, R. M. (2018). Innovative perception on using Tiron to modulate the hepatotoxicity induced by titanium dioxide nanoparticles in male rats. *Biomedicine & Pharmacotherapy*, *103*, 553-561.

Moselhy, W. A., Ibrahim, M. A., Khalifa, A. G., El-Nahass, E. S., & Hassan, N. E. Y. (2024). The effects of TiO_2 , ZnO, IONs and Al2O3 metallic nanoparticles on the CYP1A1 and NBN transcripts in rat liver. *Toxicol Res (Camb)*, *13*(2), tfae034. https://doi.org/10.1093/toxres/tfae034

Mota, M., Banini, B. A., Cazanave, S. C., & Sanyal, A. J. (2016). Molecular mechanisms of lipotoxicity and glucotoxicity in nonalcoholic fatty liver disease. *Metabolism*, *65*(8), 1049-1061.

MPI, M. f. P. I. (2017). *Food control plan: Food service and food retail. Template – March 2017. Specialist retail – butchery safe. Ministry for Primary Industries*. https://www.mpi.govt.nz/dmsdocument/11794-Food-Control-Plan-Food-Service-and-Food-Retail.-Specialist-Retail-Butchery-Safe.-Suitable-for-commercial-printing

Mugudamani, I. (2022). *Geochemical characterisation of soil and road dust from an informal settlement and their possible health implications: a study of Winnie Mandela informal settlement, Gauteng, South Africa* Central University of Technology].

Müller, F. A., & Sturla, S. J. (2019). Human in vitro models of nonalcoholic fatty liver disease. *Current Opinion in Toxicology*, *16*, 9-16. https://doi.org/https://doi.org/10.1016/j.cotox.2019.03.001

Muriel, P., López-Sánchez, P., & Ramos-Tovar, E. (2021). Fructose and the Liver. *International Journal of Molecular Sciences*, *22*(13), 6969.

Nagaya, T., Tanaka, N., Suzuki, T., Sano, K., Horiuchi, A., Komatsu, M., Nakajima, T., Nishizawa, T., Joshita, S., & Umemura, T. (2010). Down-regulation of SREBP-1c is associated with the development of burned-out NASH. *Journal of hepatology*, *53*(4), 724-731.

Nakamuta, M., Fujino, T., Yada, R., Yada, M., Yasutake, K., Yoshimoto, T., Harada, N., Higuchi, N., Kato, M., & Kohjima, M. (2009). Impact of cholesterol metabolism and the LXRα-SREBP-1c pathway on nonalcoholic fatty liver disease. *International journal of molecular medicine*, *23*(5), 603-608.

Nassir, F., & Ibdah, J. A. (2014). Role of mitochondria in nonalcoholic fatty liver disease. *International Journal of Molecular Sciences*, *15*(5), 8713-8742.

Natarajan, V., Wilson, C. L., Hayward, S. L., & Kidambi, S. (2015). Titanium Dioxide Nanoparticles Trigger Loss of Function and Perturbation of Mitochondrial Dynamics in Primary Hepatocytes. *PLoS One*, *10*(8), e0134541. https://doi.org/10.1371/journal.pone.0134541

National Research Council. (2002). *Dietary reference intakes for vitamin A, vitamin K, arsenic, boron, chromium, copper, iodine, iron, manganese, molybdenum, nickel, silicon, vanadium, and zinc*. National Academies Press.

Nguyen, P., Leray, V., Diez, M., Serisier, S., Bloc'h, J. L., Siliart, B., & Dumon, H. (2008). Liver lipid metabolism. *JOURNAL OF ANIMAL PHYSIOLOGY AND ANIMAL NUTRITION*, *92*(3), 272-283.

NHMRC. (2006). *Nutrient reference values for Australia and New Zealand. Canberra: NHMRC*. Australian Government Department of Health and Ageing, & New Zealand Ministry of Health. (2006). https://www.eatforhealth.gov.au/nutrient-reference-values/nutrients/chromium

Nie, P., Wang, M., Zhao, Y., Liu, S., Chen, L., & Xu, H. (2021). Protective Effect of Lactobacillus rhamnosus GG on TiO_2 Nanoparticles-Induced Oxidative Stress Damage in the Liver of Young Rats. *Nanomaterials*, *11*(3), 803.

Niu, L., Shao, M., Liu, Y., Hu, J., Li, R., Xie, H., Zhou, L., Shi, L., Zhang, R., & Niu, Y. (2017). Reduction of oxidative damages induced by titanium dioxide nanoparticles correlates with induction of the Nrf2 pathway by GSPE supplementation in mice. *Chemico-biological interactions*, *275*, 133-144.

Nkenda, R., Van Den Neucker, S., Demaegdt, H., Mast, J., & Cheyns, K. (2023). Titanium analyses in food before and after ban of the food additive E171. *Brussels, Belgium: Sciensano*.

NRC., N. R. C. (2002). *Dietary reference intakes for vitamin A, vitamin K, arsenic, boron, chromium, copper, iodine, iron, manganese, molybdenum, nickel, silicon, vanadium, and zinc*. National Academies Press.

NZ Health survey. (2025). *Annual Update of Key Results 2024/25: New Zealand Health Survey*. https://www.health.govt.nz/publications/annual-update-of-key-results-202425-new-zealand-health-survey

Ogunsuyi, O., Ogunsuyi, O., Akanni, O., Alabi, O., Alimba, C., Adaramoye, O., Cambier, S., Eswara, S., Gutleb, A. C., & Bakare, A. (2022). Physiological and histopathological alterations in male Swiss mice after exposure to titanium dioxide (anatase) and zinc oxide nanoparticles and their binary mixture. *Drug and chemical toxicology*, *45*(3), 1188-1213.

Orazizadeh, M., Fakhredini, F., Mansouri, E., & Khorsandi, L. (2014). Effect of glycyrrhizic acid on titanium dioxide nanoparticles-induced hepatotoxicity in rats. *Chemico-biological interactions*, *220*, 214-221.

Orazizadeh, M., OrazizadehKhorsandi, L., Mansouri, E., & Fakhredini, F. (2020). The effect of glycyrrhizin acid on Bax and Bcl2 expression in hepatotoxicity induced by Titanium dioxide

nanoparticles in rats [Article]. *Gastroenterology and Hepatology from Bed to Bench*, *13*(2), 168-176. https://doi.org/10.22037/ghfbb.v13i2.1882

Ortiz, A. E., & Alster, T. S. (2012). Rising concern over cosmetic tattoos. *Dermatologic Surgery*, *38*(3), 424-429.

Papa, G., Di Prisco, G., Spini, G., Puglisi, E., & Negri, I. (2021). Acute and chronic effects of Titanium dioxide (TiO_2) PM1 on honey bee gut microbiota under laboratory conditions. *Scientific Reports*, *11*(1), Article 5946. https://doi.org/10.1038/s41598-021-85153-1

Parrino, F., & Palmisano, L. (2020). *Titanium dioxide (TiO_2) and its applications*. Elsevier.

Patri, A., Umbreit, T., Zheng, J., Nagashima, K., Goering, P., Francke-Carroll, S., Gordon, E., Weaver, J., Miller, T., Sadrieh, N., McNeil, S., & Stratmeyer, M. (2009). Energy dispersive X-ray analysis of titanium dioxide nanoparticle distribution after intravenous and subcutaneous injection in mice. *J Appl Toxicol*, *29*(8), 662-672. https://doi.org/10.1002/jat.1454

Pearson, A., Gibbs, M., Lau, K., Edmonds, J., Alexander, D., & Nicolas, J. (2018). 2016 New Zealand total diet study.

Pedata, P., Ricci, G., Malorni, L., Venezia, A., Cammarota, M., Volpe, M. G., Iannaccone, N., Guida, V., Schiraldi, C., Romano, M., & Iacomino, G. (2019). In vitro intestinal epithelium responses to titanium dioxide nanoparticles. *Food Research International*, *119*, 634-642. https://doi.org/10.1016/j.foodres.2018.10.041

Pei, K., Gui, T., Kan, D., Feng, H., Jin, Y., Yang, Y., Zhang, Q., Du, Z., Gai, Z., Wu, J., & Li, Y. (2020). An Overview of Lipid Metabolism and Nonalcoholic Fatty Liver Disease. *Biomed Res Int*, *2020*, 4020249. https://doi.org/10.1155/2020/4020249

Pele, L. C., Thoree, V., Bruggraber, S. F., Koller, D., Thompson, R. P., Lomer, M. C., & Powell, J. J. (2015). Pharmaceutical/food grade titanium dioxide particles are absorbed into the bloodstream of human volunteers. *Particle and fibre toxicology*, *12*(1), 1-6.

Perez, L., Scarcello, E., Ibouraadaten, S., Yakoub, Y., Leinardi, R., Ambroise, J., Bearzatto, B., Gala, J. L., Paquot, A., Muccioli, G. G., Bouzin, C., van den Brule, S., & Lison, D. (2021). Dietary nanoparticles alter the composition and function of the gut microbiota in mice at dose levels relevant for human exposure. *Food and Chemical Toxicology*, *154*, Article 112352. https://doi.org/10.1016/j.fct.2021.112352

Periasamy, V. S., Athinarayanan, J., Al-Hadi, A. M., Juhaimi, F. A., & Alshatwi, A. A. (2015). Effects of titanium dioxide nanoparticles isolated from confectionery products on the metabolic stress pathway in human lung fibroblast cells. *Archives of Environmental Contamination and Toxicology*, *68*(3), 521-533.

Perry, R. J., Samuel, V. T., Petersen, K. F., & Shulman, G. I. (2014). The role of hepatic lipids in hepatic insulin resistance and type 2 diabetes. *Nature*, *510*(7503), 84-91.

Peters, R. J., van Bemmel, G., Herrera-Rivera, Z., Helsper, H. P., Marvin, H. J., Weigel, S., Tromp, P. C., Oomen, A. G., Rietveld, A. G., & Bouwmeester, H. (2014). Characterization of titanium dioxide nanoparticles in food products: analytical methods to define nanoparticles. *Journal of agricultural and food chemistry*, *62*(27), 6285-6293.

Petković, J., Žegura, B., Stevanović, M., Drnovšek, N., Uskoković, D., Novak, S., & Filipič, M. (2011). DNA damage and alterations in expression of DNA damage responsive genes induced by TiO_2 nanoparticles in human hepatoma HepG2 cells. *Nanotoxicology*, *5*(3), 341-353.

Pflücker, F., Wendel, V., Hohenberg, H., Gärtner, E., Will, T., Pfeiffer, S., Wepf, R., & Gers-Barlag, H. (2001). The human stratum corneum layer: an effective barrier against dermal uptake of

different forms of topically applied micronised titanium dioxide. *Skin Pharmacology and Physiology*, *14*(Suppl. 1), 92-97.

Phillips, D. H., & Arlt, V. M. (2009). Genotoxicity: damage to DNA and its consequences. *Molecular, clinical and environmental toxicology*, 87-110.

Pogribna, M., Koonce, N. A., Mathew, A., Word, B., Patri, A. K., Lyn-Cook, B., & Hammons, G. (2020). Effect of titanium dioxide nanoparticles on DNA methylation in multiple human cell lines. *Nanotoxicology*, *14*(4), 534-553.

Poornima, M. S., Sindhu, G., Billu, A., Sruthi, C. R., Nisha, P., Gogoi, P., Baishya, G., & K, G. R. (2022). Pretreatment of hydroethanolic extract of Dillenia indica L. attenuates oleic acid induced NAFLD in HepG2 cells via modulating SIRT-1/p-LKB-1/AMPK, HMGCR & PPAR-α signaling pathways. *J Ethnopharmacol*, *292*, 115237. https://doi.org/10.1016/j.jep.2022.115237

Praphawatvet, T., Peters, J. I., & Williams, R. O., 3rd. (2020). Inhaled nanoparticles-An updated review. *Int J Pharm*, *587*, 119671. https://doi.org/10.1016/j.ijpharm.2020.119671

Prasad, R. Y., Simmons, S. O., Killius, M. G., Zucker, R. M., Kligerman, A. D., Blackman, C. F., Fry, R. C., & DeMarini, D. M. (2014). Cellular interactions and biological responses to titanium dioxide nanoparticles in HepG2 and BEAS-2B cells: Role of cell culture media. *Environmental and Molecular Mutagenesis*, *55*(4), 336-342.

Proquin, H., Rodríguez-Ibarra, C., Moonen, C. G., Urrutia Ortega, I. M., Briedé, J. J., de Kok, T. M., van Loveren, H., & Chirino, Y. I. (2017). Titanium dioxide food additive (E171) induces ROS formation and genotoxicity: contribution of micro and nano-sized fractions. *Mutagenesis*, *32*(1), 139-149. https://doi.org/10.1093/mutage/gew051

Putra, C., Bello, D., Tucker, K. L., Kelleher, S. L., & Mangano, K. M. (2022). Estimation of Titanium Dioxide Intake by Diet and Stool Assessment among US Healthy Adults. *The Journal of Nutrition*, *152*(6), 1525-1537. https://doi.org/10.1093/jn/nxac061

Radosavljevic, T., Brankovic, M., Samardzic, J., Djuretić, J., Vukicevic, D., Vucevic, D., & Jakovljevic, V. (2024). Altered mitochondrial function in MASLD: key features and promising therapeutic approaches. *Antioxidants*, *13*(8), 906.

Ramoju, S., Andersen, M. E., Nong, A., Karyakina, N., Shilnikova, N., Krishnan, K., & Krewski, D. (2020). Derivation of whole blood biomonitoring equivalents for titanium for the interpretation of biomonitoring data. *Regulatory Toxicology and Pharmacology*, *114*, 104671. https://doi.org/https://doi.org/10.1016/j.yrtph.2020.104671

Ramoju, S., Andersen, M. E., Nong, A., Karyakina, N., Shilnikova, N., Krishnan, K., & Krewski, D. (2020). Derivation of whole blood biomonitoring equivalents for titanium for the interpretation of biomonitoring data. *Regulatory Toxicology and Pharmacology*, *114*, 104671. https://doi.org/https://doi.org/10.1016/j.yrtph.2020.104671

Ramos, M. J., Bandiera, L., Menolascina, F., & Fallowfield, J. A. (2022). In vitro models for non-alcoholic fatty liver disease: Emerging platforms and their applications. *iScience*, *25*(1), 103549. https://doi.org/10.1016/j.isci.2021.103549

Rao, M. S., & Reddy, J. K. (2001). Peroxisomal β-oxidation and steatohepatitis. Seminars in liver disease,

Rashid, M. M., Forte Tavčer, P., & Tomšič, B. (2021). Influence of titanium dioxide nanoparticles on human health and the environment. *Nanomaterials*, *11*(9), 2354.

Rastar, A., Yazdanshenas, M. E., Rashidi, A., & Bidoki, S. M. (2017). Estimation and prediction of optical properties of PA6/TiO2 nanocomposites. *ARABIAN JOURNAL OF CHEMISTRY*, *10*, S219-S224. https://doi.org/https://doi.org/10.1016/j.arabjc.2012.07.025

Raza, S., Rajak, S., Anjum, B., & Sinha, R. A. (2019). Molecular links between non-alcoholic fatty liver disease and hepatocellular carcinoma. *Hepatoma research*, *5*.

Reddy, J. K., & Hashimoto, T. (2001). Peroxisomal β-oxidation and peroxisome proliferator–activated receptor α: an adaptive metabolic system. *Annual review of nutrition*, *21*(1), 193-230.

Reed, R., Schoepf, J., Masles, M., & Westerhoff, P. (2015). Detecting Engineered Nanomaterials in Processed Foods From Australia. *Friends of the Earth*.

Regulation, E. (2012). No 231-2012 on food additives. *Official Journal of the European Union*.

research., G. v. (2024). *Titanium Dioxide Market (2024 - 2030)*. https://www.grandviewresearch.com/industry-analysis/titanium-dioxide-industry

Riazi, K., Azhari, H., Charette, J. H., Underwood, F. E., King, J. A., Afshar, E. E., Swain, M. G., Congly, S. E., Kaplan, G. G., & Shaheen, A.-A. (2022). The prevalence and incidence of NAFLD worldwide: a systematic review and meta-analysis. *The lancet Gastroenterology & hepatology*.

Rodrigues, R. M., Stinckens, M., Ates, G., & Vanhaecke, T. (2023). Neutral red uptake assay to assess cytotoxicity in vitro. In *Cell Viability Assays: Methods and Protocols* (pp. 237-245). Springer.

Rompelberg, C., Heringa, M. B., van Donkersgoed, G., Drijvers, J., Roos, A., Westenbrink, S., Peters, R., van Bemmel, G., Brand, W., & Oomen, A. G. (2016). Oral intake of added titanium dioxide and its nanofraction from food products, food supplements and toothpaste by the Dutch population. *Nanotoxicology*, *10*(10), 1404-1414.

Ropers, M., Terrisse, H., Mercier-Bonin, M., & Humbert, B. (2017). Titanium Dioxide as Food Additive, Application of Titanium Dioxide. *Magdalena Janus, IntechOpen*.

Russwurm, S., Stonans, I., Stonane, E., Weigand, G., Wiederhold, M., Jäger, L., & Reinhart, K. (2002). HepG2 hepatocytes express IFN-γ, TNF-α, TGF-β, M-CSF, oncostatin-M, ICAM-1, IL-4, IL-5, IL-7, IL-10, IL-11, IL-12 and IL-6 receptor genes in vitro. *Critical Care*, *2*(Suppl 1), P005.

Şahin, S., Azarkan, S. Y., & Türksoy, V. A. (2024). Evaluation of the effect of cannabidiol on the THLE-2 liver cell line exposed to lead. *Sci Total Environ*, *923*, 170901. https://doi.org/10.1016/j.scitotenv.2024.170901

SAHPRA. (2025). *Lipitor Patient Information Sheet.* . Retrieved 17 Nov from https://www.sahpra.org.za/wp-content/uploads/2020/04/LIPITOR_PIL_Pfizer_MCC-Format-19-February-2016.pdf,

Sallam, M. F., Ahmed, H. M., Diab, K. A., El-Nekeety, A. A., Abdel-Aziem, S. H., Sharaf, H. A., & Abdel-Wahhab, M. A. (2022a). Improvement of the antioxidant activity of thyme essential oil against biosynthesized titanium dioxide nanoparticles-induced oxidative stress, DNA damage, and disturbances in gene expression in vivo. *Journal of Trace Elements in Medicine and Biology*, *73*, 127024.

Sallam, M. F., Ahmed, H., El-Nekeety, A. A., Diab, K. A., Abdel-Aziem, S. H., Sharaf, H. A., & Abdel-Wahhab, M. A. (2022b). Assessment of the Oxidative Damage and Genotoxicity of Titanium Dioxide Nanoparticles and Exploring the Protective Role of Holy Basil Oil Nanoemulsions in Rats. *Biological Trace Element Research*, 1-16.

Salman, A. S., Al-Shaikh, T. M., Hamza, Z. K., El-Nekeety, A. A., Bawazir, S. S., Hassan, N. S., & Abdel-Wahhab, M. A. (2021). Matlodextrin-cinnamon essential oil nanoformulation as a potent protective against titanium nanoparticles-induced oxidative stress, genotoxicity, and reproductive disturbances in male mice. *Environmental Science and Pollution Research*, *28*(29), 39035-39051.

Samat, M., Ali, A., Taib, M., Hassan, O., & Yahya, M. (2016). Hubbard U calculations on optical properties of 3d transition metal oxide TiO_2. *Results in physics*, *6*, 891-896.

Sampath, A. H. J., Wickramasinghe, N. D., de Silva, K. M. N., & de Silva, R. M. (2023). Methods of extracting TiO_2 and other related compounds from ilmenite. *Minerals, 13*(5), Article 662. https://doi.org/10.3390/min13050662

Sanders, F. W., & Griffin, J. L. (2016). De novo lipogenesis in the liver in health and disease: more than just a shunting yard for glucose. *Biological Reviews*, *91*(2), 452-468.

Sang, X., Zheng, L., Sun, Q., Li, N., Cui, Y., Hu, R., Gao, G., Cheng, Z., Cheng, J., & Gui, S. (2012). The chronic spleen injury of mice following long-term exposure to titanium dioxide nanoparticles. *Journal of Biomedical Materials Research Part A*, *100*(4), 894-902.

Savage, D. B., Choi, C. S., Samuel, V. T., Liu, Z.-X., Zhang, D., Wang, A., Zhang, X.-M., Cline, G. W., Yu, X. X., & Geisler, J. G. (2006). Reversal of diet-induced hepatic steatosis and hepatic insulin resistance by antisense oligonucleotide inhibitors of acetyl-CoA carboxylases 1 and 2. *The Journal of clinical investigation*, *116*(3), 817-824.

Sayes, C. M., Wahi, R., Kurian, P. A., Liu, Y., West, J. L., Ausman, K. D., Warheit, D. B., & Colvin, V. L. (2006). Correlating nanoscale titania structure with toxicity: a cytotoxicity and inflammatory response study with human dermal fibroblasts and human lung epithelial cells. *Toxicol Sci*, *92*(1), 174-185. https://doi.org/10.1093/toxsci/kfj197

Schaudien, D., Hansen, T., Tillmann, T., Pohlmann, G., Kock, H., & Creutzenberg, O. (2025). Comparative toxicity study of three surface-modified titanium dioxide nanoparticles following subacute inhalation. *Particle and fibre toxicology*, *22*(1), 5.

Schindelin, J., Arganda-Carreras, I., Frise, E., Kaynig, V., Longair, M., Pietzsch, T., Preibisch, S., Rueden, C., Saalfeld, S., & Schmid, B. (2012). Fiji: an open-source platform for biological-image analysis. *Nature methods*, *9*(7), 676-682.

Schulz, J., Hohenberg, H., Pflücker, F., Gärtner, E., Will, T., Pfeiffer, S., Wepf, R., Wendel, V., Gers-Barlag, H., & Wittern, K.-P. (2002). Distribution of sunscreens on skin. *Advanced drug delivery reviews*, *54*, S157-S163.

Schwab, N. V., Da-Col, J. A., Terra, J., & Bueno, M. I. (2012). Fast direct determination of titanium dioxide in toothpastes by X-Ray fluorescence and multivariate calibration. *Journal of the Brazilian Chemical Society*, *23*, 546-554.

Sefried, S., Häring, H. U., Weigert, C., & Eckstein, S. S. (2018). Suitability of hepatocyte cell lines HepG2, AML12 and THLE-2 for investigation of insulin signalling and hepatokine gene expression. *Open Biol*, *8*(10). https://doi.org/10.1098/rsob.180147

Servier Canada Inc. (2016). *Product monograph for perindopril arginine film-coated tablets 2.5 mg, 5 mg and 10 mg and perindopril arginine orodispersible tablets 2.5 mg, 5 mg and 10 mg.* Retrieved 17 Nov from https://pdf.hres.ca/dpd_pm/00037213.PDF

Sha, B., Gao, W., Wang, S., Xu, F., & Lu, T. (2011). Cytotoxicity of titanium dioxide nanoparticles differs in four liver cells from human and rat. Composites Part B: Engineering,

Shahmoradi, S. S., Salehzadeh, A., Ranji, N., & Habibollahi, H. (2023). Trigger of apoptosis in human liver cancer cell line (HepG2) by titanium dioxide nanoparticles functionalized by glutamine and conjugated with thiosemicarbazone. *3 Biotech*, *13*(6), 195. https://doi.org/10.1007/s13205-023-03609-9

Shajari, Z., Golestani, A., & Nowrouzi, A. (2021). Acute cytotoxic effects of Titanium dioxide (TiO2) and chronic exposure to safe dose of nanoparticle on Hepatocarcinoma cell line (HepG2). *Nanomedicine Research Journal*, *6*(3), 269-278.

Shakeel, M., Jabeen, F., Iqbal, R., Chaudhry, A. S., Zafar, S., Ali, M., Khan, M. S., Khalid, A., Shabbir, S., & Asghar, M. S. (2018). Assessment of titanium dioxide nanoparticles (TiO_2 -NPs) induced

hepatotoxicity and ameliorative effects of Cinnamomum cassia in Sprague-Dawley rats. *Biological Trace Element Research*, *182*(1), 57-69.

Shakeel, M., Jabeen, F., Qureshi, N. A., & Fakhr, E. A. M. (2016). Toxic Effects of Titanium Dioxide Nanoparticles and Titanium Dioxide Bulk Salt in the Liver and Blood of Male Sprague-Dawley Rats Assessed by Different Assays. *Biol Trace Elem Res*, *173*(2), 405-426. https://doi.org/10.1007/s12011-016-0677-4

Shang, J., Yan, J., Lou, H., Shou, R., Zhan, Y., Lu, X., & Fan, X. (2024). Genome-wide DNA methylation sequencing reveals the involvement of ferroptosis in hepatotoxicity induced by dietary exposure to food-grade titanium dioxide. *Part Fibre Toxicol*, *21*(1), 37. https://doi.org/10.1186/s12989-024-00598-2

Sharma, J., Al-Omran, A., & Parvathy, S. (2007). Role of nitric oxide in inflammatory diseases. *Inflammopharmacology*, *15*(6), 252-259.

Shi, H., Magaye, R., Castranova, V., & Zhao, J. (2013). Titanium dioxide nanoparticles: a review of current toxicological data. *Part Fibre Toxicol*, *10*, 15. https://doi.org/10.1186/1743-8977-10-15

Shi, H., Magaye, R., Castranova, V., & Zhao, J. (2013). Titanium dioxide nanoparticles: a review of current toxicological data. *Particle and fibre toxicology*, *10*(1), 1-33.

Shi, J. Q., Ma, Y., Zhang, Y., Chen, Z. J., & Jia, G. (2023). [Effects of titanium dioxide nanoparticles on circRNA expression profiles in human hepatocellular carcinoma cells HepG2]. *Beijing Da Xue Xue Bao Yi Xue Ban*, *55*(3), 392-399. https://doi.org/10.19723/j.issn.1671-167X.2023.03.002

Shi, J., Ma, Y., Yu, N., Zhang, Y., Cao, Z., Guan, L., Liu, X., Chen, Z., & Jia, G. (2025). Key toxic pathways of hepatotoxicity induced by titanium dioxide nanoparticles through multi-omics analysis. *Food Chem Toxicol*, *201*, 115457. https://doi.org/10.1016/j.fct.2025.115457

Shinohara, N., Danno, N., Ichinose, T., Sasaki, T., Fukui, H., Honda, K., & Gamo, M. (2014). Tissue distribution and clearance of intravenously administered titanium dioxide (TiO_2) nanoparticles. *Nanotoxicology*, *8*(2), 132-141. https://doi.org/10.3109/17435390.2012.763001

Shiratori, Y., Ohmura, K., Hikiba, Y., Matsumura, M., Nagura, T., Okano, K. I., Kamii, K., & Omata, M. (1998). Hepatocyte nitric oxide production is induced by Kupffer cells. *Digestive diseases and sciences*, *43*(8), 1737-1745.

Shirdare, M., Jabbari, F., Salehzadeh, M., Ziamajidi, N., Nourian, A., Heidarisasan, S., Ghavimishamekh, A., Azandariani, M. T., & Abbasalipourkabir, R. (2022). Curcuma reduces kidney and liver damage induced by titanium dioxide nanoparticles in male Wistar rats [Article]. *Avicenna Journal of Phytomedicine*, *12*(5), 537-547. https://doi.org/10.22038/AJP.2021.53346.2727

Shrivastava, R., Raza, S., Yadav, A., Kushwaha, P., & Flora, S. J. S. (2014). Effects of sub-acute exposure to TiO_2, ZnO and Al2O3 nanoparticles on oxidative stress and histological changes in mouse liver and brain. *Drug and chemical toxicology*, *37*(3), 336-347. https://doi.org/10.3109/01480545.2013.866134

Shukla, R. K., Kumar, A., Gurbani, D., Pandey, A. K., Singh, S., & Dhawan, A. (2013). TiO_2 nanoparticles induce oxidative DNA damage and apoptosis in human liver cells. *Nanotoxicology*, *7*(1), 48-60.

Shukla, R. K., Kumar, A., Vallabani, N. V., Pandey, A. K., & Dhawan, A. (2014). Titanium dioxide nanoparticle-induced oxidative stress triggers DNA damage and hepatic injury in mice. *Nanomedicine (Lond)*, *9*(9), 1423-1434. https://doi.org/10.2217/nnm.13.100

Silvestrini, A., Meucci, E., Ricerca, B. M., & Mancini, A. (2023). Total antioxidant capacity: biochemical aspects and clinical significance. *International Journal of Molecular Sciences*, *24*(13), 10978.

Simon-Deckers, A., Gouget, B., Mayne-L'hermite, M., Herlin-Boime, N., Reynaud, C., & Carrière, M. (2008). In vitro investigation of oxide nanoparticle and carbon nanotube toxicity and intracellular accumulation in A549 human pneumocytes. *Toxicology*, *253*(1-3), 137-146. https://doi.org/10.1016/j.tox.2008.09.007

Siwulski, M., Budka, A., Budzyńska, S., Gąsecka, M., Kalač, P., Niedzielski, P., & Mleczek, M. (2021). Mineral composition of traditional and organic-cultivated mushroom Lentinula edodes in Europe and Asia–Similar or different? *LWT*, *147*, 111570.

Skipitari, M., Kalaitzopoulou, E., Papadea, P., Varemmenou, A., Gavriil, V. E., Sarantopoulou, E., Cefalas, A.-C., Tsakas, S., Rosmaraki, E., & Margiolaki, I. (2023). Titanium dioxide nanoparticle-based hydroxyl and superoxide radical production for oxidative stress biological simulations. *Journal of Photochemistry and Photobiology A: Chemistry*, *435*, 114290.

Skocaj, M., Filipic, M., Petkovic, J., & Novak, S. (2011). Titanium dioxide in our everyday life; is it safe? *RADIOLOGY AND ONCOLOGY*, *45*(4), 227.

Smajis, S., Gajdošík, M., Pfleger, L., Traussnigg, S., Kienbacher, C., Halilbasic, E., Ranzenberger-Haider, T., Stangl, A., Beiglböck, H., & Wolf, P. (2020). Metabolic effects of a prolonged, very-high-dose dietary fructose challenge in healthy subjects. *The American journal of clinical nutrition*, *111*(2), 369-377.

Smith, C., Parnell, W., & Blakey, C. (2017). Simulated typical diets for use in the 2016 New Zealand Total Diet Study. *Report Prepared for Ministry for Primary Industries*.

Song, B., Zhou, T., Yang, W., Liu, J., & Shao, L. (2016). Contribution of oxidative stress to TiO_2 nanoparticle-induced toxicity. *Environmental Toxicology and Pharmacology*, *48*, 130-140.

Spadaro, L., Magliocco, O., Spampinato, D., Piro, S., Oliveri, C., Alagona, C., Papa, G., Rabuazzo, A. M., & Purrello, F. (2008). Effects of n-3 polyunsaturated fatty acids in subjects with nonalcoholic fatty liver disease. *Dig Liver Dis*, *40*(3), 194-199. https://doi.org/10.1016/j.dld.2007.10.003

Spahis, S., Delvin, E., Borys, J.-M., & Levy, E. (2017). Oxidative stress as a critical factor in nonalcoholic fatty liver disease pathogenesis. *Antioxidants & redox signaling*, *26*(10), 519-541.

Sprong, C., Bakker, M., Niekerk, M., & Vennemann, M. (2016). Exposure assessment of the food additive titanium dioxide (E 171) based on use levels provided by the industry.

Stefan, N., Staiger, H., & Häring, H.-U. (2011). Dissociation between fatty liver and insulin resistance: the role of adipose triacylglycerol lipase. *Diabetologia*, *54*, 7-9.

Steinberg, G. R., Valvano, C. M., De Nardo, W., & Watt, M. J. (2025). Integrative metabolism in MASLD and MASH: pathophysiology and emerging mechanisms. *Journal of hepatology*.

Styles, R. (2024). *How we got a supermarket duopoly. Article for Consumer New Zealand*. Retrieved 10 june from https://www.consumer.org.nz/articles/how-we-got-a-supermarket-duopoly

Su, H., Song, X., Li, J., Iqbal, M. Z., Kenston, S. S. F., Li, Z., Wu, A., Ding, M., & Zhao, J. (2018). Biosafety evaluation of Janus Fe(3)O(4)-TiO(2) nanoparticles in Sprague Dawley rats after intravenous injection. *Int J Nanomedicine*, *13*, 6987-7001. https://doi.org/10.2147/ijn.S167851

Su, L.-J., Zhang, J.-H., Gomez, H., Murugan, R., Hong, X., Xu, D., Jiang, F., & Peng, Z.-Y. (2019). Reactive oxygen species-induced lipid peroxidation in apoptosis, autophagy, and ferroptosis. *Oxidative Medicine and Cellular Longevity*, *2019*(1), 5080843.

Suker, D. K., & Jasim, F. A. (2018). Liver histopathological alteration after repeated intra-tracheal instillation of titanium dioxide in male rats. *Gastroenterology and Hepatology from Bed to Bench*, *11*(2), 159.

Sul, Y. T. (2010). Electrochemical growth behavior, surface properties, and enhanced in vivo bone response of TiO_2 nanotubes on microstructured surfaces of blasted, screw-shaped titanium implants. *Int J Nanomedicine*, *5*, 87-100. https://doi.org/10.2147/ijn.s8012

Sun, T., Kang, Y., Liu, J., Zhang, Y., Ou, L., Liu, X., Lai, R., & Shao, L. (2021). Nanomaterials and hepatic disease: toxicokinetics, disease types, intrinsic mechanisms, liver susceptibility, and influencing factors. *J Nanobiotechnology*, *19*(1), 108. https://doi.org/10.1186/s12951-021-00843-2

Sungur, Ş., Kaya, P., & Koroglu, M. (2020). Determination of titanium dioxide nanoparticles used in various foods. *Food Additives & Contaminants: Part B*, *13*(4), 260-267. https://doi.org/10.1080/19393210.2020.1769193

Sunshine, H., & Iruela-Arispe, M. L. (2017). Membrane lipids and cell signaling. *Current opinion in lipidology*, *28*(5), 408-413.

Survey., U. S. G. (2025). *Titanium Statistics and Information. U.S. Department of the Interior.* Retrieved 17 NOV from https://www.usgs.gov/centers/national-minerals-information-center/titanium-statistics-and-information

Syed-Abdul, M. M. (2023). Lipid metabolism in metabolic-associated steatotic liver disease (MASLD). *METABOLITES*, *14*(1), 12.

Takahara, I., Akazawa, Y., Tabuchi, M., Matsuda, K., Miyaaki, H., Kido, Y., Kanda, Y., Taura, N., Ohnita, K., Takeshima, F., Sakai, Y., Eguchi, S., Nakashima, M., & Nakao, K. (2017). Toyocamycin attenuates free fatty acid-induced hepatic steatosis and apoptosis in cultured hepatocytes and ameliorates nonalcoholic fatty liver disease in mice. *PLoS One*, *12*(3), e0170591. https://doi.org/10.1371/journal.pone.0170591

Talamini, L., Gimondi, S. R., Violatto, M. B., Fiordaliso, F., Pedica, F., Tran, N. L., Sitia, G., Aureli, F., Raggi, A., Nelissen, I., Cubadda, F., Bigini, P., & Diomede, L. (2019). Repeated administration of the food additive E171 to mice results in accumulation in intestine and liver and promotes an inflammatory status. *Nanotoxicology*, *13*(8), 1087-1101. https://doi.org/10.1080/17435390.2019.1640910

Talbot, P., Radziwill-Bienkowska, J. M., Kamphuis, J. B. J., Steenkeste, K., Bettini, S., Robert, V., Noordine, M. L., Mayeur, C., Gaultier, E., Langella, P., Robbe-Masselot, C., Houdeau, E., Thomas, M., & Mercier-Bonin, M. (2018). Food-grade TiO(2) is trapped by intestinal mucus in vitro but does not impair mucin O-glycosylation and short-chain fatty acid synthesis in vivo: implications for gut barrier protection. *J Nanobiotechnology*, *16*(1), 53. https://doi.org/10.1186/s12951-018-0379-5

Targher, G., Byrne, C. D., & Tilg, H. (2024). MASLD: a systemic metabolic disorder with cardiovascular and malignant complications. *Gut*, *73*(4), 691-702.

Targher, G., Lonardo, A., & Byrne, C. D. (2018). Nonalcoholic fatty liver disease and chronic vascular complications of diabetes mellitus. *Nature reviews endocrinology*, *14*(2), 99-114.

Targher, G., Marchesini, G., & Byrne, C. (2016). Risk of type 2 diabetes in patients with non-alcoholic fatty liver disease: causal association or epiphenomenon? *Diabetes & metabolism*, *42*(3), 142-156.

Tassinari, R., Tammaro, A., Martinelli, A., Valeri, M., & Maranghi, F. (2023). Sex-Specific Effects of Short-Term Oral Administration of Food-Grade Titanium Dioxide Nanoparticles in the Liver and Kidneys of Adult Rats. *Toxics*, *11*(9). https://doi.org/10.3390/toxics11090776

TDMA, T. D. M. A. (2022). *EU's withdrawal of E171 approval moves ahead despite confirmations of its safety by authorities around the globe*. Retrieved 09 December from

https://www.tdma.info/news/eus-withdrawal-of-e171-approval-moves-ahead-despite-confirmations-of-its-safety-by-authorities-around-the-globe

Teixeira, F. S., Pimentel, L. L., Vidigal, S. S., Azevedo-Silva, J., Pintado, M. E., & Rodríguez-Alcalá, L. M. (2023). Differential lipid accumulation on HepG2 cells triggered by palmitic and linoleic fatty acids exposure. *MOLECULES*, *28*(5), 2367.

Teubl, B. J., Leitinger, G., Schneider, M., Lehr, C. M., Frohlich, E., Zimmer, A., & Roblegg, E. (2015a). The buccal mucosa as a route for TiO_2 nanoparticle uptake. *Nanotoxicology*, *9*(2), 253-261. https://doi.org/10.3109/17435390.2014.921343

Teubl, B. J., Schimpel, C., Leitinger, G., Bauer, B., Frohlich, E., Zimmer, A., & Roblegg, E. (2015b). Interactions between nano-TiO_2 and the oral cavity: Impact of nanomaterial surface hydrophilicity/hydrophobicity. *Journal of Hazardous Materials*, *286*, 298-305. https://doi.org/10.1016/j.jhazmat.2014.12.064

Tolosa, L., Gómez-Lechón, M. J., Jiménez, N., Hervás, D., Jover, R., & Donato, M. T. (2016). Advantageous use of HepaRG cells for the screening and mechanistic study of drug-induced steatosis. *Toxicol Appl Pharmacol*, *302*, 1-9. https://doi.org/10.1016/j.taap.2016.04.007

Trebolazabala, J., Maguregui, M., Morillas, H., García-Fernandez, Z., de Diego, A., & Madariaga, J. M. (2017). Uptake of metals by tomato plants (Solanum lycopersicum) and distribution inside the plant: field experiments in Biscay (Basque Country). *Journal of Food Composition and Analysis*, *59*, 161-169.

Uribe-García, A., Medina-Reyes, E. I., Flores-Reyes, C. A., Zagal-Salinas, A. A., Ispanixtlahuatl-Meraz, O., Delgado-Armenta, E., Santibáñez-Andrade, M., Flores, C. M., Sánchez-Pérez, Y., García-Cuéllar, C. M., & Chirino, Y. I. (2025). Food grade titanium dioxide induced endoplasmic reticulum stress in colon cells: Comparison between normal and colorectal carcinoma cells. *Toxicol In Vitro*, *102*, 105957. https://doi.org/10.1016/j.tiv.2024.105957

Urrutia-Ortega, I. M., Garduno-Balderas, L. G., Delgado-Buenrostro, N. L., Freyre-Fonseca, V., Flores-Flores, J. O., Gonzalez-Robles, A., Pedraza-Chaverri, J., Hernandez-Pando, R., Rodriguez-Sosa, M., Leon-Cabrera, S., Terrazas, L. I., van Loveren, H., & Chirino, Y. I. (2016). Food-grade titanium dioxide exposure exacerbates tumor formation in colitis associated cancer model. *Food and Chemical Toxicology*, *93*, 20-31. https://doi.org/10.1016/j.fct.2016.04.014

US Geological Survey. (2025). *Titanium Statistics and Information. U.S. Department of the Interior.* Retrieved 17 NOV from https://www.usgs.gov/centers/national-minerals-information-center/titanium-statistics-and-information

USFDA. (2016). *US Food and Drug Administration regulation on Titanium dioxide. Code of Federal Regulations Title 21, Section 73.575.*

USFDA. (2024). *Highlights of Prescribing Information Sheet for Lipitor (atorvastatin calcium) tablets, for oral use.* Retrieved 17 Nov from https://www.accessdata.fda.gov/drugsatfda_docs/label/2024/020702s081lbl.pdf

Vacca, M., Kamzolas, I., Harder, L. M., Oakley, F., Trautwein, C., Hatting, M., Ross, T., Bernardo, B., Oldenburger, A., Hjuler, S. T., Ksiazek, I., Lindén, D., Schuppan, D., Rodriguez-Cuenca, S., Tonini, M. M., Castañeda, T. R., Kannt, A., Rodrigues, C. M. P., Cockell, S., Govaere, O., Daly, A. K., Allison, M., Honnens de Lichtenberg, K., Kim, Y. O., Lindblom, A., Oldham, S., Andréasson, A. C., Schlerman, F., Marioneaux, J., Sanyal, A., Afonso, M. B., Younes, R., Amano, Y., Friedman, S. L., Wang, S., Bhattacharya, D., Simon, E., Paradis, V., Burt, A., Grypari, I. M., Davies, S., Driessen, A., Yashiro, H., Pors, S., Worm Andersen, M., Feigh, M., Yunis, C., Bedossa, P., Stewart, M., Cater, H. L., Wells, S., Schattenberg, J. M., Anstee, Q. M., Tiniakos, D., Perfield, J. W., Petsalaki, E., Davidsen, P., & Vidal-Puig, A. (2024). An unbiased ranking of murine dietary models based

on their proximity to human metabolic dysfunction-associated steatotic liver disease (MASLD). *Nat Metab*, *6*(6), 1178-1196. https://doi.org/10.1038/s42255-024-01043-6

Vacca, M., Leslie, J., Virtue, S., Lam, B. Y., Govaere, O., Tiniakos, D., Snow, S., Davies, S., Petkevicius, K., & Tong, Z. (2020). Bone morphogenetic protein 8B promotes the progression of non-alcoholic steatohepatitis. *Nature Metabolism*, *2*(6), 514-531.

Valdiglesias, V., Costa, C., Sharma, V., Kiliç, G., Pásaro, E., Teixeira, J. P., Dhawan, A., & Laffon, B. (2013). Comparative study on effects of two different types of titanium dioxide nanoparticles on human neuronal cells. *Food and Chemical Toxicology*, *57*, 352-361.

Valentini, X., Rugira, P., Frau, A., Tagliatti, V., Conotte, R., Laurent, S., Colet, J. M., & Nonclercq, D. (2019). Hepatic and Renal Toxicity Induced by TiO(2) Nanoparticles in Rats: A Morphological and Metabonomic Study. *J Toxicol*, *2019*, 5767012. https://doi.org/10.1155/2019/5767012

Verleysen, E., Brassinne, F., Van Steen, F., Waegeneers, N., Cheyns, K., Machiels, R., Mathioudaki, S., Jimenez, I. O., Ledecq, M., & Mast, J. (2022b). Towards a generic protocol for measuring the constituent particle size distribution of E171 in food by electron microscopy. *Food Control*, *132*, 108492.

Verleysen, E., Ledecq, M., Siciliani, L., Cheyns, K., Vleminckx, C., Blaude, M.-N., De Vos, S., Brassinne, F., Van Steen, F., Nkenda, R., Machiels, R., Waegeneers, N., Van Loco, J., & Mast, J. (2022a). Titanium dioxide particles frequently present in face masks intended for general use require regulatory control. *Scientific Reports*, *12*(1), 2529. https://doi.org/10.1038/s41598-022-06605-w

Verleysen, E., Waegeneers, N., Brassinne, F., De Vos, S., Jimenez, I. O., Mathioudaki, S., & Mast, J. (2020). Physicochemical Characterization of the Pristine E171 Food Additive by Standardized and Validated Methods. *Nanomaterials (Basel)*, *10*(3). https://doi.org/10.3390/nano10030592

Vesković, M., Šutulović, N., Hrnčić, D., Stanojlović, O., Macut, D., & Mladenović, D. (2023). The interconnection between hepatic insulin resistance and metabolic dysfunction-associated steatotic liver disease—the transition from an adipocentric to liver-centric approach. *Current Issues in Molecular Biology*, *45*(11), 9084-9102.

Vincent, J. B. (2010). Chromium: celebrating 50 years as an essential element? *Dalton Transactions*, *39*(16), 3787-3794.

Vincent, J. B. (2013). Chromium: is it essential, pharmacologically relevant, or toxic? *Interrelations between essential metal ions and human diseases*, 171-198.

Wang, H., Ni, J., Guo, X., Zhou, T., Ma, X., Xue, J., & Wang, X. (2018). Shelterin differentially respond to oxidative stress induced by TiO_2 -NPs and regulate telomere length in human hepatocytes and hepatocarcinoma cells in vitro. *Biochemical and biophysical research communications*, *503*(2), 697-702.

Wang, J. X., Zhou, G. Q., Chen, C. Y., Yu, H. W., Wang, T. C., Ma, Y. M., Jia, G., Gao, Y. X., Li, B., Sun, J., Li, Y. F., Jiao, F., Zhao, Y. L., & Chai, Z. F. (2007). Acute toxicity and biodistribution of different sized titanium dioxide particles in mice after oral administration. *Toxicology Letters*, *168*(2), 176-185. https://doi.org/10.1016/j.toxlet.2006.12.001

Wang, K., Hao, Z., Ma, L., Zhang, W., Mo, J., Li, L., & Jin, C. (2024). Nrf2-dependent hepatoprotective effect of ellagic acid in titanium dioxide nanoparticles-induced liver injury. *Phytomedicine*, *135*, 156064.

Wang, L., Wang, Q., Xiong, Y., Shi, W., & Qi, X. (2025). Obesity and its comorbidities: current treatment options, emerging biological mechanisms, future perspectives and challenges. *Diabetes, Metabolic Syndrome and Obesity*, 3427-3445.

Wang, X., Xie, H., Wang, P., & Yin, H. (2023). Nanoparticles in plants: uptake, transport and physiological activity in leaf and root. *Materials*, *16*(8), 3097.

Wang, Y., Chen, C., Chen, J., Sang, T., Peng, H., Lin, X., Zhao, Q., Chen, S., Eling, T., & Wang, X. (2022). Overexpression of NAG-1/GDF15 prevents hepatic steatosis through inhibiting oxidative stress-mediated dsDNA release and AIM2 inflammasome activation. *Redox Biol*, *52*, 102322. https://doi.org/10.1016/j.redox.2022.102322

Wang, Y., Chen, Z., Ba, T., Pu, J., Chen, T., Song, Y., Gu, Y., Qian, Q., Xu, Y., Xiang, K., Wang, H., & Jia, G. (2013). Susceptibility of young and adult rats to the oral toxicity of titanium dioxide nanoparticles. *Small*, *9*(9-10), 1742-1752. https://doi.org/10.1002/smll.201201185

Wang, Y., Chen, Z., Ba, T., Pu, J., Gu, Y., Guo, J., & Jia, G. (2014). [Genotoxic effects of oral-exposed TiO_2 nanoparticles on bone marrow cells in young rats]. *Zhonghua Yu Fang Yi Xue Za Zhi*, *48*(9), 815-818.

Wang, Y., Cui, H., Zhou, J., Li, F., Wang, J., Chen, M., & Liu, Q. (2015). Cytotoxicity, DNA damage, and apoptosis induced by titanium dioxide nanoparticles in human non-small cell lung cancer A549 cells. *Environmental Science and Pollution Research*, *22*(7), 5519-5530.

Warheit, D. B. (2024). Safety of titanium dioxide (E171) as a food additive for humans. *Front Toxicol*, *6*, 1333746. https://doi.org/10.3389/ftox.2024.1333746

Warheit, D. B., & Brown, S. C. (2019). What is the impact of surface modifications and particle size on commercial titanium dioxide particle samples? – A review of in vivo pulmonary and oral toxicity studies – Revised 11-6-2018 [Short survey]. *Toxicology Letters*, *302*, 42-59. https://doi.org/10.1016/j.toxlet.2018.11.008

Warheit, D. B., Webb, T. R., Reed, K. L., Frerichs, S., & Sayes, C. M. (2007). Pulmonary toxicity study in rats with three forms of ultrafine-TiO_2 particles: differential responses related to surface properties. *Toxicology*, *230*(1), 90-104. https://doi.org/10.1016/j.tox.2006.11.002

Warheit, D., Reed, K., & Webb, T. (2003). Pulmonary toxicity studies in rats with triethoxyoctylsilane (OTES)-coated, pigment-grade titanium dioxide particles: bridging studies to predict inhalation hazard. *Experimental Lung Research*, *29*(8), 593-606.

Waseem, M., Kaushik, P., Dutta, S., Chakraborty, R., Hassan, M. I., & Parvez, S. (2022). Modulatory Role of Quercetin in Mitochondrial Dysfunction in Titanium Dioxide Nanoparticle-Induced Hepatotoxicity. *ACS omega*, *7*(4), 3192-3202.

Wasim, M., Tariq, A., Qureshi, R. N., & Shafique, M. A. (2023). Characterization of toothpastes for fluorine and other elements by INAA and ICP-OES. *Radiochimica Acta*, *111*(2), 129-136.

Watt, M. J., Miotto, P. M., De Nardo, W., & Montgomery, M. K. (2019). The Liver as an Endocrine Organ-Linking NAFLD and Insulin Resistance. *Endocr Rev*, *40*(5), 1367-1393. https://doi.org/10.1210/er.2019-00034

Weir, A., Westerhoff, P., Fabricius, L., Hristovski, K., & von Goetz, N. (2012). Titanium Dioxide Nanoparticles in Food and Personal Care Products. *Environmental Science & Technology*, *46*(4), 2242-2250. https://doi.org/10.1021/es204168d

Wells, C., Pogribna, M., Sharmah, A., Paredes, A., Word, B., Patri, A. K., Lyn-Cook, B., & Hammons, G. (2024). Exposure to a Titanium Dioxide Product Alters DNA Methylation in Human Cells. *Nanomaterials (Basel)*, *14*(24). https://doi.org/10.3390/nano14242037

Wu, J. H., Liu, W., Xue, C. B., Zhou, S. C., Lan, F. L., Bi, L., Xu, H. B., Yang, X. L., & Zeng, F. D. (2009). Toxicity and penetration of TiO_2 nanoparticles in hairless mice and porcine skin after subchronic dermal exposure. *Toxicology Letters*, *191*(1), 1-8. https://doi.org/10.1016/j.toxlet.2009.05.020

Wu, Y., Zhang, H., Liu, G., Zhang, J., Wang, J., Yu, Y., & Lu, S. (2016). Concentrations and health risk assessment of trace elements in animal-derived food in southern China. *Chemosphere*, *144*, 564-570.

Xia, M.-C., Du, Y., Zhang, S., Feng, J., & Luo, K. (2022). Differences in multielement concentrations in rice (Oryza sativa L.) between longevity and non-longevity areas in China and their relations with lifespan indicators. *Food Research International*, *162*, 112056.

Xia, Z., He, J., Li, B., He, K., Yang, W., Chen, X., Zhang, J., & Xiang, G. (2018). Titanium dioxide nanoparticles induce mitochondria-associated apoptosis in HepG2 cells. *RSC advances*, *8*(55), 31764-31776.

Xie, G. P., Wang, C., Sun, J., & Zhong, G. R. (2011). Tissue distribution and excretion of intravenously administered titanium dioxide nanoparticles. *Toxicology Letters*, *205*(1), 55-61. https://doi.org/10.1016/j.toxlet.2011.04.034

Xu, Q., Chen, Y., Zhang, H., Zhou, K., Zhao, Y., Deng, W., Wang, Z., Guo, L., Liu, H., & Ren, Z. (2025). CDKN1A and EGR1 are key genes for endoplasmic reticulum stress-induced ferroptosis in MASH. *Free Radical Biology and Medicine*.

Yamada, S., Ogawa, H., Funato, M., Kato, M., Nakadate, K., Mizukoshi, T., Kawakami, K., Kobayashi, R., Horii, T., & Hatada, I. (2025). Induction of MASH-like pathogenesis in the Nwd1−/− mouse liver. *Communications Biology*, *8*(1), 348.

Yamashita, H., Takenoshita, M., Sakurai, M., Bruick, R. K., Henzel, W. J., Shillinglaw, W., Arnot, D., & Uyeda, K. (2001). A glucose-responsive transcription factor that regulates carbohydrate metabolism in the liver. *Proceedings of the National Academy of Sciences*, *98*(16), 9116-9121.

Yang, J., Luo, M., Tan, Z., Dai, M., Xie, M., Lin, J., Hua, H., Ma, Q., Zhao, J., & Liu, A. (2017). Oral administration of nano-titanium dioxide particle disrupts hepatic metabolic functions in a mouse model. *Environmental Toxicology and Pharmacology*, *49*, 112-118.

Yang, W., Peters, J. I., & Williams, R. O., 3rd. (2008). Inhaled nanoparticles--a current review. *Int J Pharm*, *356*(1-2), 239-247. https://doi.org/10.1016/j.ijpharm.2008.02.011

Yang, Y., Doudrick, K., Bi, X., Hristovski, K., Herckes, P., Westerhoff, P., & Kaegi, R. (2014). Characterization of food-grade titanium dioxide: the presence of nanosized particles. *Environmental Science & Technology*, *48*(11), 6391-6400.

Yeo, S.-H., Noh, J.-R., Kim, Y.-H., Gang, G.-T., Kim, S.-W., Kim, K.-S., Hwang, J. H., Shong, M., & Lee, C.-H. (2013). Increased vulnerability to β-cell destruction and diabetes in mice lacking NAD (P) H: quinone oxidoreductase 1. *Toxicology Letters*, *219*(1), 35-41.

Yin, Z. F., Wu, L., Yang, H. G., & Su, Y. H. (2013). Recent progress in biomedical applications of titanium dioxide. *Phys Chem Chem Phys*, *15*(14), 4844-4858. https://doi.org/10.1039/c3cp43938k

Younes, M., Aggett, P., Aguilar, F., Crebelli, R., Dusemund, B., Filipič, M., Frutos, M. J., Galtier, P., & Gott, D. (2018). Evaluation of four new studies on the potential toxicity of titanium dioxide used as a food additive (E 171). *Efsa Journal*, *16*(7), e05366.

Younes, M., Aquilina, G., Castle, L., Engel, K. H., Fowler, P., Frutos Fernandez, M. J., Fürst, P., Gundert-Remy, U., Gürtler, R., Husøy, T., Manco, M., Mennes, W., Moldeus, P., Passamonti, S., Shah, R., Waalkens-Berendsen, I., Wölfle, D., Corsini, E., Cubadda, F., De Groot, D., FitzGerald, R., Gunnare, S., Gutleb, A. C., Mast, J., Mortensen, A., Oomen, A., Piersma, A., Plichta, V., Ulbrich, B., Van Loveren, H., Benford, D., Bignami, M., Bolognesi, C., Crebelli, R., Dusinska, M., Marcon, F., Nielsen, E., Schlatter, J., Vleminckx, C., Barmaz, S., Carfí, M., Civitella, C., Giarola, A., Rincon, A. M., Serafimova, R., Smeraldi, C., Tarazona, J., Tard, A., & Wright, M. (2021). Safety assessment of titanium dioxide (E171) as a food additive. *Efsa j*, *19*(5), e06585. https://doi.org/10.2903/j.efsa.2021.6585

Younossi, Z. M., Golabi, P., de Avila, L., Paik, J. M., Srishord, M., Fukui, N., Qiu, Y., Burns, L., Afendy, A., & Nader, F. (2019). The global epidemiology of NAFLD and NASH in patients with type 2 diabetes: a systematic review and meta-analysis. *Journal of hepatology*, *71*(4), 793-801.

Younossi, Z. M., Golabi, P., Paik, J. M., Henry, A., Van Dongen, C., & Henry, L. (2023). The global epidemiology of nonalcoholic fatty liver disease (NAFLD) and nonalcoholic steatohepatitis (NASH): a systematic review. *Hepatology*, *77*(4), 1335-1347.

Younossi, Z. M., Golabi, P., Price, J. K., Owrangi, S., Gundu-Rao, N., Satchi, R., & Paik, J. M. (2024). The global epidemiology of nonalcoholic fatty liver disease and nonalcoholic steatohepatitis among patients with type 2 diabetes. *Clinical Gastroenterology and Hepatology*, *22*(10), 1999-2010. e1998.

Younossi, Z. M., Zelber-Sagi, S., Lazarus, J. V., Wong, V. W., Yilmaz, Y., Duseja, A., Eguchi, Y., Castera, L., Pessoa, M. G., Oliveira, C. P., El-Kassas, M., Tsochatzis, E., Fan, J. G., Spearman, C. W., Tacke, F., Castellanos Fernandez, M. I., Alkhouri, N., Schattenberg, J. M., Romero-Gómez, M., Noureddin, M., Allen, A. M., Ong, J. P., Roberts, S. K., Shubrook, J. H., Burra, P., Kohli, R., Kautz, A., Holleboom, A. G., Lam, B., Isaacs, S., Macedo, P., Gastaldelli, A., Henry, L., Ivancovsky-Wajcman, D., Nader, F., de Avila, L., Price, J. K., Mark, H. E., Villota-Rivas, M., Barberá, A., Kalligeros, M., Gerber, L. H., & Alqahtani, S. A. (2025). Global Consensus Recommendations for Metabolic Dysfunction-Associated Steatotic Liver Disease and Steatohepatitis. *Gastroenterology*, *169*(5), 1017-1032.e1012. https://doi.org/10.1053/j.gastro.2025.02.044

Yu, N., Shi, J., Ma, Y., Zhang, Y., Guan, L., Chen, Z., & Jia, G. (2025). Absolute quantitative lipidomics reveals the disturbance of lipid metabolism induced by oral exposure of titanium dioxide nanoparticles. *NanoImpact*, *37*, 100554. https://doi.org/10.1016/j.impact.2025.100554

Yusoff, R., Nguyen, L. T. H., Chiew, P., Wang, Z. M., & Ng, K. W. (2018). Comparative differences in the behavior of TiO2 and SiO2 food additives in food ingredient solutions. *Journal of nanoparticle research*, *20*(3), 76. https://doi.org/10.1007/s11051-018-4176-8

Zelber-Sagi, S., Ivancovsky-Wajcman, D., Fliss-Isakov, N., Hahn, M., Webb, M., Shibolet, O., Kariv, R., & Tirosh, O. (2020). Serum malondialdehyde is associated with non-alcoholic fatty liver and related liver damage differentially in men and women. *Antioxidants*, *9*(7), 578.

Zhang, J., Shi, J., Han, S., Zheng, P., Chen, Z., & Jia, G. (2022). Titanium dioxide nanoparticles induced reactive oxygen species (ROS) related changes of metabolomics signatures in human normal bronchial epithelial (BEAS-2B) cells. *Toxicol Appl Pharmacol*, *444*, 116020. https://doi.org/10.1016/j.taap.2022.116020

Zhang, W., Sun, J., Liu, F., Li, S., Wang, X., Su, L., & Liu, G. (2023). Alleviative Effect of Lactoferrin Interventions Against the Hepatotoxicity Induced by Titanium Dioxide Nanoparticles. *Biological Trace Element Research*. https://doi.org/10.1007/s12011-023-03702-3

Zhang, X. L., Wei, Y. Y., Li, C. J., Wang, W. Y., Zhang, R., Jia, J. B., & Yan, B. (2021). Intracellular Exposure Dose-Associated Susceptibility of Steatotic Hepatocytes to Metallic Nanoparticles. *International Journal of Molecular Sciences*, *22*(23), Article 12643. https://doi.org/10.3390/ijms222312643

Zhang, Z., Yang, H., Han, F., & Guo, P. (2025). Reactive Oxygen Species as Key Molecules in the Pathogenesis of Alcoholic Fatty Liver Disease and Nonalcoholic Fatty Liver Disease: Future Perspectives. *Current Issues in Molecular Biology*, *47*(6), 464.

Zhao, Y., Tang, Y., Liu, S., Jia, T., Zhou, D., & Xu, H. (2021). Foodborne TiO_2 nanoparticles induced more severe hepatotoxicity in fructose-induced metabolic syndrome mice via exacerbating oxidative stress-mediated intestinal barrier damage. *Foods*, *10*(5), 986.

Zheng, Y., Sun, J., Luo, Z., Li, Y., & Huang, Y. (2024). Emerging mechanisms of lipid peroxidation in regulated cell death and its physiological implications. *Cell death & disease*, *15*(11), 859.

Zhou, J., Li, W., Chi, X., Li, D., Yang, C., & Duan, Z. (2025). Inhibition of mmu_circ_0009303 improves metabolic dysfunction-associated steatotic liver disease by regulating lipid metabolism and oxidative stress. *Endocrine journal*, *72*(1), 79-91.

Zhou, Z., Xu, M.-J., & Gao, B. (2016). Hepatocytes: a key cell type for innate immunity. *Cellular & Molecular Immunology*, *13*(3), 301-315. https://doi.org/10.1038/cmi.2015.97

Zhu, X., Zhao, L., Liu, Z., Zhou, Q., Zhu, Y., Zhao, Y., & Yang, X. (2021). Long-term exposure to titanium dioxide nanoparticles promotes diet-induced obesity through exacerbating intestinal mucus layer damage and microbiota dysbiosis [Article]. *Nano Research*, *14*(5), 1512-1522. https://doi.org/10.1007/s12274-020-3210-1

Zhu, Y., Eaton, J. W., & Li, C. (2012). Titanium dioxide (TiO_2) nanoparticles preferentially induce cell death in transformed cells in a Bak/Bax-independent fashion. *PLoS One*, *7*(11), e50607.

Ziamajidi, N., Khaghani, S., Hassanzadeh, G., Vardasbi, S., Ahmadian, S., Nowrouzi, A., Ghaffari, S. M., & Abdirad, A. (2013). Amelioration by chicory seed extract of diabetes- and oleic acid-induced non-alcoholic fatty liver disease (NAFLD)/non-alcoholic steatohepatitis (NASH) via modulation of PPARα and SREBP-1. *Food Chem Toxicol*, *58*, 198-209. https://doi.org/10.1016/j.fct.2013.04.018

Zierden, M. R., & Valentine, A. M. (2015). Contemplating a role for titanium in organisms. *Metallomics*, *8*(1), 9-16. https://doi.org/10.1039/c5mt00231a

Appendices

Appendix Table 2.1 Effects of TiO_2 NPs in the rat and mouse liver (*in vivo*)

Study model	Oral daily dosage (mg/kg/bw)	Treatment timeline	Type/ Particle size	Effects on the liver	References
CD-1 mice (M, F)	5000/single dose	1 day	NG/25, 80 degeneration, and 155 nm	↑ALT/AST ratios HC: Ti accumulation in the liver, hydropic, spotty necrosis of hepatocytes	(Wang et al., 2007)
CD-1 Mice (F)	62.5, 125, 250	30 days	Anatase/ 5 nm	↑ ALT, ALP, AST, LDH, ChE, TP, TG, TCHO, NO ↓ ALB to GLB (A/G), TBIL, IL-2 H.C: Blurred hepatocytes, congested interstitial vessels.	(Duan et al., 2010)
CD-1 Mice (F)	5, 10, 50	60 days	Anatase/ 6-7 nm	↑ H_2O_2, MDA, NO, O_2^-, CYP1A gene ↓ SOD, CAT, GSH-Px, MT, GST, HSP70, p53, TF Genes H.C: Mitochondrial swelling, apoptotic bodies, chromatin condensation.	(Cui et al., 2010)
CD-1 Mice (F)	5, 10, 50	60 days	Anatase/ 5 nm	↑ ALT, AST, ALP, LDH, PChE, LAP, TLR2, TLR4, IKK1, IKK2, NF-κB, NF-κBP52, NF-κBP65, TNF-α, NIK ↓ IκB, Il-2, IgM H.C: TiO_2 accumulation in the liver, fatty degeneration with large vacuoles and congestion, necrosis, inflammatory cell infiltration, mitochondria swelling, and apoptotic cells with chromatin condensation.	(Cui et al., 2011)
Sprague-Dawley Rats (M)	10, 50, 200	30 days	Anatase/ 75 nm	↑ Glu, LDL-C, ALT/AST ratio, BUN, GSH/GSSG ↓ AST, HBDH, CK, TBIL H.C: liver injury, oedema, hepatic cord disarray, peri-lobular cell swelling, hydropic degeneration, and inflammatory cell infiltration.	(Y. Wang et al., 2013)
Swiss albino mice (M)	10, 50, 100	14 days	anatase/ 20-50 nm	↑ ALT/AST ratio, ALT, AST, ALP, MDA, ROS, Hsp60, Hsp70, p53, Bax, caspase-3 & 9 ↓ GSH, Bcl-2 H.C: increased liver weight, accumulation of mononuclear cells near the sinusoidal vesicle, angiectasis.	(Shukla et al., 2014)
Wistar Rats (M)	300	14 days	N.G/ 50-100 nm	↑ AST, ALT, ALP, MDA ↓ GPx, SOD H.C: centrilobular necrosis, congestion, swelling, and vacuolisation, inflammatory cells infiltration, and high apoptotic index.	(Orazizadeh et al., 2014)
CD-1 Mice (M)	2.5, 5, 10	6 m	Anatase/ 5 to 6 nm	↑ ALT, AST, ALP, LDH, TC, TG, IL-4, IL-5, IL-12, IFN-γ, GATA3, GATA4, T-bet, STAT3, STAT6, eotaxin, MCP-1, MIP-2 genes	(Jie Hong et al., 2014)

Study model	Oral daily dosage (mg/kg/bw)	Treatment timeline	Type/ Particle size	Effects on the liver	References
				↓ STAT1, TBIL H.C: TiO_2 accumulation in the liver, angiectasis, hyperaemia, infiltration of inflammatory cells, macrophage aggregation, hepatic tissue crevice, necrosis, apoptosis, mitochondrial swelling, nuclear membrane collapse, and chromatin marginalisation.	
Swiss Albino Mice (M)	500	21 days	Anatase/ Rutile / 50-75 nm	↑ ROS, GSH, TBARS ↓ SOD, CAT, GPX H.C: TiO_2 particles are entrapped in endosomes and Kupffer cells.	(Shrivastava et al., 2014)
Sprague-Dawley Rats (M)	10, 50, 200	30 days	Anatase/ 75 nm	↑ T-SOD, GSH/GSSG ratio, Rb, ALT, AST, ALP, MDA ↓ Mo, co, Mn, P, GPx, SOD.	(Wang et al., 2014)
Wistar Rats (M)	300	14 days	N.G/ <100 nm	H.C: Damaged lobular structures, vacuolisation and congestion, inflammatory cells Infiltration.	(Khorsandi et al., 2015)
CD-1 Mice (M)	64	28 days	Anatase/ 18 and 120 nm	↑ MDA, TNF-α, IL-6 ↓ T-SOD, GSH No effects on plasma glucose and ROS levels H.C: Fracture in tissue fibres.	(Gu et al., 2015)
Albino Mice (M)	150	14 days	Anatase/ 21 nm	↑ ALT, AST, MDA, TNF-α, IL-6, Nrf2, NF-κB, CD68, Bax, caspase-3 ↓ GSH, Bcl-2 H.C: Focal degeneration, necrosis, DNA damage, inflammatory cells infiltration.	(Azim et al., 2015)
CD-1 Mice (M)	13, 64, 320	14 weeks	Anatase/ 25 nm	↑ MDA, JNK1, p38 MAPK, TNF-α, IL-6, IR, plasma glucose ↓ SOD, GSH ↑ TiO_2 accumulation in the liver with increasing dose.	(H. Hu et al., 2015)
Kun Ming Mice (M, F)	2000	7 days	Anatase/ 25 nm	↑ AST, ALT, TBIL, MDA ↓ SOD, GSH-PX, Nrf2, NQO1, HO-1, GCLC H.C: Dilatation of sinusoids, deranged and swollen hepatocytes, vacuoles, necrosis.	(Niu et al., 2017)
Sprague-Dawley Rats (M)	150	6 weeks	N.G/ 21 nm	↑ AST, ALT, LPO, TNF-α ↓ GSH, TBARS H.C: congestion and dilatation, degenerative changes, vacuolar degeneration, necrosis, mononuclear infiltration.	(Hassanein & El-Amir, 2017)
C57/BL6 Mice (M)	250, 500	14 days	N.G/ 21 nm	↑ ILIB, TBIL, ALP, TBA, Oapt1, Mrp3, Cyp2b10, 2c37 H.C: Number of mitochondria increased and oedema in ER.	(Yang et al., 2017)
ICR Mice (M, F)	5, 10, 50	60 days	Anatase/ 10, 60, 90 nm	↑ ALP, ALT, ALB, LAP, PChe, TBIL, TP, O_2-, H_2O_2, NO, MDA, CYP1A ↓ SOD, CAT, MT, GST, HSP70, p53, TF, GSHPx	(X. C. Jia et al., 2017)

Study model	Oral daily dosage (mg/kg/bw)	Treatment timeline	Type/ Particle size	Effects on the liver	References
				H.C: TiO_2 accumulation in the liver, vascular obstruction, dilation, increased basophils, partial ischemia, swelling mitochondria, vacuoles in mitochondria, nucleolus collapse, scattered chromatin, apoptosis.	
Sprague-Dawley Rats (M)	150	28 days	Anatase/ 30–80 nm	↑ ALP, ALT, AST, LPO ↓ CAT, GST H.C: Destructed blood vessels, infiltration of neutrophils and apoptosis, damaged and congested vein, vacuolation, haemorrhage, pyknotic nuclei, dilated sinusoids.	(Shakeel et al., 2018)
Albino Rats (M)	100	60 days	Anatase/ 10 nm	↑ ALT, AST, ALP, MDA, Bax ↓ GPx, SOD, GSH, Bcl-2 H.C: Hepatic apoptosis, hepatocellular necrosis, steatosis, sinusoidal dilation with leucocytosis, distortion, disorganisation of the hepatic cords.	(Morgan et al., 2018)
Wistar Rats (M)	100, 200	60 days	Anatase/ 40 nm	↑ ALT, AST, ALP, ALB, MDA ↓ SOD, GPx, CAT, GSH H.C: Liver tissue damage, sinusoidal dilation, vacuolisation, and leukocyte infiltration.	(Jafari et al., 2018)
Sprague-Dawley Rats (M)	300	14 days	N. G	↑ AST, ALT, LPO ↓ TBARS H.C: Congestion of the central veins, dilatation of the hepatic sinusoids, focal haemorrhagic, coagulative necrosis, proliferation of Kupffer cells, lymphocytic aggregations, vacuolar degeneration.	(K. M. A. Hassanein & Y. O. El-Amir, 2018)
Wistar Albino Rats (M)	1000	21 days	Anatase/ 60 nm	↑ ALT, TNF-α, IL-6, CRP, IgG, NO, VEGF, caspase-3, LPO ↓ Cytochrome-P450 H.C: Severe degeneration, nuclear pyknosis, karyolysis, cytoplasmic vacuolation, increase in collagen, and DNA damage.	(Fadda et al., 2018)
Sprague-Dawley Rats (M)	0, 2, 10, 50	90 days	Anatase/ 29 nm	↑ TP, ALB, GLB, GSSG, MDA, IL-1α, IL-4, TNF-α ↓ GSH, GSH-Px, SOD H.C: Fatty degeneration, fat vacuoles, vacuolation of mitochondria, changes in hepatic metabolomics, disrupted energy metabolism.	(Z. Chen et al., 2019)
Wistar Rats (M)	10, 50, 100	30 days	Rutile/ 30 nm	↑ ALT, AST, LDH, ALP, MDA, TOS, Bax, p53, NLRP3, caspase-1 & 3, IL-1β, TNF-α, iNOS ↓ SOD, GPX, CAT, TAC, Bcl-2 H.C: liver cell degeneration, necrosis, congestion of the sinusoids,	(Abbasi-Oshaghi et al., 2019)

Study model	Oral daily dosage (mg/kg/bw)	Treatment timeline	Type/ Particle size	Effects on the liver	References
				lymphocytic infiltration, deposition of collagen, and apoptosis.	
Wistar Rats (M)	300	14 days	80% anatase + 20% rutile / 20 nm	↑ ALT, AST, ALP, LDH, MDA, TOS, TNF-α, NF-κB ↓ SOD, GPx, CAT, TAC H.C: dilatation of the congested portal vein, hypertrophy of Kupffer cells, hydropic and vacuolar degeneration, oedema and necrosis, and inflammatory cell infiltration.	(Moradi et al., 2019)
Swiss Albino Mice (M)	50, 250, 500	5 days	N.G/ 21 and 80 nm	↑ AST, ALT, MDA, NO, CAT ↓ GSH H.C: chromosomal fragments and dilatations, distorted and loss in lobular architecture, micro regenerating nodules, mild ballooning and infiltration by lymphocytes, mild fibrosis, swelling and degeneration, significant haemorrhage.	(Ali et al., 2019)
Wistar Albino Rats (F)	0.5, 5, 50	14 days	N.G/ 21 nm	↑ CAT ↓ GST, SOD, GPX H.C: TiO_2 accumulation in the liver.	(Canli et al., 2019)
NFR Mice (M)	5	21 days	Anatase E171/ 201 nm	↑ Accumulation of TiO_2 in the liver, TNF-α, IL-1β, circulatory cytokines (IL-6, SDF-1) ↓ IL-10 H.C: Increased necro-inflammatory foci infiltrated with F4/80 positive cells, macrophage recruitment.	(Talamini et al., 2019)
CD-1 Mice (M)	50	8 and 26 weeks	N.G/ 25 nm	↑ Cyp2b9, Cyp2c70, Cyp4a14, GRP78, CHOP, PERK, p-eIF2α, GRP78, CHOP, XBP1-s, ATF6, XBP1-s/XBP1-t, Nrf2, Nqo1, (HO-1), NF-κB Activation of MAPK pathways, IR, and an increase in plasma glucose level.	(Hu et al., 2020)
Mice	2.5, 5, 10	9 months	N. G	↑ HIF-1α, Wnt3, Wnt4, NF-κB, TGF-β1, TGF-β1R, Smad-2, ILK, ECM, calpain 2, α-SMA, c-Myc, collagen I, p38 MAPK phosphorylation, GSK-3β, β-catenin ↓ cyclin D H.C: hepatic inflammatory cell infiltration, hepatic fibrosis.	(Hong et al., 2020)
Sprague-Dawley Rats (M)	2, 10, 50	90 days	Anatase/ 29 nm	↑ GSSG, MDA ↓ GSH, GSH/GSSG, SOD, hepatic phosphatidylcholine (PC) H.C: High oxidative stress, fatty degeneration of hepatocytes, altered lipid metabolism.	(Z. J. Chen et al., 2020)
Albino Rats (M)	500	14 days	N.G/ 63–142 nm	↑ ALT, ALP, MDA, TLR-4, NF-κB, NIK, TNF-α ↓ GSH, CAT, Acetyl cholinesterase H.C: congested and dilated central vein, vacuolated and degenerated	(Mohammed & Safwat, 2020)

Study model	Oral daily dosage (mg/kg/bw)	Treatment timeline	Type/ Particle size	Effects on the liver	References
				hepatocytes with Kupffer cells, leucocyte infiltration, endothelial hyperplasia, and leucocytic aggregates.	
Wistar Rats (M)	300	14 days	N.G/ 50-100 nm	↑ ALT, AST, Bax ↓ Bcl-2 H.C: Apoptosis in all lobules.	(Orazizadeh et al., 2020)
Sprague-Dawley Rats (F)	50	21 days	N.G / 100 nm	↑ ALT, AST, T.BIL, D.BIL, creatinine, urea, uric acid, Cho, TG, LDL-Cho, MDA, NO, Bax, TNF-α ↓ TP, Alb, HDL-Cho, CAT, SOD, GPx, Bcl-2 H.C: portal vein dilatation, congestion, periportal necrosis, proliferative bile ducts, aggregation of mononuclear cellular infiltration, and fibrous tissues.	(Abdel-Wahhab et al., 2021b)
Kunming Mice (M)	2, 20	8 weeks	Anatase/ 10–25 nm	↑ ALP, TNF-α, IL-1β, IL-6, TLR-4, caspase-3 & 9, VEGFA, TGF-β, IFN-γ, MDA ↓ SOD, CAT, GSH H.C: Hepatocyte swelling, fat accumulation, and inflammatory infiltration.	(Zhao et al., 2021)
Sprague Dawley Rats (F)	150	7 days	N.G/ 33 nm	↑ AST, ALT, AST/ALT, ALP ↓ SOD1, SOD2, HO-1, GSH, CAT, GCLC, GCLM H.C: Ti accumulation in the liver, disordered arrangement of hepatocytes, and ballooning degeneration.	(Nie et al., 2021)
Wistar Rats (M)	100	30 days	N.G/ 21 nm	↑ LDH, ALT, AST, TC, TG, LDL, VLDL, Plasma Glucose ↓ HDL H.C: congestion, dilatation in the central vein.	(Bakour et al., 2021)
Balb/c Mice (M)	25	21 days	N.G/ 28.9 nm	↑ ALT, AST, TC, TG, LDL, MDA, NO, AFP, TNF-α, CEA ↓ CAT, SOD, TP, Alb, TAC, HDL H.C: DNA fragmentation, hepatocytes necrosis, dilated and congested blood vessels, fatty droplets.	(Salman et al., 2021)
Sprague-Dawley Rats (M)	50	21 days	N.G/ 28 nm	↑ AST, ALT, MDA, NO, TG, Chol, LDL, Bax, caspase 3, p53 ↓ HDL, GPx, CAT, Bcl-2 H.C: Portal tract dilation, proliferation of bile ducts, necrosis in their epithelial cells, fibrosis, and DNA fragmentation in hepatic tissue.	(Sallam et al., 2022b)
Wistar Rats (M)	300	21 days	Anatase (80%)/Rutile (20%) 20 nm	↑ ALT, AST, ALP, LDH, TOS, MDA ↓ TAC, SOD, GPx H.C: WBCs infiltration, central vein hyperaemia, enlargement of Kupffer cells, dilation of sinusoids,	(Shirdare et al., 2022)

Study model	Oral daily dosage (mg/kg/bw)	Treatment timeline	Type/ Particle size	Effects on the liver	References
				accumulation of inflammatory cells, hepatocyte necrosis.	
Sprague-Dawley Rats (M)	50	21 days	N.G/50 nm	↑ AST, ALT, T.BIL, D.BIL, Cho, TG, LDL-Cho, AFP, CEA, NO, MDA, IL-1β, IL-6, TNF-α ↓ Alb, TP, HDL-Cho, CAT, GPx, SOD, IL-10 H.C: Dilatation in the central vein and hepatic sinusoid, vacuolar degeneration, nuclear degeneration, necrosis, pyknosis, karyolysis, peripheral chromatin clumps, fibrosis, proliferation of bile ducts.	(Sallam et al., 2022a)
Sprague-Dawley Rats (M)	2, 10, 50	90 days	Anatase/ 29 nm	↑ MDA, imbalance in the liver metabolites, effects on the glycerophospholipid metabolism pathway, impact on the liver metabolism ↓ differentially expressed phosphatidylcholine (PCs).	(Chen et al., 2022a)
Wistar Rats (M)	100	28 days	N. G	↑ AST, ALT, ALP, TC, TG, MDA, IL-1β, IL-6, TNF-α, IFN-γ, γH2A, Bax, α-SMA, fibronectin ↓CAT, GPx, SOD, GSH, IL-10, Bcl-2, PI3K/AKT signalling pathway. H.C: hepatic fibrosis, inflammatory cell infiltration, hepatic sinusoid congestion, widening liver tissue gap, and lamellar tissue necrosis.	(Zhang et al., 2023)
ICR mice (M)	50	30 days	Anatase/ 7 nm	↑ AST, ALT, ALP, MDA, Bax, caspase-3 & 9, p53, p-p38, p-p38/p38 ↓ SOD, GSH-Px, GSH, T-AOC, Bcl-2 H.C: hepatocytes were blurred and disordered, swollen, and vacuolated, increased apoptosis, steatosis, congestion and dilation of the central veins, and infiltration of inflammatory cells around the blood vessels.	(Chang et al., 2023)
Sprague-Dawley Rats (M)	50	60 days	N. G/<30 nm	↑ ALT, AST, ALP, bilirubin,TC, TG, VLDL, LDL, MDA, hepatic Ti accumulation, TNF-α ↓ HDL, GPx and SOD H.C: Hepatocellular necrosis, increased inflammatory reaction.	(Abd-Elhakim et al., 2023)
Sprague-Dawley Rats (M, F)	1, 2	5 days	Anatase/ < 25 nm	H.C: Significant increase hepatocyte vacuolisation/steatosis, increase in intralobular lymphoid infiltration and congestion in the central vein with enlargement of the sinusoids, focal	(Tassinari et al., 2023)

Study model	Oral daily dosage (mg/kg/bw)	Treatment timeline	Type/ Particle size	Effects on the liver	References
				intralobular necrosis in the middle zone of the liver lobule.	
C57BL/6 mice (M)	150	8 weeks	N.G/ 21 nm	↑ AST, ALT, MDA, Ogg1 protein, IL-6, TNF-α, CXCL2, and IL-1β, Cox2, Nos2, Col1α1, αSma, Ctgf, Tgfβ1, and Timp1 ↓ GSH, GSH/GSSG ratio H.C: Liver nodule destruction, hepatocyte swelling, fat vacuoles, and inflammatory cell infiltration around the portal vein, mitochondrial swelling and a reduction in the number of cristae, reflecting a partial membrane phenotype.	(Wang et al., 2024)
Swiss webster mice (M)	50	5 days	Mix of Rutile and Anatase/ < 100 nm	↑ DNA damage, p53, MDA, ↓ SOD, Gpx H.C: Diffusion and degeneration of hepatocytes.	(Mohamed et al., 2024)
BALB/c mice (M)	8, 80, 320	28 and 84 days	E171	↑ IGF-1 and HSP90B1, High-dose E 171 exposure for 84 days increased ALT and AST levels, especially in the high-dose E 171-1 group ↓ TBIL and TG plasma levels, Ferroptosis related proteins FTH1 and FTL, the liver coefficients (ratio of liver to body weight) of mice exposed to the high dose of E171 for 84 days decreased significantly. H.C: Inflammatory cell infiltration was found in the liver tissues of mice exposed to all three E 171-1 and E 171-2 doses for 84 days. E 171 for 84 days results in changes in global DNA methylation and hydroxy methylation in the liver of mice.	(Shang et al., 2024)
Albino rats (M)	500	60 days	N.G/72.1 nm	↑ up regulation of both *CYP1A1* and *nbn* genes	(Moselhy et al., 2024)
Wistar Rats (M)	10	30 days	E171	H.C: Disorganized hepatic tissue, cellular infiltration, and hemorrhage mitochondrial damage, dilated rough ER, and less electro-dense nuclei.	(Bautista-Pérez et al., 2024)
Wistar Albino (M)	100	14 days	Mix of Rutile and Anatase/ < 100 nm	↑ α-SMA, 8-oHdG immunoreactivity, MDA, TNF-α, IL-6, AST, ALT, ALP ↓ GSH-Px, SOD H.C: Increased hepatocyte**,** sinusoid, central vein diameter**,** and plaque thickness**.** centrilobular necrosis and obliterations of the central vein. The cytoplasmic clearing (signet ring	(Başak et al., 2025)

Study model	Oral daily dosage (mg/kg/bw)	Treatment timeline	Type/ Particle size	Effects on the liver	References
				appearance) was abundant in the areas of microsteatosis. Fibrotic regions encircled by interlobular and perivascular degenerations, intracytoplasmic vacuolated patches, a rise in activated Kuppfer cells, and perivascular lymphocytic infiltrations.	
Albino Rats (M)	150	14 days	Anatase/ 50–55 nm	↑ ALT, AST, ALP, bilirubin, total protein, albumin, globulin levels, Caspase-3, BAX, IL-1β ↓ GSH, catalase, GPx, GST, SOD, GST, TNF-α H.C: Cellular alterations, degenerative hydropic changes and cellular infiltration in numerous hepatocytes, necrosis, congestion of sinusoidal blood vessels, disturbed hepatic architecture in most of the lobule and central vein congestion.	(Halawa et al., 2025)
Sprague-Dawley Rats (M)	2, 10, 50	90 days	Anatase/ 29 ± 9nm	↑ DAG, TAG ↓ LPC Significantly changed the liver lipid metabolites in rats.	(Yu et al., 2025)
Sprague-Dawley Rats (M)	50	90 days	Anatase/ 25± 5 nm	↑ES1, Ig-like domain-containing protein, GATD3A ↓ GZMA, FAM114A2, MMP9 Pathways significantly affected are Terpenoid backbone biosynthesis, Steroid biosynthesis, and alpha-Linolenic acid metabolism, Riboflavin metabolism, Histidine metabolism, and Alanine, aspartate and glutamate metabolism.	(Shi et al., 2025)

Appendix 2.2: Effects of TiO_2 NPs on liver cells (*in vitro*)

Cell type	Dosage (µg/ml)	Treatment timeline (hours)	Type/ size	Effects on liver cells	References
HepG2	1, 10, 100, 250	4, 24, 48	Anatase/ <25 nm Rutile/ <100 nm	Anatase: 2-fold increase in ROS Persistent DNA-strand breaks. ↑ Fpg-sensitive sites, p53, mdm2, p21, gadd45α Rutile: 1.4-fold increase in ROS, DNA-strand breaks, but not persistent ↑ Fpg-sensitive sites, p53, mdm2, p21, gadd45α.	(Petković et al., 2011)
SMMC-7721 HL-7702	0.1, 0.5, 1, 5, 10, 50, 100	12, 36, 24, 48	N.G/3.7 nm	↑ Cell shrinkage, nuclear condensation, ROS, cytotoxicity ↓ GSH	(Sha et al., 2011)
C3A	0.5–256	4, 6, 24	Rutile/ 7 and 10 nm	↑ DNA damage, ROS, oxidative stress, genotoxicity, IL8 ↓ GSH.	(Kermanizadeh et al., 2012)
HepG2	1, 10, 20, 40, 80	6, 24, 48	Anatase/30-70 nm	↑ Cellular uptake, cytotoxicity, oxidative DNA damage, apoptosis, micronucleated cells, ROS, Hsp60, Hsp70, p53, Bax, Cyto-c, Apaf-1, caspase-3 & 9, hydroperoxide ↓ MSD, GSH, MMP, Bcl-2.	(Shukla et al., 2013)
HepG2	100	24	Anatase 86% Rutile 14%/ P25 (21 nm)	↑ DNA damage, MN frequencies, NF-κB activity No significant transcriptional activation of AP1.	(Prasad et al., 2014)
C3A	10-100	4	Rutile/ 30.5 nm	↑ ROS Limited effect on glycogen breakdown, glucose, LP release, and metabolism.	(Filippi et al., 2015)
HepG2	5, 20, 80, 160, 320	1, 9, 12, 16, 24	Anatase/ 10 nm Rutile/ 50 nm	↑ Cytotoxicity, immunogenicity, TNF-α, MAPK, NF-κB pathway, p38, ERK1/2 phosphorylation, inflammation, Young's modulus, and adhesion force. ↓ A20.	(Chen et al., 2016)
QGY	40, 80	72	N.G/21 nm	↑ H_2O_2, chromosome instability, ROS ↑ Telomer length, TRF1, TRF2, POT1, Nrf-2.	(Wang et al., 2018)
HepG2	2.5, 5, 7.5, 10	12, 24, 48	Anatase/10 nm	↑ G1 phase, caspase-3 &7, apoptosis, VDAC1, Cyt c, αENaC, SIRT3, ADP/ATP, depolarisation, and disruption of mitochondria ↓ Cell growth and proliferation, S phase, ACSS1, ATP.	(Xia et al., 2018)
HepG2	100, 150, 200, 300	24	Rutile/ 30 nm	↑ LDH, AST, ALT, ROS, apoptosis ↓ Cell viability, GSH.	(Abbasi-Oshaghi et al., 2019)
HepG2	100	24, 72	P25/21 nm	↑ Promoter methylation in CDKN1A, DNAJC15, GADD45A,	(Pogribna et al., 2020)

Cell type	Dosage (µg/ml)	Treatment timeline (hours)	Type/ size	Effects on liver cells	References
				GDF15, INSIG1, SCARA3, TP53, BNIP3 ↓ Global methylation, DNMT3a, DNMT3b, MBD2, UHRF-1.	
HepG2	10, 50, 100, 200	3, 24	Anatase (80%), Rutile (20%)/ 25 nm	↑ NPs uptake No micronuclei expression.	(Brandão et al., 2020)
HepG2	2.5, 5, 7.5, 10	48	N.G	↑ Apoptosis, cell cycle arrest at G1 stage, ROS, ER stress, PERK, ATF6, Bax ↓ Cell growth.	(Li et al., 2020)
HepG2	4, 8, 12, 50	24	N.G/21 nm N.G/125 nm	↑ Cytotoxicity, oxidative stress, TiO_2 uptake ↓ fatty acid oxidation.	(Zhang et al., 2021)
HepG2	1.56, 3.13, 6.25, 12.5, 25, 50, 100, 200	48	Anatase/25 nm	↑ Cytotoxicity, epigenetic changes ↓ HADHB, BRIP1, ZNF562.	(Shi et al., 2023)
L02	5, 10, 20	5-72	N.G/21 nm	↑ Cytotoxicity, ROS levels, cell nuclei fragmentation, MDA, IL-1β, IL-6, TNF-α, Cxcl2 ↓ GSH, GSH/GSSG ratio.	(Wang et al., 2024)
HepG2	10, 100	24, 72	Anatase/ 242.3 ± 93.6 nm	↑ promoter methylation of DNAJC15, GDF15, TP53 ↓ global methylation.	(Wells et al., 2024)
HepG2	1.57, 3.13, 6.25, 12.5, 25, 50, 100, 200	12, 24, 48	Anatase/25± 5 nm	↑ Cytotoxicity at higher dose, SPP1, MDK, CCL20 ↓ NLRP10, H1-2, ISCA2 Significantly affected in the 100 µg/mL TiO_2 NPs treatment group included aminoglycan and nucleotide sugar metabolism, glycerophospholipid metabolism, linoleic acid metabolism, fructose and mannose metabolism, and phosphatidylinositol signaling system.	(Shi et al., 2025)

Appendix 4.1. Composite design. Figures shown are grams of food ingested per 14 days.

Major (operational) category	Compo-site number	Composite Group	Key food	Age and gender group									
				Males 19 - 24 yrs	Males >25 yrs	Females >25 yrs	Pacific Females >15 yrs	Pacific Males >15 yrs	Boys (11-14 yrs)	Girls (11 - 14 yrs)	Children (5 - 6 yrs)	Pre-school (1-3 yrs)	Infants (6-12 mo)
Fruits	1	Pip fruit/Kiwi fruit	Apple	557	586	452	452	586	960	1010	1050	350	270
Fruits			Pear	161	161	161	161	161	120	150	120	140	50
Fruits			Kiwifruit	124	124	124	124	124	20	40	80	80	15
Fruits	2	Stone fruit	Avocado	60	60	100	60	60	30	30	20	58	30
Fruits			Nectarines	70	108	108	108	108	100	90	130	30	50
Fruits			Peaches, canned	96	96	109	96	96	30	45	60	50	50
Fruits			Prunes	30	40	20	20	40	15	20	20	20	15
Fruits	3	Citrus	Mandarins	86	144	86	43	43	86	86	86	36	36
Fruits			Oranges	185	185	261	185	185	430	710	610	260	110
Fruits													
Fruits	4	Berries	Mixed berries	39	48	33	33	48	16	16	16	10	10
Fruits			Grapes	28	28	56	56	28	20	30	40	40	10
Fruits			Strawberries	130	80	55	55	80	20	45	55	30	20
Fruits	5	Tomato	Tomato, fresh	180	281	260	195	281	240	280	50	65	40
Fruits			Tomato, canned	109	168	139	52	120	110	65	50	45	40

Appendix 4.1 Continued…

Major (operational) category	Compo-site number	Composite Group	Key food	Age and gender group									
				Males 19 - 24 yrs	Males >25 yrs	Females >25 yrs	Pacific Females >15 yrs	Pacific Males >15 yrs	Boys (11-14 yrs)	Girls (11 - 14 yrs)	Children (5 - 6 yrs)	Pre-school (1-3 yrs)	Infants (6-12 mo)
Fruits	6	Others	Pineapple, canned	128	50	50	50	50	25	30	70	20	20
Fruits			Banana	544	544	475	645	544	360	260	420	530	460
Fruits			Melon	133	40	22	22	40	20	30	40	30	30
Vegetables & fungi	7	Root vegetables	Beetroot	40	50	30	30	50	30	30	10	0	0
Vegetables & fungi			Carrot	167	221	181	137	221	180	150	160	115	70
Vegetables & fungi			Onions	109	123	102	74	123	130	85	70	15	10
Vegetables & fungi	8	Tubers	Potatoes with skin	452	422	257	215	350	450	360	280	60	40
Vegetables & fungi			Potatoes peeled	917	858	523	436	710	720	670	540	240	150
Vegetables & fungi			Potatoes, hot chips	714	430	255	322	430	700	560	320	210	90
Vegetables & fungi			Taro	40	40	40	445	480	40	40	20	10	10
Vegetables & fungi			Kumara	109	109	80	109	109	30	70	20	40	40
Vegetables & fungi	9	Leafy vegetables	Broccoli/Cauliflower	150	160	120	70	160	130	90	80	70	40

Appendix 4.1 Continued…

Major (operational) category	Compo-site number	Composite Group	Key food	Age and gender group									
				Males 19 - 24 yrs	Males >25 yrs	Females >25 yrs	Pacific Females >15 yrs	Pacific Males >15 yrs	Boys (11-14 yrs)	Girls (11 - 14 yrs)	Children (5 - 6 yrs)	Pre-school (1-3 yrs)	Infants (6-12 mo)
Vegetables & fungi			Cabbage	105	105	58	75	145	140	100	60	15	15
Vegetables & fungi			Lettuce	100	125	125	75	125	190	130	30	15	0
Vegetables & fungi			Celery	15	15	27	27	15	50	30	15	15	0
Vegetables & fungi			Silver beet	80	91	60	40	91	40	30	25	20	15
Vegetables & fungi			Courgette	45	45	60	45	45	40	20	14	10	10
Vegetables & fungi	10	Squash/Creeping veg	Capsicum	45	45	45	45	45	40	40	15	10	0
Vegetables & fungi			Cucumber	24	40	40	40	40	40	20	15	15	15
Vegetables & fungi			Pumpkin	110	184	188	93	184	60	50	45	80	65
Vegetables & fungi			Peas	83	83	55	20	83	165	130	90	60	40
Vegetables & fungi	11	Seed/Other	Mixed vegetables	193	183	200	100	183	29	28	29	20	0
Vegetables & fungi			Mushrooms	35	35	60	30	35	60	40	15	15	15
Vegetables & fungi			Corn	50	50	25	25	50	70	50	85	30	30
Vegetables & fungi	12	Dried fruits	Sultanas/raisins	30	30	20	20	30	30	30	30	99	65

Appendix 4.1 Continued…

Major (operational) category	Compo-site number	Composite Group	Key food	Age and gender group									
				Males 19 - 24 yrs	Males >25 yrs	Females >25 yrs	Pacific Females >15 yrs	Pacific Males >15 yrs	Boys (11-14 yrs)	Girls (11 - 14 yrs)	Children (5 - 6 yrs)	Pre-school (1-3 yrs)	Infants (6-12 mo)
Grain and cereal-based	13	Bread	Bread, grain	436	622	556	276	502	757	597	618	172	0
Grain and cereal-based			Bread, wheatmeal	210	160	156	156	200	295	175	150	115	75
Grain and cereal-based			Bread, white	1200	743	464	806	649	1173	843	857	283	265
Grain and cereal-based	14	Rice or rice-based	Hummus	40	40	21	21	40	16	8	8	8	8
Grain and cereal-based			Rice	791	676	544	544	1092	360	200	220	55	30
Grain and cereal-based			Rice dish	400	280	220	280	280	120	100	110	0	0
Grain and cereal-based	15	Breakfast cereals	Sushi	45	140	45	45	45	45	45	45	0	0
Grain and cereal-based			Bran flakes	50	50	30	30	30	42	42	15	30	20
Grain and cereal-based			Cornflakes	72	72	50	50	72	73	35	78	60	30
Grain and cereal-based			Oats	50	100	50	100	100	75	80	70	120	70
Grain and cereal-based			Muesli	75	150	60	120	150	40	35	15	15	0
Grain and cereal-based			Other breakfast cereals	60	50	36	36	50	37	37	74	60	30

Appendix 4.1 Continued…

Major (operational) category	Compo-site number	Composite Group	Key food	Age and gender group									
				Males 19 - 24 yrs	Males >25 yrs	Females >25 yrs	Pacific Females >15 yrs	Pacific Males >15 yrs	Boys (11-14 yrs)	Girls (11 - 14 yrs)	Children (5 - 6 yrs)	Pre-school (1-3 yrs)	Infants (6-12 mo)
Grain and cereal-based	16	Pasta, spaghetti, noodles	Noodle dish	743	728	427	611	818	120	100	100	0	0
Grain and cereal-based			Noodles, instant	375	195	195	290	585	300	460	300	160	50
Grain and cereal-based			Spaghetti	210	210	133	133	210	200	150	120	150	100
Grain and cereal-based			Pasta, dried	450	450	450	300	450	390	270	220	150	110
Grain and cereal-based	17	Biscuits	Biscuit, chocolate	72	69	36	86	69	276	216	166	115	45
Grain and cereal-based			Biscuit, cracker	40	40	40	40	40	70	70	70	60	50
Grain and cereal-based			Biscuit, plain	44	60	60	40	60	85	90	90	165	65
Grain and cereal-based			Wheat biscuits	165	120	90	60	120	200	100	150	180	70
Grain and cereal-based	18	Cakes	Cakes and slices	360	364	180	194	425	100	160	60	60	20
Grain and cereal-based			Muffins and scones	180	130	120	120	130	170	250	140	70	35
High protein foods	19	Chicken	Chicken	808	432	468	840	1260	670	440	340	60	40
High protein foods			Chicken takeaway	279	186	186	279	372	120	100	42	56	28

Appendix 4.1 Continued…

Major (operational) category	Compo-site number	Composite Group	Key food	Age and gender group									
				Males 19 - 24 yrs	Males >25 yrs	Females >25 yrs	Pacific Females >15 yrs	Pacific Males >15 yrs	Boys (11-14 yrs)	Girls (11 - 14 yrs)	Children (5 - 6 yrs)	Pre-school (1-3 yrs)	Infants (6-12 mo)
High protein foods			Sausages	280	240	100	100	240	300	200	200	150	70
High protein foods			Liver	30	30	30	30	30	0	0	0	0	0
High protein foods			Beef, rump	170	170	108	108	170	200	150	90	50	30
High protein foods	20	Beef	Beef, corned	140	130	85	197	260	80	50	50	35	25
High protein foods			Beef, mince	70	120	87	80	90	280	140	150	120	80
High protein foods			Lamb	190	142	115	284	426	100	80	45	40	30
High protein foods			Bacon	104	90	35	35	90	45	20	20	30	20
High protein foods	21	Pork	Pork	130	118	86	160	192	110	80	45	20	20
High protein foods			Ham	240	118	80	40	70	180	100	70	70	20
High protein foods			Fish cakes	50	100	50	100	100	0	0	0	0	0
High protein foods	22	Fish	Fish, battered	216	216	189	210	216	100	60	80	45	25
High protein foods			Fish, canned	100	100	100	150	200	40	40	14	20	25
High protein foods			Fish, fingers	23	23	23	23	23	20	30	40	40	30

Appendix 4.1 Continued…

Major (operational) category	Compo-site number	Composite Group	Key food	Age and gender group									
				Males 19 - 24 yrs	Males >25 yrs	Females >25 yrs	Pacific Females >15 yrs	Pacific Males >15 yrs	Boys (11-14 yrs)	Girls (11 - 14 yrs)	Children (5 - 6 yrs)	Pre-school (1-3 yrs)	Infants (6-12 mo)
High protein foods			Fish, fresh	238	238	195	290	318	170	70	45	30	15
High protein foods			Oysters	30	50	30	30	50	0	0	0	0	0
High protein foods	23	Other seafood	Prawns	46	46	46	46	46	0	0	0	0	0
High protein foods			Mussels	90	90	50	50	90	15	15	0	0	0
High protein foods	24	Eggs	Eggs	310	269	275	162	269	220	190	160	110	60
High protein foods	25	Nuts	Almonds	30	30	25	25	30	15	15	15	0	0
High protein foods			Peanuts	40	40	40	40	40	20	20	20	0	0
High protein foods			Hamburger	351	236	102	234	236	300	265	100	80	40
High protein foods			Meat pie	408	348	174	348	174	360	320	200	90	50
High protein foods	26	Others (composite foods, tofu, and beans)	Pizza	250	190	150	150	190	150	180	130	70	40
High protein foods			Tofu	80	60	60	60	60	10	10	0	0	0
High protein foods			Baked beans	170	170	85	80	170	100	90	90	100	60

Appendix 4.1 Continued…

Major (operational) category	Compo-site number	Composite Group	Key food	Age and gender group									
				Males 19 - 24 yrs	Males >25 yrs	Females >25 yrs	Pacific Females >15 yrs	Pacific Males >15 yrs	Boys (11-14 yrs)	Girls (11 - 14 yrs)	Children (5 - 6 yrs)	Pre-school (1-3 yrs)	Infants (6-12 mo)
Dairy foods	27	Milk	Milk, 0.5% fat	877	1401	1039	658	1401	320	300	230	260	0
Dairy foods			Milk, 3.25% fat	1734	1489	842	1183	1489	2290	1560	2010	4294	960
Dairy foods			Milk, flavoured	628	370	350	350	370	180	130	130	100	10
Dairy foods			Milk, soy	120	243	438	438	243	154	250	150	100	0
Dairy foods			Yoghurt	300	300	410	180	150	294	294	294	890	785
Dairy foods	28	Milk products 1	Cheese	195	221	176	56	73	205	205	100	145	105
Dairy foods			Butter	126	146	92	146	146	100	70	70	55	40
Dairy foods			Coconut cream	0	0	0	332	400	0	0	0	0	0
Dairy foods	29	Milk products 2	Ice Cream	300	200	130	155	200	470	370	370	150	80
Dairy foods			Dairy dessert	150	150	150	150	150	75	130	290	460	130

Appendix 4.1 Continued…

Major (operational) category	Compo-site number	Composite Group	Key food	Age and gender group									
				Males 19 - 24 yrs	Males >25 yrs	Females >25 yrs	Pacific Females >15 yrs	Pacific Males >15 yrs	Boys (11-14 yrs)	Girls (11 - 14 yrs)	Children (5 - 6 yrs)	Pre-school (1-3 yrs)	Infants (6-12 mo)
Drinks and soup	30	Water	Water, bottled	434	350	350	350	350	632	634	673	455	70
Drinks and soup			Water, municipal	2516	2700	3800	3800	2700	4228	4246	4507	3045	1810
Drinks and soup			Fruit drink	1780	540	260	260	540	970	700	1200	830	350
Drinks and soup	31	Juices and carbonated beverages	Orange juice	260	260	260	260	522	50	80	80	280	110
Drinks and soup			Apple juice	260	260	260	260	260	50	80	80	380	130
Drinks and soup			Carbonated beverage	4163	1500	1050	1500	1770	1370	1150	570	300	125
Drinks and soup	32A	Warm or caffeinated beverages	Tea	900	4844	5586	2860	2860	250	250	200	0	0
Drinks and soup	32B	Warm or caffeinated beverages	Coffee instant	3878	7770	5796	3878	3878	98	154	0	0	0

Appendix 4.1 Continued…

Major (operational) category	Compo-site number	Composite Group	Key food	Age and gender group									
				Males 19 - 24 yrs	Males >25 yrs	Females >25 yrs	Pacific Females >15 yrs	Pacific Males >15 yrs	Boys (11-14 yrs)	Girls (11 - 14 yrs)	Children (5 - 6 yrs)	Pre-school (1-3 yrs)	Infants (6-12 mo)
Drinks and soup	32C	Warm or caffeinated beverages	Caffeinated beverage	720	260	260	260	260	200	150	0	0	0
Drinks and soup			Chocolate beverage	535	250	130	130	130	900	900	800	300	100
Drinks and soup	33	Alcoholic drinks	Wine, red	150	300	300	150	300	0	0	0	0	0
Drinks and soup			Wine, white	200	300	400	200	300	0	0	0	0	0
Drinks and soup			Beer	4322	3322	450	355	3322	0	0	0	0	0
Drinks and soup	34	Soup	Soup	250	250	340	150	250	150	150	100	50	30
Spreads, condiments flavourings	35	Spreads	Jam	75	74	85	61	62	40	30	30	20	15
Spreads, condiments flavourings			Honey	55	66	33	33	44	40	22	32	20	20
Spreads, condiments flavourings			Peanut butter	24	12	12	24	24	70	45	60	20	0
Spreads, condiments flavourings			Yeast extract	16	8	8	8	8	15	15	20	25	25
Spreads, condiments flavourings			Table spread	264	210	168	210	220	125	95	85	35	30

Appendix 4.1 Continued…

Major (operational) category	Compo-site number	Composite Group	Key food	Age and gender group									
				Males 19 - 24 yrs	Males >25 yrs	Females >25 yrs	Pacific Females >15 yrs	Pacific Males >15 yrs	Boys (11-14 yrs)	Girls (11 - 14 yrs)	Children (5 - 6 yrs)	Pre-school (1-3 yrs)	Infants (6-12 mo)
Spreads, condiments flavourings	36	Condiments and flavourings	Salad dressing	28	28	18	18	28	30	30	20	0	0
Spreads, condiments flavourings			Simmer sauce	100	100	80	80	100	50	50	50	0	0
Spreads, condiments flavourings			Tomato sauce	120	51	28	54	51	115	75	45	50	30
Snack foods and chocolate	37	Snack foods and chocolate	Snack bars	35	35	70	35	17	120	115	115	30	20
Snack foods and chocolate			Chocolate	180	100	80	40	100	180	130	100	20	10
Snack foods and chocolate			Confectionery	50	50	50	50	50	190	130	95	35	20
Snack foods and chocolate			Potato crisps	38	38	26	38	38	140	155	90	35	15
Snack foods and chocolate			Snacks, flavoured	50	40	30	30	40	130	135	110	60	35

Appendix 4.1 Continued…

Major (operational) category	Compo-site number	Composite Group	Key food	Age and gender group									
				Males 19 - 24 yrs	Males >25 yrs	Females >25 yrs	Pacific Females >15 yrs	Pacific Males >15 yrs	Boys (11-14 yrs)	Girls (11 - 14 yrs)	Children (5 - 6 yrs)	Pre-school (1-3 yrs)	Infants (6-12 mo)
Infant foods	38A	Infant foods (Pre-school)	Infant food, cereal	0	0	0	0	0	0	0	0	0	0
Infant foods			Infant food, fruit/custard	0	0	0	0	0	0	0	0	120	0
Infant foods			Infant food, savoury	0	0	0	0	0	0	0	0	120	0
Infant foods			Infant and follow-on formula	0	0	0	0	0	0	0	0	196	0
Infant foods	38B	Infant foods (Toddler)	Infant food, cereal	0	0	0	0	0	0	0	0	0	90
Infant foods			Infant food, fruit/custard	0	0	0	0	0	0	0	0	0	360
Infant foods			Infant food, savoury	0	0	0	0	0	0	0	0	0	340

Appendix 4.1 Concluded…

Major (operational) category	Compo-site number	Composite Group	Key food	Age and gender group									
				Males 19 - 24 yrs	**Males >25 yrs**	**Females >25 yrs**	**Pacific Females >15 yrs**	**Pacific Males >15 yrs**	**Boys (11-14 yrs)**	**Girls (11 - 14 yrs)**	**Children (5 - 6 yrs)**	**Pre-school (1-3 yrs)**	**Infants (6-12 mo)**
Infant foods			Infant and follow-on formula	0	0	0	0	0	0	0	0	0	5600
Others	39	Sugar	Sugar	134	190	150	146	195	95	95	55	25	15
Oil	40	Oil	Oil	215	182	110	110	182	85	60	40	35	10

Appendix 4.2: Concentrations of Ti in the inorganic ash of the food composite samples. Note that results for samples 39 and 40 (sugar and oil) are unreliable, due to the very low (negligible) ash content of both sample types. In four cases, these gave apparently negative weights due to the relative dominance of the measurement errors associated with weighing the Pyrex beaker before and after ashing, when there is essentially no ash.

Major category	Compo-site No	Composite group	Concentrations of Ti in the inorganic ash (mg/kg)				
			Sample A	Sample B	Sample C	Mean	Std dev
Fruits	1	Pip fruit/Kiwi fruit	110.3	95.1	84	96.5	13.2
	2	Stone fruit	59.6	45.3	37	47.3	11.4
	3	Citrus	146.7	72.8	73.9	97.8	42.4
	4	Berries	72.7	87.4	57.7	72.6	14.8
Vegetables and fungi	5	Tomato	32.3	25	24.2	27.1	4.4
	6	Others	223.1	85.5	52.2	120.3	90.6
	7	Root vegetables	54.5	65.4	58	59.3	5.6
	8	Tubers	33.9	76.1	26.5	45.5	26.8
	9	Leafy vegetables	31.6	33	57.9	40.9	14.8
	10	Squash/Creeping veg	25.8	16.4	14.8	19	5.9
	11	Seed/Other	99.7	60.2	53.3	71.1	25
Grain and cereal-based foods (carbohydrate rich)	12	Dried fruits	32.6	35.6	30.3	32.8	2.7
	13	Bread	28.1	26.1	21.8	25.3	3.2
	14	Rice or rice-based	183.8	92.3	114.5	130.2	47.7
	15	Breakfast cereals	45.5	62.2	32.3	46.7	14.9
	16	Pasta, spaghetti, noodles	120.1	101.5	134	118.5	16.3
	17	Biscuits	36.7	39.4	39.4	38.5	1.5
	18	Cakes	24.3	19.8	23.5	22.5	2.4
High protein foods (meat/chicken/fish/other)	19	Chicken	46.6	49.2	52.7	49.5	3.1
	20	Beef	65	92.7	47	68.2	23
	21	Pork	22	38.9	35.1	32	8.9
	22	Fish	29.3	25.4	24.5	26.4	2.5
	23	Other seafood	46.8	21.8	35.1	34.5	12.5
	24	Eggs	114.4	146	71	110.5	37.7
	25	Nuts	32	23.3	30	28.4	4.6
	26	Others (composite foods, tofu, and beans)	6.7	10.5	7.2	8.1	2
Dairy foods	27	Milk	14.5	13.3	10.4	12.7	2.1
	28	Milk products 1	15.1	11.3	9	11.8	3.1
	29	Milk products 2	5731	792	1493	2672	2672

Appendix 4.2 continued…

Major category	Compo-site No	Composite group	Concentrations of Ti in the inorganic ash (mg/kg)				
			Sample A	Sample B	Sample C	Mean	Std dev
Drinks (beverages) and soup	30	Water	286.4	233.4	208.3	242.7	39.9
	31	Juices and carbonated beverages	22.1	21.2	18.5	20.6	1.9
	32A	Tea	94.2	101.3	76.4	90.6	12.9
	32B	Coffee instant & drinking chocolate	43.3	52	59.8	51.7	8.2
	32C	Caffeinated beverage	142	25.4	27.1	64.9	66.8
	33	Alcoholic drinks	7.3	3.2	6.8	5.8	2.3
	34	Soup	17.5	19.1	13.1	16.6	3.1
Spreads, condiments and flavourings	35	Spreads	54.2	41.5	39.3	45	8.1
	36	Condiments and flavourings	7.6	6.9	9	7.8	1.1
Snack foods and chocolate	37	Snack foods and chocolate	9.4	12	12.7	11.4	1.8
Infant foods	38A	Infant foods - preschool	20.9	17.4	13.1	17.2	3.9
	38B	Infant foods - toddler	45.7	25.4	22.8	31.3	12.5
Others	39	Sugar	26381	(negative)	(negative)	6182	17501
	40	Oil	8078	(negative)	(negative)	1437	5804

Appendix 4.3: Calculated intakes of Cr in the 43 composites across the 10 age and gender groups and estimated overall intakes and doses. 14-day intakes are calculated by multiplying Cr concentrations in each composite **(Table 4.2)** by the amounts of that food ingested **(Appendix 4.1).**

Operational food group	Compo-site number	Composite or sample name	Cr intakes by composite group as 14-day values (µg/14 days)									
			Age and gender group									
			Males 19 to 24 years	Males 25 years +	Females 25 years +	Pacific Females 15 years +	Pacific Males 15 years +	Boys (11 to 14 years)	Girls (11 to 14 years)	Children (5 to 6 years)	Pre-school (1 to 3 years)	Infants (6 to 12 months)
Fruits	1	Pip fruit/Kiwi fruit	11.7	12.1	10.3	10.3	12.1	15.3	16.7	17.4	7.9	4.7
Fruits	2	Stone fruit	5.8	6.9	7.6	6.4	6.9	4.0	4.2	5.2	3.6	3.3
Fruits	3	Citrus	3.0	3.6	3.8	2.5	2.5	5.6	8.7	7.6	3.2	1.6
Fruits	4	Berries	4.7	3.8	3.5	3.5	3.8	1.3	2.2	2.7	1.9	1.0
Fruits	5	Tomato	4.0	6.3	5.6	3.5	5.6	4.9	4.8	1.4	1.5	1.1
Fruits	6	Others	4.8	3.8	3.2	4.2	3.8	2.4	1.9	3.1	3.4	3.0
Vegetables and fungi	7	Root vegetables	0.5	0.6	0.5	0.4	0.6	0.5	0.4	0.4	0.2	0.1
Vegetables and fungi	8	Tubers	17.6	14.7	9.1	12.0	16.4	15.3	13.4	9.3	4.4	2.6
Vegetables and fungi	9	Leafy vegetables	1.0	1.1	0.8	0.6	1.1	1.2	0.8	0.4	0.3	0.1
Vegetables and fungi	10	Squash/creeping veg	1.3	1.9	2.0	1.3	1.9	1.1	0.8	0.5	0.7	0.5
Vegetables and fungi	11	Seed/Other	8.1	7.9	7.7	3.9	7.9	7.3	5.6	4.9	2.8	1.9
Vegetables and fungi	12	Dried fruits	3.0	3.0	2.0	2.0	3.0	3.0	3.0	3.0	10.0	6.6

Appendix 4.3 continued…

Operational food group	Compo-site number	Composite or sample name	Cr intakes by composite group as 14 day values (µg/14 days)									
			Age and gender group									
			Males 19 to 24 years	Males 25 years +	Females 25 years +	Pacific Females 15 years +	Pacific Males 15 years +	Boys (11 to 14 years)	Girls (11 to 14 years)	Children (5 to 6 years)	Pre-school (1 to 3 years)	Infants (6 to 12 months)
Grain and cereal-based	13	Bread	44.6	36.8	28.4	29.9	32.6	53.7	39.0	39.3	13.8	8.2
Grain and cereal-based	14	Rice or rice-based	22.8	20.3	14.8	15.9	26.0	9.7	6.3	6.8	1.1	0.7
Grain and cereal-based	15	Breakfast cereals	23.8	32.7	17.5	26.1	31.2	20.7	17.8	19.6	22.1	11.6
Grain and cereal-based	16	Pasta, spaghetti, noodles	28.7	25.5	19.4	21.5	33.3	16.3	15.8	11.9	7.4	4.2
Grain and cereal-based	17	Biscuits	13.5	12.1	9.5	9.5	12.1	26.5	20.0	20.0	21.8	9.6
Grain and cereal-based	18	Cakes	18.1	16.6	10.1	10.5	18.6	9.1	13.8	6.7	4.4	1.8
High protein foods	19	Chicken	53.9	33.9	29.8	48.1	73.9	43.0	29.2	23.0	10.5	5.4
High protein foods	20	Beef	20.4	20.1	14.4	23.7	33.1	22.4	14.3	11.4	8.3	5.6
High protein foods	21	Pork	11.3	7.8	4.8	5.6	8.4	8.0	4.8	3.2	2.9	1.4
High protein foods	22	Fish	34.7	37.4	30.8	42.8	47.4	18.3	11.1	9.9	7.5	5.3
High protein foods	23	Other seafood	11.9	13.4	9.1	9.1	13.4	1.1	1.1	0.0	0.0	0.0
High protein foods	24	Eggs	3.7	3.2	3.3	1.9	3.2	2.6	2.3	1.9	1.3	0.7
High protein foods	25	Nuts	7.6	7.6	7.1	7.1	7.6	3.8	3.8	3.8	0.0	0.0
High protein foods	26	Others	51.0	40.6	23.1	35.3	33.6	37.2	35.0	21.0	13.8	7.7

Appendix 4.3 continued…

Operational food group	Compo-site number	Composite or sample name	Cr intakes by composite group as 14 day values (µg/14 days)									
			Age and gender group									
			Males 19 to 24 years	Males 25 years +	Females 25 years +	Pacific Females 15 years +	Pacific Males 15 years +	Boys (11 to 14 years)	Girls (11 to 14 years)	Children (5 to 6 years)	Pre-school (1 to 3 years)	Infants (6 to 12 months)
Dairy foods	27	Milk	30.2	31.5	24.0	23.6	31.5	26.5	20.1	22.7	42.7	8.7
Dairy foods	28	Milk products 1	23.8	25.5	25.9	14.6	14.1	22.9	21.8	17.7	41.7	35.6
Dairy foods	29	Milk products 2	13.2	10.3	8.2	18.8	22.1	16.0	14.7	19.4	18.0	6.2
Drinks and soup	30	Water	0.1	0.1	0.1	0.1	0.1	0.1	0.1	0.1	0.1	0.0
Drinks and soup	31	Juices and carb bevs	13.5	5.3	3.8	4.8	6.5	5.1	4.2	4.0	3.7	1.5
Drinks and soup	32A	Tea	0.7	3.5	4.0	2.1	2.1	0.2	0.2	0.1	0.0	0.0
Drinks and soup	32B	Coffee & drinking choc	128.9	234.2	173.0	117.0	117.0	29.1	30.8	23.4	8.8	2.9
Drinks and soup	32C	Caffeinated beverage	2.4	0.9	0.9	0.9	0.9	0.7	0.5	0.0	0.0	0.0
Drinks and soup	33	Alcoholic drinks	22.5	18.9	5.5	3.4	18.9	0.0	0.0	0.0	0.0	0.0
Drinks and soup	34	Soup	5.5	5.5	7.5	3.3	5.5	3.3	3.3	2.2	1.1	0.7

Appendix 4.3 continued…

Operational food group	Compo-site number	Composite or sample name	Cr intakes by composite group as 14 day values (µg/14 days)									
			Age and gender group									
			Males 19 to 24 years	Males 25 years +	Females 25 years +	Pacific Females 15 years +	Pacific Males 15 years +	Boys (11 to 14 years)	Girls (11 to 14 years)	Children (5 to 6 years)	Pre-school (1 to 3 years)	Infants (6 to 12 months)
Spreads, condiments	35	Spreads	5.2	4.4	3.7	4.0	4.3	3.5	2.5	2.7	1.4	1.1
Spreads, condiments	36	Condiments flavourings	9.5	6.9	4.8	5.8	6.9	7.5	6.0	4.4	1.9	1.2
Spreads, condiments	37	Snack foods, chocolate	29.0	21.6	21.0	15.8	20.1	62.3	54.5	41.8	14.8	8.2
Infant foods	38A	Preschool	0.0	0.0	0.0	0.0	0.0	0.0	0.0	0.0	21.1	0.0
Infant foods	38B	Toddler	0.0	0.0	0.0	0.0	0.0	0.0	0.0	0.0	0.0	210.9
Others	39	Sugar	0.4	0.6	0.5	0.5	0.6	0.3	0.3	0.2	0.1	0.0
Oil	40	Oil	0.2	0.2	0.1	0.1	0.2	0.1	0.1	0.0	0.0	0.0
Intake sums as Cr		µg/14 days	697	743	561	552	691	512	436	373	310	366
		µg/day	50	53	40	39	49	37	31	27	22	26
From 2016/18 NZTDS, Appendix 3.1->		body weight (kg)	79.5	86.7	73.3	88.1	98.1	54.0	54.0	23.0	13.0	9.0
Estimated doses		µg/kg-bw/day	0.63	0.61	0.55	0.45	0.50	0.68	0.58	1.16	1.71	2.90

Appendix 4.4: Calculated intakes of Zn in the 43 composites across the 10 age and gender groups and estimated overall intakes and doses. 14-day intakes are calculated by multiplying Zn concentrations in each composite **(Table 4.2)** by the amounts of that food ingested **(Appendix 4.1).**

Operational food group	Compo-site number	Composite or sample name	Zn intakes by composite group as 14-day values (µg/14 days)									
			Age and gender group									
			Males 19 to 24 years	Males 25 years +	Females 25 years +	Pacific Females 15 years +	Pacific Males 15 years +	Boys (11 to 14 years)	Girls (11 to 14 years)	Children (5 to 6 years)	Pre-school (1 to 3 years)	Infants (6 to 12 months)
Fruits	1	Pip fruit/Kiwi fruit	1972	2040	1726	1726	2040	2576	2810	2927	1335	785
Fruits	2	Stone fruit	963	1144	1268	1068	1144	658	696	865	594	545
Fruits	3	Citrus	301	366	386	254	254	574	885	774	329	162
Fruits	4	Berries	237	188	173	173	188	67	110	134	96	48
Fruits	5	Tomato	441	686	609	377	612	535	527	153	168	122
Fruits	6	Others	2059	1621	1399	1834	1621	1036	818	1355	1483	1304
Vegetables and fungi	7	Root vegetables	2393	2983	2370	1825	2983	2575	2007	1817	984	606
Vegetables and fungi	8	Tubers	5289	4405	2737	3618	4926	4597	4028	2796	1327	782
Vegetables and fungi	9	Leafy vegetables	2237	2465	1938	1426	2664	2734	1889	1044	671	348
Vegetables and fungi	10	Squash/creeping veg	539	755	801	536	755	433	313	214	277	216
Vegetables and fungi	11	Seed/Other	1311	1275	1235	635	1275	1177	901	795	454	309
Vegetables and fungi	12	Dried fruits	109	109	73	73	109	109	109	109	361	237
Grain and cereal-based	13	Bread	18367	15173	11701	12318	13442	22138	16069	16168	5671	3383
Grain and cereal-based	14	Rice or rice-based	7710	6864	5015	5378	8804	3269	2133	2314	381	230

Appendix 4.4 continued…

Operational food group	Compo-site number	Composite or sample name	Zn intakes by composite group as 14-day values (µg/14 days)									
			Age and gender group									
			Males 19 to 24 years	Males 25 years +	Females 25 years +	Pacific Females 15 years +	Pacific Males 15 years +	Boys (11 to 14 years)	Girls (11 to 14 years)	Children (5 to 6 years)	Pre-school (1 to 3 years)	Infants (6 to 12 months)
Grain and cereal-based	15	Breakfast cereals	7101	9761	5227	7772	9298	6176	5297	5829	6592	3469
Grain and cereal-based	16	Pasta, spaghetti, noodles	14865	13235	10075	11153	17248	8444	8193	6187	3846	2174
Grain and cereal-based	17	Biscuits	1800	1621	1267	1267	1621	3539	2669	2669	2916	1290
Grain and cereal-based	18	Cakes	1859	1701	1033	1081	1911	930	1412	689	448	189
High protein foods	19	Chicken	14264	8953	7868	12720	19534	11374	7722	6073	2776	1440
High protein foods	20	Beef	35623	35148	25233	41501	57947	39185	24936	19890	14546	9796
High protein foods	21	Pork	8036	5527	3408	3984	5967	5679	3391	2289	2034	1017
High protein foods	22	Fish	2040	2202	1812	2515	2788	1074	651	582	439	309
High protein foods	23	Other seafood	6397	7167	4855	4855	7167	578	578	0	0	0
High protein foods	24	Eggs	5444	4724	4829	2845	4724	3863	3336	2810	1932	1054
High protein foods	25	Nuts	1770	1770	1643	1643	1770	885	885	885	0	0
High protein foods	26	Others	7701	6141	3493	5334	5077	5628	5291	3181	2080	1162
Dairy foods	27	Milk	4362	4549	3466	3414	4549	3823	2909	3272	6173	1260
Dairy foods	28	Milk products 1	7420	7969	8101	4564	4409	7157	6798	5544	13023	11111
Dairy foods	29	Milk products 2	155	121	97	220	259	188	172	228	210	72

Appendix 4.4 continued…

Operational food group	Compo-site number	Composite or sample name	Zn intakes by composite group as 14-day values (µg/14 days)									
			Age and gender group									
			Males 19 to 24 years	Males 25 years +	Females 25 years +	Pacific Females 15 years +	Pacific Males 15 years +	Boys (11 to 14 years)	Girls (11 to 14 years)	Children (5 to 6 years)	Pre-school (1 to 3 years)	Infants (6 to 12 months)
Drinks and soup	30	Water	37	38	52	52	38	61	61	65	44	24
Drinks and soup	31	Juices and carb beverage	370	147	105	131	177	140	115	111	103	41
Drinks and soup	32A	Tea	16	88	102	52	52	5	5	4	0	0
Drinks and soup	32B	Coffee & drinking choc	1303	2367	1749	1183	1183	295	311	236	89	30
Drinks and soup	32C	Caffeinated beverage	20	7	7	7	7	5	4	0	0	0
Drinks and soup	33	Alcoholic drinks	821	690	202	124	690	0	0	0	0	0
Drinks and soup	34	Soup	101	101	138	61	101	61	61	40	20	12
Spreads, condiments	35	Spreads	184	157	130	143	152	123	88	96	51	38
Spreads, condiments	36	Condiments flavourings	74	53	38	45	53	58	46	34	15	9
Spreads, condiments	37	Snack foods, chocolate	3403	2535	2468	1861	2362	7327	6411	4917	1735	964

Appendix 4.4 concluded…

Operational food group	Compo-site number	Composite or sample name	Zn intakes by composite group as 14-day values (µg/14 days)									
			Age and gender group									
			Males 19 to 24 years	Males 25 years +	Females 25 years +	Pacific Females 15 years +	Pacific Males 15 years +	Boys (11 to 14 years)	Girls (11 to 14 years)	Children (5 to 6 years)	Pre-school (1 to 3 years)	Infants (6 to 12 months)
Infant foods	38A	Preschool	0	0	0	0	0	0	0	0	4842	0
Infant foods	38B	Toddler	0	0	0	0	0	0	0	0	0	148677
Others	39	Sugar	6	9	7	7	9	4	4	3	1	1
Oil	40	Oil	1	1	1	1	1	0	0	0	0	0
Intake sums as Zn		µg/14 days	169101	156856	118834	139775	189911	149077	114640	97098	78045	193217
		µg/day	12079	11204	8488	9984	13565	10648	8189	6936	5575	13801
		mg/day	12.1	11.2	8.5	10.0	13.6	10.6	8.2	6.9	5.6	13.8
From 2016/18 NZTDS, Appdx 3.1->		body weight (kg)	79.5	86.7	73.3	88.1	98.1	54.0	54.0	23.0	13.0	9.0
Estimated doses		µg/kg-bw/day	152	129	116	113	138	197	152	302	429	1533

Appendix 5.1: Identities and associated metadata for the food items and other products tested as part of this survey

Identity	Brand	Made in	Category 1	Category 2	Category 3	E171 Label
Perinaise peri peri mayonnaise	Nandos	Netherlands	Condiments	Condiments	Mayonnaise	No
Portuguese style peri peri hot flavour sauce	Porto Peri-Peri	Australia	Condiments	Condiments	Peri Peri Sauce	No
Sweet and sour sauce	Lee Kum Kee	China	Condiments	Condiments	Sweet and sour sauce	No
Sweet chilli sauce	Barkers	New Zealand	Condiments	Condiments	Sweet chilli sauce	No
Picnic	Cadbury	Australia	Confectionery	Chocolate confectioneries	Chocolate-containing bars	No
Twirl	Cadbury	Australia	Confectionery	Chocolate confectioneries	Chocolate-containing bars	No
Dairy milk	Cadbury	Australia	Confectionery	Chocolate confectioneries	Chocolate-containing bars	No
Snickers	Mars Wrigley	Australia	Confectionery	Chocolate confectioneries	Chocolate-containing bars	No
Pinky	Cadbury	Australia	Confectionery	Chocolate confectioneries	Chocolate-containing bars	No
Milky bar	Nestle	Australia	Confectionery	Chocolate confectioneries	Chocolate-containing bars	No
Raspberry white chocolate bumper bar	Cookie Time	New Zealand	Confectionery	Chocolate confectioneries	Chocolate-containing bars	No
Crunchie	Cadbury	Australia	Confectionery	Chocolate confectioneries	Chocolate-containing bars	No
Mars	Mars Wrigley	Australia	Confectionery	Chocolate confectioneries	Chocolate-containing bars	No
Moro	Cadbury	Australia	Confectionery	Chocolate confectioneries	Chocolate-containing bars	No

Appendix 5.1 continued…

Identity	Brand	Made in	Category 1	Category 2	Category 3	E171 Label
Perky nana	Cadbury	Australia	Confectionery	Chocolate confectioneries	Chocolate-containing bars	No
Flake	Cadbury	Australia	Confectionery	Chocolate confectioneries	Chocolate-containing bars	No
Kit kat	Nestle	Australia	Confectionery	Chocolate confectioneries	Chocolate-containing bars	No
Twix	Mars Wrigley	Egypt	Confectionery	Chocolate confectioneries	Chocolate-containing bars	No
Peanut slab	Whittaker's	New Zealand	Confectionery	Chocolate confectioneries	Chocolate-containing bars	No
Fruit and nut	Whittaker's	New Zealand	Confectionery	Chocolate confectioneries	Chocolate-containing bars	No
Bounty	Mars Wrigley	Netherlands	Confectionery	Chocolate confectioneries	Chocolate-containing bars	No
Aero	Nestle	Australia	Confectionery	Chocolate confectioneries	Chocolate-containing bars	No
Pixie caramel	Nestle	Australia	Confectionery	Chocolate confectioneries	Chocolate-containing bars	No
Creamy milk	Whittaker's	New Zealand	Confectionery	Chocolate confectioneries	Chocolate-containing bars	No
Whittaker's sante bar	Whittaker's	New Zealand	Confectionery	Chocolate confectioneries	Chocolate-containing bars	No
Chantal organics choc almond probiotic protein bar	Chantal Organics	New Zealand	Confectionery	Chocolate confectioneries	Chocolate-containing bars	No
Weight watcher's choc coconut delight bar	Tasti	New Zealand	Confectionery	Chocolate confectioneries	Chocolate-containing bars	Yes

Appendix 5.1 continued…

Identity	Brand	Made in	Category 1	Category 2	Category 3	E171 Label
Kinder surprise (egg shape)	Ferrero Rocher	Italy	Confectionery	Chocolate confectioneries	Chocolate-containing items (other)	No
Bueno	Ferrero Rocher	Italy	Confectionery	Chocolate confectioneries	Chocolate-containing items (other)	No
Turkish delight	Frys	Australia	Confectionery	Chocolate confectioneries	Chocolate-containing items (other)	No
Christmas tree mallows	Lolliland	China	Confectionery	Chocolate confectioneries	Chocolate-containing items (other)	No
Kinder chocolate	Kinder	Germany	Confectionery	Chocolate confectioneries	Chocolate-containing items (other)	No
Christmas stocking	Potter Brothers	New Zealand	Confectionery	Chocolate confectioneries	Chocolate-containing items (other)	No
Milk chocolate Santas	Pams	Italy	Confectionery	Chocolate confectioneries	Chocolate-containing items (other)	No
Christmas mallow pop	Nice	China	Confectionery	Chocolate confectioneries	Chocolate-containing sweets	No

Appendix 5.1 continued…

Identity	Brand	Made in	Category 1	Category 2	Category 3	E171 Label
M&Ms minis	Mars Wrigley	China	Confectionery	Chocolate confectioneries	Chocolate-containing sweets	No
RJs sweets Jaffas	RJs	Australia	Confectionery	Chocolate confectioneries	Chocolate-containing sweets	No
Maltesers chocolate original	Maltesers	Australia	Confectionery	Chocolate confectioneries	Chocolate-containing sweets	No
Pascall chocolate lollies pineapple lumps	Pascall	Australia	Confectionery	Chocolate confectioneries	Chocolate-containing sweets	No
M&Ms chocolate crispy	Mars Wrigley	Australia	Confectionery	Chocolate confectioneries	Chocolate-containing sweets	Yes
M&Ms chocolate brownie	Mars Wrigley	Australia	Confectionery	Chocolate confectioneries	Chocolate-containing sweets	Yes
M&Ms chocolate peanut	Mars Wrigley	China	Confectionery	Chocolate confectioneries	Chocolate-containing sweets	No
Darrell Lea chocolates minty crunchy balls	Darrell Lea	Australia	Confectionery	Chocolate confectioneries	Chocolate-containing sweets	Yes
M&Ms sweets cookie dough	Mars Wrigley	Australia	Confectionery	Chocolate confectioneries	Chocolate-containing sweets	Yes

Appendix 5.1 continued…

Identity	Brand	Made in	Category 1	Category 2	Category 3	E171 Label
M&Ms chocolate milk choc	Mars Wrigley	China	Confectionery	Chocolate confectioneries	Chocolate-containing sweets	No
M&Ms milk chocolate	Mars Wrigley	Australia	Confectionery	Chocolate confectioneries	Chocolate-containing sweets	Yes
Apricot blueberry bites	Loaf	New Zealand	Confectionery	Chocolate confectioneries	Chocolate-containing sweets	No
Queen Anne	Queen Anne	New Zealand	Confectionery	Chocolate confectioneries	Chocolates	No
Lindor	Lindt	Germany	Confectionery	Chocolate confectioneries	Chocolates	No
Roses	Cadbury	Australia	Confectionery	Chocolate confectioneries	Chocolates	No
Ferrero Rocher	Ferrero Rocher	Italy	Confectionery	Chocolate confectioneries	Chocolates	No
Chocolate coins	Pams	New Zealand	Confectionery	Chocolate confectioneries	Chocolates	No
Tunys	Tonys Choco Lonely	Netherlands	Confectionery	Chocolate confectioneries	Chocolates	No
Chocotalia	Praline	Italy	Confectionery	Chocolate confectioneries	Chocolates	No
Cookie bears hundreds and thousands	Griffins	New Zealand	Confectionery	Flour or cereal confectioneries	Biscuits	No
Vanilla cream biscuits	Oki Doki	India	Confectionery	Flour or cereal confectioneries	Biscuits	No

Appendix 5.1 continued…

Identity	Brand	Made in	Category 1	Category 2	Category 3	E171 Label
Wafers (strawberry and vanilla)	Woolworths	Malaysia	Confectionery	Flour or cereal confectioneries	Biscuits	No
White choc and raspberry 1 piece	Kapiti	New Zealand	Confectionery	Flour or cereal confectioneries	Biscuits	No
Donut factory 12 mini iced	The Donut Factory	New Zealand	Confectionery	Flour or cereal confectioneries	Biscuits	Yes
Double filled frooze balls cookie dough	Tasti	New Zealand	Confectionery	Flour or cereal confectioneries	Biscuits	No
Monte carlo biscuits	Arnotts	Australia	Confectionery	Flour or cereal confectioneries	Biscuits	No
Short bread cream biscuits	Arnotts	Australia	Confectionery	Flour or cereal confectioneries	Biscuits	No
Strawberry flavoured thick shake bar (manufacturer redacted)*	---------	New Zealand	Confectionery	Flour or cereal confectioneries	Biscuits (chewable bars)	No
Tasti milkies choc vanilla snack size bars	Tasti	New Zealand	Confectionery	Flour or cereal confectioneries	Biscuits (chewable bars)	Yes
LCMs cereal bars unicorn	Kellogg's	Thailand	Confectionery	Flour or cereal confectioneries	Biscuits (chewable bars)	Yes
Strawberry coulis cheesecake 410 g	Sara Lee	Australia	Confectionery	Flour or cereal confectioneries	Cakes	No
Birthday cake Cube Bakery	New World Thorndon	New Zealand	Confectionery	Flour or cereal confectioneries	Cakes	No
Birthday cake New World	Cube Bakery Taranaki Street	New Zealand	Confectionery	Flour or cereal confectioneries	Cakes	No
Choc iced mini donuts biscuits	Griffins	New Zealand	Confectionery	Flour or cereal confectioneries	Cakes	No

Appendix 5.1 continued…

Identity	Brand	Made in	Category 1	Category 2	Category 3	E171 Label
Chocolate brownie natural flavour	Bar Clif	USA	Confectionery	Flour or cereal confectioneries	Cakes	No
100s & 1000s	Dollar Sweets	Australia	Confectionery	Sugar confectioneries	Cake decorations	No
Sprinkle medley eyes eyes baby 80g	Sweet Moments	New Zealand	Confectionery	Sugar confectioneries	Cake decorations	Yes
Jumbo hearts red 75g	Sweet Moments	China	Confectionery	Sugar confectioneries	Cake decorations	No
Medley natural blue 85g	Sweet Moments	New Zealand	Confectionery	Sugar confectioneries	Cake decorations	Yes
Sprinkle medley circus circus 85g	Gobake	New Zealand	Confectionery	Sugar confectioneries	Cake decorations	No
Sprinkle medley dancing unicorn 80g	Gobake	New Zealand	Confectionery	Sugar confectioneries	Cake decorations	Yes
Sprinkle medley vintage pearl 80g	Gobake	New Zealand	Confectionery	Sugar confectioneries	Cake decorations	Yes
Sugar natural crystal pink 90g	Gobake	New Zealand	Confectionery	Sugar confectioneries	Cake decorations	Yes
Pettinice white icing	Bakels	New Zealand	Confectionery	Sugar confectioneries	Cake icings	Yes
Ready-made white icing	Wilson	Australia	Confectionery	Sugar confectioneries	Cake icings	Yes
Eclipse chew mints	Mars Wrigley	Australia	Confectionery	Sugar confectioneries	Chewable candies	No
Mentos raspberry	Mentos	China	Confectionery	Sugar confectioneries	Chewable candies	No

Appendix 5.1 continued…

Identity	Brand	Made in	Category 1	Category 2	Category 3	E171 Label
Tic tac white	Tic Tac	Australia	Confectionery	Sugar confectioneries	Chewable candies	No
Tic tac colour	Tic Tac	Australia	Confectionery	Sugar confectioneries	Chewable candies	No
Mentos Fruit	Mentos	China	Confectionery	Sugar confectioneries	Chewable candies	No
Sherbet Fizzies	The CareFillery	New Zealand	Confectionery	Sugar confectioneries	Chewable candies	No
Berries and cream	The CareFillery	New Zealand	Confectionery	Sugar confectioneries	Chewable candies	Yes
Giant Python	The CareFillery	China	Confectionery	Sugar confectioneries	Chewable candies	No
Licorice allsorts	The CareFillery	New Zealand	Confectionery	Sugar confectioneries	Chewable candies	No
Tangy sticks	Pascall	New Zealand	Confectionery	Sugar confectioneries	Chewable candies	No
Gumi yum surprise	Zuru	New Zealand	Confectionery	Sugar confectioneries	Chewable candies	No
Pascal explorers	Pascall	Australia	Confectionery	Sugar confectioneries	Chewable candies	No
Curiously strong mints	Wrigleys	Australia	Confectionery	Sugar confectioneries	Chewable candies	No
Macey’s crocodile’s grandpa recipes	Macey’s	New Zealand	Confectionery	Sugar confectioneries	Chewable candies	No
Marshmallows pink and white	Pascall	Australia	Confectionery	Sugar confectioneries	Chewable candies	No

Appendix 5.1 continued…

Identity	Brand	Made in	Category 1	Category 2	Category 3	E171 Label
Sour lollies	The CareFillery	China	Confectionery	Sugar confectioneries	Chewable candies	Yes
Party times eggs	The CareFillery	New Zealand	Confectionery	Sugar confectioneries	Chewable candies	Yes
Sour peaches	Macey's	New Zealand	Confectionery	Sugar confectioneries	Chewable candies	Yes
Skittles	Mars Wrigley	Australia	Confectionery	Sugar confectioneries	Chewable candies	Yes
Pascal wine gums	Pascall	Australia	Confectionery	Sugar confectioneries	Chewable candies	No
Iddy Biddy fruit bits Disney Princess mixed berry flavoured snacks	Iddy Biddy	China	Confectionery	Sugar confectioneries	Chewable candies	No
Pascall fruit burst	Pascall	Thailand	Confectionery	Sugar confectioneries	Chewable candies	No
Pascall Lollies Jet Planes	Pascall	Australia	Confectionery	Sugar confectioneries	Chewable candies	No
Mayceys sour fruit mix	Macey's	New Zealand	Confectionery	Sugar confectioneries	Chewable candies	Yes
Woolworths Lollies Milk Bottles	Woolworths	New Zealand	Confectionery	Sugar confectioneries	Chewable candies	Yes
Pascall lollies milkshakes	Pascall	Thailand	Confectionery	Sugar confectioneries	Chewable candies	No
Skittles sweets fruits	Mars Wrigley	Australia	Confectionery	Sugar confectioneries	Chewable candies	Yes
Skittles sours lollies large bag	Mars Wrigley	Australia	Confectionery	Sugar confectioneries	Chewable candies	Yes

Appendix 5.1 continued…

Identity	Brand	Made in	Category 1	Category 2	Category 3	E171 Label
Haribo strawberry balla stixx	Haribo	Spain	Confectionery	Sugar confectioneries	Chewable candies	No
Extra white gum	Mars Wrigley	Australia	Confectionery	Sugar confectioneries	Chewing gums	Yes
Watermelon burst gum	Mars Wrigley	China	Confectionery	Sugar confectioneries	Chewing gums	No
PK gum	Mars Wrigley	Australia	Confectionery	Sugar confectioneries	Chewing gums	No
Hubba bubba	Mars Wrigley	UK	Confectionery	Sugar confectioneries	Chewing gums	No
Peak	Peak	Australia	Confectionery	Sugar confectioneries	Chewing gums	Yes
Extra spearmint	Mars Wrigley	Australia	Confectionery	Sugar confectioneries	Chewing gums	No
Pam's peppermint candy canes	Pams	China	Confectionery	Sugar confectioneries	Hard candies	No
Cream candies	Werther’s Original	Germany	Confectionery	Sugar confectioneries	Hard candies	No
Crystal sticks cotton candy flavoured sticks	Candy Showcase	South Africa	Confectionery	Sugar confectioneries	Hard candies	Yes
Chupa chup	Chupa Chup	Spain	Confectionery	Sugar confectioneries	Hard candies	No
Oki Doki Christmas candy cane with jellybean	Oki Doki	China	Confectionery	Sugar confectioneries	Hard candies	Yes
Unicorn spinner lollipop	Tutti Fruiti	China	Confectionery	Sugar confectioneries	Hard candies	Yes

Appendix 5.1 continued…

Identity	Brand	Made in	Category 1	Category 2	Category 3	E171 Label
Swirly heart pops raspberry flavoured	Candy Showcase	China	Confectionery	Sugar confectioneries	Hard candies	Yes
QuickEze	QuickEze	Australia	Confectionery	Sugar confectioneries / pharmaceutical	Chewable candies	No
Soothers	Nestle	Australia	Confectionery	Sugar confectioneries / pharmaceutical	Hard candies	No
Halls throaties	Halls	Thailand	Confectionery	Sugar confectioneries / pharmaceutical	Hard candies	No
Fisherman's friend	Fisherman's Friend	England	Confectionery	Sugar confectioneries / pharmaceutical	Hard candies	No
Coconut ice cream bites 6 pieces (manufacturer redacted)*	----------	Thailand	Dairy foods	Ice creams/ dairy desserts	Ice cream biscuits	No
Oreo frozen cookie sandwich 1 pack	Tip Top	New Zealand	Dairy foods	Ice creams/ dairy desserts	Ice cream biscuits	No
Samanco red bean	Binggrae	South korea	Dairy foods	Ice creams/ dairy desserts	Ice cream biscuits	No
Mochi bites golden blonde chocolate	Little Moons	UK	Dairy foods	Ice creams/ dairy desserts	Ice cream bites	No
Yukimi frozen dessert vanilla 1 pack	Lotte	Japan	Dairy foods	Ice creams/ dairy desserts	Ice creams	No
Marlborough salted caramel 1 L	Kapiti	New Zealand	Dairy foods	Ice creams/dairy desserts	Ice creams	No

Appendix 5.1 continued…

Identity	Brand	Made in	Category 1	Category 2	Category 3	E171 Label
Triple choc 1 L	Kapiti	New Zealand	Dairy foods	Ice creams / dairy desserts	Ice creams	No
French Vanilla 2L	Tip top	New Zealand	Dairy foods	Ice creams / dairy desserts	Ice creams	No
Premium awesome boysenberry stracciatella 2L	MuchMoore	New Zealand	Dairy foods	Ice creams / dairy desserts	Ice creams	No
Boysenberry ripple 2L	Tip Top	New Zealand	Dairy foods	Ice creams / dairy desserts	Ice creams	No
The Laughing Cow original cheese wedges	Laughing Cow	France	Dairy products	Dairy products	Cheeses	No
Coffeemate	Nestle	Thailand	Drink additives	Powders	Coffee creamers	No
Caramel syrup for coffee	Quarterpast	New Zealand	Drink additives	Syrups	Coffee syrups	No
E^2 lemon and lime liquid energy	Coca Cola	New Zealand	Drinks	Energy, sports or fruit drinks	Liquids	No
Slushy lemonade and raspberry 1 pack	Tip Top	New Zealand	Drinks	Energy, sports or fruit drinks	Liquids	No
Fierce berry gatorade	Gatorade	New Zealand	Drinks	Energy, sports or fruit drinks	Liquids	No
Electrolite rehydration	Vitasport	New Zealand	Drinks	Energy, sports or fruit drinks	Powders	No
Fruit drink powder (mango, orange, sweet navel orange, blackcurrant)	Raro	New Zealand	Drinks	Energy, sports or fruit drinks	Powders	No
So good almond	Sanitarium	Australia	Drinks	Plant-based milks	Almond milk	No
Oat milk	Vitasoy	Australia	Drinks	Plant-based milks	Oat milk	No

Appendix 5.1 continued…

Identity	Brand	Made in	Category 1	Category 2	Category 3	E171 Label
Rice milk	Vitasoy	Australia	Drinks	Plant-based milks	Rice milk	No
So good barista soy	Sanitarium	Australia	Drinks	Plant-based milks	Soy milk	No
Soy milk regular	Vitasoy	Australia	Drinks	Plant-based milks	Soy milk	No
Gel color neon blue	Gobake	China	Food additives or ingredients	Food colorants	Blue	Yes
Gel color neon orange	Gobake	China	Food additives or ingredients	Food colorants	Orange	Yes
Gel color super white	Gobake	China	Food additives or ingredients	Food colorants	White	Yes
Gel color neon yellow	Gobake	China	Food additives or ingredients	Food colorants	Yellow	Yes
Wheatmeal sliced bread	Essentials	New Zealand	Grain-based foods	Baked goods	Breads	No
Baby dry milk	S26 Gold	Singapore	Infant foods	Baby foods	Milk formulas	No
Baby dry milk	Aptamil	New Zealand	Infant foods	Baby foods	Milk formulas	No
Pumpkin and potato with NZ beef pouch	Natureland	New Zealand	Infant foods	Baby foods	Pouches	No
Banana and berries with NZ apple pouch	Natureland	New Zealand	Infant foods	Baby foods	Pouches	No
Strawberry fruit custard pouch	Smiling Tums	Australia	Infant foods	Baby foods	Pouches	No
Chicken and vegetables pouch	Smiling Tums	Australia	Infant foods	Baby foods	Pouches	No
Beef, butternut pumpkin and rice with spinach pouch	Watties Organic	Australia	Infant foods	Baby foods	Pouches	No
Apple blueberry and strawberry pouch	Watties	Australia	Infant foods	Baby foods	Pouches	No

Appendix 5.1 continued…

Identity	Brand	Made in	Category 1	Category 2	Category 3	E171 Label
Creamy custard with banana pouch	Watties	Australia	Infant foods	Baby foods	Pouches	No
Pear banana and apple pouch	Only Organic	New Zealand	Infant foods	Baby foods	Pouches	No
Banana blueberry and quinoa pouch	Only Organic	New Zealand	Infant foods	Baby foods	Pouches	No
Muesli with apple	Farex	Australia	Infant foods	Baby foods	Pouches	No
Watties baby food	Watties	Australia	Infant foods	Baby foods	Pouches	No
Berocca	Bayer	New Zealand	Nutraceuticals	Nutraceuticals	Tablets (dissovable)	No
Paracetamol	Febrex	Australia	Pharmaceuticals	Pharmaceuticals	Tablets (to swallow)	No
Polident fresh denture adhesive cream	Polident	Ireland	Toothpastes and related products	Toothpastes and related products	Adhesive denture cream	No
Red seal kids' toothpaste gel	Red seal	New Zealand	Toothpastes and related products	Toothpastes and related products	Toothpastes	No
Colgate advanced whitening	Colgate	Thailand	Toothpastes and related products	Toothpastes and related products	Toothpastes	No
Macleans protect fresh mint	Macleans	South Africa	Toothpastes and related products	Toothpastes and related products	Toothpastes	Yes
Sensodyne rapid relief	Haelon	New Zealand	Toothpastes and related products	Toothpastes and related products	Toothpastes	Yes
Colgate sensitive whitening	Colgate	Thailand	Toothpastes and related products	Toothpastes and related products	Toothpastes	Yes
Mouth fresh cool mint toothpaste	Mouth Fresh	India	Toothpastes and related products	Toothpastes and related products	Toothpastes	Yes

Appendix 5.1 concluded…

Identity	Brand	Made in	Category 1	Category 2	Category 3	E171 Label
Oral-B 3D white	P&G	China	Toothpastes and related products	Toothpastes and related products	Toothpastes	Yes
Kids mild mint flavour toothpaste (manufacturer redacted)*	----------	Germany	Toothpastes and related products	Toothpastes and related products	Toothpastes	No
Pronamel gentle whitening fresh mint	Haelon	Thailand	Toothpastes and related products	Toothpastes and related products	Toothpastes	Yes
Steradent active plus denture paste	Steradent	Australia	Toothpastes and related products	Toothpastes and related products	Toothpastes	Yes

* The identity of the manufacturer is redacted due to a mismatch where some E171 was present though not listed in the product labelling. These are being referred to the applicable regulator. In all other cases, E171 detection was either consistent with the labelling, or (in 7 cases) E171 was not present despite being listed on the product labelling.

Appendix 5.2: Analytical results for titanium in individual products sampled as part of this study.

Results are expressed as both [Ti] and [TiO_2] equivalents. Concentrations in products are wet weight as used or consumed. Concentration in ash are those in the inorganic component of each item which survived ashing at 600 °C. All numerical values in this table have been rounded to three significant figures for consistency. Values less than 100 have been rounded to two decimal places where appropriate.

Identity	**Type** (Category 3 in **Appendix 5.1**)	**Concentration in product (mg/kg)**		**Concentration in ash (mg/kg ash)**	
		[Ti]	**[TiO_2] equiv**	**[Ti]**	**[TiO_2] equiv**
Perinaise peri peri mayonnaise	Mayonnaise	0.13	0.21	3.80	6.35
Portuguese style peri peri hot flavour sauce	Peri Peri Sauce	0.19	0.32	14.1	23.5
Sweet and sour sauce	Sweet and sour sauce	0.12	0.20	13.3	22.3
Sweet chilli sauce	Sweet chilli sauce	0.21	0.36	12.6	21.1
Picnic	Chocolate-containing bars	<0.35	<0.59	<445	<742
Twirl	Chocolate-containing bars	<0.36	<0.60	<3250	<5430
Dairy milk	Chocolate-containing bars	<0.32	<0.53	<3120	<5200
Snickers	Chocolate-containing bars	<0.32	<0.54	<79.8	<133
Pinky	Chocolate-containing bars	<0.42	<0.70	<25.8	<43.0
Milky bar	Chocolate-containing bars	<0.22	<0.37	<13.8	<22.9
Raspberry white chocolate bumper bar	Chocolate-containing bars	<0.39	<0.65	<36.5	<60.9
Crunchie	Chocolate-containing bars	0.98	1.63	20.1	33.5
Mars	Chocolate-containing bars	0.49	0.82	889	1480
Moro	Chocolate-containing bars	0.76	1.27	4390	7320
Perky nana	Chocolate-containing bars	0.39	0.66	78.3	131

Appendix 5.2 continued…

Identity	**Type** (Category 3 in **Appendix 5.1**)	**Concentration in product (mg/kg)**		**Concentration in ash (mg/kg ash)**	
		[Ti]	**[TiO_2] equiv**	**[Ti]**	**[TiO_2] equiv**
Flake	Chocolate-containing bars	0.37	0.62	958	1600
Kit kat	Chocolate-containing bars	0.51	0.85	1930	3220
Twix	Chocolate-containing bars	0.47	0.79	1490	2490
Peanut slab	Chocolate-containing bars	0.88	1.46	30900	51500
Fruit and nut	Chocolate-containing bars	0.54	0.90	1510	2520
Bounty	Chocolate-containing bars	0.81	1.35	57.4	95.7
Aero	Chocolate-containing bars	0.45	0.75	35.1	58.5
Pixie caramel	Chocolate-containing bars	1.76	2.93	31.9	53.2
Creamy milk	Chocolate-containing bars	1.02	1.69	53.7	89.6
Whittaker's sante bar	Chocolate-containing bars	4.43	7.39	278	464
Chantal organics chocolate almond probiotic protein bar	Chocolate-containing bars	0.84	1.41	39.4	65.8
Weight watchers chocc coconut delight bar	Chocolate-containing bars	0.58	0.97	59.7	99.6
Kinder surprise (egg shape)	Chocolate-containing (other)	<0.46	<0.76	<28.7	<47.8
Bueno	Chocolate-containing (other)	<0.45	<0.74	<5.00	<8.35
Turkish delight	Chocolate-containing (other)	<0.22	<0.37	<55.0	<91.8
Christmas tree mallows	Chocolate-containing (other)	<0.03	<0.04	<884	<1470

Appendix 5.2 continued…

Identity	**Type** (Category 3 in **Appendix 5.1**)	**Concentration in product (mg/kg)**		**Concentration in ash (mg/kg ash)**	
		[Ti]	**[TiO_2] equiv**	**[Ti]**	**[TiO_2] equiv**
Kinder chocolate	Chocolate-containing (other)	0.45	0.76	39.3	65.5
Christmas stocking	Chocolate-containing (other)	3.41	5.70	1220	2040
Milk chocolate Santas	Chocolate-containing (other)	6.01	10.0	470	783
Christmas mallow pop	Chocolate-containing sweets	<0.07	<0.11	<557	<929
M&Ms minis	Chocolate-containing sweets	2.04	3.40	176	294
RJs sweets Jaffas	Chocolate-containing sweets	4.48	7.48	506	844
Maltesers chocolate original	Chocolate-containing sweets	1.31	2.19	75.1	125
Pascall chocolate lollies pineapple lumps	Chocolate-containing sweets	2.19	3.66	369	616
M&Ms chocolate crispy	Chocolate-containing sweets	1250	2080	87100	145000
M&Ms chocolate brownie	Chocolate-containing sweets	795	1330	57100	95300
M&Ms chocolate peanut	Chocolate-containing sweets	1.92	3.21	146	243
Darrell Lea chocolates minty crunchy balls	Chocolate-containing sweets	284	474	27000	45000
M&Ms sweets cookie dough	Chocolate-containing sweets	942	1570	98700	165000
M&Ms chocolate milk choc	Chocolate-containing sweets	1.99	3.3	167	279
M&Ms milk chocolate	Chocolate-containing sweets	422	704	30100	50300
Apricot blueberry bites	Chocolate-containing sweets	0.29	0.50	22.4	37.3

Appendix 5.2 continued…

Identity	**Type** (Category 3 in **Appendix 5.1**)	**Concentration in product (mg/kg)**		**Concentration in ash (mg/kg ash)**	
		[Ti]	**[TiO_2] equiv**	**[Ti]**	**[TiO_2] equiv**
Queen Anne	Chocolates	<0.38	<0.64	<137	<228
Lindor	Chocolates	<0.41	<0.69	<908	<1520
Roses	Chocolates	<0.31	<0.51	<19.0	<31.7
Ferrero Rocher	Chocolates	1.15	1.92	60.8	101
Chocolate coins	Chocolates	0.70	1.17	49.9	83.3
Tunys	Chocolates	0.57	0.95	35.0	58.4
Chocotalia	Chocolates	1.10	1.83	106	177
Cookie bears hundreds and thousands	Biscuits	<0.20	<0.33	<21.1	<35.2
Vanilla cream biscuits	Biscuits	<0.14	<0.23	<15.7	<26.2
Wafers (strawberry and vanilla)	Biscuits	<0.18	<0.30	<67.9	<113
White choc and raspberry 1 piece	Biscuits	0.49	0.82	78.4	131
Donut factory 12 mini iced	Biscuits	0.66	1.10	43.3	72.2
Double-filled frooze balls cookie dough	Biscuits	1.28	2.14	57.2	95.4
Monte carlo biscuits	Biscuits	0.41	0.69	44.7	74.6
Short bread cream biscuits	Biscuits	0.41	0.69	35.5	59.1
Strawberry flavoured thick shake bar (manufacturer redacted)*	Biscuits (chewable bars)	280	467	29300	48800

Appendix 5.2 continued…

Identity	Type (Category 3 in **Appendix 5.1**)	Concentration in product (mg/kg)		Concentration in ash (mg/kg ash)	
		[Ti]	[TiO_2] equiv	[Ti]	[TiO_2] equiv
Tasti milkies choc vanilla snack size bars	Biscuits (chewable bars)	234	391	17200	28800
LCMs cereal bars unicorn	Biscuits (chewable bars)	1.96	3.30	245	408
Strawberry coulis cheesecake 410 g	Cakes	0.43	0.70	57.5	96.0
Birthday cake, Cube Bakery	Cakes	1.07	1.80	298	498
Birthday cake New World	Cakes	1.44	2.40	364	607
Choc iced mini donut biscuits	Cakes	0.92	1.50	88.0	146
Chocolate brownie natural flavour	Cakes	1.89	3.10	709	1180
100s & 1000s	Cake decorations	<0.30	<0.50	<478	<798
Sprinkle medley eyes eyes baby 80g	Cake decorations	<0.19	<0.32	<652	<1090
Jumbo hearts red 75g	Cake decorations	0.45	0.80	563	939
Medley natural blue 85g	Cake decorations	10.4	17.3	35100	58600
Sprinkle medley circus circus 85g	Cake decorations	0.84	1.40	2730	4560
Sprinkle medley dancing unicorn 80g	Cake decorations	54.7	91.3	78600	131000
Sprinkle medley vintage pearl 80g	Cake decorations	17.3	28.8	45900	76500
Sugar natural crystal pink 90g	Cake decorations	84.1	140	46900	78200
Pettinice white icing	Cake icings	465	776	265000	443000

Appendix 5.2 continued…

Identity	Type (Category 3 in **Appendix 5.1**)	Concentration in product (mg/kg)		Concentration in ash (mg/kg ash)	
		[Ti]	[TiO_2] equiv	[Ti]	[TiO_2] equiv
Ready-made white icing	Cake icings	1250	2090	421000	702000
Eclipse chew mints	Chewable candies	<0.09	<0.15	<6.10	<10.1
Mentos raspberry	Chewable candies	<0.13	<0.22	<28.1	<46.8
Tic tac white	Chewable candies	<0.13	<0.21	<13.3	<22.2
Tic tac colour	Chewable candies	<0.11	<0.18	<7.63	<12.7
Mentos Fruit	Chewable candies	<0.08	<0.13	<4.01	<6.69
Sherbet Fizzies	Chewable candies	<0.42	<0.70	<8.62	<14.4
Berries and cream	Chewable candies	<0.25	<0.41	<441	<735
Giant Python	Chewable candies	<0.26	<0.43	<1480	<2470
Licorice allsorts	Chewable candies	<0.38	<0.63	<75.3	<126
Tangy sticks	Chewable candies	<0.17	<0.28	<1530	<2560
Gumi yum surprise	Chewable candies	<0.17	<0.28	<537	<896
Pascal explorers	Chewable candies	<0.14	<0.24	<1400	<2330
Curiously strong mints	Chewable candies	<0.42	<0.71	<1930	<3210
Macey’s crocodile’s grandpa recipes	Chewable candies	<0.07	<0.11	<33.7	<56.2
Marshmallows pink and white	Chewable candies	<0.27	<0.46	<582	<972

Appendix 5.2 continued…

Identity	Type (Category 3 in **Appendix 5.1**)	Concentration in product (mg/kg)		Concentration in ash (mg/kg ash)	
		[Ti]	[TiO_2] equiv	[Ti]	[TiO_2] equiv
Sour lollies	Chewable candies	186	311	479000	799000
Party times eggs	Chewable candies	32.9	54.9	125000	209000
Sour peaches	Chewable candies	16.8	28.0	21200	35300
Skittles	Chewable candies	10.7	17.9	30100	50100
Pascal wine gums	Chewable candies	0.70	1.16	2100	3510
Iddy Biddy fruit bits Disney Princess mixed berry flavoured snacks	Chewable candies	0.78	1.30	1090	1820
Pascall fruit burst	Chewable candies	0.46	0.77	9740	16200
Pascall Lollies Jet Planes	Chewable candies	0.46	0.76	2400	4000
Macey's sour fruit mix	Chewable candies	11.9	19.8	15100	25200
Woolworths Lollies Milk Bottles	Chewable candies	753	1256	1320000	220000
Pascall lollies milkshakes	Chewable candies	1.35	2.25	240	401
Skittles sweets fruits	Chewable candies	6.70	11.2	38100	63600
Skittles sours lollies large bag	Chewable candies	5.85	9.75	13000	21800
Haribo strawberry balla stixx	Chewable candies	0.64	1.07	0.17	0.30

Appendix 5.2 continued…

Identity	**Type** (Category 3 in **Appendix 5.1**)	**Concentration in product (mg/kg)**		**Concentration in ash (mg/kg ash)**	
		[Ti]	**[TiO_2] equiv**	**[Ti]**	**[TiO_2] equiv**
Extra white gum	Chewing gums	1.21	2.02	73.7	123
Watermelon burst gum	Chewing gums	2.57	4.28	200	334
PK gum	Chewing gums	1.72	2.88	101	169
Hubba bubba	Chewing gums	3.55	5.93	64.6	108
Peak	Chewing gums	1330	2220	14900	24900
Extra spearmint	Chewing gums	2.18	3.60	32.1	53.5
Pams peppermint candy canes	Hard candies	<0.22	<0.36	<1150	<1920
Cream candies	Hard candies	<0.15	<0.25	<14.3	<23.8
Crystal sticks cotton candy flavoured sticks	Hard candies	<0.33	<0.55	<36400	<60700
Chupa chup	Hard candies	2.00	3.30	4370	7290
Oki Doki Christmas candy cane with jelly bean	Hard candies	83.0	139	752000	1250000
Unicorn spinner lollipop	Hard candies	832	1390	1210000	2030000
Swirly heart pops raspberry flavoured	Hard candies	1080	1800	569000	949000
QuickEze	Chewable candies	1.16	1.93	61.0	102
Soothers	Hard candies	<0.27	<0.46	<17.9	<29.9

Appendix 5.2 continued…

Identity	**Type** (Category 3 in **Appendix 5.1**)	**Concentration in product (mg/kg)**		**Concentration in ash (mg/kg ash)**	
		[Ti]	**[TiO_2] equiv**	**[Ti]**	**[TiO_2] equiv**
Halls throaties	Hard candies	<0.21	<0.35	<42.2	<70.4
Fisherman's friend	Hard candies	0.46	0.77	43.6	72.7
Coconut ice cream bites 6 pieces (manufacturer redacted)*	Ice cream biscuits	96.0	160	20400	34100
Oreo frozen cookie sandwich 1 pack	Ice cream biscuits	2.46	4.10	181	301
Samanco red bean	Ice cream biscuits	0.39	0.64	99.7	166
Mochi bites golden blonde chocolate	Ice cream bites	<0.08	<0.13	<9.21	<15.4
Yukimi frozen dessert vanilla 1 pack	Ice creams	0.42	0.71	80.1	134
Marlborough salted caramel 1 L	Ice creams	0.37	0.61	39.2	65.5
Triple choc 1L	Ice creams	1.34	2.23	117	196
French Vanilla 2L	Ice creams	0.31	0.51	56.8	94.8
Premium awesome boysenberry stracciatella 2L	Ice creams	1.04	1.73	202	337
Boysenberry ripple 2L	Ice creams	0.68	1.13	160	268
The Laughing Cow original cheese wedges	Cheeses	<0.43	<0.72	<10.3	<17.1
Coffeemate	Coffee creamers	0.53	0.88	17.3	28.9
Caramel syrup for coffee	Coffee syrups	<0.04	<0.07	<38.4	<64.0

Appendix 5.2 continued…

Identity	**Type** (Category 3 in **Appendix 5.1**)	**Concentration in product (mg/kg)**		**Concentration in ash (mg/kg ash)**	
		[Ti]	**[TiO_2] equiv**	**[Ti]**	**[TiO_2] equiv**
E^2 lemon and lime liquid energy	Liquids	<0.04	<0.06	<32.0	<53.4
Slushy lemonade and raspberry 1 pack	Liquids	0.61	1.02	1870	3120
Fierce berry gatorade	Liquids	0.07	0.12	29.4	49.0
Electrolite rehydration	Powders	<0.19	<0.31	<5.29	<8.82
Fruit drink powder (mango orange, sweet navel orange, blackcurrant)	Powders	<0.12	<0.21	<14.1	<23.5
So good almond	Almond milk	0.09	0.15	16.4	27.4
Oat milk	Oat milk	<0.03	<0.05	<4.31	<7.19
Rice milk	Rice milk	0.07	0.10	21.1	35.2
So good barista soy	Soy milk	<0.03	<0.06	<2.84	<4.74
Soy milk regular	Soy milk	0.11	0.20	25.1	41.8
Gel colour neon blue	Food colouring	28400	47400	461000	769000
Gel colour neon orange	Food colouring	26800	44700	379000	632000
Gel colour super white	Food colouring	143000	239000	335000	558000
Gel colour neon yellow	Food colouring	27300	45600	314000	524000
Wheatmeal sliced bread	Breads	<0.11	<0.19	<6.27	<10.5

Appendix 5.2 continued…

Identity	**Type** (Category 3 in **Appendix 5.1**)	**Concentration in product (mg/kg)**		**Concentration in ash (mg/kg ash)**	
		[Ti]	**[TiO_2] equiv**	**[Ti]**	**[TiO_2] equiv**
Baby dry milk	Milk formulas	<0.23	<0.39	<7.43	<12.4
Baby dry milk	Milk formulas	<0.24	<0.40	<8.88	<14.8
Pumpkin and potato with NZ beef pouch	Pouches	<0.23	<0.39	<52.4	<87.5
Banana and berries with NZ apple pouch	Pouches	<0.24	<0.39	<54.7	<91.3
Strawberry fruit custard pouch	Pouches	<0.24	<0.40	<40.6	<67.7
Chicken and vegetables pouch	Pouches	<0.24	<0.40	<38.5	<64.2
Beef, butternut pumpkin and rice with spinach pouch	Pouches	<0.24	<0.40	<57.4	<95.8
Apple blueberry and strawberry pouch	Pouches	<0.23	<0.38	<73.1	<122
Creamy custard with banana pouch	Pouches	<0.24	<0.40	<67.4	<112
Pear banana and apple pouch	Pouches	<0.24	<0.40	<58.4	<97.5
Banana blueberry and quinoa pouch	Pouches	<0.24	<0.40	<29.2	<48.7
Muesli with apple	Pouches	0.79	1.32	60.6	101
Wattie’s baby food	Pouches	0.45	0.75	163	273
Berocca	Tablets (dissolvable)	0.60	1.00	2.75	4.59
Paracetamol	Tablets (to swallow)	4.99	8.33	238	396

Appendix 5.2 continued…

Identity	**Type** (Category 3 in **Appendix 5.1**)	**Concentration in product (mg/kg)**		**Concentration in ash (mg/kg ash)**	
		[Ti]	**[TiO_2] equiv**	**[Ti]**	**[TiO_2] equiv**
Polident fresh denture adhesive cream	Adhesive denture cream	<0.09	<0.15	<0.82	<1.36
Red seal kids toothpaste gel	Toothpastes	<0.41	<0.69	<2.21	<3.69
Colgate advanced whitening	Toothpastes	4.80	8.00	19.3	32.1
Macleans protect fresh mint	Toothpastes	3810	6350	17300	28900
Sensodyne rapid relief	Toothpastes	2540	4230	12500	20800
Colgate sensitive whitening	Toothpastes	714	1190	3320	5540
Mouth fresh cool mint toothpaste	Toothpastes	2860	4780	14800	24700
Oral-B 3D white	Toothpastes	1120	1870	4660	7770
Kids mild mint flavour toothpaste (manufacturer redacted)*	Toothpastes	553	922	2580	4300
Pronamel gentle whitening fresh mint	Toothpastes	11.9	19.9	60.1	100
Steradent active plus denture paste	Toothpastes	1020	1690	2670	4450

* The identity of the manufacturer is redacted due to a mismatch where some E171 was present though not listed in the product labelling. These are being referred to the applicable regulator. In all other cases, E171 detection was either consistent with the labelling, or (in 7 cases) E171 was not present despite being listed on the product labelling.

Appendix 5.3: Origins for each of the portion size weights selected in Table 5.8.

Food product subset	Weights are for…	Weight (g)	Additional information
Cake icings (N=2)	The icing on one slice	40	Around 400 g of cake icing is needed for a 6 inch two layered cake (this cake can have 10 moderate portions which leads us to around 40 g/piece).
Biscuits (chewable bars) (N=2)	One bar	20	Pack of 6 bars with a net weight of 120 g
Chewable candies (N=8)	Small bag of sour lollies or similar (1 person)	180	This is for woolsworth lollies milk bottles
Chocolate-containing sweets (N=5)	One pack of M&Ms (49 g)	130	M&Ms comes in different weights ranging (100, 120, 130, 145, 345). The one used was 130 g.
Hard candies (N=3)	One Unicorn spinner lolipop	23	Comes as an individually wrapped piece
Ice cream biscuits (N=1)	NOM - 1 pack of 6	26	Pack of 6 bars with a serving size weight of 26 g
Maxima for chewable candies (1256), chocolate-containing sweets (2076), and hard candies (1797) (N=3)	Average of the three above	111	Average of all the three (180g, 130g, and 23g)
Chewing gums (N=1)	A pack	28	Comes in a pack of 14 x 2 g pieces with a net weight of 28 g
Toothpastes (N=8)	One bead on a toothbrush	2.8	Average of 5 beads